# Control of molecular movement based on porphyrins

Ivan Meshkov

# UNIVERSITÉ DE STRASBOURG

*ÉCOLE DOCTORALE DES SCIENCES CHIMIQUES*

**UMR 7140**

# THÈSE présentée par :

**Ivan MESHKOV**

soutenue le : **31 mars 2016**

pour obtenir le grade de : **Docteur de l'université de Strasbourg**

Discipline/ Spécialité : Chimie

co-tutelle

# Contrôle du Mouvement Moléculaire à Base de Porphyrines

**THÈSE dirigée par :**

| | |
|---|---|
| **M. HOSSEINI Mir Wais** | Professeur, Université de Strasbourg |
| **Mme BULACH Véronique** | Professeur, Université de Strasbourg |
| **M. TSIVADZE Aslan** | Professeur, IPCE RAS, Moscou |
| **Mme GORBUNOVA Yulia** | Professeur, IPCE RAS, Moscou |

**RAPPORTEURS :**

| | |
|---|---|
| **M. LEMERCIER Gilles** | Professeur, Université de Reims Champagne-Ardenne |
| **M. TRIFONOV Alexander** | Professeur, IOMC RAS, Nijni Novgorod |

## Acknowledgements

First of all, I would like to thank the members of the jury: Prof. Gilles Lemercier and Prof. Alexander Trifonov for the time they spent to appreciate my thesis and for their remarks and comments.

I would like to express plenty of gratitude to my supervisors: Prof. Mir Wais Hosseini and Prof. Aslan Tsivadze for the opportunity to work on this subject in the collaboration of two countries and for their scientific help. Many thanks to Prof. Véronique Bulach for supporting me in Strasbourg, for the discussions and for spending her time. Especially I would like to thank Prof. Yulia Gorbunova for supporting me in Moscow, for her ideas (which helped to develop the work), for teaching me and for fixing my mistakes.

All members of both laboratories (French and Russian) have been the source of motivation for me. Thanks to Prof. Sylvie Ferlay, Dr. Abdelaziz Jouaiti, Dr. Stéphane Baudron, Dr. Aurélie Guenet, Dr. Alexander Martynov, Dr. Kirill Birin, Dr. Yulia Enakieva, Dr. Anna Sineltchikova, Dr. Marina Polovkova and Dr. Ludmila Lapkina for their readiness to help and answer to my questions. Special thanks to Nathalie Kyritsakas-Gruber and Dr. Mikhail Grigoriev for their perfect X-ray skills; to Audrey Fluck-Salomon for her help with lab equipment and not killing me for broken things; to our secretary Valérie Rey for all administrative help in Strasbourg. I would like to thank all my lab mates: Patrick, Mohamed, Antoine, Bowen, Fan, Takumi, Hervé, Romain, Berangere, Cyril, Georges, Maxime, Katya, Damien, Elsa, Dimby (for fitness trainings), Nico Z (for turnstile spirit in the office), Nico M (for wonderful French music in the lab), Sasha (for advices and support), Chaojie (for keeping high morale in the office); Evgeniya (for wonderful Russian music in the lab), Marina (for Dijon interventions), Taisiya (for singlet oxygen and good mood), Elena (too much “for” to write) and many more whom I missed to note for making my time in Strasbourg and Moscow unforgettable.

Especially I would like to thank NMR service in Strasbourg (Lionel Allouche, Maurice Coupe, Bruno Vincent) and Dr. Gayane Kirakosyan (NMR in Moscow) for their participation in my work.

Last, I would like to thank my friends: Alexey L, Irina S, Stanislav S, Alexander P, Nikolay K, Jan H; my brother and my parents for their encouragement, their right words in difficult moments and their believing in me. Without them, this work would be impossible to be completed.

# Contents

**Introduction** **1**

**Chapter I. Molecular Turnstiles Based on Phosphorus (V) Porphyrins** **17**

**Chapter II. Phosphorus (V) Porphyrins: Photochemical Properties** **75**

**Chapter III. A Molecular Break Based on a Zn(II) Porphyrin Dimer** **105**

**General Conclusions** **129**

**Experimental Part** **133**

**Crystallographic Data** **163**

**Résumé (French)** **171**

## Abbreviations

| | |
|---|---|
| DABCO | 1,4-diazabicyclo[2.2.2]octane |
| DCM | Dichloromethane |
| DHP | 3,4-dihydro-2H-pyrane |
| DMAP | 4-dimethylaminopyridine |
| DMF | Dimethylformamide |
| DMSO | Dimethylsulfoxide |
| EtOH | Ethanol |
| $Et_3N$ | Triethylamine |
| eq | Equivalent |
| GPC | Gel permeation chromatography |
| MeOH | Methanol |
| NMR | Nuclear magnetic resonance |
| ppm | Part per million |
| TBAF | Tetrabutylammonium fluoride |
| TFA | Trifluoroacetic acid |
| THF | Tetrahydrofuran |
| THP | Tetrahydropyrane |
| UV | Ultraviolet |

# Introduction

# Contents


1. **General introduction** 5
2. **Kinesin a walking protein** 6
3. **Translatory motion** 7
4. **Rotatory motion** 8
5. **Molecular devices on surfaces** 12
6. **References** 15

# 1. General introduction

The world around us includes multitude of objects. They can be of different shapes, colors, sizes *etc*. however they are all in permanent motion relative to each other. Giant planetary systems rotate around the galactic centers. Simultaneously galaxies move with enormous speeds relatively to supermassive black holes, quasars and other galaxies. Planetary system consists in complex movements of planets, satellites, asteroids… They also include moving parts. This series can be continued to micro objects, such as atoms and subatomic particles. Even at 0 K the movement of micro particles does not stop due to quantum effects. Thus the motion pierces all the matter around us and it never stops.

Since ancient ages, humanity is concerned with the control movement. This process started with constructing of simple mechanic devices like a wheel before it became more and more sophisticated. The evolution of movement control evolved in two ways based on increasing and decreasing the size of moving parts. Today, for example ships with size greater than medieval cities, or airplanes of the cargo type capable of transporting hundreds of tons have been constructed. In more recent years, the opposite trend, *i. e*. constructing even smaller devices, is under active investigations. Where are the limits of devices miniaturization? Is it possible to construct operational devices based on the control of single molecules or atoms? These questions are topics of current research.

In 1959, Richard Feynman, an American physicist, gave a famous lecture "*There is plenty of room at the bottom*".[1] This lecture postulated the principle of individual atoms manipulations. At that time, this proposal was visionary. Years after, in 1981, Gerd Karl Binnig and Heinrich Rohrer from Swiss department of IBM invented the scanning tunneling microscope (STM) with atomic resolution. This instrument, not only allowed to analyze samples with nanometric resolution but also to move single atoms. In 1989, Don Eigler made an IBM logo with 35 Xe atoms at a surface.[2,3] In 2012, again IBM researchers showed the cartoon "A Boy and His Atom" based on motion animation of 65 molecules of carbon monoxide on a copper substrate.[4]

At the same time biologists, interested in movements in biological systems, initiated research on biological machines within living organisms. Single molecules or clusters of molecules play a major role in dynamics of movement in complex biological systems. This domain, although well investigated today still remains in its infancy and requires further studies. Our understanding of complex biological systems at different length scale has increased dramatically as our experimental ability to observe nature has expanded from macro to molecular scale. Today, we see the mergence of biomimetic approaches based, *i.e.* bio-inspired design of devices and systems for solving technological problems in medicine and engineering.

## 2. Kinesin a walking protein

One of the most striking examples of the biological motors is kinesin. The latter is a protein based motor present in eukaryotic cells. This protein moves along cytoskeleton microtubules. Kinesin plays very important roles in cellular functions. In particular, as a cellular cargo responsible for transport of matter inside cells. The energy source required for kinesin motion is ATP (adenosine triphosphate). The structure of the kinesin family is variable with common features. But in general, kinesin-1 is a heterotetramer **(Fig. 1)**. It contains two motor subunits (called "heavy chains", green on the figure) and two "light chains" (blue in the figure). Heavy chains of the protein form two mobile heads. Through amino groups, the head is connected to a flexible linker "stalk" (grey part). The stalk includes a carboxy tail that binds to light chains of kinesin. The stalk forms a coiled-coil domain. Usually the cargo section is connected to the light chains (blue).

**Fig. 1** Representation of the structure of kinesin-1.

The protein head possesses two binding sites: one for the microtubule, the other for ATP. The ATP binding and hydrolysis with simultaneous release of ADP (adenosine diphosphate) lead to changes of the conformation of microtubule binding part and then to movement of the protein along the microtubule. **(Fig. 2)**. The direction of movement is controlled. Microtubules are polar in nature and kinesin heads are connected to microtubules with imposed orientation with ATP controlling the direction of each step. The two heads function as two legs. Two mechanisms have been suggested for the movement. The "Hand-over-hand" mechanism assumes that leading head changes in each step. The other mechanism "inchworm" postulates that one of the two heads leads and the second one follows. However, it has been established that the first mechanism prevales.[5]

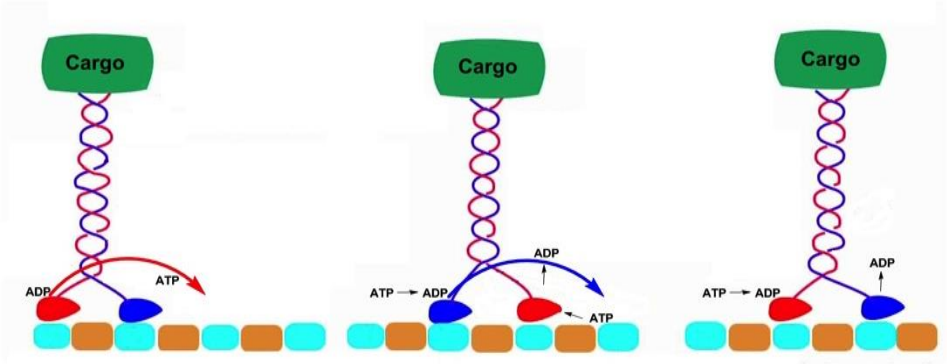


**Fig. 2** Principe of kinesin-1 "walking" along the cell microtubule.

Some examples of artificial systems with translational motion are described below.

## 3. Translatory motion

Rotaxanes are one of the well-known peculiar molecular architectures. The first prototype was described in 1967[6]. A typical rotaxane contains two parts: a dumbbell molecule and a macrocycle as the ring **(Fig. 3).** Two bulky groups (stoppers) are located at both ends of the dumbbell to prevent dissociation of the macrocycle. The first attempt was based on the reaction of two halves of the dumbbell and the macrocycle. However, more effective synthetic strategies were elaborated subsequently.[7] For [2]-rotaxanes, the dumbbell contains two interaction sites. Thus the macrocycle may be positioned at two possible stations. The interaction between the two parts may be insured by either coordination bonding[8] or by hydrogen bonding[9].

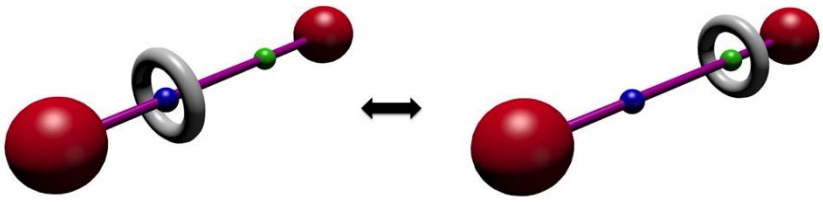

**Fig. 3** Translatory motion in [2]-rotaxane.

In such a system, the ring may be regarded as a shuttle travelling between two terminal stations. In the context of binary logic, this may be seen as "0" and "1" states. This concept was tested as a molecular electronic memory in 2007.[10]

The rotaxane design principle was extended to three component architectures. Examples of so-called "molecular elevators" were described **(Fig. 4)**.[11,12] The system was based on two "floors" based on amine and viologen moieties. The elevator was shown to move between the two floors based on basicity/acidity.

**Fig. 4** Translatory motion in a molecular elevator.

Rotaxanes are close to another class of molecular motors, namely catenanes, which undergo rotatory motion (**Fig. 6)**. The switching between these two classes of molecular motors was described.[13] Indeed, using anthracene based stoppers connected to the dumbbell, irradiation under UV light triggers their reaction leading thus to a catenane (**Fig. 5)**. Interestingly, irradiation using

another wavelength or heating breaks the bonds between anthracenes leading to the initial rotaxane. This process is reversible and can be repeated several times.

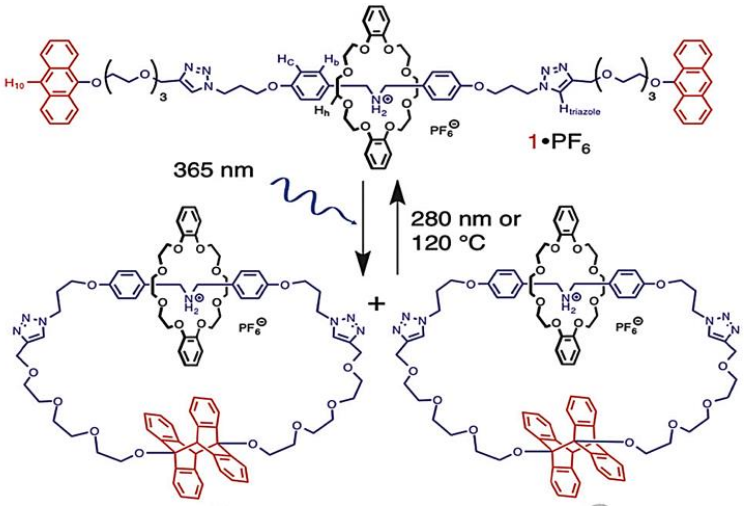


**Fig. 5** Rotaxane-catenane transformations.

## 4. Rotatory motion

Catenanes mentioned above, are described more precisely here after. In general, a catenane contains two similar interlocked parts. For [2]catenanes, the two parts are macrocyclic rings **(Fig. 6)**.

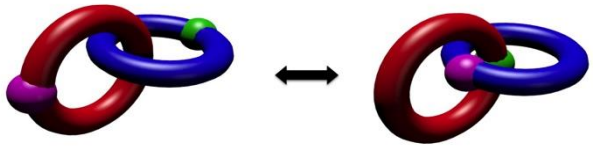

**Fig. 6** Rotary motion in a [2]catenane.

Principles used to control in motion are similar to those described for rotaxanes. For example, the process may be based on hydrogen bonding between the two rings **(Fig. 7)**.[14] The authors described a [2]catenane for which the movement can be induced by changing the polarity of the solvent. Thus, in halogenated solvent such as chloroform, the two rings of the catenane interact with each other by H-bonds. In DMSO, a polar solvent breaking H-bonds, a conformational change occurs. Indeed, the amide moieties of the two rings do not form H bonds with each other leading to the location of the hydrophobic alkyl chains in the center of the architecture.

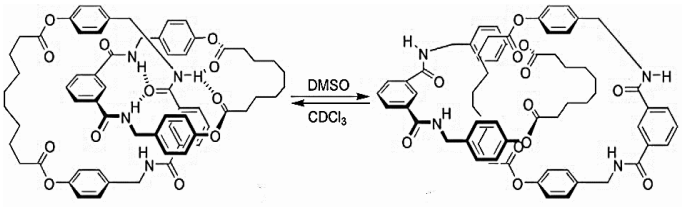


**Fig. 7** The [2]catenane motion based on hydrogen bonding.

A similar design based on coordination bonding was also described **(Fig. 8)**.[15–18] The interactions of phenanthroline coordinating sites with Cu(I) lead to formation of bonds between two rings. Removal of the metal cation induces a conformational change leading to the initial state of the catenane.

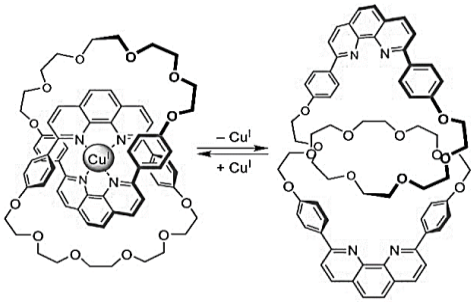


**Fig. 8** The [2]catenane motion based on copper (I)-ligand interactions.

The catenane rings may possess different sizes. Using a larger ring, more than one binding sites may be introduced (**Fig. 9)**. This type of system undergoes two dynamic processes: shuttle motion owing to its in rotaxane architecture and rotation within the catenane part. Switching between three different stations allows to achieve a controlled directional motion.[19] The directionality of the movement is based on differences in the binding affinities of stations A, B, C leading to selective coordination which induces unidirectional rotation of the smaller ring. Two fumaramide station A and B display different coordinative properties due to methylation of B. Furthermore A connected to the benzophenone unit allows photoisomerization of A at 350 nm before the station B (254 nm). Station C is photo inactive and its coordination propensity is between A and B. These features are responsible for the stepwise motion of the small ring in a sequential manner A → B → C.

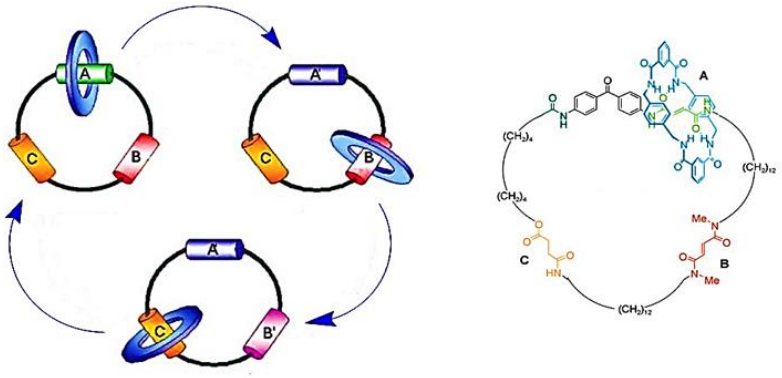


**Fig. 9** Unidirectional motion in [2]catenane.

Several other molecular rotors have been also reported. For example, metallocene based molecular rotors **(Fig. 10)** were described.[20] Both species (triptycene and metallocene) cannot rotate independently due to bulkiness of the two mobile parts which interact with each other like a gear. No precise mechanism for this mobile system was described.

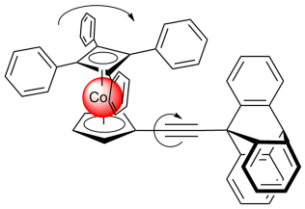


**Fig. 10** Molecular gear.

Subsequently, the triptycene fragment was equipped with a recognition site **(Fig. 11)**.[21] The system called "molecular brakes", undergoes free rotation of the two parts. For steric reasons, a conformational change is induced by the binding Hg(II) cation which locks the rotational movement.

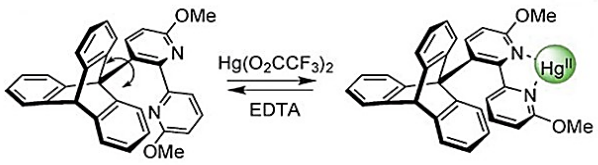


**Fig. 11** Molecular brakes: stopping the motion by coordination of mercury.

This system was further modified **(Fig. 12)** through the incorporation of coordinating sites on both fragments.[22,23] Since energetic and steric barriers are rather substantial, only an oscillation of the system is expected. Reaction with phosgene molecule leads to formation of isocyanate moiety. Owing to the close proximity of the hydroxy and isocyano groups, they react together. The system may be switched to the next position by thermal events. After hydrolysis of amide group, the final conformation of the machine is shifted by 120° when compared to the initial state.

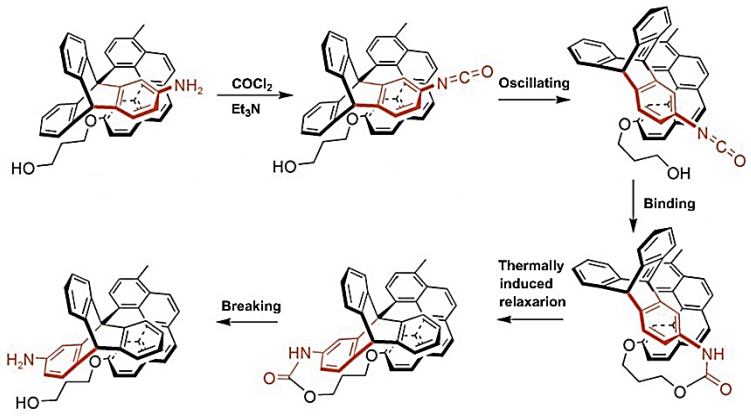


**Fig. 12** Unidirectional molecular oscillating rotor.

More recent examples describe "molecular robotic arm" **(Fig. 13)**.[24] The system is based on two interconnected units. The rotation of the two parts is induced by a double protonation process. The first protonation leads to disconnection of the pyridine moiety and isomerization of the system around the double bond. The second protonation leads to the disconnection of the quinoline unit and the rotation around the N-quinoline bond. Deprotonation affords a metastable isomer, which

slowly transforms into the initial state. Thus the pyridine fragment (red) may be considered as the arm that moves the cargo from one side of the machine to the other.

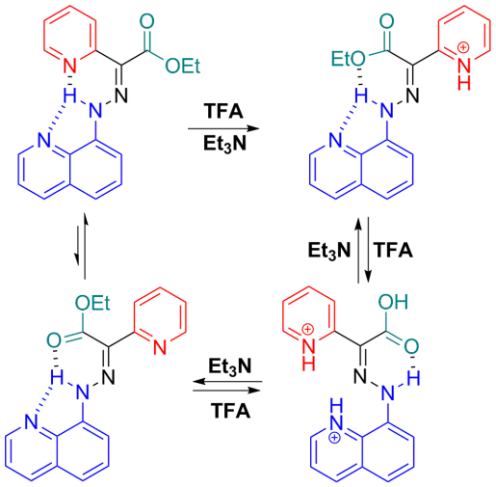


**Fig. 13** A hydrazone-based molecular switch.

Porphyrin-based compounds have been also widely applied as molecular machines. For example, Ce(IV) double-decker porphyrin based complexes undergo rotary motion which can be interrupted by binding with bidentate external molecules **(Fig. 14)**.[25,26] In replacement of dicarboxylic acids, several other stoppers were reported.[27–30]

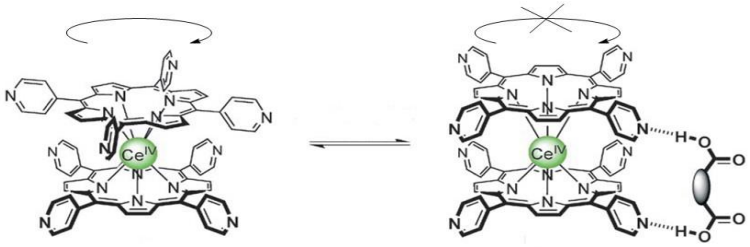

**Fig. 14** Double-deck porphyrin based molecular rotor.

A very inspiring porphyrin based caterpillar was synthesized by Harry Anderson's group (**Fig. 15)**.[31] For this rather elaborated system, motions of several movable parts was demonstrated by NMR exchange spectroscopy (EXSY). These experiments show that these complexes exhibit correlated motion for which the conrotatory rotation of the two template wheels is coupled to rotation of the nanoring track. In the case of the 10-porphyrin system, the correlated motion can be locked by binding palladium (II) dichloride between the two templates.

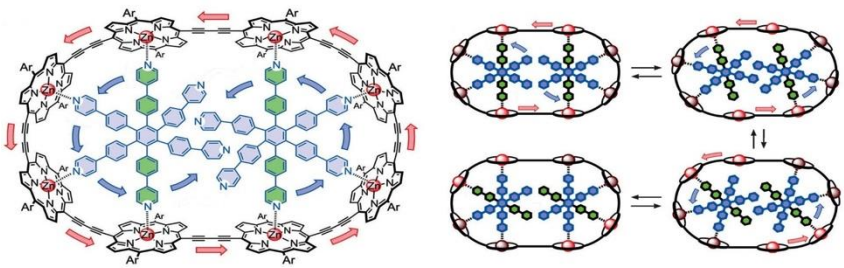

**Fig. 15** Supramolecular caterpillar.

## 5. Molecular devices on surfaces

Surface confined molecular motion is a topic of interest. Several examples of molecular rotors deposited different substrates have been described.

Metallocene based fluorinated and non fluorinated rotors equipped with thioether moieties as "legs" was reported.[32] The rotors **(Fig. 16)** was adsorbed on gold surface. According to NMR data in solution, almost no barrier for the rotation process is detected for the polar fluorinated rotor solution. The surface deposited samples were investigated by X-ray photoelectron microscopy, STM and grazing incident IR microscopy. Only for the polar fluorinated rotor, the electric field of STM tip induces the rotation of the system on the surface.

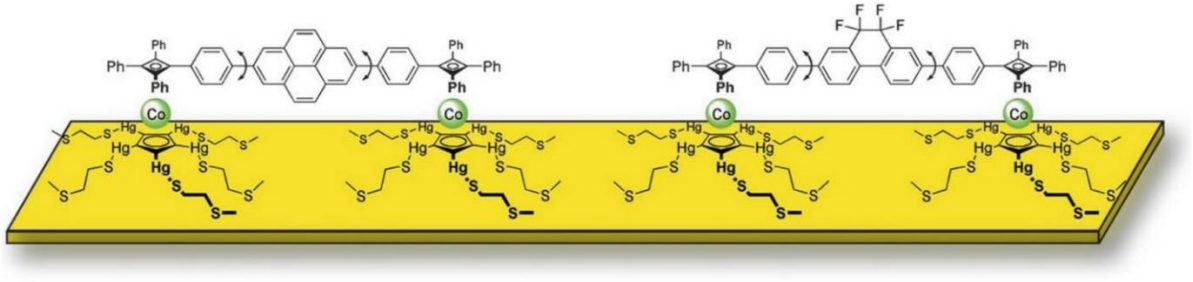

**Fig. 16** Nonpolar and polar surface deposited molecular motors.

Another molecular rotor was reported by Jian and Tour **(Fig. 17)**.[33] Four caltrop-shaped molecules that might be useful as surface-bound electric field-driven molecular motors have been synthesized. The caltrops are based on a pair of electron donor-acceptor arms and a tripod base. A monolayer of such compound deposited on golden substrate was generated. The movement of the zwitterionic molecular arms was induced by electric fields applied around the caltrops.

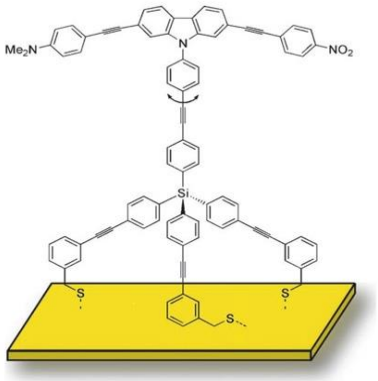

**Fig. 17** Dipolar rotor designed to be attached to gold surfaces.

Another organometallic molecular rotor designed to be deposited on surface was synthesized.[34,35] Due to five ferrocene groups at the ends of propeller blades, the system is expected to be electroactive (**Fig. 18)**. The stator (red) was placed on a platinum grid. It was placed between an anode and a cathode. The proposed mechanism implies selective oxidation of one of the ferrocene units and the repulsion of the resulting cation by the anode. Upon rotation, the oxidized ferrocene unit is replaced by the second which is oxidized in its turn. However, it was not clearly

demonstrated that the conductivity observed was due to the rotation of the molecule since a direct tunneling from cathode to anode could also take place.

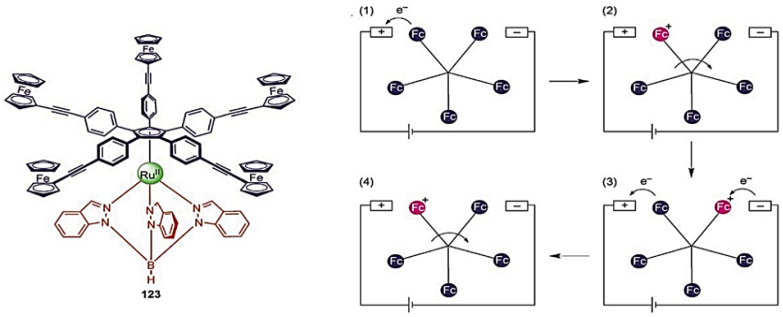

**Fig. 18** Ferrocene molecular rotor and proposed mechanism for its rotation.

Other similar systems have been also investigated (**Fig. 19)**.[36,37] Direct tunneling electron transfer from STM tip to ferrocene (position 2) and empty hands (position 1) of the rotor induced anticlockwise and clockwise rotation respectively. This behaviour was explained by modeling of different excited electronic states. It was determined that tunneling through different arms involves different electronic states with opposite potential landscapes that lead to different directions of rotation.

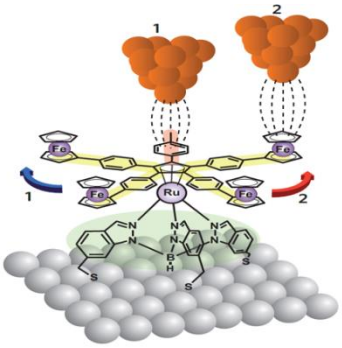

**Fig. 19** Direct STM control of the directional motion of an unsymmetrical ferrocene based rotor.

A very important step in development of molecular machines is the shift to materials (from solution to the solid state). Unidirectional rotating devices **(Fig. 20)** and liquid crystals films were reported by Feringa et al.[38–40]

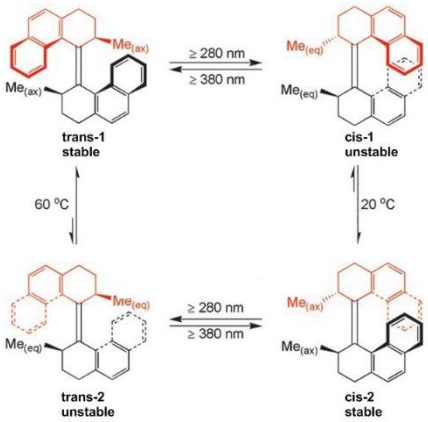


**Fig. 20** Operation of an unidirectional molecular rotor.

The rotor in trans-1 conformation is transforms into its cis-1 conformation under irradiation (λ >280 nm). This form is not stable at temperatures above -55 $^{o}$C because methyl substituents are in unfavorable equatorial positions. This isomer relaxes to cis-2 stable form by helix inversion around double bond. Thus anticlockwise rotation further continues. Irradiation leads to the formation of trans-2 isomer. Methyl groups are again in energetically unfavorable positions. Heating to ~60 $^{o}$C leads to 360$^{o}$ rotation of the upper part of the molecule upon reaching the initial trans-1 isomer. Since each turn of the system induces a change in the helicity, all conformations can be monitored by CD spectroscopy. This unique molecular rotor was incorporated in liquid crystal films.[40] Three isomers of the rotor can be isolated at room temperature. A liquid-crystalline film doped with the trans-1 conformer gave a right-handed cholesteric violet phase (**Fig. 21)**. UV irradiation at room temperature switches the trans-1 conformer to the cis-1 isomer. Further irradiation leads to the trans-2 isomer with a left-handed helical twist. This process is observed directly by the film's color change from violet to red. Heating of the film affords the initial violet color due to relaxation to the trans-1 molecule.

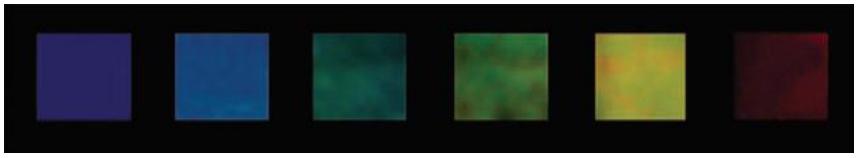

**Fig. 21** Color changing of liquid crystalline film containing the unidirectional molecular rotor.

There are many other examples of molecular machines controlled by different external and internal factors. Among them, considerable interest has been focused over the last years on molecular "turnstiles". In particular, during the last decade, several studies have been reported on molecular turnstiles based on porphyrin backbones. The main topic of this PhD thesis was to develop approaches towards new turnstiles based on phosphorus (V) porphyrin derivatives. The state of art and detailed investigations of this topic are described in the following chapters.

**Conclusion**

Although abiotic molecular dynamic systems are still much less sophisticated and complex than biological motors, however, combinations of molecular design, synthetic procedures and theoretical calculations should allow to increase the sophistication of synthetic molecular devices and their use in a variety of applications such as molecular computing, catalysis, sensors, transport of matter etc.

## 6. References


1 R. P. Feynman, *Eng. Sci.*, 1960, **23**, 22–36.

2 C. Toumey, *Nat. Nanotechnol.*, 2007, **2**, 9–10.

3 D. M. Eigler and E. K. Schweizer, *Nature*, 1990, **344**, 524–526.

4 A. Heinrich, C. Lutz, S. Baumann and I. Rau, *http://www.research.ibm.com/articles/madewithatoms.shtml*, 2012.

5 R. D. Vale and R. A. Milligan, *Science*, 2000, **288**, 88–95.

6 I. T. Harrison and S. Harrison, *J. Am. Chem. Soc.*, 1967, **89**, 5723–5724.

7 C. A. Schalley, K. Beizai and F. Vögtle, *Acc. Chem. Res.*, 2001, **34**, 465–476.

8 J.-P. Sauvage, *Acc. Chem. Res.*, 1998, **31**, 611–619.

9 P. R. Ashton, R. Ballardini, V. Balzani, I. Baxter, A. Credi, M. C. T. Fyfe, M. T. Gandolfi, M. Gómez-López, M. V. Martínez-Díaz, A. Piersanti, N. Spencer, J. Fraser Stoddart, M. Venturi, A. J. P. White and D. J. Williams, *J. Am. Chem. Soc.*, 1998, **120**, 11932–11942.

10 J. E. Green, J. Wook Choi, A. Boukai, Y. Bunimovich, E. Johnston-Halperin, E. DeIonno, Y. Luo, B. A. Sheriff, K. Xu, Y. Shik Shin, H.-R. Tseng, J. F. Stoddart and J. R. Heath, *Nature*, 2007, **445**, 414–417.

11 J. D. Badjic, V. Balzani, A. Credi, S. Silvi and J. Fraser Stoddart, *Science*, 2004, **303**, 1845–1849.

12 J. D. Badjic, M. Ronconi, J. F. Stoddart, V. Balzani, S. Silvi, A. Credi, *J. Am. Chem. Soc.*, 2006, **99**, 1489–1499.

13 A. Tron, H.-P. Jacquot de Rouville, A. Ducrot, J. H. R. Tucker, M. Baroncini, A. Credi and N. D. McClenaghan, *Chem. Commun.*, 2015, **51**, 2810–2813.

14 D. A. Leigh, K. Moody, J. P. Smart, K. J. Watson and A. M. Z. Slawin, *Angew. Chem. Int. Ed.*, 1996, **35**, 306–310.

15 J. Sauvage and J. Kern, *J. Am. Chem. Soc.*, 1984, **106**, 3045–3046.

16 M. Cesario, C. O. Dietrich, A. Edel, J. Guilhem, J. P. Kintzinger, C. Pascard and J. P. Sauvage, *J. Am. Chem. Soc.*, 1986, **108**, 6250–6262.

17 B. Mohr, M. Weck, J.-P. Sauvage and R. H. Grubbs, *Angew. Chem. Int. Ed. Engl.*, 1997, **36**, 1308–1310.

18 M. Koizumi, C. Dietrich-Buchecker and J.-P. Sauvage, *European J. Org. Chem.*, 2004, **2004**, 770–775.

19 D. A. Leigh, J. K. Y. Wong, F. Dehez and F. Zerbetto, *Nature*, 2003, **424**, 174–179.

20 A. M. Stevens and C. J. Richards, *Tetrahedron Lett.*, 1997, **38**, 7805–7808.

21 T. R. Kelly, *Acc. Chem. Res.*, 2001, **34**, 514–522.

22 T. Ross Kelly, R. a. Silva, H. De Silva, S. Jasmin and Y. Zhao, *J. Am. Chem. Soc.*, 2000,

**122**, 6935–6949.

23 T. R. Kelly, H. De Silva and R. a Silva, *Nature*, 1999, **401**, 150–152.

24 I. Aprahamian, *Nat. Chem.*, 2015, published online 21 December.

25 M. Takeuchi, T. Imada and S. Shinkai, *Angew. Chemie Int. Ed.*, 1998, **37**, 2096–2099.

26 A. Sugasaki, M. Ikeda, M. Takeuchi, A. Robertson and S. Shinkai, *J. Chem. Soc. Perkin Trans. 1*, 1999, **1**, 3259–3264.

27 A. Sugasaki, K. Sugiyasu, M. Ikeda, M. Takeuchi and S. Shinkai, *J. Am. Chem. Soc.*, 2001, **123**, 10239–10244.

28 A. Sugasaki, M. Ikeda, M. Takeuchi and S. Shinkai, *Angew. Chemie Int. Ed.*, 2000, **39**, 3839–3842.

29 M. Ikeda, T. Tanida, M. Takeuchi and S. Shinkai, *Org. Lett.*, 2000, **2**, 1803–1805.

30 A. Robertson, M. Ikeda, M. Takeuchi and S. Shinkai, *Bull. Chem. Soc. Jpn.*, 2001, **74**, 883–888.

31 S. Liu, D. V. Kondratuk, S. A. L. Rousseaux, G. Gil-Ramírez, M. C. O'Sullivan, J. Cremers, T. D. W. Claridge and H. L. Anderson, *Angew. Chemie Int. Ed.*, 2015, **54**, 5355–5359.

32 X. Zheng, M. E. Mulcahy, D. Horinek, F. Galeotti, T. F. Magnera and J. Michl, *J. Am. Chem. Soc.*, 2004, **126**, 4540–4542.

33 H. Jian and J. M. Tour, *J. Org. Chem.*, 2003, **68**, 5091–5103.

34 A. Carella, G. Rapenne and J.-P. Launay, *New J. Chem.*, 2005, **29**, 288–290.

35 G. Rapenne, *Org. Biomol. Chem.*, 2005, **3**, 1165–1169.

36 K. Ernst, *Nat. Nanotechnol.*, 2013, **8**, 7–8.

37 U. G. E. Perera, F. Ample, H. Kersell, Y. Zhang, G. Vives, J. Echeverria, M. Grisolia, G. Rapenne, C. Joachim and S.-W. Hla, *Nat. Nanotechnol.*, 2012, **8**, 46–51.

38 B. L. Feringa, *Acc. Chem. Res.*, 2001, **34**, 504–513.

39 N. Koumura, R. W. Zijlstra, R. a van Delden, N. Harada and B. L. Feringa, *Nature*, 1999, **401**, 152–155.

40 R. A. Van Delden, N. Koumura, N. Harada and B. L. Feringa, *Proc. Natl. Acad. Sci. U. S. A.*, 2002, **99**, 4945–4949.

# Chapter I. Molecular Turnstiles Based on Phosphorus (V) Porphyrins

# Contents


**1. Introduction 21**

**1.1 The general idea on multiple station molecular turnstiles 21**

**1.2 Non-porphyrin turnstiles 22**
**1.2.1 Organometallic Pt(II) turnstiles 23**
**1.2.2 Organic turnstiles 26**

**1.3 Porphyrin-based turnstiles 27**
**1.3.1 Strapped porphyrin based turnstiles 27**
**1.3.2 Sn-based turnstiles 28**

**2. Model turnstile based on P(V) tetraphenylporphyrin 31**

**2.1 Synthesis of phosphorus tetraphenylporphyrins 32**
**2.1.1 Insertion of the phosphorus (V) into the porphyrin cavity 32**
**2.1.2 Substitution of the axial ligands 34**

**2.2 Synthesis of the handle#1 39**

**2.3 Synthesis of the turnstile with handle#1 40**
**2.3.1 Application of standard method 40**
**2.3.2 Microwave synthesis 41**

**3. Synthesis of the single station turnstile 43**

**3.1 Synthesis of P(V) meso-pyridylporphyrins 43**
**3.1.1 Insertion of the phosphorus atom into the pyridyl-containing porphyrin 43**
**3.1.2 Axial ligands exchange 45**

**3.2 X-ray diffraction data of phosphorus (V) MPyP complexes 46**

**3.3 Approaches toward the turnstile#1 49**

**3.4 Synthesis of the handle#2 51**

**3.5 Synthesis of the handle #2 based turnstiles 51**
**3.5.1 Synthesis of the model turnstile#2 51**
**3.5.2 Synthesis of the turnstile#2 54**
**3.5.3 Turnstile #1 synthesis through Br-derivative 55**

**4. Dynamic behaviour of the molecular turnstile#1 59**

**4.1 Use of silver triflate 59**
**4.1.1 1D NMR investigations 59**
**4.1.2 Analysis by Mass-spectrometry 61**
**4.1.3 2-D NMR investigation 61**
**4.1.4 Reversibility of the dynamic closing/opening process 63**

**4.2 The turnstile in the presence of triflic acid 64**
**4.2.1 1-D NMR investigations 64**
**4.2.2 2-D NMR investigations 67**
**4.2.3 Reversibility of the locking/unlocking process 68**

**4.3 Competition between $Ag^+$ and $H^+$ as closing agents** **69**

**5. Conclusion of the chapter** **70**

**6. References** **72**

# 1. Introduction

## 1.1 The general idea on multiple station molecular turnstiles

During the last decade, our group has focused on the control of intramolecular movements. We have mainly studied a special class of dynamic molecular devices called "molecular turnstiles".[1–16] These mobile systems may be described as a molecule composed of interconnected rotating two parts with respect to each other. In **Fig. 1.1.** a schematic representation is given.

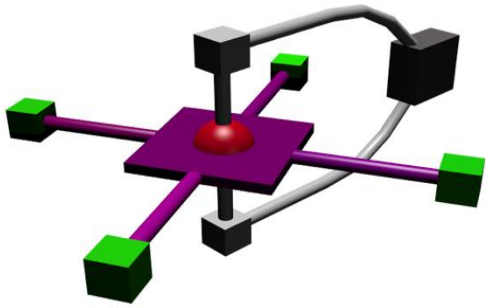

**Fig. 1.1** Schematic representation of a turnstile bearing four static and one mobile stations.

The grey part, so-called the "handle", contains one recognition site (mobile station) (dark grey box in **Fig. 1.1**). The central purple part acts as the "stator". It contains variable number of static stations (green parts in **Fig. 1.1**). Both types of stations may take part in interactions with effectors or external stimuli. The connection between the handle and the stator is achieved through using a "hinge" (red sphere in the center of the stator).

The handle either freely rotates around the stator (open state, **Fig. 1.2**) or may be blocked (close state) by simultaneous interaction between one of the static stations and the dynamic station through an effector using molecular recognition events.

The recognition processes between the two parts and the effector may be based on different type of intermolecular interactions such as electrostatic interactions, coordination bonds or H-bonds.

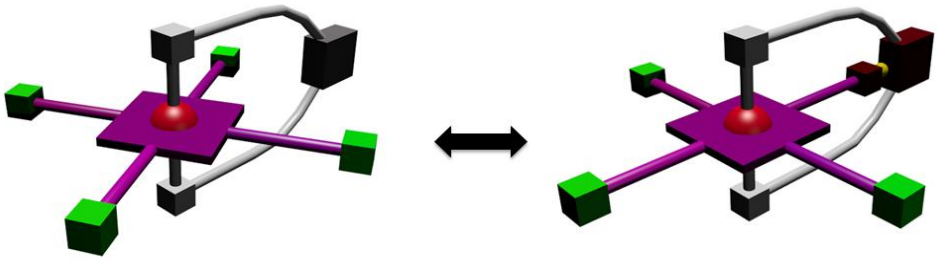

**Fig. 1.2** Schematic representation of the open and the close states of the turnstile.

By introducing at least three different stations in the periphery of the stator, one may control the direction of rotation through appropriate choices of interaction sites and their relative localisations on the stator. The design proposed above may be based on different propensities of

different stations to bind a metal and/or a proton. For example, if dealing with a handle bearing a pyridine moiety, one may introduce sequentially a 2,6-lutidine, a pyridine and a benzonitrile units on the stator. In the presence of a metal cation as the effector, the first locked state may be generated through its binding to lutidine possessing the highest affinity for the metallic centre. Then a decrease of pH should lead to gradual protonation of the different stations from the more basic (lutidine) to the less basic one (benzonitrile) and thus the movement of the handle (**Fig. 1.3)**. Obviously, one must take into account the stability of the "hinge" at different pH, in particular in acidic media.

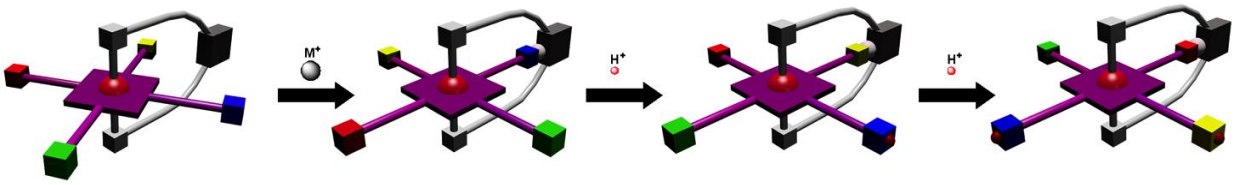


**Fig. 1.3** The motion control of the system with three coordination sites (blue – lutidine, yellow – pyridine, red – benzonitrile) by selective binding and protonation.

Moreover, these processes being achieved in solution, the equilibrium constants involved in the different process should be high enough in order to avoid the formation of mixtures of close and open states. In order to shift the equilibrium, one may use non-coordinating and apolar solvents or/and low temperature.

During this work, our aim was to synthetize a 4 stations molecular turnstile based on P(V) *meso*-substituted porphyrins. The handle would be connected to the porphyrin stator through the axial positions of the P(V) atom located in the cavity of the porphyrin and acting as the "hinge". In order to study the stability of the system under acidic conditions, we have studied first an analogue, a porphyrin bearing only one station at the *meso* position.

NMR techniques are perfectly suited for studying the behaviour of turnstile in solutions, namely, the open and the close states. Indeed, during the movement process, we should observe a change in symmetry together with shifts of resonance of specific protons of the handle. In addition, 2D NMR techniques should reveal specific correlations between protons of the handle and of the porphyrin due to their near proximity in the close state.

The molecular turnstiles previously obtained in the laboratory are described in the following parts divided in two different categories depending on the nature of the stator.

## 1.2 Non-porphyrin turnstiles

A series of turnstiles with two coordinating sites was synthesized and described few years ago[10,11,13–16]. The design principles are represented in **Fig. 1.4.**

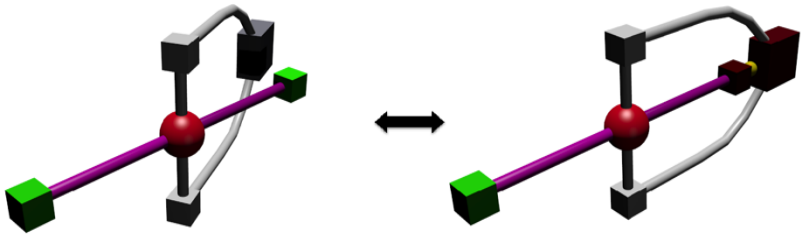

**Fig. 1.4** Schematic representation of the open and the close states of the non-porphyrin based turnstile.

In the absence of any external stimulus, the handle freely rotates around the stator. In the presence of the metal ion, the rotation is blocked and the turnstile is in its closed state. Two alternative handles combined with two types of stator were elaborated.

### 1.2.1 Organometallic Pt(II) turnstiles

The systems with a pyridyl unit as coordinating site within the handle were synthesized **(Fig. 1.5)**.[10,11,16] Two of them (**A** and **B**) are symmetrical whereas the turnstile **C** is unsymmetrical.

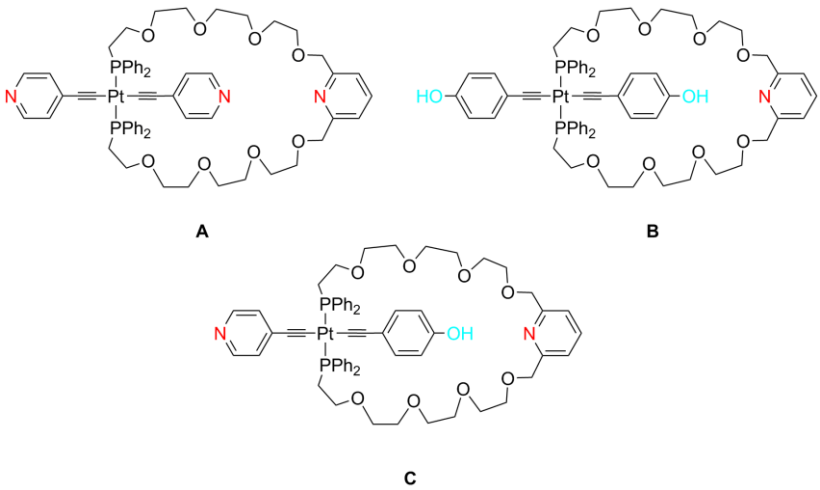


**Fig. 1.5** Organometallic turnstiles equipped with a handle bearing a pyridyl unit

The Pt(II) turnstile **A** was combined with silver cations. In the presence of the $AgSbF_6$, it forms a 1:1 complex **(Fig. 1.6)**. At room temperature, both pyridyl groups of stator were found to be equivalent according to $^1$H-NMR investigations. Owing to the presence of two ethynylpyridine moieties on the rotor, at room temperature, the turnstile oscillates between two closed states through rotation around the P–Pt–P axis. Cooling of the system to -70 $^{\circ}$C locks the oscillatory movement. The reversibility of the opening and closing process was studied in solution using $^1$H- and $^{31}$P-NMR. At RT, the addition of $Et_4NBr$ to a solution of **A**–$Ag^+$ caused the precipitation of AgBr which was filtered leaving thus the turnstile **A** in its open state. The process can be repeated several times.[11]

The turnstile **B** even in the absence of any external effector is in its locked state owing to the formation of a weak hydrogen bond between the phenol and the pyridyl moieties. Again, the

turnstile oscillates between two close states owing to the presence of two phenol units. All attempts to distinguish between the two different phenols at low temperature were unsuccessful. However, ROESY NMR demonstrated the formation of a closed state even at room temperature.[16]

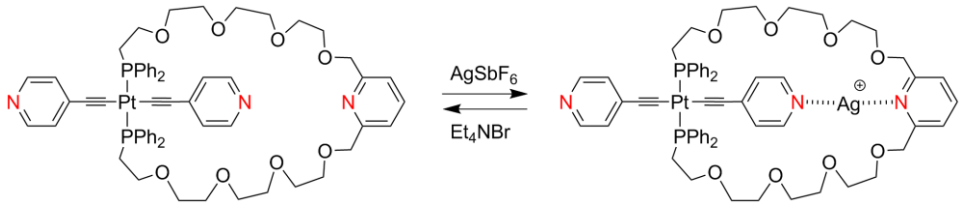


**Fig. 1.6** Close and open states of the organometallic turnstile **A.**

The unsymmetrical turnstile **C** shows an interesting behaviour in the solution. In the absence of effector, it first forms a closed state by hydrogen bonding between the phenol moiety of the stator and the pyridyl unit of the handle. The presence of $Ag^{+}$ cation in the solution leads to the second closed state **(Fig. 1.7)**.[16]

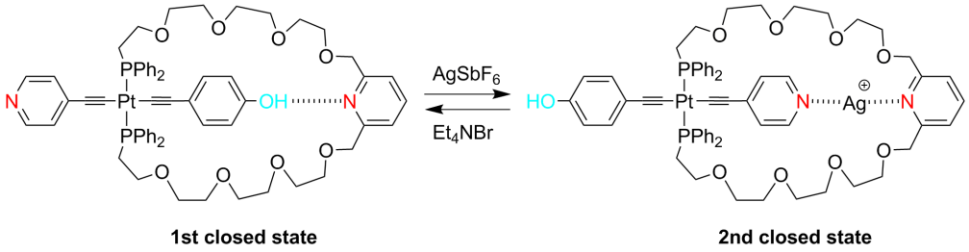


**Fig. 1.7** Switching between two states of the organometallic turnstile **C.**

Both states were identified at room temperature by NMR techniques. Switching between different states was achieved. However, the system bearing only two interaction sites, it is impossible to impose the direction of the rotation.

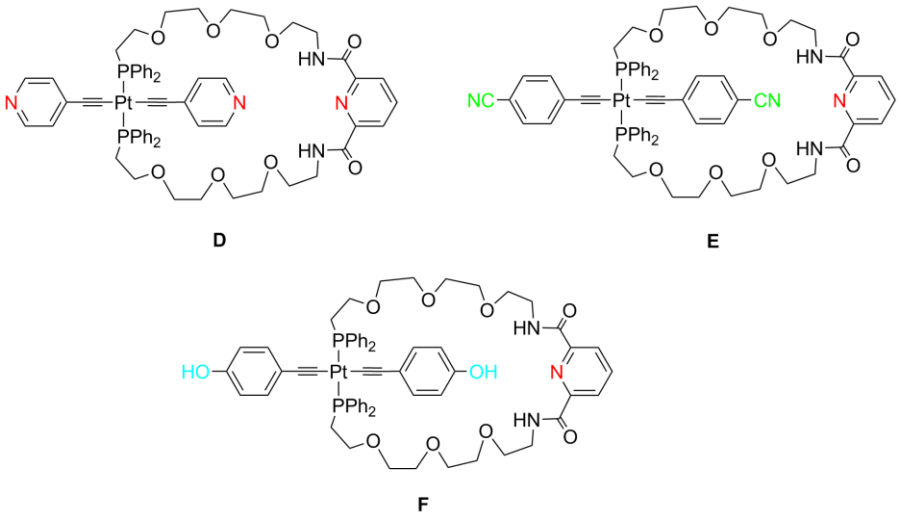


**Fig. 1.8** Organometallic turnstiles equipped with a pyridine-amide type handle.

In addition to the above mentioned turnstiles, another series based on a different handle was reported.[10,15] Instead of a pyridyl as coordinating site, an amide moiety is used **(Fig. 1.8)**. This

substitution leads to an increase in the handle denticity from one to three. This design requires the use of metal ions with coordination number 4 (1 for the stator and 3 for the handle). Instead of Ag(I) cation, Pd(II) was used as the locking agent.

The turnstile **D**, similar to **A** was successfully closed with $Pd(AcO)_2$ **(Fig. 1.9)**.

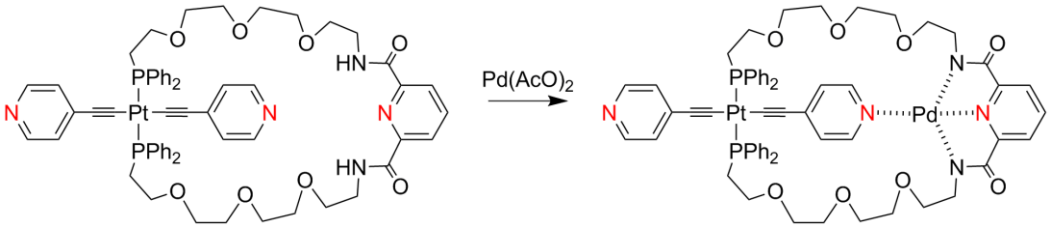


**Fig. 1.9** Open and closed states of the organometallic turnstile **D**.

In comparison with turnstile **A**, no oscillation between two pyridyl units was observed. Indeed, even at room temperature, two different sets of signals have been observed for the two pyridyl units of the stator. It should be noted that in the solid state in the absence of Pd(II) the turnstile is in its closed state owing to the formation of hydrogen bonds between the pyridyl moiety of the stator and the H atoms of the amide unit of handle[10].

The turnstile **E**, for which the pyridyl coordinating sites were replaced by benzonitrile groups, was also reported.[15] The benzonitrile unit possesses weaker binding propensity than pyridyl group. As expected, this indeed facilitated the opening process. Again, the turnstile was successfully closed using $Pd(AcO)_2$ **(Fig. 1.10)**.

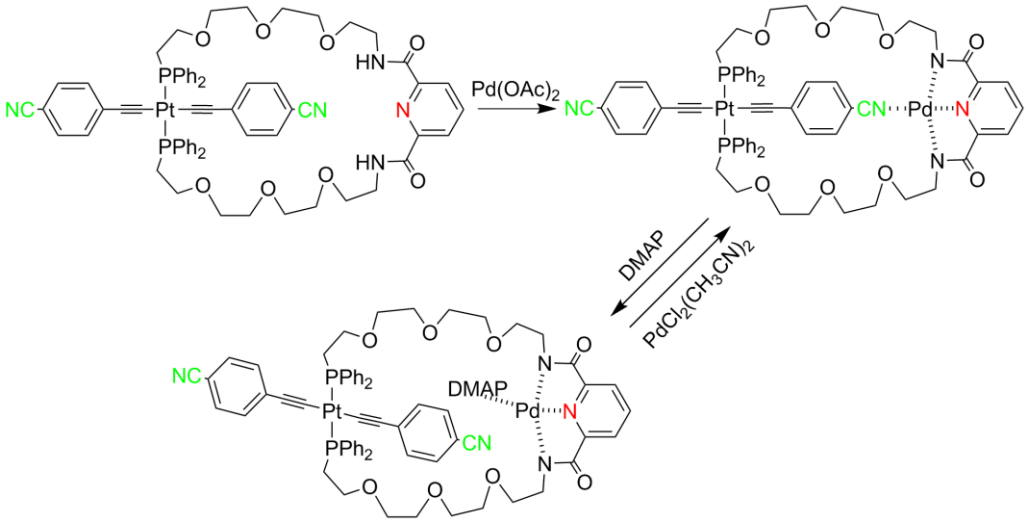


**Fig. 1.10** Open and closed states of the organometallic turnstile **E** and its reversible opening.

At room temperature, the turnstile **E** forms a stable 1:1 complex with Pd(II). No oscillation between the two benzonitrile moieties was observed. For the reopening of the system, DMAP (*para*-DimethylAminoPyridine) was used. DMAP, binding more strongly Pd(II) than benzonitrile,

leads thus to another open state of the turnstile. Further addition of $PdCl_2(CH_3CN)_2$ leads to the closed state. Several cycles could be achieved.

Another possibility fro the reopening of the turnstile **E** was investigated **(Fig. 1.11)**. Addition of a strong acid such as methanesulfonic acid, upon protonation of DMAP leads to its decoordination and the turnstile returns back to its closed state upon recoordination of the benzonitrile units. Addition of a strong base (triethylamine for example) leads to the deprotonates of DMAP in the solution and recoordination to Pd(II) and generation of the open state of the turnstile.[15]

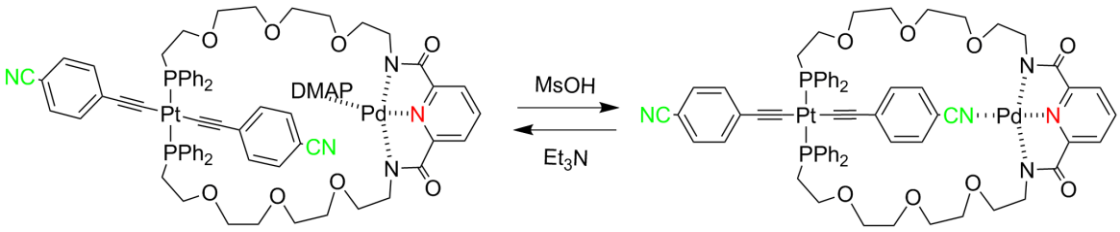


**Fig. 1.11** Acid-base opening and closing of the organometallic turnstile **E**.

The turnstile **F** with two phenols attached to the stator was also investigated. In solution, the hydroxy group of phenol occurs in fast exchange with water (which always exists in solvents). Thus, no closed state was observed. Attempts to deprotonate the phenol moiety afforded partial decomposition of the turnstile.[10]

### 1.2.2 Organic turnstiles

A series of turnstiles mainly organic in nature was also synthesized **(Fig. 1.12)**.[10,13,14] An amide based handle was used. All turnstiles **G-K** have been closed using Pd(II) as locking agent as described above for turnstiles **D, E**.[10] Again, both closed and open states were investigated by multidimensional NMR techniques which revealed the reversibility of the opening and closing processes for turnstiles **I** and **J**.[13,14] Interestingly, as expected from the design of turnstiles **I** and **J,** different luminescence properties have been observed for their open and closed states. Whereas the open state is strongly luminescent, for the closed state, the emission is quenched by the presence of Pd(II) leading to an optical reading of the two states. Thus, it was demonstrated that the dynamics of the turnstile can be monitored either by NMR or by luminescence techniques.

The major advantage of non-porphyrin based turnstiles described above is their simplicity and high yields of synthesis. However, by principle, for the turnstiles mentioned above only a maximum of two interaction sites may be introduced. This implies that with such design principles, the directionality of the movement, which requires at least three different sites, can not be controlled.

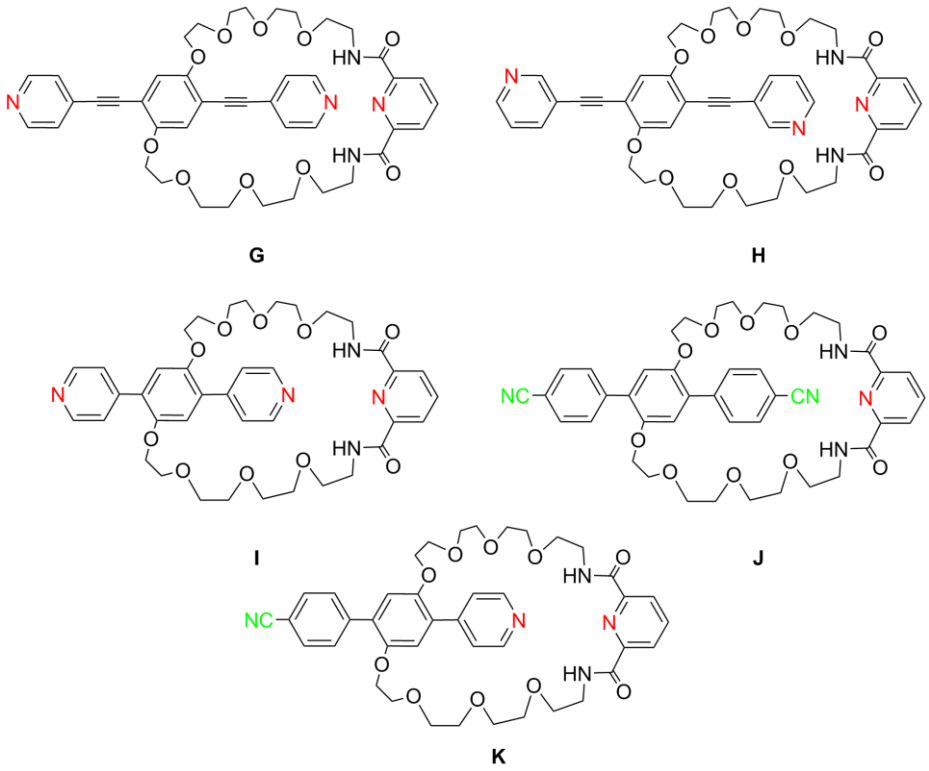


**Fig. 1.12** Organic turnstiles **G-K**.

### 1.3 Porphyrin-based turnstiles

In the laboratory, several studies dealing with molecular turnstiles based on porphyrins have been undertaken over the last decade. As stated above, for Pt(II) as well as for organic systems reported, the turnstile may be equipped only with two stations. In contrast, for porphyrin based turnstiles, one may introduce up to four stations using the *meso* positions.

Porphyrin based turnstiles synthesized in the group may be separated into two groups: strapped porphyrin and Sn(IV) porphyrin based systems.

#### 1.3.1 Strapped porphyrin based turnstiles

The schematic principle of the turnstile is represented in **Fig. 1.13**. The purple part represents the porphyrin backbone, the handle (in grey) is connected to the porphyrin *via* the *meso* positions of two trans *meso*-substituents. Several related systems were investigated **(Fig. 1.14)**.[4,9,12]

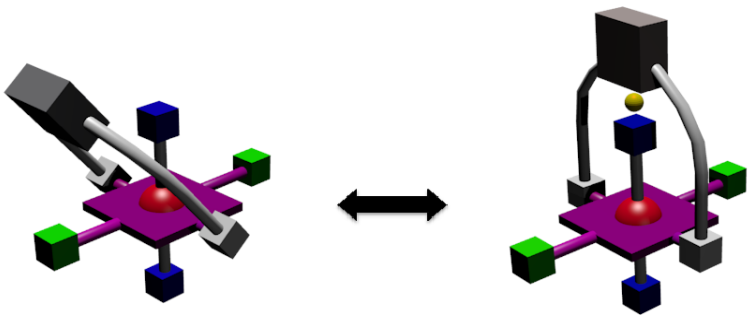

**Fig. 1.13** Schematic representation of strapped porphyrin turnstiles.

Depending on the metal cations located within the cavity of the porphyrin, the turnstiles may contain up to 4 stations. Indeed, the pyridyl moiety of the handle may interact with two *meso* substituents (Ph-X and Ph-Y) for M= 2H or Pd(II), while the presence of ligands in the apical position of Zn(II) and Sn(IV) leads to one or two additional stations respectively.

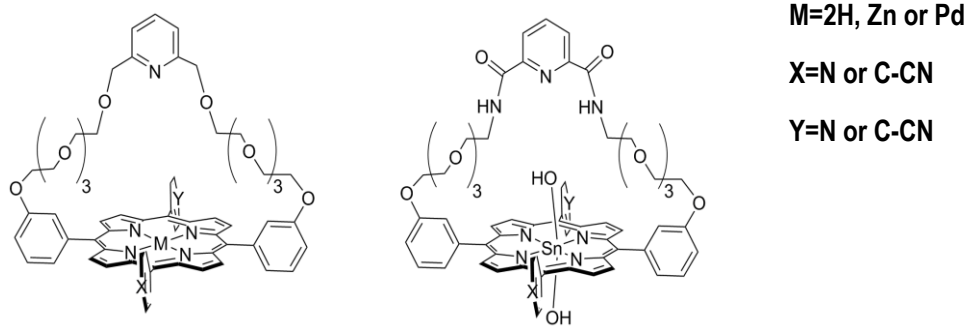


**Fig. 1.14** Strapped porphyrin turnstiles.

Due to the structure of the strapped porphyrin based turnstiles (connection of the handle to the stator at *meso*-positions), full rotation may be expected depending on the length of the spacers used to connect the handle to the porphyrin. Hence, one of the two opposite axial sites may be involved in the interactions with the free or metallated handle.

### 1.3.2 Sn-based turnstiles

The most interesting results have been obtained with Sn(IV) porphyrin based turnstiles. In the latter case, the handle is connected to the stator *via* two axial positions of the octahedron around Sn(IV) cation.

The first Sn(IV) based turnstile synthetized in our laboratory (**Fig. 1.15**)[1–3] was composed of a *meso*-monopyridylporphyrin as the stator (**A**$_P$).

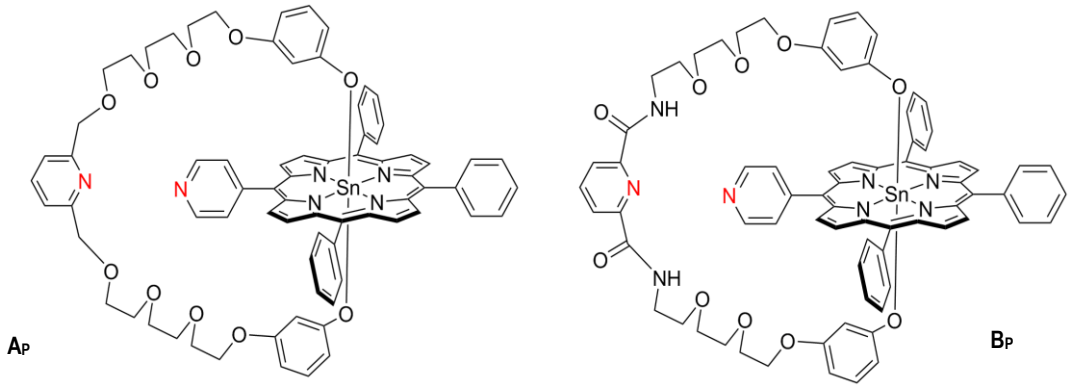


**Fig. 1.15** Sn(IV) porphyrin based turnstiles.

The handle, containing pyridyl moiety is connected to the porphyrin *via* the two axial position of the octahedron around the Sn(IV) center acting as a hinge. A similar system, **B**$_P$, bearing two amide linkers within the handle has also been reported **(Fig. 1.15)**.[6] The molecule **A**$_P$ can be viewed as a molecular gate. In its open state, the handle is free to rotate around the porphyrin. The addition

of $Ag^+$ leads to the closed state through the coordination of the metal cations by the two pyridyl coordinating units **(Fig. 1.16)**.

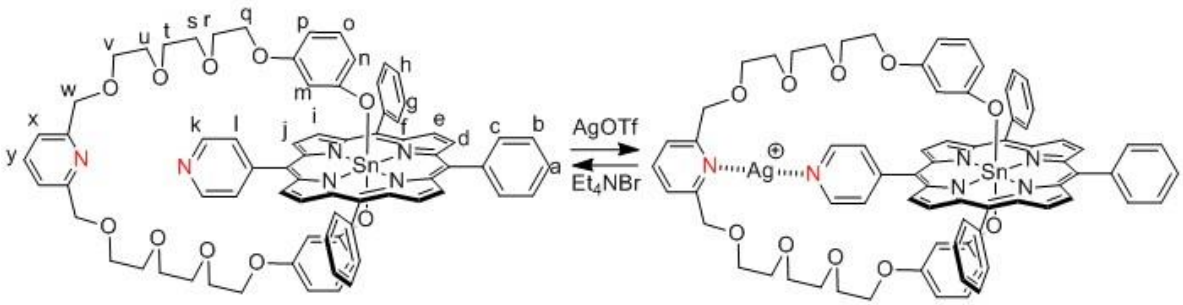


**Fig. 1.16** Open and closed states of a Sn(IV) porphyrin based turnstile $\mathbf{A_P}$.

Both the open and closed states were characterized by $^1$H-NMR and by mass spectrometry. The absence of rotation at room temperature was confirmed by ROESY NMR techniques which showed specific correlations between hydrogen atoms of the porphyrin and some of the handle **(Fig. 1.17)**. These correlations are not observed for the open state of the turnstile.

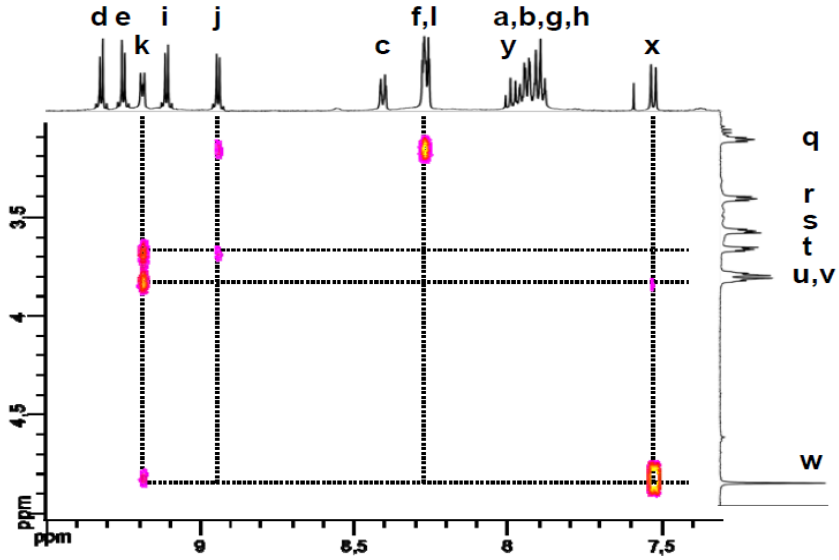


**Fig. 1.17** Portions of the ROESY NMR map for $\mathbf{A_P}$ closed state.

The addition of an excess of silver ion in solution did not lead to further changes. The stability constant was calculated to be logK = 3.75 in $CH_3CN$.

The addition of $Et_4NBr$ leads to the reopening of the system and to the precipitation of AgBr **(Fig. 1.16)**. Several close-open cycles of the system were performed without any decomposition. The turnstile was found to be stable under the conditions used.

Concerning the molecular turnstile $\mathbf{B_P}$, the addition of Pd(II) leads to the formation of the closed state while the reopening could be performed by adding an excess of $CN^-$ anion or DMAP.[6] The next step was to extend the principle to turnstiles offering two stations. This was achieved using *trans*-$A_2B_2$ Sn(IV) porphyrins as stators **(Fig. 1.18)**.[4,5,7,8] Four new systems have been obtained.

They differ by the presence of the amide linkages in the handle (**$D_P$ – $F_P$**) when compared to **$C_P$** and by the nature of the stations at the *meso* positions: pyridyl, methoxyphenyl and benzonitrile.

Similarly to **$A_P$**, the turnstile **$C_P$** is locked in the presence of $Ag^+$ cation. However, at room temperature an oscillation between the two equivalent *meso*-pyridyl units was observed.[8]The closing of the turnstile at a single station was reached at -70 °C. The close-open processes were again achieved by precipitation of AgBr from the solution.

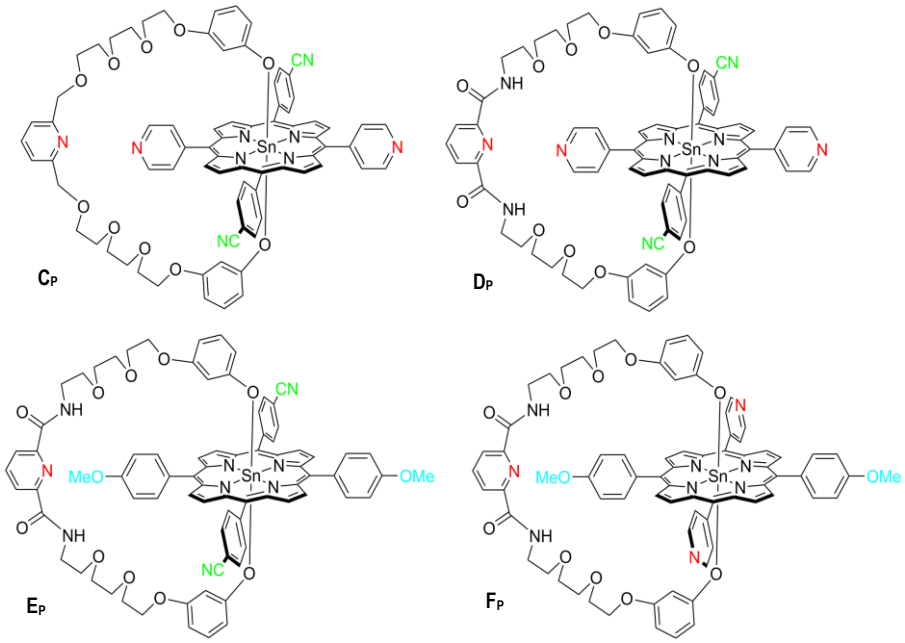


**Fig. 1.18** Several examples of $A_2B_2$ Sn (IV) based turnstiles.

The "amide" turnstile **$D_P$** was investigated.[4] Its closed state was generated in the presence of Pd(II) **(Fig. 1.19)**. For the turnstile **$G_P$**, the aim was to achieve the movement of the handle from the *meso*-pyridyl to *meso*-benzonitrile (**$H_P$**) stations by the presence of an external stimuli. Unfortunately, the addition of the Pt(II) complex **L** does not lead to the cleavage of the Pd-pyridyl coordination bond and the turnstile remained locked at the pyridyl station.

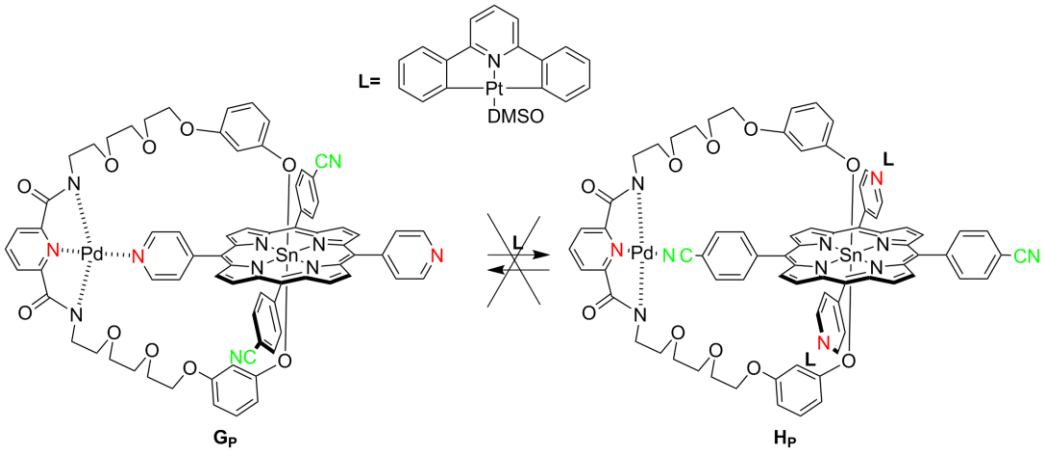


**Fig. 1.19** Attempt to switch the turnstile from the pyridyl to benzonitrile station.

However, the bond cleavage was observed for **$E_P$**. In this system, the benzonitrile group displays a weaker binding propensity than the pyridyl unit **$G_P$**. Indeed, addition of DMAP leads to the generation of the open state **$J_P$ (Fig. 1.20)**. This process is reversible and the closed state **$I_P$** is formed by the addition of $Pd(CH_3CN)Cl_2$.

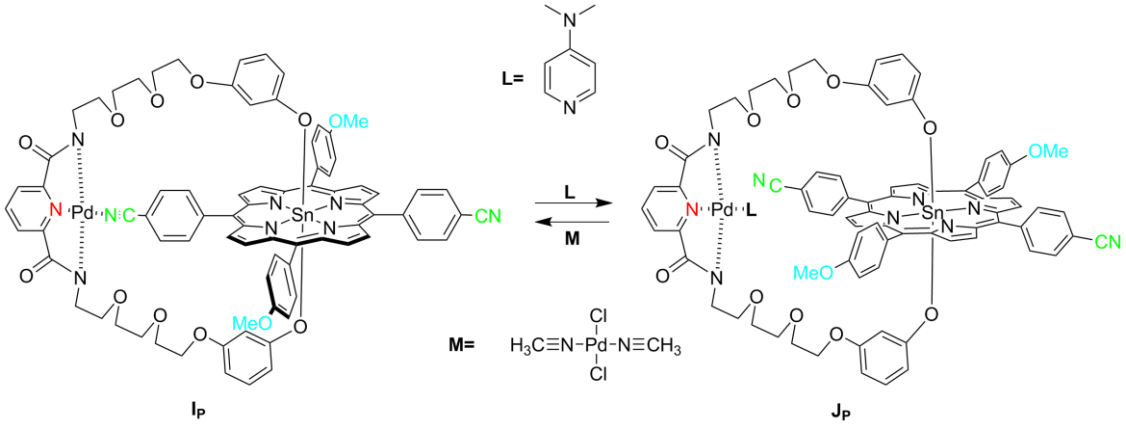


**Fig. 1.20** Closed and open states of the turnstile **$E_P$.**

Unfortunately, in all systems studied, it was not possible to observe the movement of the handle from one station to the adjacent one.

Moreover, although these Sn (IV) molecular turnstiles showed high efficiency, the Sn-O bond was found to be unstable under acidic conditions, even in the presence of weak acids preventing thus the use of acid/base tuning of the movement.

In order to increase the stability of the system under acidic conditions, it appeared compulsory to replace the Sn(IV) center by other metals or metalloids to generate less reactive bonds for the connection of the handle to the stator. For achieving that, phosphorus appeared to be the candidate of choice. The main topic of this PhD thesis is to synthetize new turnstiles based on phosphorus (V) porphyrin. The development of synthetic approaches for the preparation of such turnstiles as well as their properties are described in the following chapters.

## 2. Model turnstile based on P(V) tetraphenylporphyrin

As stated above, Sn(IV) porphyrin based turnstiles were shown to be effective dynamic systems. However, their potential could not be fully exploited owing to the reactivity of the Sn-O bond under acidic conditions. Due to an ability of phosphorus cation to form strong P-O bonds as well as the coordination number 6 of P(V), phosphorus porphyrin based turnstiles appeared to be promising candidates to replace Sn(IV) based derivatives. We planned to use the same synthetic strategy as for Sn(IV) based turnstiles. This multistep strategy involves several key synthetic issues:

- Synthesis of free-base porphyrins
- Insertion of P(V) within the porphyrins

- The synthesis of handles
- Connection of the handle to P(V) porphyrin
- Investigation of turnstile dynamic properties.

The previously described approaches toward the synthesis of phosphorus porphyrins can be divided into two main groups: β-substituted porphyrins and *meso*-arylporphyrins. Phosphorus β-porphyrins (octaethylporphyrin-OEP) was described first in 1977 by M. Gouterman.[17] The reaction was achieved with $PCl_3$ in boiling pyridine. This method was used afterwards with some modifications.[18–21] $PBr_3$ was also used for the metallation of *meso*-porphyrin diethyl ester.[18] Unfortunately, these techniques are not appropriate for *meso*-arylporphyrins which are targeted for our project.

The metallation of *meso*-tetraphenylporphyrins ($H_2TPP$) with phosphorus (V) was described for the first time by Carrano and Tsutsui also in 1977.[22] The method consists in the reaction of porphyrin with $POCl_3$ in boiling pyridine. This method is the most used one to date.[23–27] For the series of *meso*-alkylporphyrins, a mixture of $PCl_3$ and lutidine was found to be successful.[28] It is interesting to notice that the insertion of phosphorus into *meso*-pyridylporphyrins was not described previously.

## 2.1 Synthesis of phosphorus tetraphenylporphyrins

### 2.1.1 Insertion of the phosphorus (V) into the porphyrin cavity

The insertion of a metal cation into a porphyrin cavity proceeds usually under smooth conditions and in high yields.[29] However, in the case of phosphorus (V), the insertion takes place only under harsh conditions. At room temperature, the reaction does not proceed. To complete the metallation reaction, it is compulsory to carry out the reaction during almost 24 h in refluxing pyridine in the presence $POCl_3$ as the phosphorus source. Pyridine must be dried by distillation since residual water promotes the formation of hydroxy-complexes as impurities. To avoid this, dry pyridine or $PCl_5$ should be applied. Following this procedure, the dichloro-complex $[P(TPP)Cl_2]^+Cl^-$ is obtained in rather high yield (up to 82%) **(Fig. 1.21)**.

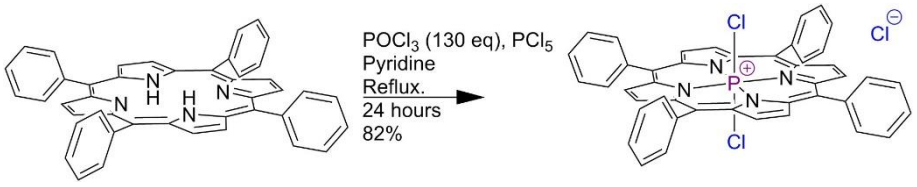


**Fig. 1.21** Standard method for the insertion of phosphorus atom into the porphyrin cavity.

The crude product is purified by column chromatography on $SiO_2$ and the desired product is eluted with a mixture of $CH_2Cl_2$-MeOH (5%), along with partial substitution of $Cl^-$ by $MeO^-$ and a small amount of side products. Further purification by gel-permeation chromatography (GPC) using Bio-Beads polymeric gel and chloroform as the eluent allows to separate different products

differing by the nature of the axial ligands based on their size. The desired product is collected as the second fraction.

The complex has been characterized by $^{1}$H-, $^{31}$P- and $^{13}$C-NMR in chloroform. It should be noted that $^{1}$H-NMR spectrum shows some interesting features. Due to the presence of phosphorus atom (spin of $^{31}$P nucleus is ½) in the porphyrin cavity, the 8 equivalent β-pyrrolic protons appear as a doublet at 9.14 ppm with $^{4}J_{P\text{-}H}$ = 4.5 Hz **(Fig. 1.22)**.

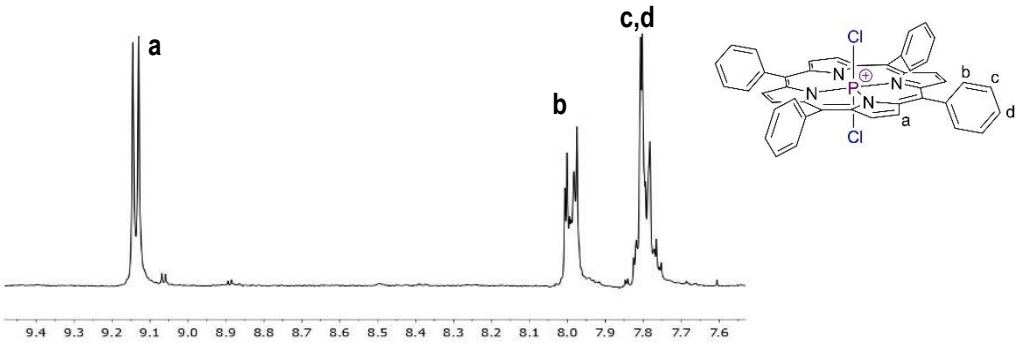


**Fig. 1.22** $^{1}$H-NMR spectrum of dichlorocomplex (300 MHz, $CDCl_3$, 25 °C).

Axial chloride ligands are labile and the complex slowly hydrolyses in air due to the presence of moister. As already noted, the exchange of $Cl^-$ anion could also be observed in the presence of MeOH.

This method is the only one described for *meso*-arylporphyrins and it works rather well for $H_2$TPP. However, as it will be described below, this procedure proceeds with rather low yields for porphyrins bearing pyridyl groups at the *meso* positions.

The insertion of phosphorus into phthalocyanines was described in the literature[30] and consists in the reaction of free-base phthalocyanines with $POBr_3$ as phosphorus source. We applied this methodology to our case and found that the use of $POBr_3$ instead of $POCl_3$ or $PCl_5$ presented several advantages **(Fig. 1.23)**. The reaction was monitored by UV-Vis spectroscopy by observing the disappearance of 4 Q-bands of TPP and the rising of new bands of P(V) porphyrin. It was found that full metallation occurs in 80 min in contrast to 24 h required for the previous method and the yield reaches 95%. In addition, this approach requires a smaller amount of reagents. The $[P(TPP)Br_2]^+$ complex is highly reactive and cannot be isolated. Its hydrolysis leads exclusively to the formation of $[P(TPP)(OH)_2]^+$**(Fig. 1.23)**.

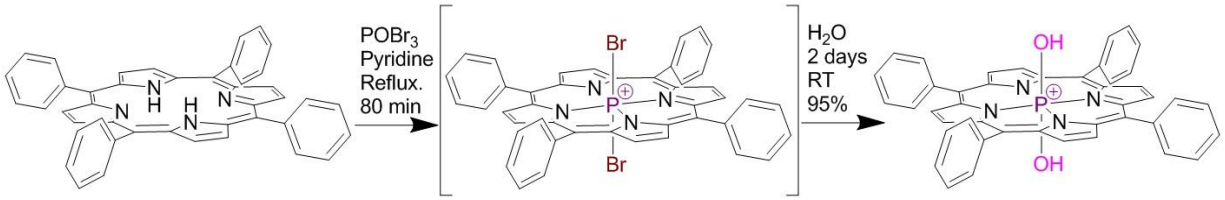


**Fig. 1.23** The phosphorus insertion method developed in this work.

It must be pointed out that the reaction with $POBr_3$ is very tricky. If we dissolve the porphyrin in pyridine under argon and add solid $POBr_3$ directly, the reaction does not take place, even under reflux. $POBr_3$ should be dissolved in pyridine and added dropwise to the free-base porphyrin in pyridine at room temperature. After refluxing, the reaction mixture cannot be evaporated. In case of evaporation of pyridine using rotary-evaporator, the concentration of $POBr_3$ increases and this leads to partial decomposition of P(V) porphyrin. Especially evaporating to dryness decreases the yield to ~15%.

Moreover, the purification of the crude product should be performed carefully and, as already mentioned, the evaporation of the pyridine should be avoided. We found that the best way to proceed is to add directly the mixture in DCM (or chloroform) and mix it with water. This mixture is then stirred during approximately 2 days to complete the hydrolysis of dibromo-complex $[P(TPP)Br_2]^+$ to the hydroxy analogue $[P(TPP)(OH)_2]^+$. Further extraction and washing with water removes the most part of pyridine. However, in addition to the desired product, some phosphorus containing compounds as well as pyridine remain in the organic layer which can not be removed by further washing. Even at that stage, the evaporation of the solvent leads to a dramatic decrease of the yield due to the decomposition of the complex. We were unable to recrystallize the complex in hexane or other non polar solvents. The purple solid complex becomes brown-green instantly in air. This is the reason why the organic layer is mixed with petroleum ether (or hexane) and the 1:1 mixture is loaded directly on a $SiO_2$ column and eluted with a 1:1 DCM-petroleum ether mixture. The free base porphyrin is eluted with DCM while the highly polar targeted P(V) complex remains at the top of the column. Gradually addition of methanol into the eluent removes the brown fractions containing impurities. Up to 10% of methanol is required to elute the desired phosphorus complex. An additional purification by gel permeation chromatography (GPC) removes small residual impurities and leads to the pure product. Following this precise procedure allows to increase the yield to 95% for TPP.

Finally, the nature of the counter ion is crucial. $Br^-$ anion must be used as the counter ion. For characterization of the complex in the solid state see the X-ray diffraction study on single crystal here after.

### 2.1.2 Substitution of the axial ligands

In the next step, we studied the exchange of the axial ligands on P(V). In porphyrin chemistry, this type of reaction is quite common,[31] and the substitution occurs in most cases quite smoothly. However, as already mentioned, the case of phosphorus is peculiar and poorly documented. A precise and systematic study is thus needed in order to find the best conditions to insert the handle in the last step of the synthesis.

As mentioned in the previous part, the axial ligands present in $[P(TPP)X_2]^+X^-$ (X = $Cl^-$ or $Br^-$), can be exchanged in the presence of water. Refluxing of $[P(TPP)Cl_2]^+Cl^-$ with water and pyridine affords the complex $[P(TPP)(OH)_2]^+$ with hydroxy axial ligands.

In order to mimic the coordination of the handle, we studied the introduction of *m*-methoxyphenol at the axial position of the P(V) (**Fig. 1.24**).

In the case of Sn(IV) porphyrin based systems, starting with the dihydroxy complex, it has been shown that 3-methoxyphenol could be introduced at both axial positions in $CHCl_3$ under reflux using a small excess of *m*-methoxyphenol (~2.4 eq.).[1]

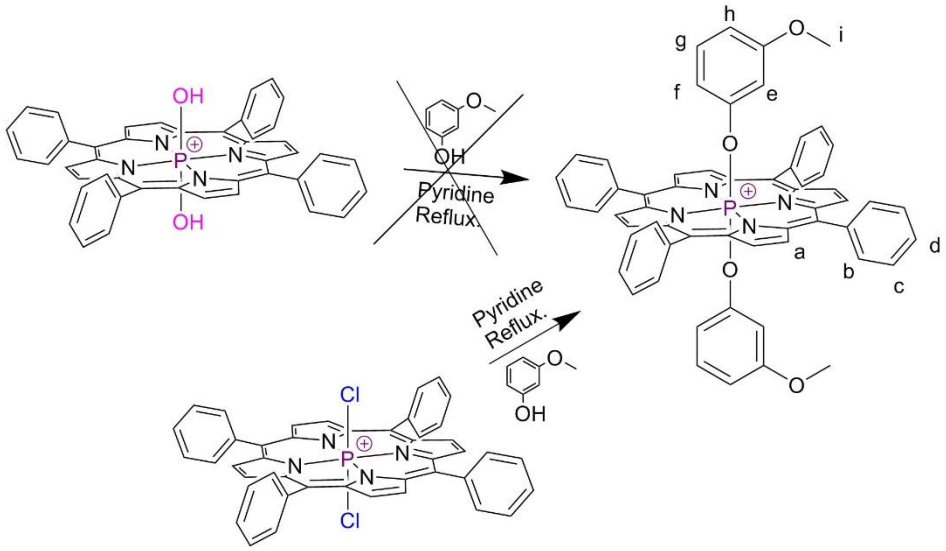


**Fig. 1.24** Exchange of the axial ligands in P(V) porphyrin.

In the case of phosphorus, these conditions did not lead to any substitution. Thus, more drastic conditions have been used. The typical procedure for the exchange of axial ligands in P(V) porphyrins requires the presence of pyridine under refluxing conditions.[24,31,32] However, starting from $[P(TPP)(OH)_2]^+$ this reaction did not lead to the desired product but mainly to the decomposition of the complex after 2 h under reflux (**Fig. 1.24**). Nevertheless, starting from $[P(TPP)Cl_2]^+Cl^-$, the desired bis(3-methoxyphenoxo) complex was obtained in 50 % yield after overnight refluxing in the presence of 3 eq. of 3-methoxyphenol. The formation of the new complex was confirmed by $^{31}$P-NMR which revealed a shift of the signal from -229 to -196 ppm **(Fig. 1.25)**. This value is however close to the value observed for dihydroxy complex (-193 ppm).

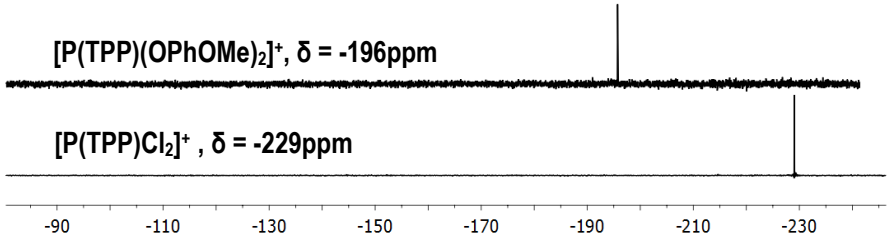


**Fig. 1.25** $^{31}$P-NMR spectra of P(V) TPP complexes with chlorine and methoxyphenoxy as axial ligands in $CDCl_3$.

The crude product was found contain in addition to the desired complex $[P(TPP)(OPhOMe)_2]^+$, a mixture of partially substituted complexes with high molecular mass, the free-base porphyrin and some unidentified compounds. The mixture could be separated by $SiO_2$ column chromatography. The final purification requires GPC. The $^1$H-NMR spectrum of target product in $CDCl_3$ (**Fig. 1.26**), as expected, contains the two signals corresponding to protons in the *ortho* positions of the phenoxy axial ligands (*e* and *f*) strongly upfield shifted ($\Delta\delta \sim 5$ ppm) when compared to the free 3-methoxyphenol. The 8 β-pyrrolic protons appear as a doublet due to their coupling with the phosphorus located in the cavity ($^4J_{P\text{-}H}$ = 3.4 Hz).

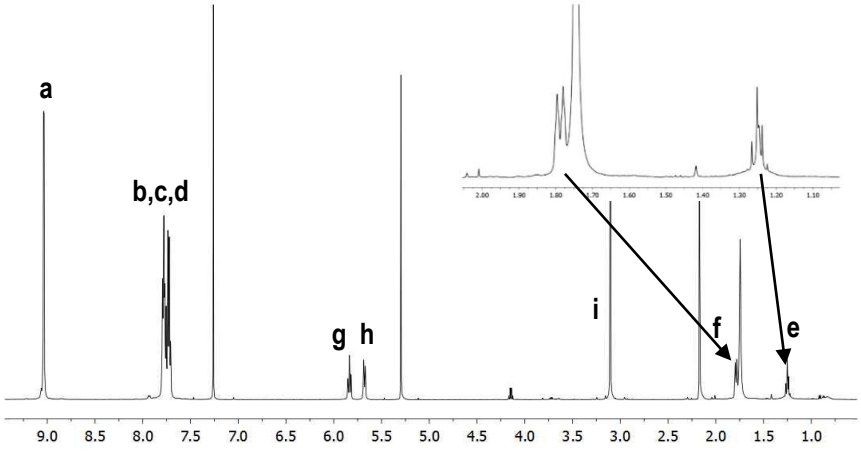


**Fig. 1.26** $^1$H-NMR ($CDCl_3$, 500 MHz, 25 $^o$C) spectrum of $[P(TPP)(OPhOMe)_2]^+$ and assignment of the signals, proton attributions are given in **Fig. 1.24**

It should be noted that the yield could be increased upon increasing the amount of methoxyphenol. However, our goal here is to define the optimal conditions for the insertion of the handle. Apart from the fact that the preparation of the handle requires a multi-step and quite expensive synthesis, the use of the bidentate handle in excess could also lead to the formation of the 2:1 side product represented in **Fig. 1.27**.

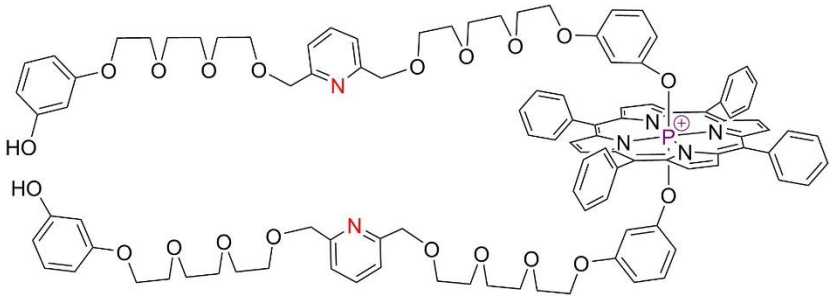


**Fig. 1.27** Side product which can be formed in the excess of the handle.

The main differences between the reaction of methoxyphenol with Sn(IV) and P(V) porphyrins concern the mechanisms of the axial ligand substitution. The one concerning Sn porphyrins[33] is represented in **Fig. 1.28**. In the case of Sn(IV), the reaction proceeds smoothly due to the weakness of Sn-O bond.

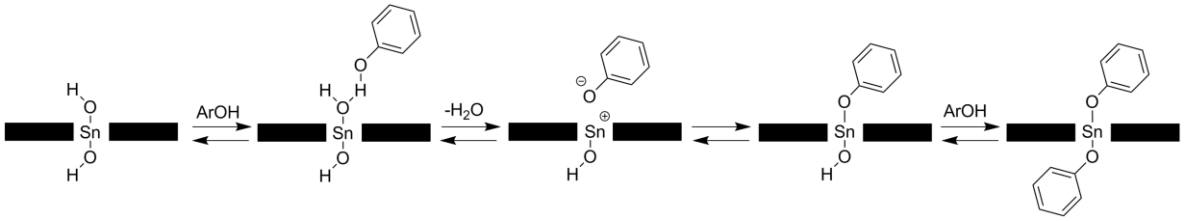


**Fig. 1.28** Mechanism for the substitution of axial ligands in Sn(IV) porphyrins. The second step of the substitution is the same.

A P-O bond is stronger than Sn-O bond. As it was shown experimentally, the presence of a base is required in order to exchange the axial ligands. Two mechanisms may be proposed for the exchange of the axial ligands. The first one is based on the use of good leaving groups on the porphyrin and a molecule (phenol in our case) that can be deprotonated by a base such as pyridine for example (**Fig. 1.29(1)**). Deprotonation of the OH moiety of phenol leads to the nucleophilic attack of phosphorus (V) located within the porphyrin cavity. Departure of $X^-$ anion leads to full exchange of the axial ligand. The second axial ligand may be exchanged by the same mechanism. Another possibility may be based on the use of two OH group on phosphorus (V) and its deprotonation leading to a nucleophile which can displace a leaving group on the incoming ligand (**Fig. 1.29(2)**). However, P(V) porphyrins are not very stable under basic conditions. Deprotonation of the axial OH ligands can lead to the decomposition of the porphyrin as experimentally demonstrated (see **Fig. 1.24**).

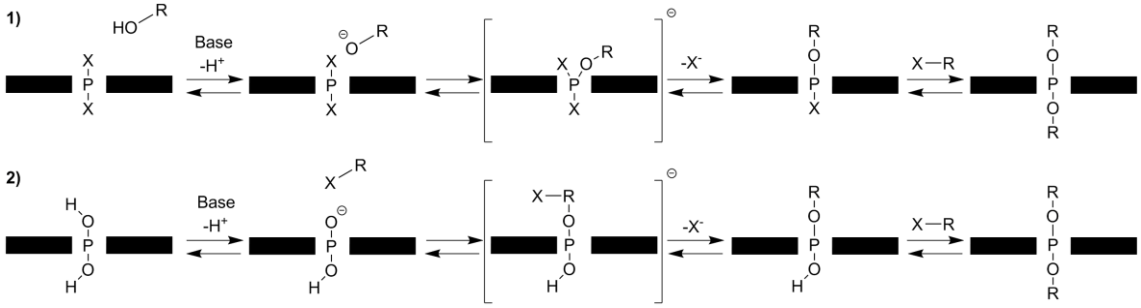


**Fig. 1.29** Two possible mechanisms for the substitution of axial ligands in P(V) porphyrins. **X =** leaving group, **R =** desired substituent. The second step of the substitution is the same.

As described above, $[P(TPP)Br_2]^+$ is a highly reactive species and hydrolyses rapidly. We decided to check its reactivity in the presence of alcohols. First, we added ethanol to the crude product and stirred the mixture at room temperature during 2 days. The diethoxy complex $[P(TPP)(OEt)_2]^+$ was obtained with a rather high yield (64%) **(Fig. 1.30)**.

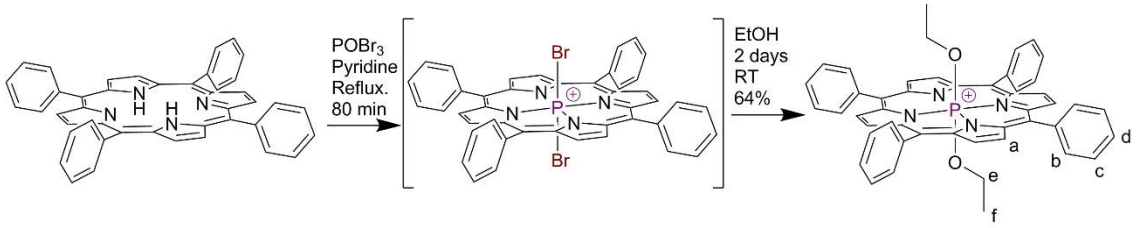


**Fig. 1.30** Synthetic pathway for $[P(TPP)(OEt)_2]^+$.

The exchange process was monitored by $^{31}$P-NMR spectroscopy: the phosphorus signal was observed at -179 ppm. The $^{1}$H-NMR spectrum are also informative (**Fig. 1.31)**. Two multiplets corresponding to the resonance of 20 phenyl protons and the doublet corresponding to the 8 β-pyrrolic protons "*a"* ($^{4}J_{P\text{-}H}$ = 2.8 Hz) are observed. The axial ligands are located in the field of influence of the porphyrin ring and thus appeared strongly upfield shifted. For EtOH, Δδ ~ 3 ppm for the $CH_3$ protons (*f*) while it is Δδ ~5.6 ppm for $CH_2$ proton (*e*) are observed. Their coupling with the $^{31}$P was also observed for both signals; the signal corresponding to *f* appears as a triplet of doublets (td, $^{3}J$ = 7.3 Hz, $^{4}J_{P\text{-}H}$ = 2.1 Hz) for the 6 protons *e*, while the signals corresponding to the 4 protons *e* appeared as a doublet of quadruplets (dq, $^{3}J_{P\text{-}H}$ = 14.0 Hz, $^{3}J$ = 7.0 Hz).

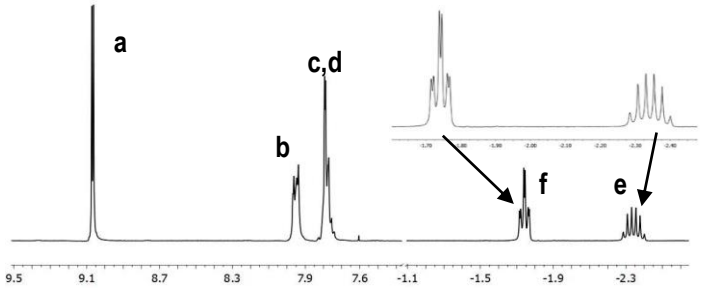


**Fig. 1.31** $^{1}$H-NMR ($CDCl_3$, 500 MHz, 25 °C) spectrum of $[P(TPP)(OEt)_2]^+$ and assignment of the signals, proton attributions are given in **Fig. 1.30.**

In addition to solution characterization, the solid-state structure of $[P(TPP)(OEt)_2]^+$ was also studied by X-ray diffraction on single crystal (**Fig. 1.32**). Purple crystals of the complex were obtained at 25 °C upon slow diffusion of pentane into a solution of the complex in chloroform with a drop of methanol. Due to the low quality of the single crystals, the structure was not finalized and it was not possible to refine the solvent presented in the asymmetric unit. The P(V) atom is localized in the center of the cavity and its small ionic radius induces a substantial deformation of the porphyrin ring. The macrocycle is strongly "ruffled". The $C_{meso}$ atoms are located out of the N4 porphyrin plane, two of them are above the main plane, the other two bellow the plane. The distance between *meso* carbons and the plane of four N and one P atom is the 0.931-0.958 Å range.

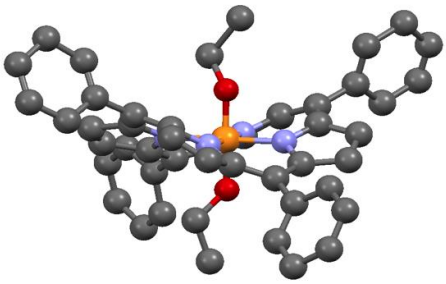

**Fig. 1.32** X-ray structure of $[P(TPP)(OEt)_2]^+$ (hydrogen atoms are omitted for clarity).

The phosphorus is hexacoordinated with 4 nitrogen of the porphyrin in the equatorial plane and two ethoxy groups located in the axial positions. Indeed, the P-N and P-O distances are small *i.e.* *ca* 1.84 Å and *ca* 1.63 Å respectively. These values are in good accordance with the data reported previously for similar complexes.[34–36] The quality of the crystal did not allow to determine the counter ion with precision. Taking into account the substantial deformation of the P(V) porphyrin macrocycle, synthetic difficulties for the preparation of the turnstile can be expected.

**Table 1.1**. Selected X-ray data for $[P(TPP)(OEt)_2]^+$.

| Bond | Length (Å) | Bond | Angle (degree) |
|---|---|---|---|
| P-O | 1.641(5)<br>1.624(5) | O-P-O | 177.3(2) |
| P-N | 1.839(5), 1.841(5),<br>1.842(5), 1.847(4) | N-P-N trans<br>N-P-N cis | 179.0(3) - 179.6(3)<br>89.6(2) - 90.5(2) |

### 2.2 Synthesis of the handle#1

Dealing with the choice of the handle, Sn(IV) porphyrin based turnstiles were equipped with the handle#1 **(Fig. 1.33)**, since its metric and shape are perfectly suited. For the phosphorus (V) porphyrin based turnstiles, the same handle was chosen. The synthetic pathway for the handle#1 was described in previous publications.[1–3] Its preparation, based on a multi-step procedure, was inspired by the published procedure, however some of them have been modified **(Fig. 1.33)**. In a first step, pyridine-2,6-diyldimethanol was converted to the dichloro-derivative **3** in 95% yield by reaction with $SOCl_2$. The triethylene glycol "spacer" in the handle was first monoprotected with 2-tetrahydropyranyl group to prevent the formation of cyclic compounds in the next step. The monoprotection reaction using dihydropyran is not selective and lead to a mixture of unprotected, monoprotected (**4**) and diprotected compounds, even with a threefold excess of the glycol. The mixture of was separated by column chromatography. The compound **4** reacts with **3** in dry refluxing THF in the presence of NaH in order to deprotonate the OH group on the glycol fragment. The compound **5** was isolated in 58% yield.

After removal of the THP protecting group, the compound **6** was obtained. Then it was transformed into the bis-mesylate compound **7**. The monoprotected resorcinol **8** was synthesized using a modification of the described synthesis.[1–3] It consisted in the direct solvent-free condensation of resorcinol with DHP[37,38] in the presence of $AlCl_3 \cdot 6H_2O$ as Lewis acid catalyst. The reaction leads to the formation of a mixture of free resorcinol, monoprotected (substance **8**) and diprotected one. This mixture could be separated by the column chromatography despite the close polarity of compounds. Derivative **9** is obtained by the reaction of **7** with **8** in dry THF and under reflux in the presence of NaH. There are two ways to isolate the product: column

chromatography or soxhlet extraction - both have similar efficiency. Soxhlet takes more time and column chromatography requires more solvent and attention. Handle#1 (**10**) is obtained upon deprotection of **9** under acidic conditions. The overall yield is 20%.

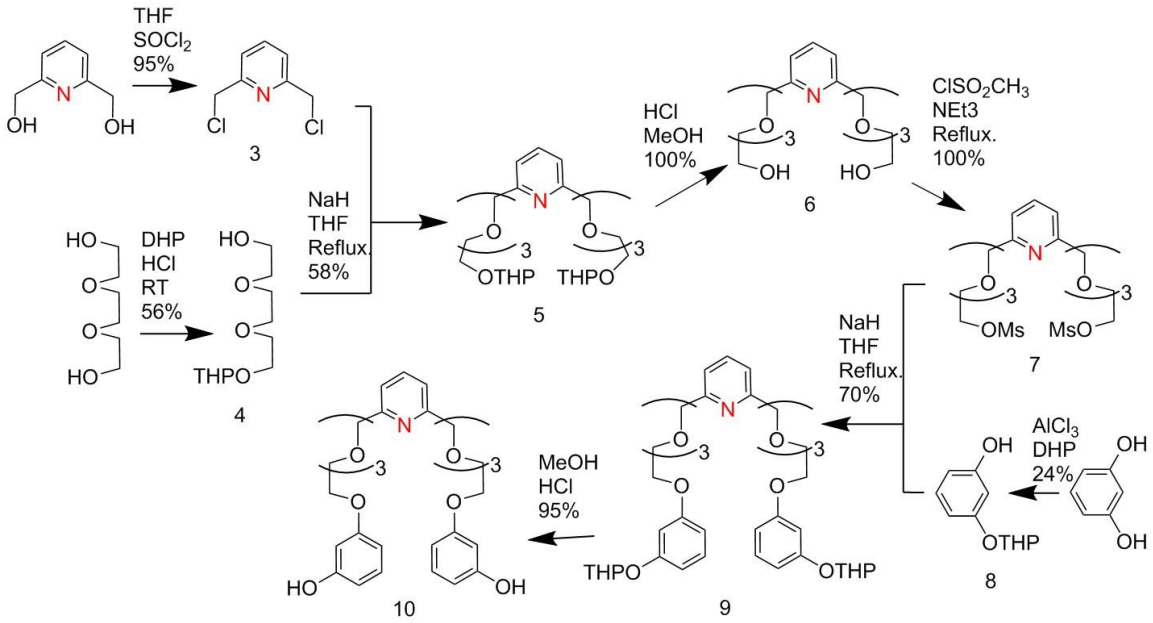


**Fig. 1.33** The synthesis of the handle#1.

## 2.3 Synthesis of the turnstile with handle#1

### 2.3.1 Application of standard method

First, we tried to use the conditions found for the introduction of 3-methoxyphenol (see previous part). As described above, the aromatic fragment can be added to the complex in refluxing pyridine. This method was applied for the reaction of $[P(TPP)Cl_2]^+$ with the handle#1 **(Fig. 1.34)** in a 1:1 ratio. Unfortunately, we observed only the formation of a mixture of $[P(TPP)(OH)_2]^+$, free-base porphyrin and high-molecular mass compounds upon overnight refluxing of $[P(TPP)Cl_2]^+$ with the handle#1. Attempts to optimize the conditions failed.

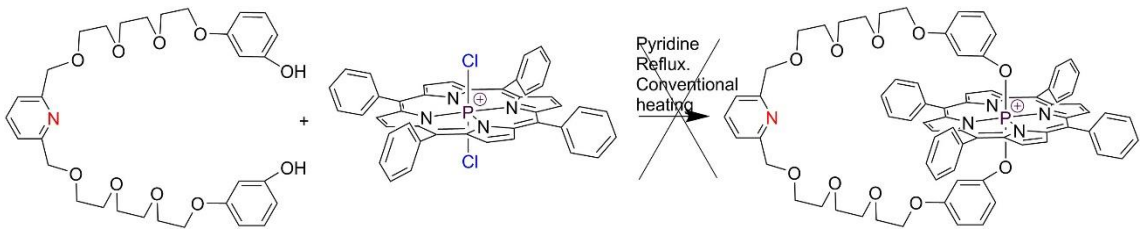


**Fig. 1.34** Application of standard method to obtain the model turnstile#1.

To avoid the hydrolysis of $[P(TPP)Cl_2]^+$, we also tried to use dried pyridine by distillation over $CaH_2$,[39] unfortunately, we observed the same result and the targeted turnstile could not be obtained.

One explanation for the different behaviour of the handle compared to the 3-methoxyphenol could be due to the severe deformation of the porphyrin macrocycle that prevents the handle to act

as a bidentate ligand and to form a 1:1 complex with the phosphorus porphyrin. In order to overcome this issue, the reaction was performed under microwave irradiation.

### 2.3.2 Microwave synthesis

Microwave irradiation and the use of special tubes, allow to reach temperatures over boiling point of the solvent. Cooling the system with an airflow allows to maintain the level of incoming energy constant without overheating of the solvent. The microwave region of the electromagnetic wavelengths includes the region from ~300 MHz to ~300 GHz. In science and industry, 2450 MHz is usually used. Comparing to IR region, microwaves contains less energy. Because microwaves can transfer energy directly to reactive species, so-called "molecular heating", they can promote transformations that are currently not possible using conventional heating. Thus, only rotation processes of molecules are involved, that exclude overheating of reaction mixture and thus preventing decomposition of reaction products.[40]

The main advantage of the microwave heating when compared to conventional techniques is direct delivering of energy from the source to molecules. During an ordinary procedure, the heat should overpass the walls of the vessel first. Next, it should heat all the mixture equally. During the microwave synthesis, there is no such threshold. There are two main mechanisms for microwave transfer energy: dipole rotation and ionic conduction. The first mechanism functions with polar molecules. In the presence of microwave field, molecules start to rotate following the quickly changing electric field of the source. The second mechanism is similar but instead of dipoles it involves ions.[40] The solvent has a great influence on the reaction. In the case of polar solvent, the advantage of microwave synthesis is not so significant. So, due to its polarity, pyridine is not the best choice. However, the deprotonation of the handle needs a basic substance (which is polar) in the mixture. Thus, we decided to keep pyridine as the solvent. Comparing to conventional heating, which includes in terms of energy mainly two parameters to be varied (time and temperature), microwave includes also the power.

A mixture of $[P(TPP)Cl_2]^+$ and handle#1 in dry pyridine heated to 150 $^oC$ at 120 W during 2 h leads to the formation of the desired turnstile $[P(TPP)handle\#1]^+$. However, under these conditions, we observed also the formation of $[P(TPP)(OH)_2]^+$, free-base porphyrin, high molecular compounds, some unidentified substances and $[P(TPP)monohandle\#1]^+$ (**Fig. 1.35**). To separate the mixture, a tedious step by step purification was applied: standard absorption chromatography and several GPC columns. The main issue was to separate the target model turnstile#1 from the similar compound with the handle acting as a monodentate ligand $[P(TPP)monohandle\#1]^+$ **(Fig. 1.35)**.

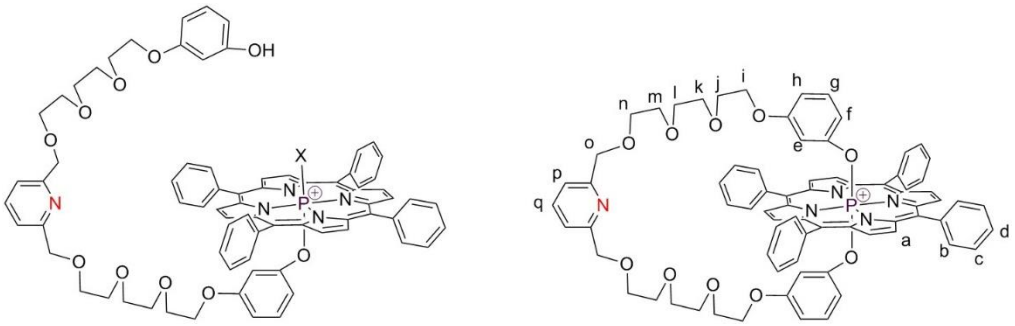

**Fig. 1.35** $[P(TPP)monohandle\#1]^+$ and model turnstile#1.

These compounds have approximately the same polarity and size. The size of the partially opened complex is a little bigger than the desired turnstile $[P(TPP)handle\#1]^+$, and this difference even small allows their separation by several GPC. After optimization of the conditions the desired model turnstile#1 could be obtained in 30% yield.

This turnstile displays rather interesting NMR spectra which needs to be described. $^{31}$P-NMR shows a signal at 195 ppm in $CDCl_3$ and in $CD_3OD$, indicating the stability of the axial bonds in these solvents (not dried). Concerning the $^1$H-NMR investigation, spectra of $[P(TPP)handle\#1]^+$ obtained in $CDCl_3$ and in $CD_3OD$ are given in **Fig. 1.36** together with the spectrum of the "free" handle#1 in $CDCl_3$. Broadening of all signals are observed in $CDCl_3$.

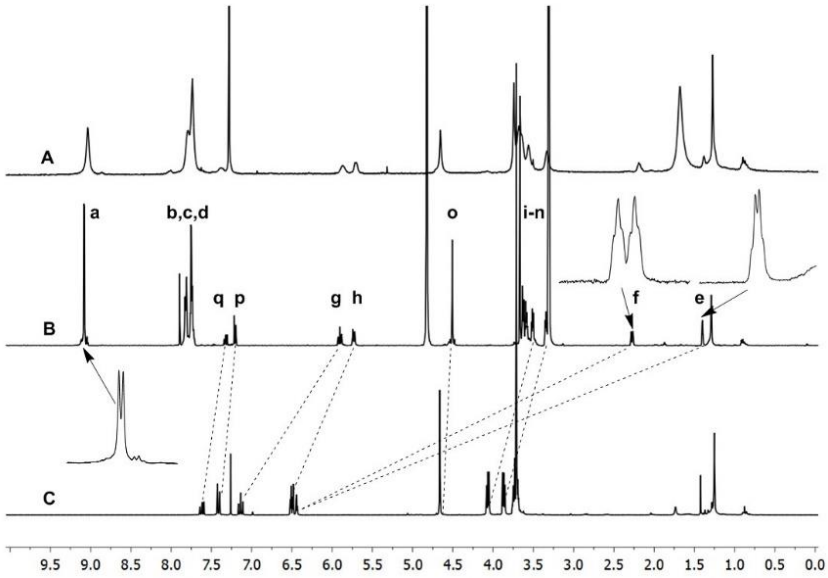


**Fig. 1.36** $^1$H NMR spectra (400 MHz, $25^0$C) of the model turnstile#1 in $CDCl_3$ (A), $CD_3OD$ (B) and of the handle#1 in $CDCl_3$ (C). Proton's designations are presented in **Fig. 1.35**

The resonance for β-pyrrolic protons *a* appears as a doublet ($^4J_{P\text{-}H}$=3.4 Hz) which is expected for P(V) porphyrins. Signals for protons *e, f* are clearly upfield shifted (Δδ of ~4 ppm and ~5 ppm respectively). Some of the proton signals of the handle are also up-field shifted, however to much less extent. Signals for the glycol protons *i-n* appear, as expected, in the 3.5 ppm range. However, the shape of the observed multiplets differs from the one observed for the Sn (IV) based turnstiles. Here, they are split into several multiplets with different chemical shifts and without overlaps[2,3].

The reason for this difference could be due to the difference in the geometry of complexes: tin systems are planar while phosphorus systems are not.

So far, several conclusions may be drawn:

- It is possible to obtain the model turnstile based on phosphorus(V) porphyrin
- The model turnstile#1 displays different solution behaviour when compared to the similar compound $[P(TPP)(OPhOMe)_2]^+$;
- The introduction of similar axial ligands (methoxyphenol and handle#1) requires different reaction conditions; probably for steric reasons since the handle#1 is rather bulky.

# 3. Synthesis of the single station turnstile

In order to occupy two distinct "open" and "closed" states, the Turnstile#1 must contain one coordinating site on the stator **(Fig. 1.2)**. The pyridyl group is the most suitable coordinating site as previously demonstrated by Sn(IV) porphyrins based turnstiles. The pyridyl unit offers two feature: binding to metal ion cations and undergoing protonation in the present of acids. The latter issue is a crucial for the control of the movement by acid/base reactions.

## 3.1 Synthesis of P(V) *meso*-pyridylporphyrins

### 3.1.1 Insertion of the phosphorus atom into the pyridyl-containing porphyrin

As already described, the standard $POCl_3$&$PCl_5$ method can be applied for TPP metallation. Our aim was to prepare a turnstile bearing a coordination site on the stator. Thus, 5-pyridyl-(10,15,20)-triphenylporphyrin ($H_2$MPyP) was chosen as the target **(Fig. 1.37)**.

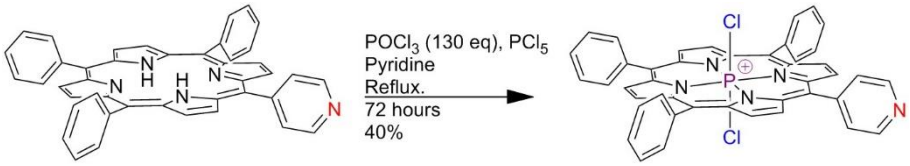


**Fig. 1.37** Standard method of the insertion of phosphorus into $H_2$MPyP.

The standard metallation method was found less effective for this porphyrin. Indeed, it needs 72 h instead of 24 h for the TPP. Even after 72 h, full conversion is not achieved *i.e.* the mixture contains the free-base porphyrin. Increasing the time did not lead to an increase of the yield. The final yield is only 40% which is lower than for MPyP.

Moreover, the dichlorocomplex $[P(MPyP)Cl_2]^+$ is more sensitive to moisture than $[P(TPP)Cl_2]^+$. It is slowly hydrolyzed in air, and the chloride axial ligands are partially substituted by OMe during column chromatography in the presence of methanol and further purification by GPC is required after the silica column. The pure product must be stored under argon in the absence

of light. However, even under these conditions, a slow decomposition of the product over the time was observed.

The metallation of the (5,15)-dipyridyl-(10,20)-diphenylporphyrin ($DPyPH_2$) was also investigated **(Fig. 1.38)**. The metallation is even more difficult when compared to the monopyridyl $H_2MPyP$. Refluxing the reaction mixture during 7 days is necessary to obtain some metallated P(V) porphyrin and only a small part of the porphyrin is converted to the desired P(V) complex. The purification is more tedious since this complex is more sensitive to moisture. The final yield for the (5,15)-dipyridyl-(10,20)-diphenylporphyrin ($H_2DPyP$) was found to be only 5%.

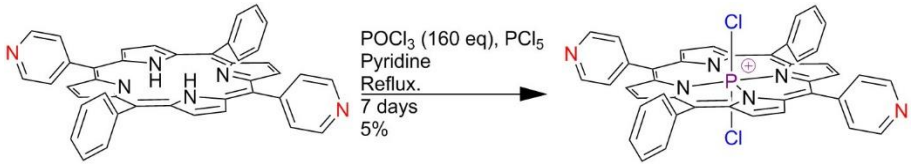


**Fig. 1.38** Standard method of insertion of phosphorus to $H_2DPyP$.

To confirm the influence of the *meso* pyridyl substituents on the yield of P(V) complex formation, the reaction was carried out with tetrapyridylporphyrin ($H_2TPyP$). No metallation was observed. Thus, it appears that the standard metallation with $POCl_3$&$PCl_5$ works well only with $H_2TPP$ and with the monopyridyl porphyrin $H_2MPyP$ however with lower efficiency. The insertion of P(V) in the cavity of porphyrins bearing more than one *meso*-pyridyl unit requires another metallation method.

The metallation of phthalocyanines usually requires stronger conditions than porphyrins.[41] The P(V) phthalocyaninates are described[30] and were obtained using $POBr_3$ as the metallation agent.

$POBr_3$ has been already successfully applied for the insertion of P(V) in $H_2TPP$ (see previous part, **Fig. 1.23**). We also applied this procedure to $H_2MPyP$ **(Fig. 1.39)**. An increased reaction time (+10 min when compared to $H_2TPP$) and a larger $POBr_3$ excess (+15 equivalents) were used. After hydrolysis, the yield of target compound reached 85% which is lower than the one observed for $H_2TPP$ (95%). It should be noted that full hydrolysis of the Br-complex needs only one day of stirring with water instead of two for $[P(TPP)Br_2]^+$ indicating that $[P(MPyP)Br_2]^+$ is more reactive.

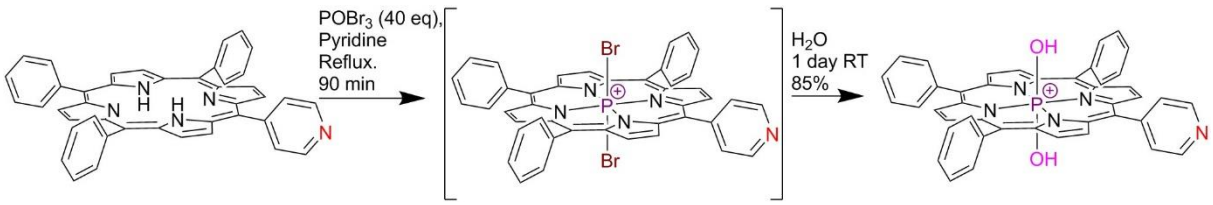


**Fig. 1.39** Insertion of phosphorus to $H_2MPyP$ using $POBr_3$.

The insertion of phosphorus to $H_2DPyP$ can be also achieved using $POBr_3$. Similar trends are observed: an increase of the number of *meso*-pyridyl leads to a decrease of the rate of the reaction

even in the presence of increasing amounts of $POBr_3$ with $H_2TPP$. The incorporation of P(V) into $H_2DPyP$ was achieved in an acceptable yield (69%).

It appeared interesting to test these conditions in the presence of tetrapyridylporphyrin $H_2TPyP$. After optimization of conditions, the best yield obtained for the incorporation of P(V) was only 13%. The $[P(TPyP)(OH)_2]^+$ displayed some unusual properties such as low solubility in chloroform and in more polar solvents. During purification on $SiO_2$, up to a 1:1 mixture of methanol and DCM was required for elution. Increasing the eluent polarity using acetic acid must be avoided since it leads to the protonation of complex. Moreover, the use of any base such as $Et_3N$ to increase the polarity was found to be also avoided. Indeed, although the complex is stable in the DCM-methanol-triethylamine mixture, upon evaporation the complex decomposes. The P(V) tetrapyridylporphyrin is highly unstable under basic conditions. Moreover, even at low temperature under the argon in the absence of light, this compound is unstable. Because of these features *i.e.* synthetic difficulties, purification problems and instability, this compound cannot be used for the generation of the turnstile.

### 3.1.2 Axial ligands exchange

The exchange of axial ligands of P(V) based DPyP and TPyP complexes was not investigated because of their instability. For $[P(DPyP)(OH)_2]^+$, a single O-alkylation was attempted (see experimental part). Here we will focus on the MPyP system. The general idea is the same as for the TPP system. The appropriate condition for the reaction is refluxing in pyridine. Since $POBr_3$ method showed its efficiency, the starting material was $[P(MPyP)(OH)_2]^+$ **(Fig. 1.40)**.

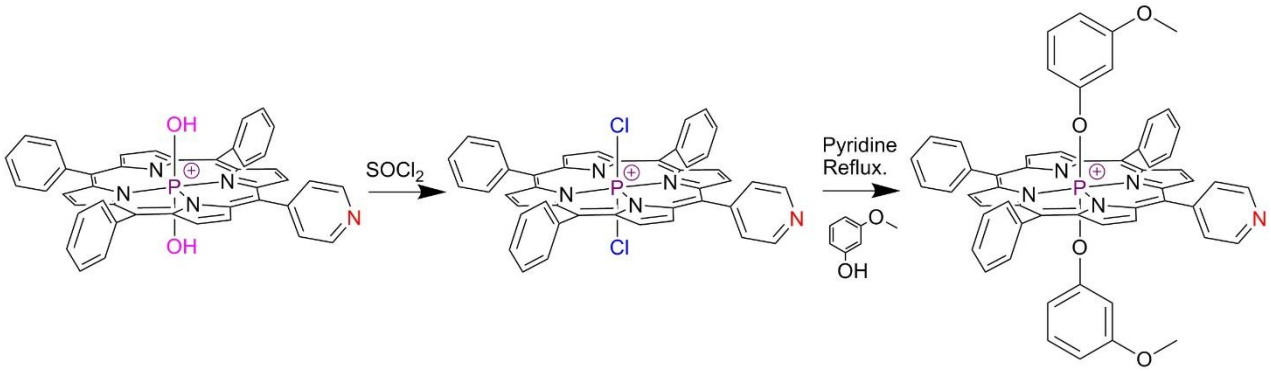


**Fig. 1.40** Exchange of the axial ligands in MPyP phosphorus(V) system.

As it was already found for $H_2TPP$, $[P(MPyP)(OH)_2]^+$ cannot be used as starting material and the hydroxy-ligands has to be replaced by more labile ones such as $Cl^-$. The formation of $[P(MPyP)Cl_2]^+$ is carried out with excess of $SOCl_2$, a strong chlorinating agent (**Fig. 1.40**). The reaction is carried out at room temperature. This procedure proceeds with 100% conversion. The excess of $SOCl_2$ is removed under reduced pressure. The product does not require further purification. It needs to be filtered through a Bio-Beads S-X1 column to remove traces of $SOCl_2$.

Pure chloroform is used as the eluent. The absence of any alcohols is required. Similarly to $[P(TPP)Cl_2]^+$, $[P(MPyP)Cl_2]^+$ reacts with *m*-methoxyphenol in boiling pyridine affording $[P(MPyP)(OPhOMe)_2]^+$ in 50% yield **(Fig. 1.40)**.

The $^1$H-NMR spectra of $[P(MPyP)Cl_2]^+$, $[P(MPyP)(OH)_2]^+$ and $[P(MPyP)(OPhOMe)_2]^+$ are presented in **Fig. 1.41**. The exchange of the axial ligands leads to significant changes of the spectrum. As in previous cases, $^{31}$P-NMR is very sensitive to the nature of the axial ligands. The chemical shits observed for $^{31}$P-NMR signals are different for all these complexes and similar to signals observed in the TPP series. The signal at -195 ppm corresponds to $[P(MPyP)(OPhOMe)_2]^+$, while signals at -193 ppm and at -229 ppm are characteristic for $[P(MPyP)(OH)_2]^+$ and $[P(MPyP)Cl_2]^+$ respectively. The nature of axial ligand was established by its specific fingerprint in $^1$H-NMR spectra. All proton signals are shifted and all signals are affected upon substitution. Moreover, in the case of $[P(MPyP)(OPhOMe)_2]^+$, the signals of aromatic protons in the *ortho*-positions of phenoxy ligands are strongly upfield shifted (close to 1.2 and 1.7 ppm).

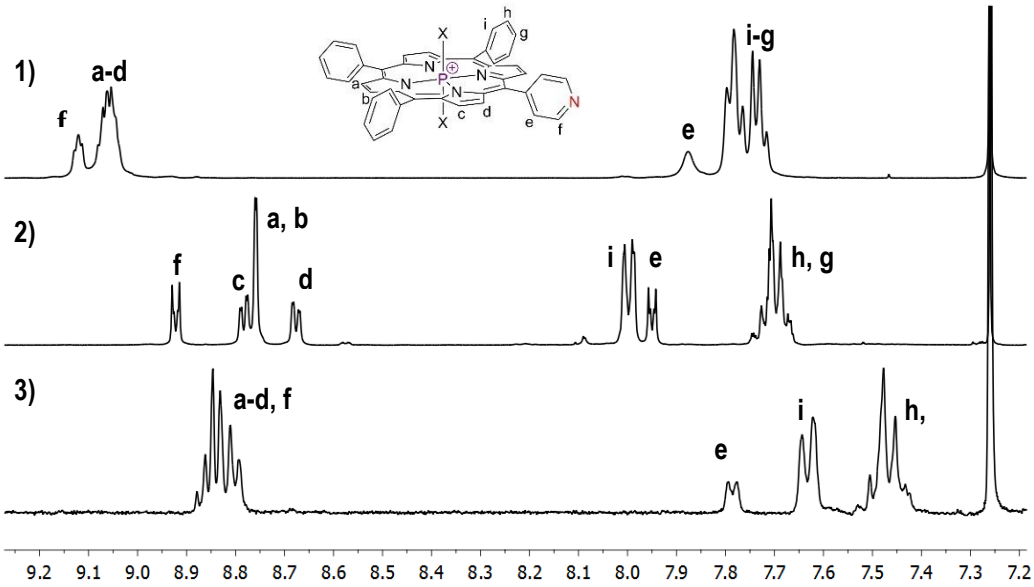


**Fig. 1.41** Portions of $^1$H-NMR spectra of $[P(MPyP)(OPhOMe)_2]^+$ (**1**), $[P(MPyP)(OH)_2]^+$ (**2**) and $[P(MPyP)Cl_2]^+$ (**3**) ($CDCl_3$, 25 $^oC$).

### 3.2 X-ray diffraction data of phosphorus (V) MPyP complexes

In addition to solution characterization, the solid-state structure of some of the phosphorus complexes with mono-pyridyl containing porphyrin were studied by single crystals X-ray diffraction. Single crystals of $[P(MPyP)(OH)_2]^+$ were obtained at 25 $^o$C upon vapor diffusion of the *n*-pentane into a chloroform solution of the complex. The latter crystallizes (triclinic, P-1 space group) with 2 chloroform molecules. The structure of $[P(MPyP)(OH)_2]^+Br^-$ is presented in **Fig. 1.42**. Selected structural parameters are presented in **table 1.2.** The phosphorus atom, adopting a distorted octahedral environment, is coordinated by four nitrogen atoms of the porphyrin core (P-N distances are in the 1.859 – 1.878 Å range) and two oxygen atoms of axial hydroxyl ligands

(with P-O distances of 1.615 and 1.638 Å). The *meso*-substituents are tilted with respect to the porphyrin plane with CCC dihedral angles of 118.43° for the pyridine moiety and from 120.75° to 121.69° for phenyl groups.

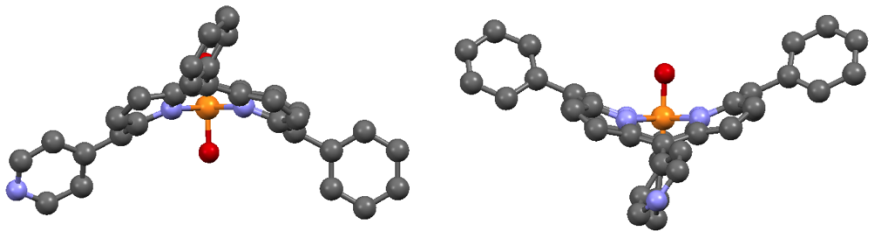

**Fig. 1.42** X-ray structure of $[P(MPyP)(OH)_2]^+$ (hydrogen atoms and bromine counterions are omitted for clarity).

As expected, the complex shows a pronounced "ruffled" deformation of the porphyrin ring. The degree of the deformation is similar to what was observed for P(V) TPP complexes. The structure correlates well with literature data reported for similar $[P(TPP)(OH)_2]^+$ complex.[27] Bromide anion was the counterion of the cationic complex.

**Table 1.2** Selected X-ray data for $[P(MPyP)(OH)_2]^+$.

| Bond | Length (Å) | Bond | Angle (degree) |
|---|---|---|---|
| P-O | 1.615(5)<br>1.638(5) | O-P-O | 178.1(3) |
| P-N | 1.859(7), 1.868(6),<br>1.876(7), 1.878(6) | N-P-N trans<br>N-P-N cis | 178.3(3) - 179.2(3)<br>89.5(3) - 91.4(3) |

Considering the crystal packing, nitrogen atom of pyridine moiety is engaged in special intermolecular interactions. It forms a hydrogen bond with the OH axial ligand of the adjacent porphyrin molecule **(Fig. 1.43)** with the formation of 1D zig-zag H-bonded network. This interaction helps to identify the pyridine moiety from the three other phenyl substituents. The second axial OH ligand forms hydrogen bond with the chloroform molecule.

Since the structure of the complex is similar to the one determined for $[P(TPP)(OH)_2]^+$, [27] it should be possible to prepare the turnstile based on this platform.

Attempts to obtain single crystal of $[P(TPP)(OPhOMe)_2]^+$ and $[P(MPyP)(OPhOMe)_2]^+$ failed. Although once very small needle type crystals of $[P(MPyP)(OPhOMe)_2]^+$ were obtained, unfortunately they were not suitable for X-ray diffraction studies. The complex $[P(MPyP)(OPhOH)_2]^+$, which was considered to be used for the synthesis of the turnstile (see below), except for the absence of methyl groups in the axial ligands, displays similar structural features. $^1$H- and $^{31}$P-NMR spectra are similar to the one observed for $[P(MPyP)(OPhOMe)_2]^+$.

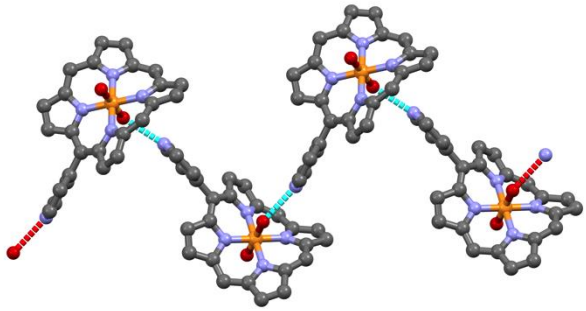

**Fig. 1.43** Fragments of crystal packing of $[P(MPyP)(OH)_2]^+Br^-$ showing the interconnection of adjacent porphyrins into a 1D zig-zag H-bonded network (phenyl *meso*-substituents, hydrogen atoms, solvent molecules and bromide counterion are omitted for clarity).

The red-brown single crystals of $[P(MPyP)(OPhOH)_2]^+$ were obtained upon slow diffusion of *n*-hexane into a chloroform solution of the complex in the presence of traces of methanol and toluene. The complex crystallizes (triclinic, P-1 space group) with one $CHCl_3$ molecule. The molecular structure of the complex is shown in **Fig. 1.44**. Selected crystal parameters are presented in **table 1.3.** Similarly to $[P(MPyP)(OH)_2]^+Br^-$, the phosphorus atom is hexacoordinated and surrounded by four nitrogen atoms of the porphyrin core (P-N distances are in the 1,82 – 1,84 Å range) and two oxygen atoms of axial hydroxyl ligands (P-O distances of 1,658 and 1,664 Å). The *meso*-substituents are tilted with respect of porphyrin plane with CCC dihedral angles in the 116.7° to 119.8° range. The pyridyl unit is disordered over all four *meso*-substituents of macrocycle and cannot be identified. No hydrogen bonds have been observed.

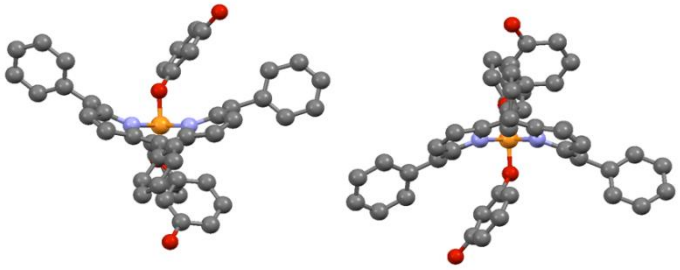

**Fig. 1.44** X-ray structure of $[P(MPyP)(OPhOH)_2]^+$ (hydrogen atoms, solvent molecules and counterion are omitted for clarity)

**Table 1.3** Selected X-ray data for $[P(MPyP)(OPhOH)_2]^+$.

| Bond | Length (Å) | Bond | Angle (degree) |
|---|---|---|---|
| P-O | 1.658(4)<br>1.664(4) | O-P-O | 173.9(2) |
| P-N | 1.822(5), 1.831(5),<br>1.839(5), 1.840(5) | N-P-N trans<br>N-P-N cis | 178.5(2) - 179.8(2)<br>89.5(2) - 90.5(2) |

As it is shown in **table 1.3,** here the N-P bond lengths are shorter than in $[P(MPyP)(OH)_2]^+$. Thus the deformation is slightly more pronounced, however the porphyrin core remains "ruffled". Phenyl rings does not form parallel planes as in the similar Sn(IV) system.[3] The mixture of $Cl^-$ and $Br^-$ counterions is present in the 1:1 ratio. Chloride anions found in the crystal arise most likely from chloroform decomposition (since the crystallization was carried out over a period of almost two months). The resorcinol OH groups forms hydrogen bonds with the counterions.

From structural studies in solution and solid state several conclusions can be made:

- Geometry of P(V) MPyP complexes is similar to the one of P(V) TPP complexes, the porphyrin plane in all case is strongly distorted
- Electronic properties are different and depend on the number of pyridyl substituents
- $[P(MPyP)(OPhOH)_2]^+$ structure is different with respect to the similar Sn(IV) analogue.

### 3.3 Approaches toward the turnstile#1

For the synthesis of the turnstile, we faced some difficulties in connecting the handle#1 to the porphyrin using the method described for TPP (for details see below).

The first attempt to connect the handle#1 to $[P(MPyP)Cl_2]^+$ was performed using conventional heating in pyridine (**approach 1**) **(Fig. 1.45)**. Due to higher reactivity of axial ligands in P(V) MPyP when compared to TPP, the exchange process should have been facilitated. Unfortunately, similarly to $[P(TPP)Cl_2]^+$, the formation of the one station turnstile was unsuccessful.

Microwave conditions were also tested. Under the same conditions as those used for the formation of $[P(TPP)handle\#1]^+$ (model turnstile#1) (120W, 150 $^oC$, 2 h), only the demetallated products was obtained. The synthesis was successful only once when the reaction was performed at 140 $^oC$ and 120W during 45 min. Unfortunately the procedure was not reproducible.

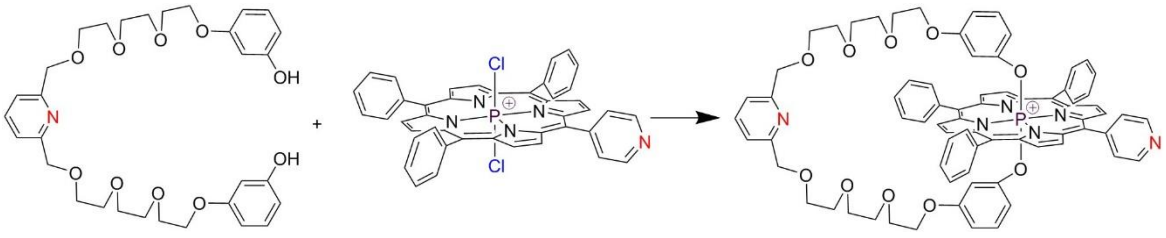

**Fig. 1.45** The suggested pathway to obtain the turnstile#1 (**approach 1**).

As we already noted, both for P(V) TPP and MPyP complexes, the targeted axial ligands may be introduced directly starting with the dibromo-complexes. The alcohol could be added directly in a second step after the treatment with $POBr_3$. By using an excess of resorcinol with respect to $[P(MPyP)Br_2]^+$, it was possible to obtain the dihydroxyphenoxy-complex $[P(MPyP)(OPhOH)_2]^+$ in 55% yield **(Fig. 1.46)**. Subsequently, in order to connect directly the handle#1 to the porphyrin, the complex was condensed with the compound **7** (**approach 2**).

This process requires basic conditions for resorcinol deprotonation. As we already mentioned, owing to the instability of P(V) porphyrins under basic conditions, the reaction leads to the demetallation of the porphyrin.

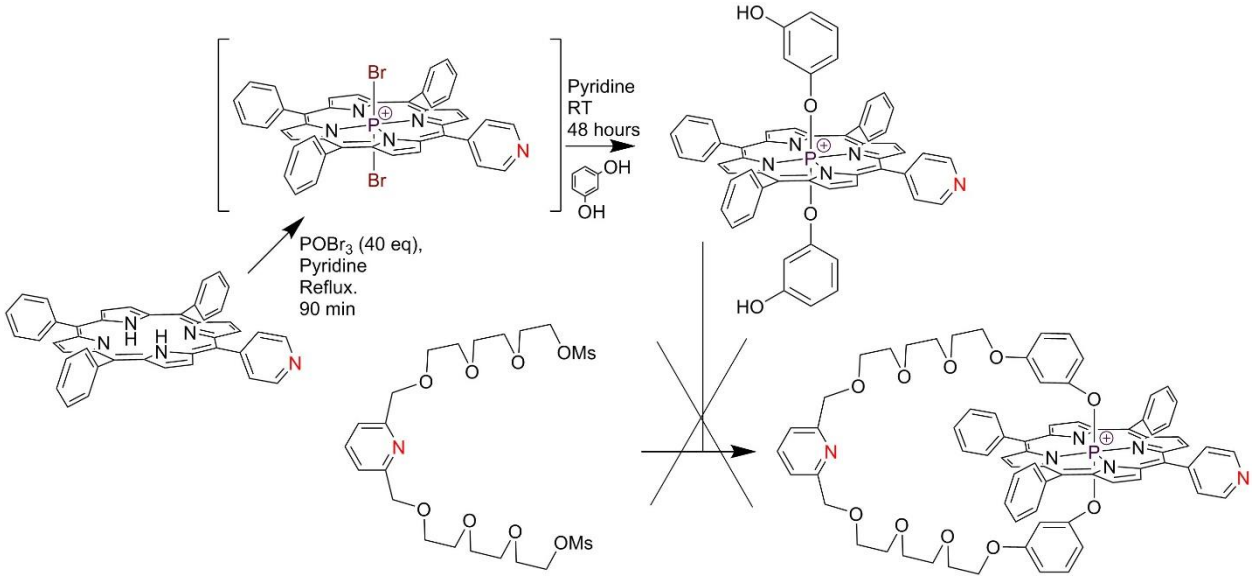


**Fig. 1.46** The explored pathway to obtain the turnstile#1 **(approach 2).**

Based on the above mentioned investigations, it appears that the synthetic approach developed for model turnstile can not be applied for the preparation of the turnstile bearing coordinating pyridyl sites. As an alternative, we have undertaken another approach for connection of the handle to the porphyrin backbone. This interconnection strategy is based on O-alkylation at P(V) center using handles bearing two terminal O-alkyl groups. It has been shown that this reaction proceeds under mild conditions.[42] For this approach, the leaving group should be incorporated within the handle. The O-alkylation of P(V) porphyrins was already described[42–44] and is based on the dihydroxy-complex as the precursor. To test this reaction with MPyP, a model reaction with ethyl tosylate was investigated (**Fig. 1.47)**. It was shown that the diethoxy derivative $[P(MPyP)(OEt)_2]^+$ can be obtained under mild conditions in acetonitrile and in the presence of cesium carbonate in 30% yield. The compound was characterized by NMR ($^1H$, $^{13}C$, $^{31}P$), HR ESI MS and UV-Vis spectroscopy. The spectroscopic features are similar to those of $[P(TPP)(OEt)_2]^+$. In marked contrast to $[P(TPP)(OEt)_2]^+$, unfortunately attempts to obtain single crystals failed.

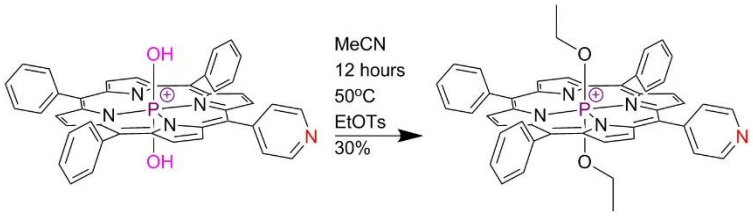


**Fig. 1.47** O-alkylation of $[P(MPyP)(OH)_2]^+$.

Subsequently, this new approach was applied to the synthesis of the turnstile using the handle bearing O-alkyl fragment (approach 3). For this purpose, another handle (**14**) was synthesized **(Fig. 1.48, 1.49)**.

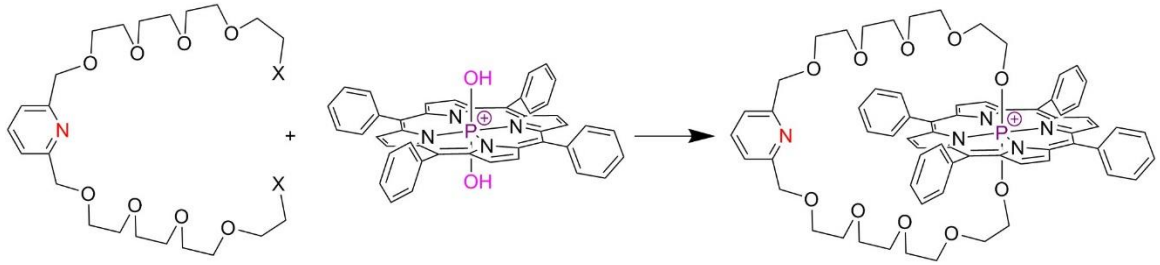

**Fig. 1.48** Suggested pathway to obtain the turnstile#1 (approach 3). X = leaving group

### 3.4 Synthesis of the handle#2

In order to facilitate the reaction between phosphorus atom and the handle, the tosylate derivative was chosen as leaving group. The multistep synthesis was inspired by the previously described procedure **(Fig. 1.49)**.[11]

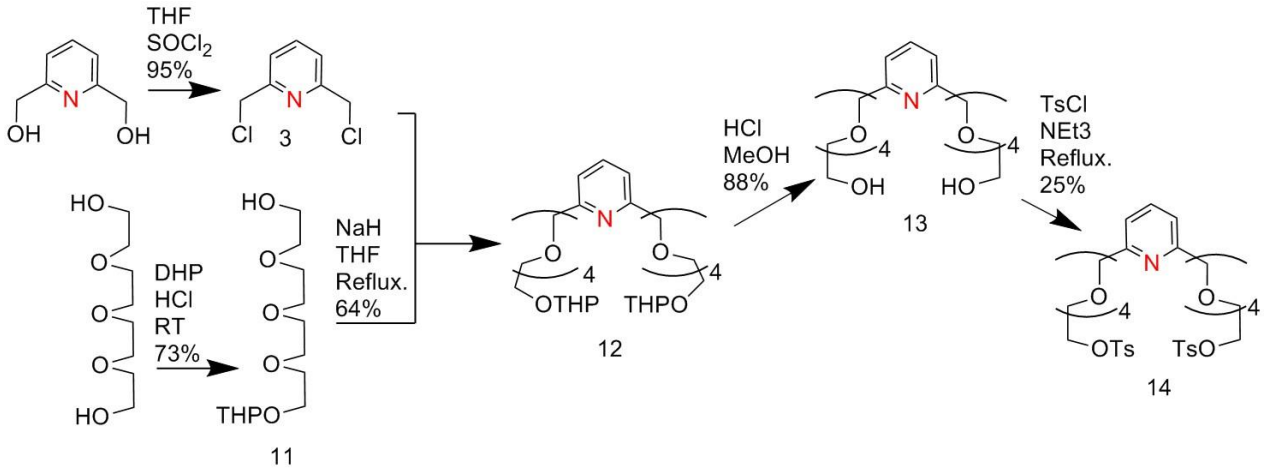


**Fig. 1.49** Synthetic pathway to obtain the handle#2.

Comparing to handle#1, several changes were made. Instead of triethylene glycol, tetraethylene glycol was used as spacer. The handle#2 does not posses the aromatic part, thus the difference in length may be compensated by addition of one glycol unit within the chain. All synthetic steps are similar to those used for the preparation of handle#1, except the final tosylation reaction. The reaction of compound **13** with tosyl chloride in the presence of triethylamine was carried out in THF at room temperature upon stirring the mixture for 5 h. After purification, *i.e.* washing with $NaHCO_3$ to remove the excess of tosyl chloride, the handle#2 was obtained in rather low yield (25%) for the last step. The overall yield for the preparation of the handle#2 bearing two active leaving groups was *ca* 10%.

### 3.5 Synthesis of the handle #2 based turnstiles

#### 3.5.1 Synthesis of the model turnstile#2

The O-alkylation process, as described in literature, can be carried out in the presence of $K_2CO_3$ in refluxing acetonitrile[43] or in DMF at room temperature.[42] Since one must avoid high temperature, several attempts to react the handle#2 with $[P(TPP)(OH)_2]^+$ in DMF at RT were made. Unfortunately, no product of the reaction was obtained.

Acetonitrile with two drops of DMF and $Cs_2CO_3$ instead of $K_2CO_3$ as more efficient base were used for the reaction. The condensation was carried out at 60 °C overnight. A two steps purification based on column chromatography on a $SiO_2$ and GPC was applied. Unfortunately, even after multiple purifications, the pure compound was not isolated. The final product $[P(TPP)monohandle\#2]^+$ **(Fig. 1.50)** always contained some unidentified impurities.

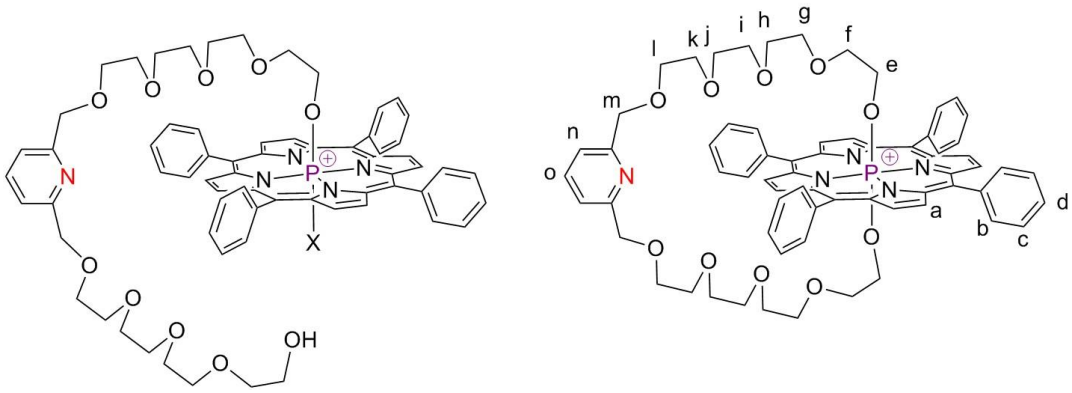


**Fig. 1.50** $[P(TPP)monohandle\#2]^+$ complex and model turnstile#2 $[P(TPP)handle\#2]^+$.

The model turnstile#2 was characterized by $^1H$- and $^{31}P$-NMR spectroscopy **(Fig. 1.51).** The $^{31}P$-NMR spectrum displays a signal at -181 ppm. The $^1H$-NMR spectrum is quite complex and is explained in details. Signals of glycol protons *e-l*, which appeared as a multiplet in the spectrum of free handle#2, are shifted upfield due to ring current of porphyrin and split into individual multiplets for the turnstile. The signals of protons *e*, appearing as a doublet of doublets ($^3J_{P\text{-}H}$ = 10 Hz, $^3J$ = 5.7 Hz), were found to be most strongly shifted ($\Delta\delta \sim 5.5$ ppm) due to close location to porphyrin ring. The signals of protons *f* are less shifted ($\Delta\delta \sim 3$ ppm). The signals for the other glycol protons appeared as broad multiplets in the 2-4 ppm spectral range. It is unclear if this shape of signals is due to the non-equivalence of two chains of the handle. If this was the case, the formation of multiplets can be explained by the overlap of expected triplets. In the spectrum of the model turnstile#2, signals of the tosylate group are also observed ($Ar_{Ts}$ and $Me_{Ts}$ markers in the **Fig. 1.51)**. The signal integration implies that the counterion is exchanged by $TsO^-$ anion.

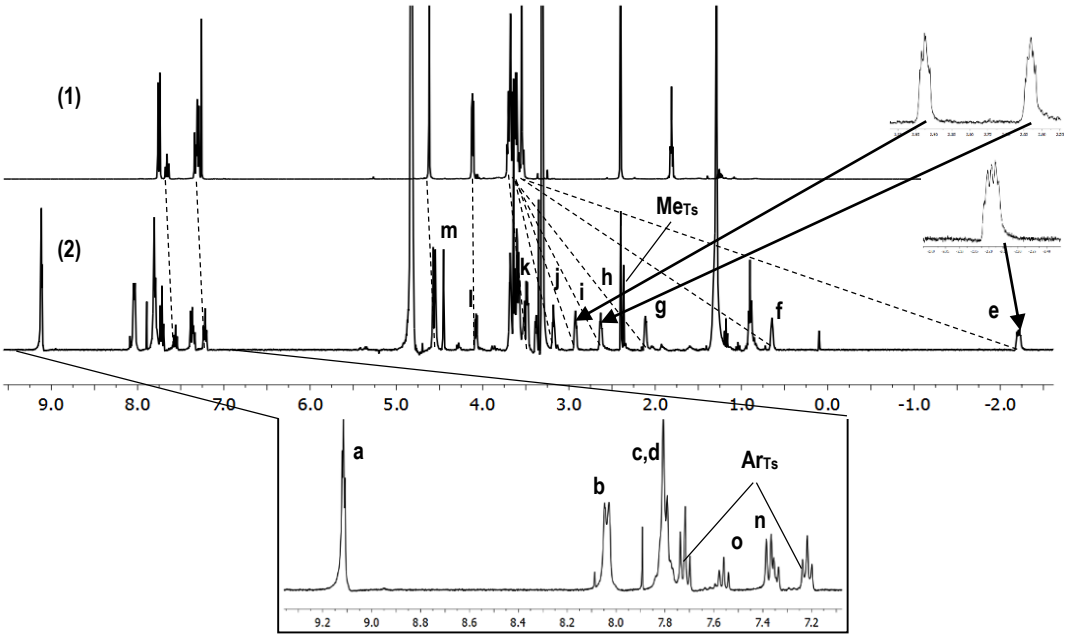


**Fig. 1.51** $^{1}$H-NMR spectra of handle#2 (1) ($CDCl_3$, 600 MHz, 25 °C) and model turnstile#2 (2) (MeOD, 400 MHz, 25 °C). Protons assignment is presented in **Fig. 1.50**.

A strong signal corresponding to impurities is observed at 3.5 ppm. The latter cannot correspond to the handle connected to the porphyrin, since *e-l* form individual signals. Most likely, it corresponds to glycol moieties of the decomposed handle. Also several other unidentified peaks were detected in the spectrum. Additional characterization of the compound was made by mass-spectrometry (MALDI-TOF) **(Fig. 1.52)**.

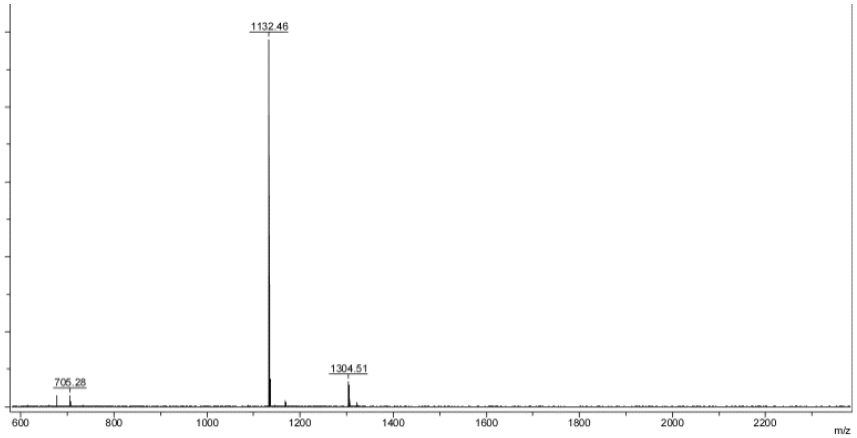


**Fig. 1.52** MALDI-TOF spectrum of model turnstile#2.

The signal corresponding to the model turnstile#2 molecular ion is observed at *m/z*=1132.46 (calculated for $[M\text{-}OTs]^+$ 1132.47). Thus, we can confirm that the $[P(TPP)handle\#2]^+$ turnstile was successfully obtained, however, we were not able to isolate it in a pure form. Each purification step leads to the partial decomposition of complex and did not decrease the amount of the impurities. We suspected a photo-destruction processes of the phosphorus turnstile to be responsible for the instability. Consequently, we have investigated this process in detail. The results are described in the second chapter of the manuscript.

### 3.5.2 Synthesis of the turnstile#2

To overcome this failure, we explored other conditions to prepare the turnstile. Several attempts to obtain the MPyP turnstile#2 were made. The reaction of the dihydroxy complex with handle#2 was performed in acetonitrile at 50 °C and in the presence of $Cs_2CO_3$ under argon **(Fig. 1.53)**. The complex was purified with the same procedure as for the model turnstile#2. Unfortunately, again the pure turnstile could not be isolated.

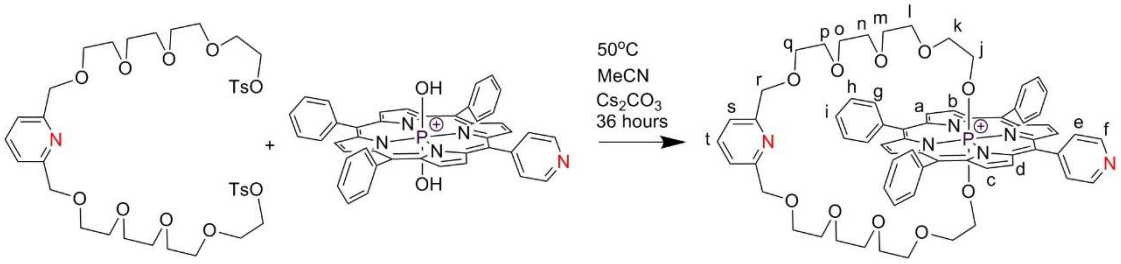


**Fig. 1.53** Synthesis of the turnstile#2 $[P(MPyP)handle\#2]^+$.

Similarly to model turnstile#2, the compound undergoes decomposition during GPC purification. This fact is probably related the photostability of turnstale#2. This phenomenon is described in the second chapter of the manuscript.

The structure and composition of turnstile#2 in solution was determined by $^1$H-and $^{31}$P-NMR spectroscopy **(Fig. 1.54).** The $^{31}$P NMR signal appeared at -181 ppm as for the model turnstile#2. The $^1$H-NMR spectrum is also similar to the one recorded for the model turnstile#2. The signal for the proton closest to the phosphorus atom appears as a doublet of doublets ($^3J_{P\text{-}H}$ = 10 Hz, $^3J$ = 5.7 Hz) with the same chemical shift. The shapes and positions of signals of other glycol protons *k*-*r* are similar to those of the model turnstile#2. The signals corresponding to the β-pyrrolic protons *a*-*d* appeared as a multiplet (δ = 9.12-9.19 ppm), while resonances for the pyridyl protons *e* and *f* appeared as two signals in the aromatic region of the spectrum. The signals of impurities appeared at the same ppm range as for the model turnstale#2.

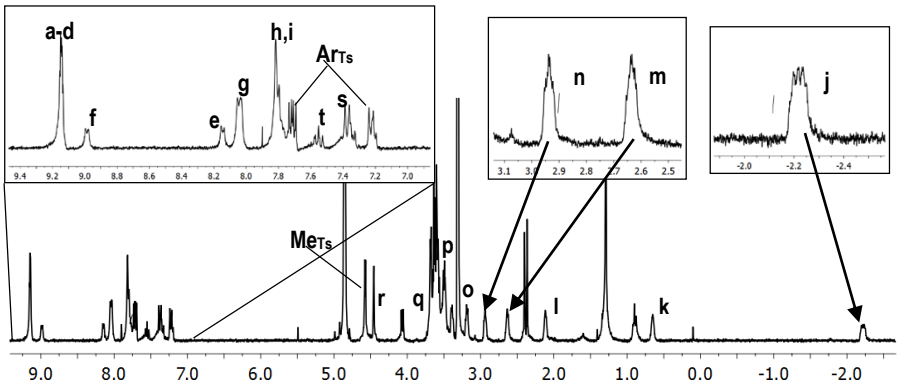


**Fig. 1.54** $^1$H-NMR spectrum of turnstile#2 (MeOD, 400 MHz, 25 °C). Proton assignment is presented in **Fig. 1.53**.

Additional characterization by mass-spectrometry (HR ESI) was also carried out **(Fig. 1.55)**. The peak corresponding to the turnstile#2 molecular ion is observed at *m/z*=1133.4598 (calculated for $[M\text{-}OTs]^+$ 1133.4573). In addition, several high-mass peaks were also detected. Again, although the turnstile#2 was formed, it was not possible to isolate it in a pure form.

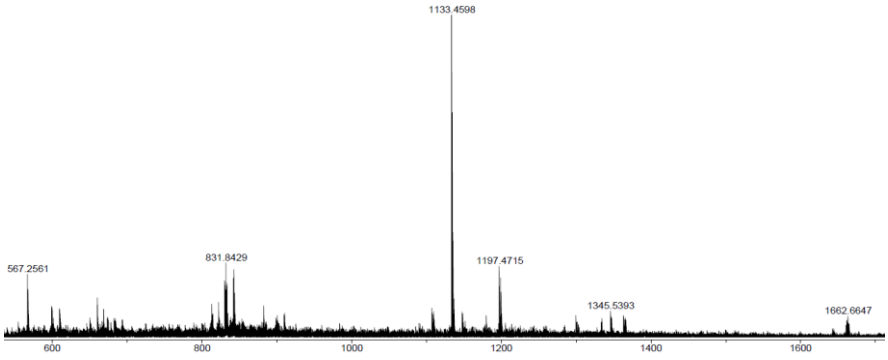


**Fig. 1.55** HR ESI spectrum of the turnstile#2.

Several conclusions may be drawn:

- The O-alkylation reaction was found to be effective for the formation of the turnstile
- The purification was found to be unfeasible et the compound appeared to unstable, probably due to photodecomposition

### 3.5.3 Turnstile #1 synthesis through Br-derivative

As stated above, we showed that the synthetic pathway leading to the turnstile#1 was operational for TPP but non operational for MPyP. It has been also demonstrated that the bromide axial ligands in P(V) porphyrins exhibit high reactivity and may be substituted directly during the complexation process. This reaction requires an excess of the incoming molecules. Considering the effective reaction with $SOCl_2$, the use of $SOBr_2$ should lead to the Br-complex.

As we expected, the stirring of $[P(MPyP)(OH)_2]^+$ in small amount of chloroform with $SOBr_2$ leads to dibromocomplex. The excess of $SOBr_2$ was removed by vacuum. However, attempts to isolate the compound failed. Traces of water in solvents or in air quickly hydrolyze the complex. The mixture of hydroxyl and bromo complexes was characterized by $^{31}$P-NMR. Two phosphorus signals were observed at -193 ppm corresponding to $[P(MPyP)(OH)_2]^+$ and at -322 ppm corresponding to $[P(MPyP)Br_2]^+$ **(Fig. 1.56).**

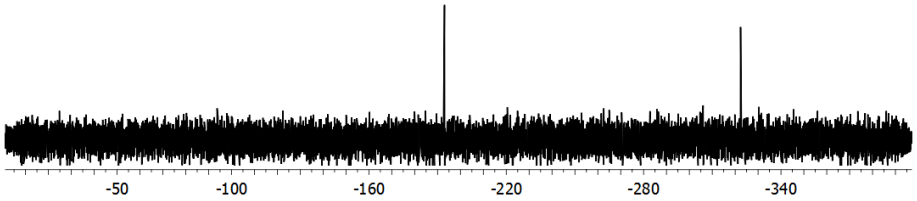


**Fig. 1.56** $^{31}$P-NMR spectrum of the mixture of $[P(MPyP)Br_2]^+$ and $[P(MPyP)(OH)_2]^+$ (162 MHz, $CDCl_3$, 25 $^oC$).

Based on these results, the synthesis of the turnstile#1 was attempted by a two step reaction **(Fig. 1.57)**. The first step consists in the bromination reaction during 3 h and storage under vacuum overnight to remove the excess of thionyl bromide. The handle#1 was also kept under the reduced pressure to remove all traces of the moisture. In order to avoid the presence of moisture, freshly distilled over $CaH_2$ pyridine was added through a cannula to both flasks containing the $[P(MPyP)Br_2]^+$ and the handle#1.

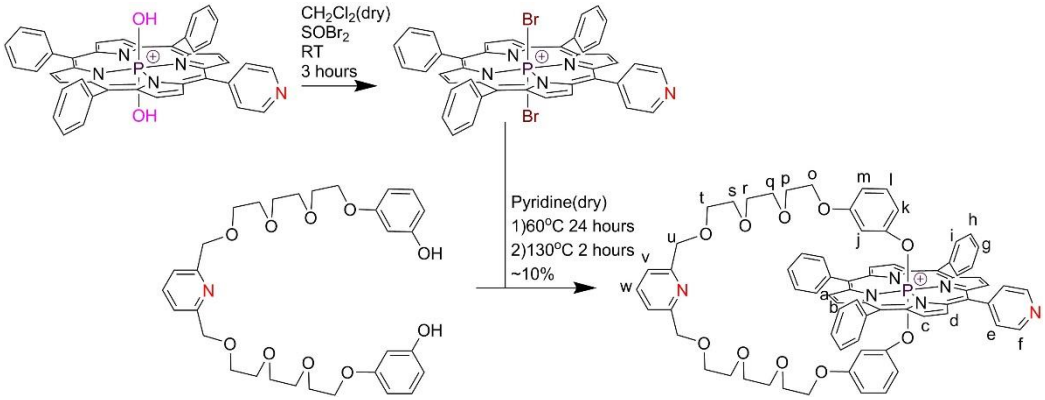


**Fig. 1.57** The novel synthetic pathway used to synthesize the turnstile#1.

During the second step, the two solutions were mixed and stirred at 60 °C during 24 h. At this temperature, the demetallation and decomposition of the P(V) porphyrin are minimized. However, the handle#1 connects to phosphorus center only from one side **(Fig. 1.58)**. Further refluxing of the mixture for 2 h is necessary to fully connect the handle#1 to phosphorus atom. Unfortunately, the reflux activates the decomposition processes thus leading the formation of the turnstile#1 in only 10% yield. It should be mentioned that direct refluxing (without the 1st step) leads only to the decomposition of the compound.

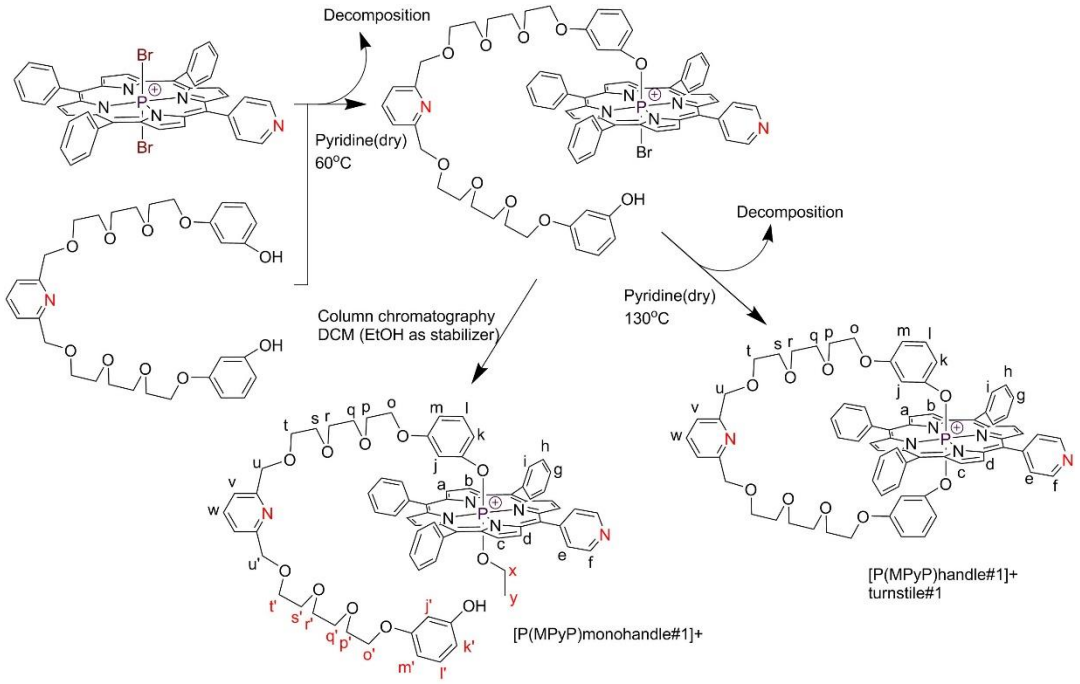


**Fig. 1.58** Scheme for the synthesis of the turnstile#1.

The purification of the reaction mixture revealed the presence of several substances. They may be divided into two main groups: P(V) porphyrins and the products of decomposition of porphyrins and the handle. The first group contains the turnstile#1, complex with the handle connected only by one side [P(MPyP)monohandle#1]$^+$ and the complexes with hydroxy, ethoxy and methoxy axial ligands. The other group includes the free-base porphyrin, the free handle, several unidentified compounds (probably corroles) and high-molecular substances. The purification process is quite similar to one used for the model turnstile#1. The two main groups of compounds were separated by column chromatography. The products of decomposition are less polar and can be eluted with DCM and MeOH (gradually increasing the ratio from 0% to 5%). These fractions contain also some pyridine. All P(V) porphyrins and high-molecular species remain at the start of the column and can be eluted with DCM-MeOH mixture (12-15v% MeOH). It is reasonable to think that the [P(MPyP)monohandle#1]$^+$ with bromo axial ligands is transformed into the ethoxy [P(MPyP)monohandle#1]$^+$ derivative during chromatography since DCM used contains 0.1-0.4 % of ethanol as stabilizer.

Preliminary separation of porphyrins was achieved by a Bio-Beads S-X3 column (chloroform 98% and methanol 2%). The handle-containing complexes are separated from other porphyrins due to the large difference between their molecule sizes. The main issue here is to isolate turnstile#1 from [P(MPyP)monohandle#1]$^+$. Several Bio-Beads S-X1 columns are usually needed to achieve this purpose. The [P(MPyP)monohandle#1]$^+$ is slightly larger but the difference of the sizes is not enough for good separation using a Bio-Beads column. Finally the turnstile#1 was isolated in 10% yield.

The UV-Vis spectra of solutions of compound [P(MPyP)monohandle#1]$^+$ and turnstile#1 are similar. However, these compounds may be easily identified by NMR (either $^1$H or $^{31}$P) **(Fig. 1.59)**.

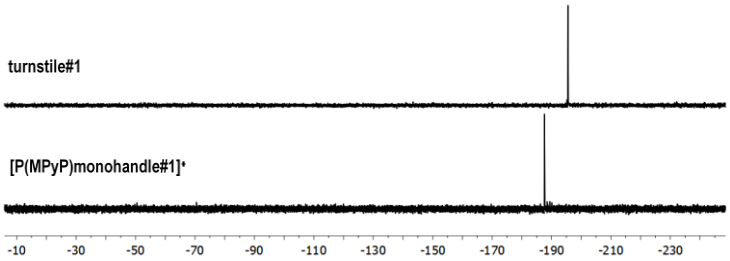


**Fig. 1.59** Comparison of $^{31}$P-NMR spectra of turnstile#1 and non-cyclic analog (162 MHz, MeOD, 25 °C).

The phosphorus signals appear at -188 ppm and -195 ppm for the open compound [P(MPyP)monohandle#1]$^+$ and for the turnstile1# respectively **(Fig. 1.59)**. It was previously described that the signal for [P(MPyP)(OEt)$_2$]$^+$ appears at -179 ppm, therefore the signal for [P(MPyP)monohandle#1]$^+$ is located between the ethoxy complex and the turstile#1. The ethoxy axial ligand can also be easily identified by $^1$H-NMR **(Fig. 1.60)**. The resonances of *x* and *y*

protons, are strongly upfield shifted due to macrocycle influence and correspond to ethoxy-group in the axial position of phosphorus porphyrin. Such a behaviour is similar to the one observed for $[P(MPyP)(OEt)_2]^+$.

Signals for the glycol protons *o-t* appear as multiplet composed of signals of the free handle and the turnstile#1 **(Fig. 1.60)**. The signals of resorcinol protons *j-m* split into two different groups. The first one *(j'-m')* corresponds to the disconnected fragment of the handle. The second group corresponds to the connected fragment. The chemical shifts are close to those observed for the turnstile#1.

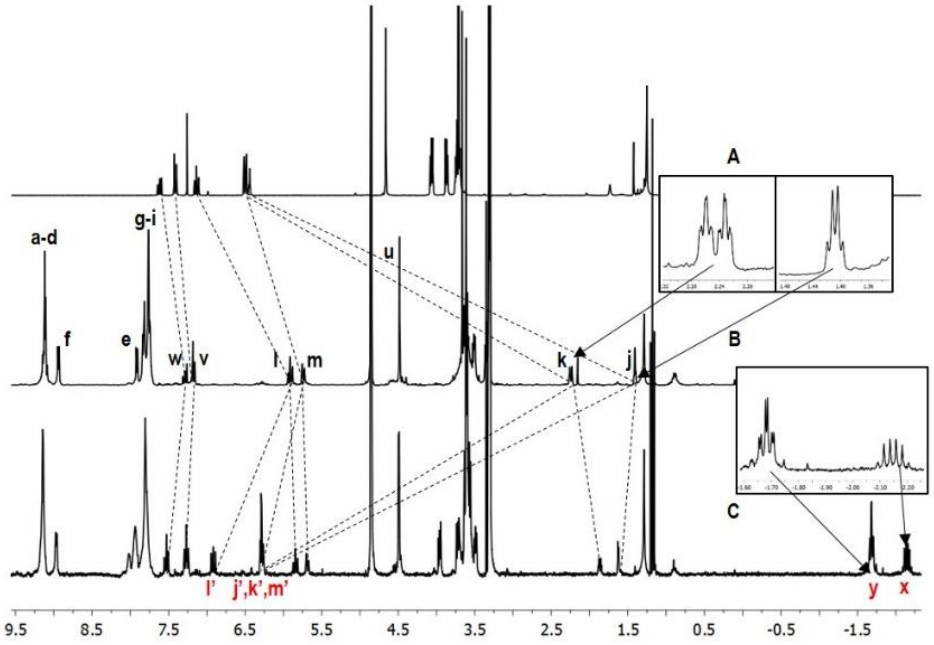


**Fig. 1.60** Comparison of $^1$H-NMR spectra of handle #1 (**A**, $CDCl_3$), turnstile#1 (**B,** MeOD), and [P(MPyP)monohandle#1]$^+$ (**C**, MeOD), 400 MHz, 25 $^\circ$C. Proton assignment is presented in **Fig. 1.58**.

Signals of the porphyrin protons of both complexes display similar chemical shifts and shapes. The Turnstile#1 $^1$H-NMR spectrum is similar to the model turnstile. The differences observed are related to the structures of porphyrins TPP and MPyP. One feature should be noted, signals corresponding to protons *j* and *k* of the turnstile#1 display the same chemical shifts and shape as the model turnstile. The absence of signals in the upfield region of the $^1$H-NMR spectrum confirms the absence of aliphatic chains connected to the phosphorus atom.

In summary, the following conclusions may be drawn:

- The turnstile#1 with one coordination site was synthesized
- The compound is stable and was isolated and fully characterized;
- A reaction mechanism for its synthesis is proposed
- Probably due to the distortion of porphyrin ring, the handle#1 preferentially undergoes a single connection to the phosphorus atom

# 4. Dynamic behaviour of the molecular turnstile#1

## 4.1 Use of silver triflate

### 4.1.1 1D NMR investigations

The study of the dynamic behaviour of the P(V) porphyrin based turnstile is inspired by the one carried out with Sn(IV) based turnstile.[2] As previously reported, the dynamic behaviour of the turnstile in solution was studied by NMR techniques. Silver cation[1] was used as the locking agent[45,46] because:

- its possible linear coordination geometry
- sufficiently high binding constant when bound to pyridyl moieties as coordinating sites
- its diamagnetic nature required for NMR investigation

Triflate anion was used for solubility reasons and its poor binding capacity to silver cation.[2]

The experiments were carried out in polar solvents (methanol-$d_4$ or acetonitrile-$d_3$). The concentration of the complex was *ca* $10^{-3}$ M unless specified otherwise.

Owing to simultaneous binding of the silver cation by both pyridyl moieties, the latter should behave as the locking agent **(Fig. 1.61)**.

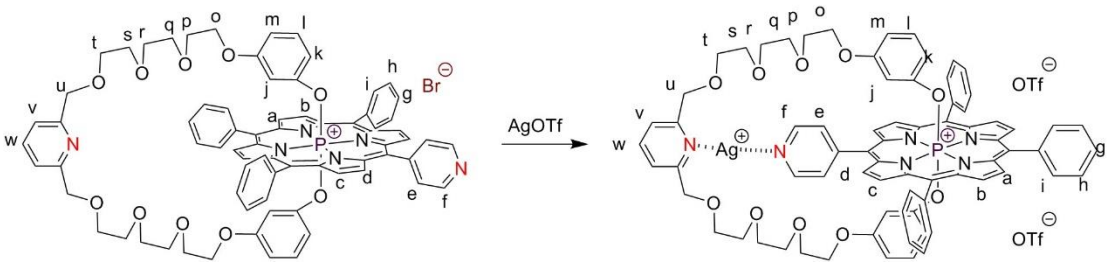


**Fig. 1.61** The closing of turnstile#1 induced by the silver cation.

The locking process was investigated by NMR ($c=2.6\cdot10^{-3}$M) upon addition of solution of silver triflate in deuterated methanol to solution of turnstile#1. Two regions of $^1$H-NMR spectra (aromatic and aliphatic) were analyzed. Owing to the binding of silver cation, one would expect shifts of protons of the pyridyl moieties and a change in the symmetry of the turnstile.

The aromatic region of the spectra (7.1-9.5 ppm) is presented in **Fig. 1.62**. Addition of 0.5 eq. of AgOTf had no effect, while addition of 1 equivalent caused few small but observable changes of the spectrum. This behaviour is expected since the counterion of the turnstile is $Br^-$ anion and thus the first equivalent of silver cation is required to remove $Br^-$ anion by precipitation of AgBr. Addition of 2 eq. of AgOTf leads to substantial changes.

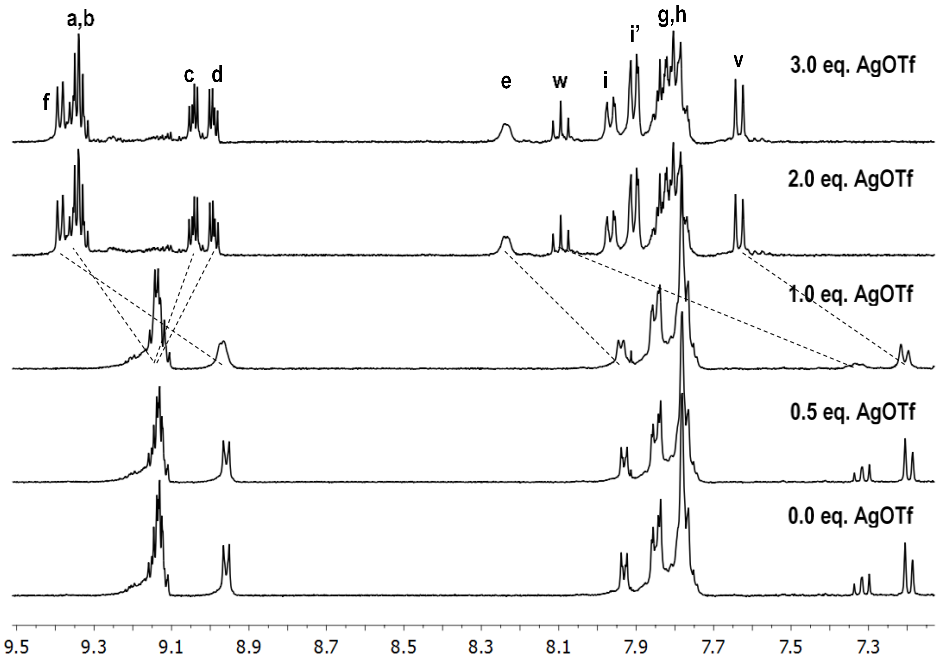


**Fig. 1.62** $^{1}$H-NMR (MeOD, 400 MHz, 25 °C) spectrum (7.1-9.5 ppm region) of the turnstile#1 in the presence of different equivalents of AgOTf. Proton assignment is presented in **Fig. 1.61.**

Signals of the porphyrin pyridyl protons *e* and *f* shift downfield by 0.30 ppm and 0.43 ppm respectively. Signals of the handle pyridyl protons *y* and *w* follow the same trend ($\Delta\delta$ = 0.78 ppm for both). A splitting of signals *a-d* (β-pyrrolic protons) into two groups is also observed. Signals of protons *a* and *b* display close chemical shifts and appear as a multiplet, while signals of protons *c* and *d* appear as a doublet of doublets. ($^{3}J$ = 5.3 Hz, $^{4}J_{P\text{-}H}$ = 3.1). These changes are due to the binding of the silver cation.

Signals of glycol protons *o-u* appear in the 3.3-5.0 ppm region **(Fig. 1.63)**. In the presence of 2 equivalents of silver triflate, the signal corresponding to *u* shifts downfield by 0.42 ppm. The multiplet splits into five distinct multiplets. Signals of protons *t, s* are found to be broad. Although the shape of signals of protons *o-r* is expected to be triplets, they appear as multiplets which may be a superposition of two triplets non equivalence of protons of the two glycol chains of the handle.

To prove that the close state of the turnstile#1 was reached, an excess of AgOTf was added. The spectrum in the presence of 3 eq. is the same as the one with 2 eq.

The binding constant for silver binding was calculated using ChemEqui software.[47,48] Signals of *e, v, t, s* protons were used for calculations. The binding constant log K is 2.83 ± 0.8.

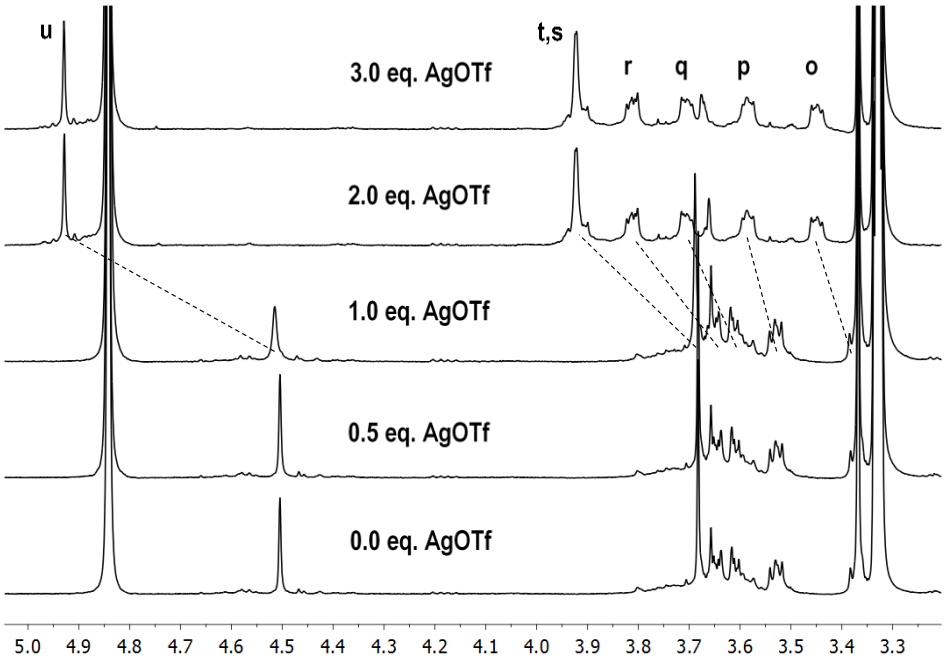


**Fig. 1.63** $^{1}$H-NMR (MeOD, 400 MHz, 25 $^{\circ}$C) spectrum (3.3-5.0 ppm region) of turnstile#1 in the presence of different equivalents of AgOTf. Proton assignment is presented in **Fig. 1.61**.

### 4.1.2 Analysis by Mass-spectrometry

The closed state of the turnstile#1, obtained in the presence of 3 equivalents of AgOTf, was analyzed my mass-spectrometry. HR electrospray ionization technique was used since it is one of the softest methods. Two main peaks were observed **(Fig. 1.64)**. One at molecular ion (*m/z 615.2309, calc. 615.2323)* corresponds to the monoprotonated turnstile#1 $[M+H]^{2+}$. The lower intensity peak at *m/z 668.1781 (calc. mass 668.1809)* corresponds to the closed state of turnstile $[M+Ag]^{2+}$, demonstrating the 1:1 stoichiometry of the complex.

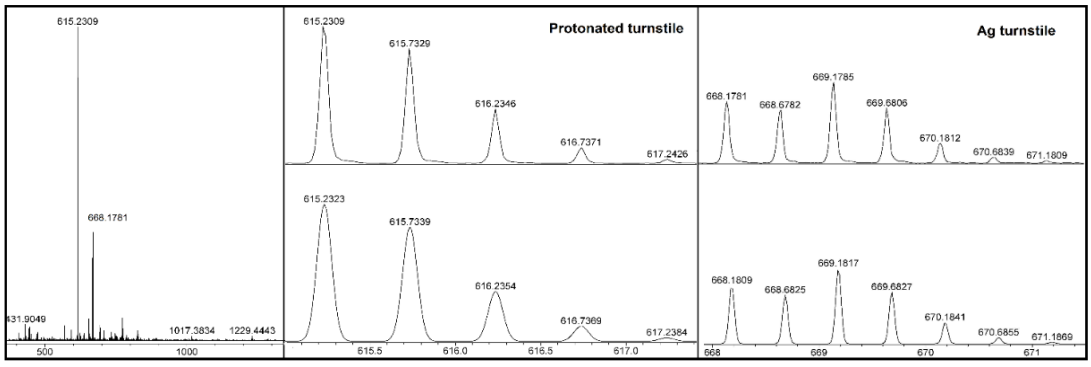


**Fig. 1.64** HR ESI spectrum of the turnstile#1 closed by $Ag^{+}$ cation.

### 4.1.3 2-D NMR investigation

2D ROESY and NOESY methods based on Nuclear Overhauser Effect (NOE) are powerful techniques to study spatial proximity of active centers even for non chemically bonded ones. Usually ROESY is applied for compounds with molar mass around 1000 g/mol. The molar mass of the turnstile#1 without silver and bromide counterion is 1310 g/mol. Thus both methods

NOESY and ROESY were used. Since the ROESY technique did not show any correlations, NOESY was used. It is worth noting that, in order to observe through space correlations, the maximum distance between the two interacting $^{1}H$ nuclei must be around 5Å.[49]

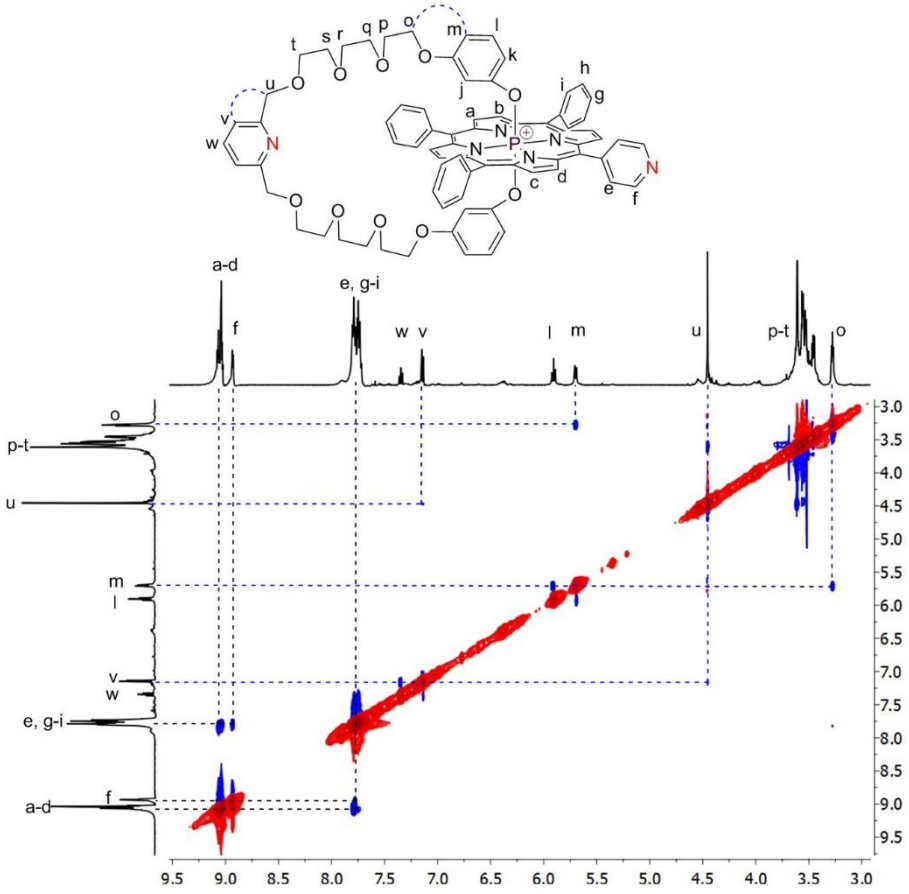


**Fig. 1.65** NOESY spectrum ($CD_3CN$, 500 MHz, 25 °C) of the open state of the turnstile#1.

Although Methanol-$d_4$ always contains residual water, in the 1D $^{1}H$-NMR spectra no overlap with turnstile#1 signals was observed. However, its presence leads to noisy 2D NOESY correlation maps. Therefore, correlations observed are rather weak and hidden due to high intensity water signal. Deuterated acetonitrile may overcome this shortcoming. Thus, the investigation was performed in acetonitrile-$d_3$. First, the turnstile in the absence of silver ions (open state) was analyzed **(Fig. 1.65)**. Several weak correlations were observed. The correlation between the porphyrin protons is marked with black dotted lines. β-pyrrolic protons show cross-peaks with both phenyl and pyridyl protons. Interactions between protons of pyridyl and phenyl moieties are also observed. Cross-peaks between *v* and *u*, *o* and *m* protons indicate through-space interactions in the handle. No specific correlations between the handle and the porphyrin were detected.

The closed state of the turnstile ($c=2.6\cdot10^{-3}M$) was investigated by the same technique. The analysis was performed in the presence of 3 equivalents AgOTf. Similar correlations, as for the open state of the turnstile, between the handle protons and porphyrin protons were detected. In addition to these correlations, other significant correlations have been observed **(Fig. 1.66)**.

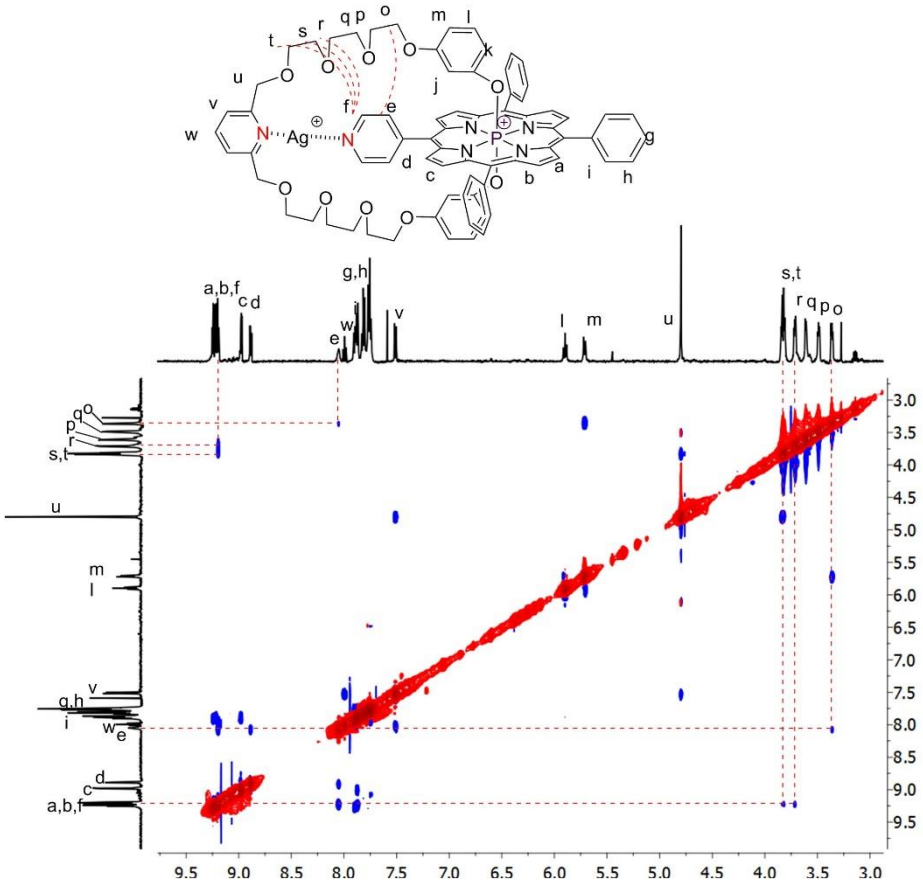


**Fig. 1.66** NOESY spectrum ($CD_3CN$, 500 MHz, 25 °C) of the closed form of the turnstile#1 in the presence of 3 equivalents of AgOTf.

Owing to the binding of $Ag^+$ cation, the rotation of the handle around the stator is blocked. The locking process imposes for the pyridyl group to be located between the two glycol chains of the handle. The rather short distance between them allows to detect $^1H$-$^1H$ through space correlations. Indeed *m*-pyridyl protons *f* being close to handle protons *s, t* and *r*, correlations between them are observed by NOESY investigation. Also *o*-pyridyl protons *e* show interactions with handle proton *o.* Thus observed correlations clearly demonstrate the closing of the turnstile by the silver cation.

### 4.1.4 Reversibility of the dynamic closing/opening process

From the previous experiments the following conclusions may be drawn:

- In the absence of the external stimulus, the handle freely rotates around the porphyrin (open state of the turnstile)
- In the presence of $Ag^+$ cation, the two pyridyl units bind the silver cation simultaneously leading thus the closed state of the turnstile as evidenced by 1D and 2D NMR techniques and ESI MS.

Since silver cations forms insoluble precipitates in the presence of halides, this feature, as previously exploited[2] was used to open the close state of the turnstile. Tetraethylammonium bromide ($Et_4NBr$) was used as the opening agent **(Fig. 1.67)**. The protocol used was the following.

Starting with the closed state of the turnstile generated by addition of two equivalents of AgOTf, two equivalents of $Et_4NBr$ is added. This procedure indeed leads to the open state of the turnstile. In order to regenerate the closed state, two equivalents of AgOTf is added. Four and a half opening-closing cycles were performed in methanol-$d_4$ and followed by $^1$H-NMR (400 MHz, 25 °C) **(Fig. 1.67)**. Although each cycle leads to the precipitation of AgBr, this had no influence on the quality of the NMR spectra.

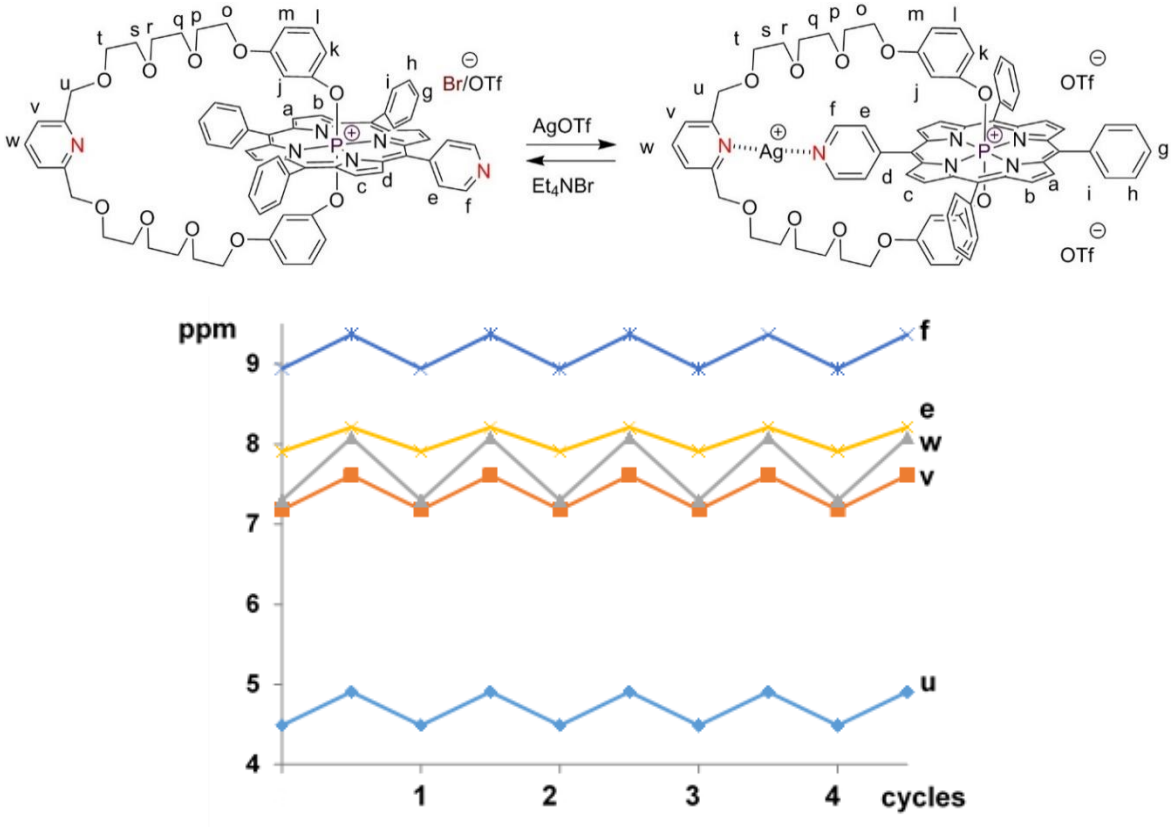


**Fig. 1.67** Selected protons chemical shifts for 4.5 "open-close" cycles.

Thus:

- The reversibility of the turnstile was demonstrated
- The molecular turnstile functions even after several cycles

## 4.2 The turnstile in the presence of triflic acid

### 4.2.1 1-D NMR investigations

Based on the design of the turnstile#1, i. e. the presence of two coordinating and basic pyridyl moieties, bearing, in stead of $Ag^+$ cation, one may use $H^+$ to lock the system **(Fig. 1.68)**. Owing to the presence of two pyridyl units (on the handle and on the stator), addition of one equivalent of a strong acid should lead to the monoprotonation of one of the two basic units, probably the pyridyl located on the handle. Further addition of acid should lead to the diprotonated derivative. Taking

into account the rather low basicity of the pyridyl moiety, the use of a strong acid is required. Thus, triflic acid, one of the strongest organic acids ($pK_a$= -12 in water[50]) was used.

The stepwise addition of the acid to the turnstile#1 in solution was monitored by $^1$H-NMR.

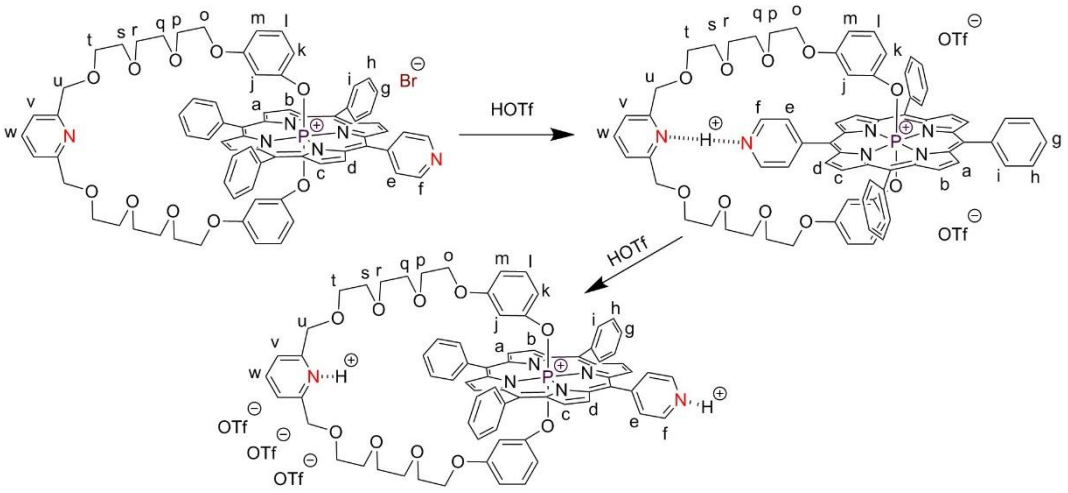


**Fig. 1.68** Proposed behaviour of the turnstile#1 in the presence of triflic acid.

The experiment was carried out in methanol-$d_4$ at room temperature ($c=2.6\cdot10^{-3}$M). HOTf was gradually added. Changes in the $^1$H-NMR spectrum were observed in the presence of 1 eq. of the acid. Two regions of the spectrum were analyzed (separately described bellow). The aromatic region (7.1-9.4 ppm) is presented in **Fig. 1.69**. In general, the behaviour is similar to the one observed when $Ag^+$ was used as the locking agent. However, 100% closing was only achieved in the presence of 8 equivalents of triflic acid. Further addition of HOTf did not lead to any change in the spectrum. We stopped the process after addition of 30 equivalents of the acid. Probably, by increasing the number of equivalent of acid, the second protonation could be reached although such large excess of acid could also lead to the decomposition of the turnstile.

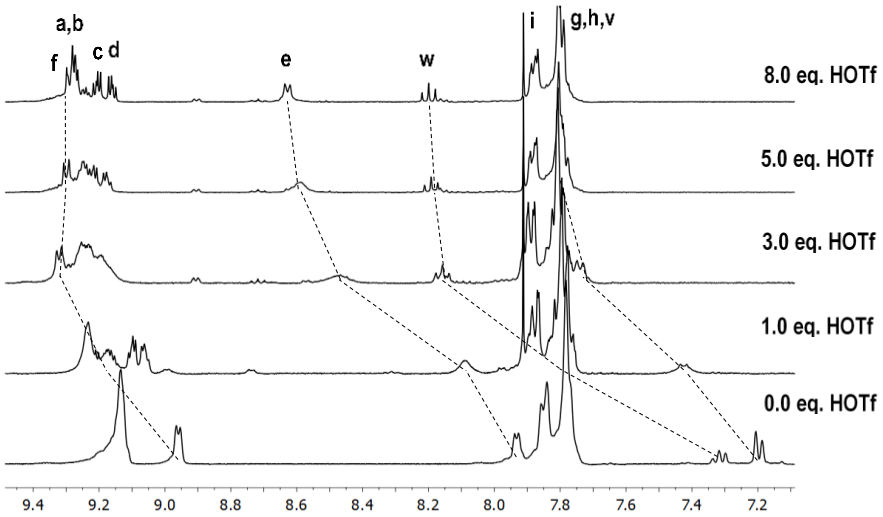


**Fig. 1.69** $^1$H-NMR (MeOD, 400 MHz, 25 °C) spectrum (7.1-9.5 ppm region) of the turnstile#1 in the presence of different equivalents of HOTf. Proton assignment is presented in **Fig. 1.68.**

The porphyrin pyridyl protons shifted downfield ($\Delta\delta(f)$ = 0.33 ppm, $\Delta\delta(e)$ = 0.70 ppm). The handle protons are also downfield shifted: $\Delta\delta(w)$ = 0.88 ppm, signal of proton *v* overlaps with the phenyl protons and cannot be identified after closing. Signals of β-pyrrolic protons are similar to those observed for the silver case: protons *a* and *b* appear as multiplets, protons *c* and *d* appear as two doublets of doublets ($^3J$ = 5.3 Hz, $^4J_{P\text{-}H}$ = 3.3). Although, signals of *a* and *b* protons should be two doublets of doublets, they overlap with signal of proton *f*. In the presence of acid, dramatic changes have been observed for the 3.3-5.0 ppm region containing resonances of protons of the glycol chains **(Fig. 1.70)**.

In the presence of 5 equivalents of triflic acid, the signal of protons *u* shifts downfield by 0.38 ppm. The final chemical shift cannot be determined because of the overlap with the water peak (due to the presence of acid in the tube, water signal changes its position). The broad and extended multiplet of *o-t* protons splits to five distinct multiplets. Every group of protons (*o, p, r, s* and *t)* displays separate signals. This is different from the silver locked system for which protons *t* and *s* show a broad and overlapped signal.

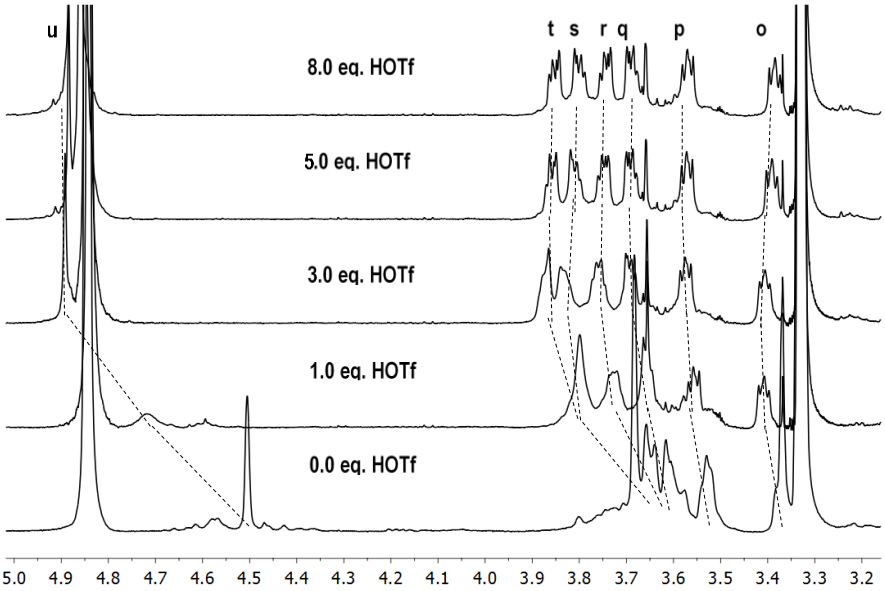


**Fig. 1.70** $^1$H-NMR (MeOD, 400 MHz, 25 °C) spectrum (3.3-5.0 ppm region) of the turnstile#1 in the presence of different equivalents of HOTf. Proton assignment is presented in **Fig. 1.68**.

We also carried out the experiment using higher concentrations ($c=9.8\cdot10^{-3}$) and found that to block the rotation, only 3 equivalents of HOTf was required.

The binding constant of the proton by the turnstile#1 leading to its closed state was also calculated using ChemEqui software. Signals of *e, u, t, s* protons were used for calculations. The obtained value is log K = 3.69 ± 0.06. The results obtained may be summarized as follows:

- The turnstile#1 can be closed using a proton (addition of HOTf)
- The closing process depends on the concentration of $H^+$

- Changes in the $^{1}$H-NMR spectrum are similar to those observed for locking with silver cation

### 4.2.2 2-D NMR investigations

2D NOESY NMR was recorded in the presence of 3 equivalents of HOTf ($c=9.8\cdot10^{-3}$) in acetonitrile-$d_3$. In general, correlations observed are similar to those previously observed in the case of silver cation **(Fig. 1.71)**.

As in the case of silver cation, the closing process by $H^+$ locks the rotation of the handle around the stator. Again, the pyridyl group should be placed between the two handle glycol chains. The *meta*-pyridyl proton *f* is located near the handle protons *s*, *t* and *r* as evidenced by the observation of correlations. Interestingly, several correlations between the glycol protons and the phenyl groups of porphyrin are detected. This may be due to the smaller size of proton (its radius is 0.31 pm *vs* 145 pm for $Ag^+$).

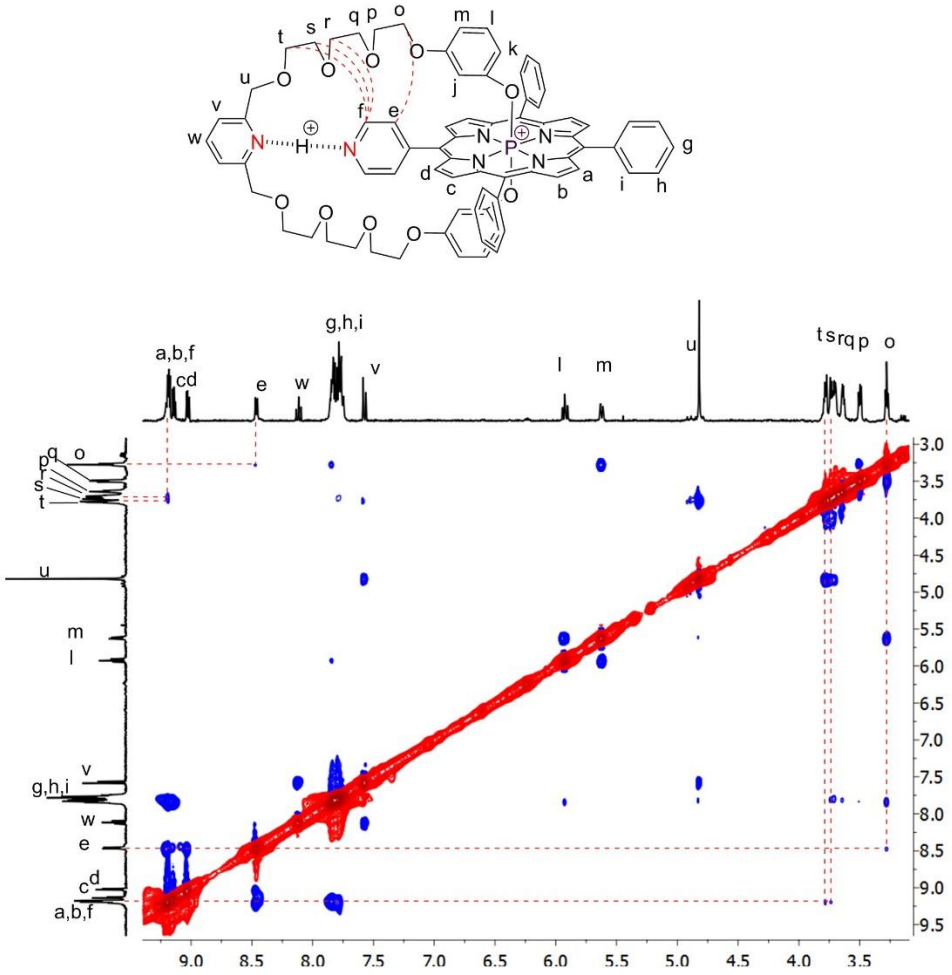


**Fig. 1.71** NOESY spectrum ($CD_3CN$, 400 MHz, 25 °C) of turnstile#1 in its closed state.

Furthermore, HR ESI investigations performed on the closed state of the turnstile showed, as expected, a peak corresponding to the protonated turnstile.

### 4.2.3 Reversibility of the locking/unlocking process

Starting from the open state of the turnstile, its closed state is generated by a proton through H-bonding between a protonated pyridyl, probably located on the handle, and the pyridyl moiety of the stator. In principle, the return to the open state should be possible upon addition of a base to deprotonate the pyridylium unit. This was indeed achieved using triethylamine ($Et_3N$) as a stronger base than pyridine. The experiment was carried out in methanol-$d_4$ at 25 °C ($c=9.8\cdot10^{-3}$ M, 400 MHz) **(Fig. 1.72)** and monitored *in situ* by NMR spectroscopy.

Starting with the closed state of the turnstile generated upon addition of 3 equivalents of HOTf, the reopening was achieved upon addition of 4 equivalents of $Et_3N$. The open state was investigated by NMR spectroscopy. The reclosing of the turnstile was achieved by addition of 2 equivalents of triflic acid. The experiment was pursued in a sequential manner by addition of 2 equivalents of base followed by 2 equivalents of acid. The opening/closing process of the turnstile#1 was found to be perfectly reversible (**Fig. 1.72**). After 4.5 cycles, the experiment was stopped.

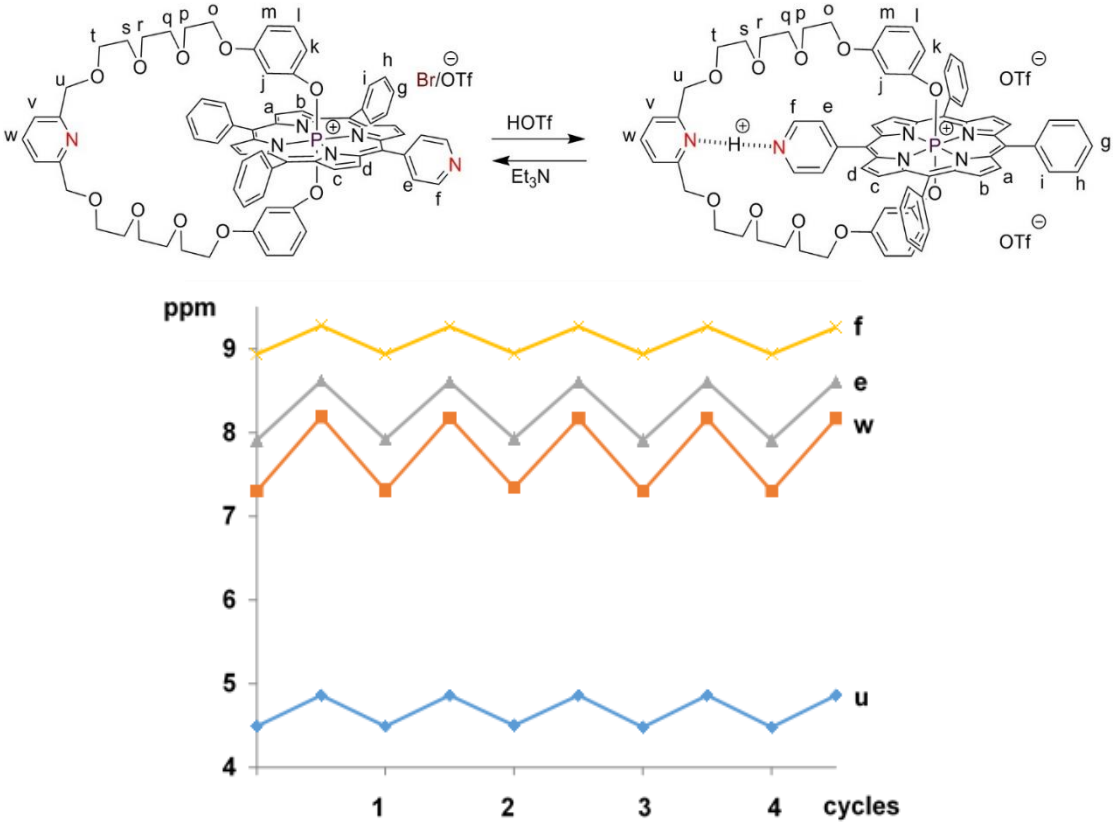


**Fig. 1.72** Selected protons chemical shifts of 4.5 "open-close" cycles.

Thus:

- the Acid/base reversibility of the closing and opening process was demonstrated
- Even after 4.5 cycles, the turnstile#1 was shown to be functional

### 4.3 Competition between $Ag^+$ and $H^+$ as closing agents

Competitions experiments between proton and silver cation was investigated **(Fig. 1.73)**. Two different experiments have been carried out:

- The turnstile (c = $7.6 \cdot 10^{-3}$ M, 400 MHz, MeOD, 25 °C) was first closed using 3 equivalents of triflic acid and then was titrated with AgOTf
- The turnstile (c = $7.6 \cdot 10^{-3}$ M, 400 MHz, MeOD, 25 °C) was closed using 1 equivalent of AgOTf (the initial counterion was already triflate one) and then it was titrated with HOTf

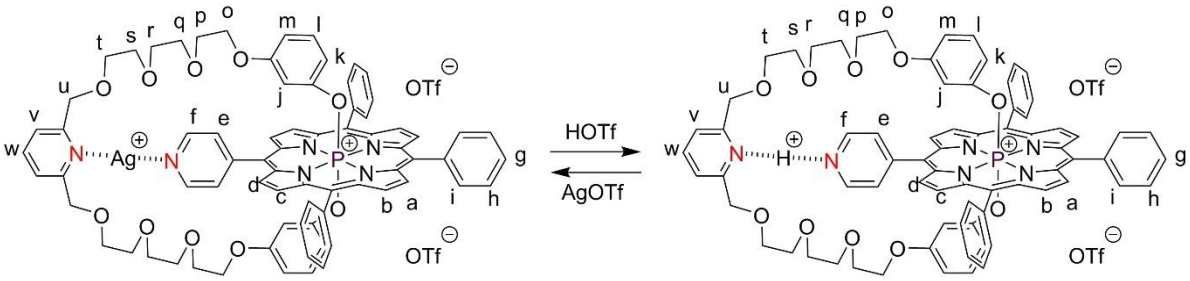


**Fig. 1.73** Competition between silver cation and proton.

Starting with the proton closed turnstile, the replacement of the proton by $Ag^+$ cation was achieved upon gradual addition of AgOTf and the process was monitored by $^1$H-NMR spectroscopy. Addition of one equivalent of AgOTf did not induce any change in the $^1$H-NMR spectrum **(Fig. 1.74)**. Further addition of silver triflate *i. e.* 17 equivalents leads to the silver closed turnstile. 3 eq. of triethylamine was added to neutralize the acid present.

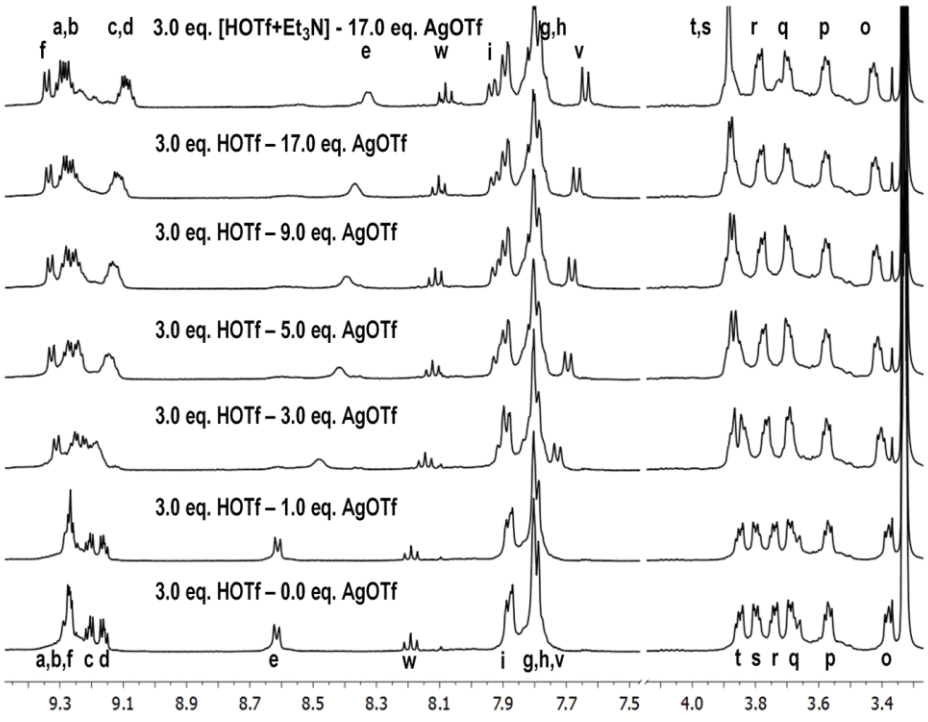


**Fig. 1.74** Portions of the $^1$H-NMR spectra for the competition experiment.

For the proton closed turnstile, protons *a, b* and *f* appeared as a multiplet. After addition of silver cation, the multiplet splits into *f* signal and *a*-*b* multiplet. Upon exchange of the locking agent, the handle signals *t* and *s*, appearing as two distinct signals for the proton locked species, became a broad signal. The signal corresponding to protons *v* was also shifted upon replacement of the proton by silver cation. The signal corresponding to *i* protons was splits into two signals with different intensities. The lower intensity signal corresponds to two *i* protons of the phenyl ring opposite to the pyridyl group located on the porphyrin. The higher intensity signal corresponds to the other two phenyl groups. Changes for the other characteristic signals have been also observed.

Although one would expect an easy replacement of the proton by the silver cation, nevertheless, a large excess (5:1 ratio) of silver triflate was required to substitute the protons. The reverse experiment was also carried out. Starting with the silver closed turnstile generated using 1 equivalent of AgOTf, stepwise addition of 9 equivalents of triflic acid was first performed and then one equivalent of $Et_4NBr$ was added to precipitate the silver cation. The reverse observations, when compared to the above mentioned competition experiment, were made **(Fig. 1.75)**.

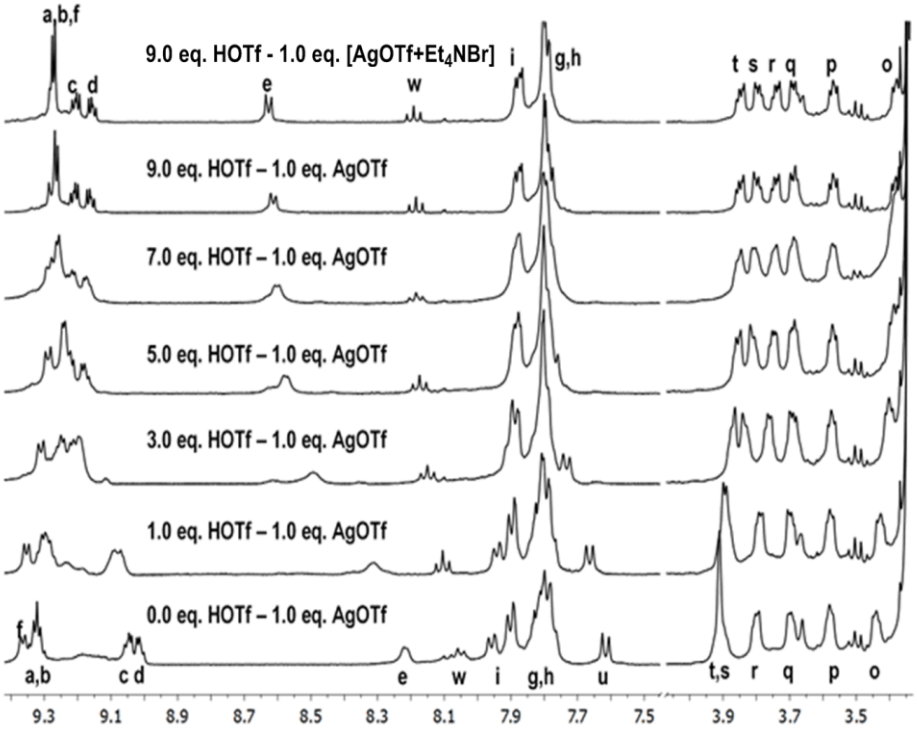


**Fig. 1.75** Portions of the $^1$H-NMR spectra for the competition experiments.

## 5. Conclusion of the chapter

In this chapter we described the synthetic pathways for the preparation of four different molecular turnstiles and studied their dynamic behaviour.

The synthesis of P(V) porphyrin derivatives was found to be delicate. We have prepared a model compound based on TPP derivatives. The syntheses of P(V) porphyrin bearing two monodentate axial ligands was achieved under reported standard conditions. However, the reaction with a bidentate handle#1 required to find specific conditions. Microwave synthesis was found to be effective. In case of Sn(IV) porphyrin based turnstile investigated previously in the group, it was possible to model the reactivity of the pyridyl bearing derivative MPyP using TPP. For P(V) porphyrin derivative, we observed large differences depending on the number of pyridyl substituents at the *meso* positions of the macrocycle. For the incorporation of the phosphorus atom into the cavity of the porphyrin, it was necessary to elaborate new method using shorter reaction time and lower amount of metallation agent. The new method was found to be effective for porphyrins that cannot be metallated by standard techniques. The number of pyridyl substituents on the porphyrin backbone was found to be crucial for axial ligands exchange. However, the method elaborated for the synthesis of the model turnstile#1 was found to be ineffective for the synthesis of the turnstile#1. In order to overcome this issue, another strategy was developed. The turnstile#1 bearing one pyridyl coordinating site was obtained and isolated.

The use of mild conditions for the connection of the handle to the porphyrin was investigated. A modified methods based on O-alkylation of the P(V) porphyrins was developed. Two turnstiles were prepared: the model turnstile #2 (without coordinating sites) and the turnstile#2 (with pyridyl group). Unfortunately, all attempts to isolate the pure products failed. The compounds prepared were found to be photo unstable and underwent decomposition during purification.

The turnstile#1 was finally successfully obtained and characterized by mass-spectrometry, 1D and 2D $^{1}$H-, $^{31}$P- and $^{13}$C-NMR techniques. The switching between the open and close states of the turnstile was investigated using silver cation as locking agent. The molecular turnstile#1 was shown to be stable. The dynamic opening/closing process was shown to be reversible. Interestingly, the closing of the turnstile using a proton was demonstrated using triflic acid. Furthermore, the dynamic reversible opening/closing process using acid (triflic acide)/base ($Et_3N$) was demonstrated.

Although our distant goal was to prepare P(V) porphyrin based turnstiles equipped with four stations at the *meso* positions, the synthetic difficulties as well as the reactivity of the phosphorous containing backbone, this was not achieved. Following this design principle seems currently illusive.

## 6. References


1 A. Guenet, *Un portail moléculaire basé sur une porphyrine à anse : synthèse, étude et premiers pas vers le développement de machines moléculaires*, Université de Strasbourg, 2007.

2 A. Guenet, E. Graf, N. Kyritsakas, L. Allouche and M. W. Hosseini, *Chem. Commun.*, 2007, 2935–2937.

3 A. Guenet, E. Graf, N. Kyritsakas and M. W. Hosseini, *Inorg. Chem.*, 2010, **49**, 1872–1883.

4 T. Lang, *Synthèse et caractérisation de machines moléculaires à base de porphyrines*, Université de Strasbourg, 2010.

5 T. Lang, A. Guenet, E. Graf, N. Kyritsakas and M. W. Hosseini, *Chem. Commun.*, 2010, **46**, 3508–3510.

6 A. Guenet, E. Graf, N. Kyritsakas and M. W. Hosseini, *Chem. Eur. J.*, 2011, **17**, 6443–6452.

7 T. Lang, E. Graf, N. Kyritsakas and M. W. Hosseini, *Dalt. Trans.*, 2011, **40**, 3517–3523.

8 T. Lang, E. Graf, N. Kyritsakas and M. W. Hosseini, *Dalt. Trans.*, 2011, **40**, 5244–5248.

9 T. Lang, E. Graf, N. Kyritsakas and M. W. Hosseini, *Chem. Eur. J.*, 2012, **18**, 10419–26.

10 N. Zigon, *Synthèse et étude de tourniquets moléculaires et conception de MOFs à base de Pt(II)*, Université de Strasbourg, 2013.

11 N. Zigon, A. Guenet, E. Graf and M. W. Hosseini, *Chem. Commun.*, 2013, **49**, 3637–3639.

12 T. Lang, E. Graf, N. Kyritsakas and M. W. Hosseini, *New J. Chem.*, 2013, **37**, 112.

13 N. Zigon, P. Larpent, A. Jouaiti, N. Kyritsakas and M. W. Hosseini, *Chem. Commun.*, 2014, **50**, 5040–5042.

14 N. Zigon, P. Larpent, A. Jouaiti, N. Kyritsakas and M. W. Hosseini, *Dalt. Trans.*, 2014, **43**, 15779–15784.

15 N. Zigon, N. Kyritsakas and M. W. Hosseini, *Dalt. Trans.*, 2014, **43**, 152–157.

16 N. Zigon and M. W. Hosseini, *Chem. Commun.*, 2015, **51**, 12486–12489.

17 P. Sayer, M. Gouterman and C. R. Connell, *J. Am. Chem. Soc.*, 1977, **99**, 1082–1087.

18 M. Gouterman, P. Sayer, E. Shankland and J. P. Smith, *Inorg. Chem.*, 1981, **20**, 87–92.

19 Y. Yamamoto, R. Nadano, M. Itagaki and K. Akiba, *J. Am. Chem. Soc.*, 1995, **117**, 8287–8288.

20 A. Yamamoto, W. Satoh, Y. Yamamoto and K. Akiba, *Chem. Commun.*, 1999, **6**, 147–148.

21 K. Y. Akiba, R. Nadano, W. Satoh, Y. Yamamoto, S. Nagase, Z. Ou, X. Tan and K. M.

Kadish, *Inorg. Chem.*, 2001, **40**, 5553–5567.

22 C. J. Carrano and M. Tsutsui, *J. Coord. Chem.*, 1977, **7**, 79–83.

23 C. A. Marrese, C. J. Carrano, V. For, E. Section, C. A. Marrese, C. J. Carrano, V. For and E. Section, *Inorg. Chem.*, 1983, **22**, 1858–1862.

24 K. Susumu, K. Tanaka, T. Shimidzu, Y. Takeuchi and H. Segawa, *J. Chem. Soc. Perkin Trans. 2*, 1999, 1521–1529.

25 M. P. Gajewski and L. Czuchajowski, *Cent. Eur. J. Chem.*, 2004, **2**, 446–455.

26 K. Hirakawa, N. Fukunaga, Y. Nishimura, T. Arai and S. Okazaki, *Bioorganic Med. Chem. Lett.*, 2013, **23**, 2704–2707.

27 S. Mangani, E. F. Meyer, D. L. Cullen, M. Tsutsui and C. J. Carrano, *Inorg. Chem.*, 1983, **22**, 400–404.

28 A. A. Ryan, M. M. Ebrahim, R. Petitdemange, G. M. Vaz, E. Paszko, N. N. Sergeeva and M. O. Senge, *Photodiagnosis Photodyn. Ther.*, 2014, **11**, 510–515.

29 J. K. M. Sanders, N. Bampos, Z. Clyde-Watson, S. L. Darling, J. C. Hawley, H.-J. Kim, C. C. Mak and S. J. Webb, in *The porphyrin handbook. Volume 3. Inorganic, Organometallic and Coordination Chemistry*, 2000, pp. 3–40.

30 M. O. Breusova, V. E. Pushkarev and L. G. Tomilova, *Russ. Chem. Bull. Int. Ed.*, 2007, **56**, 1456–1460.

31 T. Barbour, W. J. Belcher, P. J. Brothers, C. E. F. Rickard and D. C. Ware, *Inorg. Chem.*, 1992, **31**, 746–754.

32 T. A. Rao and B. G. Maiya, *Inorg. Chem.*, 1996, **35**, 4829–4836.

33 S. J. Langford, M. A. P. Lee, K. J. Macfarlane and J. A. Weigold, *J. Incl. Phenom. Macrocycl. Chem.*, 2001, **41**, 135–139.

34 Y.-H. Lin, M.-T. Sheu, C.-C. Lin, J.-H. Chen and S.-S. Wang, *Polyhedron*, 1994, **13**, 3091–3097.

35 P.-C. Cheng, I.-C. Liu, T.-N. Hong, J.-H. Chen, S.-S. Wang, S.-L. Wang and J.-C. Lin, *Polyhedron*, 1996, **15**, 2733–2740.

36 Y.-H. Lin, S.-S. Tang, C.-C. Lin, J.-H. Chen, W.-F. Zeng, S.-S. Wang and H.-J. Lin, *Aust. J. Chem.*, 1995, **48**, 1367–1372.

37 V. V. Namboodiri and R. S. Varma, *Tetrahedron Lett.*, 2002, **43**, 1143–1146.

38 A. B. Chopa, G. F. Silbestri and M. T. Lockhart, *J. Organomet. Chem.*, 2005, **690**, 3865–3877.

39 W. L. F. Armarego and C. L. L. Chai, *Purifcation of Organic Chemicals*, 2009.

40 B. L. Hayes, *Microwave Synthesis. Chemistry at the Speed of Light*, 2002.

41 Y. G. Gorbunova, A. G. Martynov and A. Y. Tsivadze, *Handb. Porphyr. Sci.*, 2012, 271–

388.

42 K. Kunimoto, H. Segawa and T. Shimidzu, *Tetrahedron Lett.*, 1992, **33**, 6327–6330.

43 Y. Andou, K. Ishikawa, K. Shima, T. Shiragami and M. Yasuda, *Bull. Chem. Soc. Jpn.*, 2002, **75**, 1757–1760.

44 J. Matsumoto, T. Kubo, T. Shinbara, N. Matsuda, T. Shiragami, M. Fujitsuka, T. Majima, M. Yasuda, *Bull. Chem. Soc. Jpn.*, 2013, **86**, 1240–1247.

45 L. Carlucci, G. Ciani, D. M. Proserpio and F. Porta, *Angew. Chemie Int. Ed.*, 2003, **42**, 317–322.

46 E. Bosch and C. L. Barnes, *Inorg. Chem.*, 2001, **40**, 3234–3236.

47 *http://www.vpsolovev.ru/programs/*.

48 V. P. Solov'ev, V. E. Baulin, N. N. Strakhova, V. P. Kazachenko, V. K. Belsky, A. A. Varnek, T. A. Volkova and G. Wipff, *J. Chem. Soc. Trans. 2*, 1998, 1489–1498.

49 G. Englert, *Pure Appl. Chem.*, 1991, **63**, 59–70.

50 E. Raamat, K. Kaupmees, G. Ovsjannikov, A. Trummal, A. Kütt, J. Saame, I. Koppel, I. Kaljurand, L. Lipping, T. Rodima, V. Pihl, I. A. Koppel and I. Leito, *J. Phys. Org. Chem.*, 2013, **26**, 162–170.

# Chapter II. Phosphorus (V) Porphyrins: Photochemical Properties

# Contents


1. Introduction 79

2. Photophysical properties of P(V) porphyrins 84

2.1 P(V) porphyrins as photosensitizers 84

2.2 Photophysical properties of P(V) porphyrins in chloroform 85
2.2.1 Experimental setup#1 85
2.2.2 Singlet oxygen generation measurements 86
2.2.3 Fluorescence measurements 88

2.3 Photophysical properties of P(V) porphyrins in DMSO 90
2.3.1 Singlet oxygen generation measurements 90
2.3.2 Fluorescence measurements 91

2.4 Photophysical properties of phosphorus porphyrins in aqueous solutions 93
2.4.1 Experimental setup#2 93
2.4.2 Singlet oxygen generation measurements 93
2.4.3 Fluorescence measurements 95

2.5 Electronic structure of aryloxy-complexes 96

3. Application of P(V) porphyrins in photocatalysis 98

3.1 Experiment description 98

3.2 Photooxidation of hydroquinone 99

4. Conclusions of the chapter 100

5. References 102

# 1. Introduction

In the first chapter, we suggested that the instability of some of P(V) porphyrins was due to their photoreactivity. Most probably it arises from generation of singlet oxygen by this type of porphyrins. Their behaviour was studied more precisely. In this chapter, we describe some photochemical properties of P(V) porphyrins. The role played by the nature of substituents and axial ligands was investigated.

The porphyrins are highly-colored compounds that possess strong absorptions in two main spectral regions. Bands localized near 400 nm are called the Soret bands. The second series of bands, called Q bands, are localized between 500-750 nm. The latter are several times less intensive than the Soret band ($\log\varepsilon$(Soret) = ~5; $\log\varepsilon$(Q) = ~4). The specific features of porphyrin's UV-vis absorption spectra were described by Martin Gouterman[1,2] with four-orbital model. According to this model **(Fig. 2.1)**, electronic transitions occur between two HOMOs and two LUMOs orbitals. LUMOs were identified as two degenerated $e_g$ orbitals; HOMOs are represented as $a_{1u}$ and $a_{2u}$ orbitals. Transitions between these orbitals afford two excited states. The transition pair to LUMO+1 gives rise to the Soret band (or B band). The transition pair to LUMO leads to Q bands.

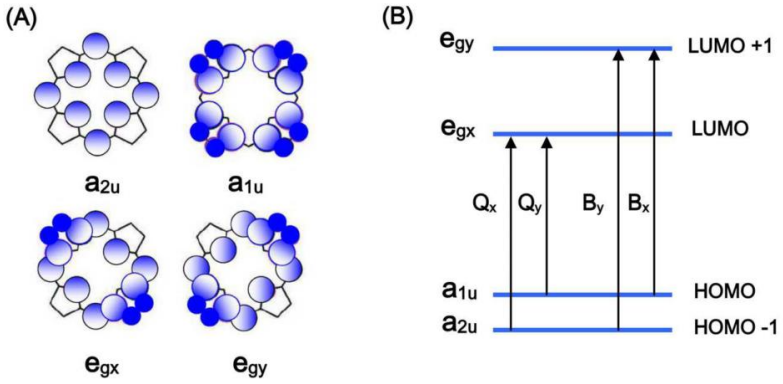


**Fig. 2.1** Gouterman 4-orbital model.

Hence, a strong Soret band corresponds to both $B_x$ and $B_y$ transitions. Since it corresponds to the LUMO+1 level, it may be called $S_0$-$S_2$ transition. Due to the small energy difference, the Soret band usually appears as one strong peak. Lower energy of $Q_x$ and $Q_y$ transitions corresponds to Q bands resulting from electronic transition to first excited state ($S_0$-$S_1$). A standard free-base porphyrin such as $H_2$TPP displays a $D_{2h}$ symmetry. Thus $Q_x$ and $Q_y$ transitions appear as four different Q bands[3] **(Fig. 2.2)**. Two of them correspond to 0-0 $Q_x$ and $Q_y$ 0-0 transitions. Two supplementary bands appear in case of 0-1 processes.

Metallated, deprotonated and diprotonated porphyrins possess $D_{4h}$ symmetry. Hence, generally only two Q-bands are observed. Indeed, insertion of metal ion (Zn(II) for example) into the porphyrin cavity leads to only two Q bands in the spectrum **(Fig. 2.3)**.

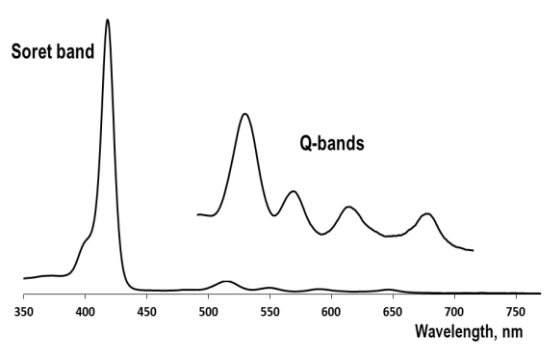


**Fig. 2.2** Typical UV-vis spectrum of a free-base porphyrin.

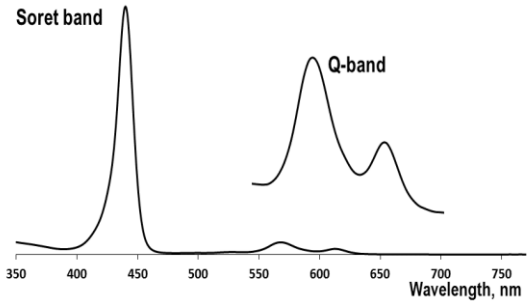


**Fig. 2.3** Typical UV-vis spectrum of a metallated porphyrin.

Relaxation processes of porphyrins are well documented[4] and depend on the nature of the porphyrin ring and the metal centre. Several main photophysical relaxation processes take place. Two types of fluorescence are observed ($S_2$-$S_0$ and $S_1$-$S_0$). $S_2$ state usually rapidly transfer into $S_1$, but $S_2$-$S_0$ transition can be detected and described.[5] Usually, fluorescence is observed in 650-800 nm spectral range and corresponds to $S_1$-$S_0$ transitions.

Another pathway for relaxation of absorbed energy in porphyrins is non-radiative processes. The efficiency of this pathway also strongly depends on the porphyrin nature. The residual energy participates in intersystem crossing processes. Due to this process, an energy transfer to the triplet state of porphyrin occurs **(Fig. 2.4)**. In the absence of oxygen, the porphyrin energy relaxes either by phosphorescence or by non-radiative pathways.

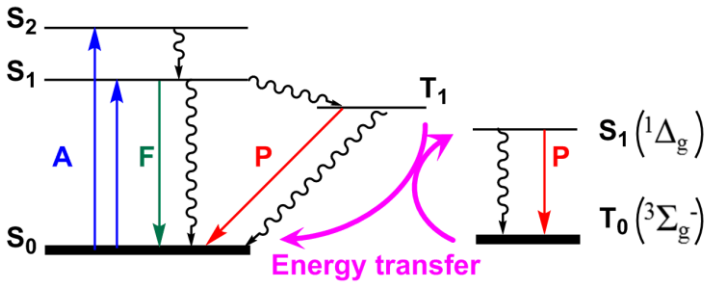


**Fig. 2.4** Jablonski diagram of energy transitions in porphyrins and oxygen: A - absorption, F - fluorescence, P – phosphorescence.

Under normal conditions, oxygen exists in its triplet state. Thus, if the porphyrin triplet state is located close to the oxygen triplet state, the energy transfer occurs. The efficiency of this process

depends on $T_1$ energy and lifetime. Several factors such as porphyrin substituents, metal center in the cavity or solvent influence the process.

Under usual conditions, $O_2$ molecule is paramagnetic. The term used for this stable form is $^3\Sigma_g^-$. The electronic structure of the molecule is represented in the **Fig. 2.5**. It can be excited into the singlet state by forbidden electronic transition. Molecular oxygen displays two lowest singlet states: $^1\Delta_g$ and $^1\Sigma_g^+$. $^1\Delta_g$ state is relatively long-lived since the transition to the triplet state is spin forbidden. $^1\Sigma_g^+$ state has an extremely short lifetime ($10^{-11}$-$10^{-9}$s in the solution in contrast with the $^1\Delta_g$ state (lifetime of $10^{-6}$-$10^{-3}$s)).[6–9] This $^1\Delta_g \rightarrow {}^3\Sigma_g^-$ transformation leads to a very weak phosphorescence at 1268.7 nm[10] which may be used as a direct method for detection of singlet oxygen. There is another possibility to detect the generation of singlet oxygen. The latter is based on the use of chemical traps, photosensitive compounds capable of reacting with singlet oxygen.[11–19]

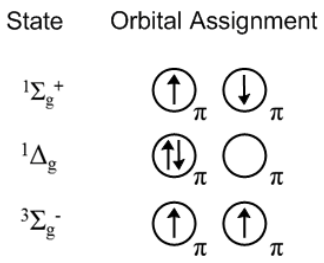


**Fig. 2.5** Representation of singlet and triplet oxygen states.

The singlet oxygen can be generated by either by chemical or photochemical processes. The first method is based on degradation of hydrogen trioxide[20] or reaction of hydrogen peroxide with sodium hypochlorite.[21] We will not focus on that pathway. The second possibility is based on the use of photosensitizers. This method is simple and controllable and requires only the oxygen molecule. This process requires the use of photons with appropriate wavelength, and a photosensitizer capable of exciting the oxygen molecule from its triplet to its singlet state. In order to promote the energy transfer from $T_1$ to $^3O_2$ leading to the excited $^1\Delta_g$, photosensitizer molecules must possess high quantum yields and the lifetime of the $T_1$ state must be longer (ms) than that of the $S_1$ state (ns). In fact, there are two competitive mechanisms of interactions between the photosensitizer molecule and oxygen. The type I mechanism involves hydrogen atom abstraction or electron-transfer between the excited sensitizer and a substrate yielding free radicals. These radicals can react with $O_2$ leading to the formation of "superoxide" anion radical $O_2^{\cdot-}$. It should be noted that superoxide is very reactive species. The type II mechanism proceeds only through energy transfer with formation of the $^1\Delta_g$ state. This pathway is presented in Jablonski diagram (**Fig. 2.4)**.

The photosensitizers efficiency could be evaluated by the quantum yield of singlet oxygen generation, defined as

$$\Phi_{\Delta}=\Phi_{T}\Phi_{transfer}$$

where $\Phi_T$ is quantum yield of photosensitizer triplet state generation and $\Phi_{transfer}$ the efficiency of energy transfer. Direct determination of these values is quite difficult. Usually the photosensitizer with known singlet oxygen quantum yield is used as a reference. The photophysical values for the investigated compound (with unknown quantum yield) and the reference are measured under the same conditions. The quantum yield is calculated by comparison of collected data. Using a special equipment, the phosphorescence of the singlet oxygen can be observed at 1268.7 nm. By comparison of the integral intensities of detected phosphorescence peaks the singlet oxygen quantum yield can be calculated. Another possibility to detect the presence of singlet oxygen and to calculate the quantum yield of its generation, may be based on the use of chemical traps. The trap must react specifically with singlet oxygen. The chemical traps may be separated into two groups: water-soluble and soluble in organic solvents (such as toluene, chloroform *etc*).

The most commonly used trap is 1,3-diphenylisobenzofuran (DPBF).[22] It can be used in non-aqueous media since it is only soluble in organic solvents. DPBF absorbs in the violet part of the spectrum ($\lambda_{max}$ = 417 nm). The reaction of DPBF with single oxygen leads to the disruption of furan ring (**Fig. 2.6)**. Since the oxidation process leads to colorless products, the bleaching of the solution indicates the presence of singlet oxygen. DPBF is photosensitive and should not be irradiated in the 410-420 nm range. In addition to the rather simplicity of its structure and its commercial availability, DPBF offers other advantages: it does not react with $^3O_2$ and superoxide; it reacts solely with singlet oxygen (there is no physical quenching of $^1\Delta_g$).[11] The photochemical behaviour of DPBF in the presence of photosensitizer was described.[15] The pathway of DPBF oxidation was also determined and described.[15]

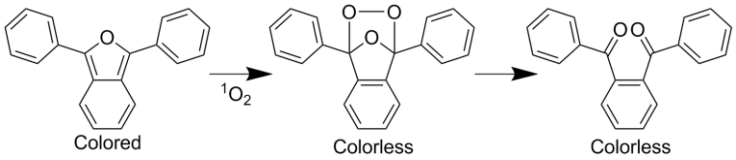


**Fig. 2.6** The reaction between DPBF and singlet oxygen.

As we already stated, DPBF is insoluble in water. Many water-soluble chemical traps are also known.[11,14,17,18,19] Mostly, they include an anthracene core sensitive to singlet oxygen and react with $^1O_2$ to yield endoperoxides **(Fig. 2.7)**.

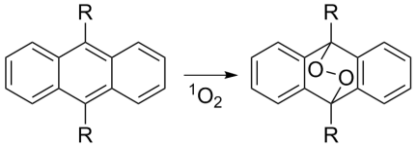


**Fig. 2.7** Singlet oxygen reaction with anthracene derivatives as chemical traps.

Water-soluble traps have been extensively investigated.[19] Simple traps such as furfuryl alcohol or 2,5-dimethylfuran shows low selectivity and thus cannot be used as efficient singlet oxygen traps. Naphthalene, anthracene and tetracene water-soluble derivatives show better results. However, these compounds are usually anionic species. Indeed, the commercially available anionic ADMA (antracene-9,10-bis-methylmalonate) **(Fig. 2.8**) is the most commonly used water-soluble trap. A cationic ammonium based trap (*bis*-9,10-anthracene-(4-trimethylphenylammonium) dichloride - BPAA) was described.[18]

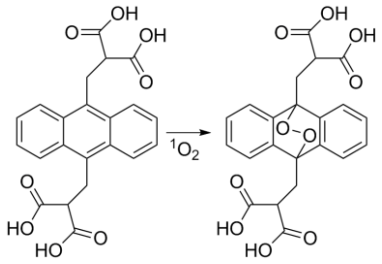


**Fig. 2.8** Water soluble trap ADMA reacts with singlet oxygen.

The commercially available Singlet Oxygen Sensor Green (SOSG) (**Fig. 2.9**.) is another trap used for singlet oxygen detection using.

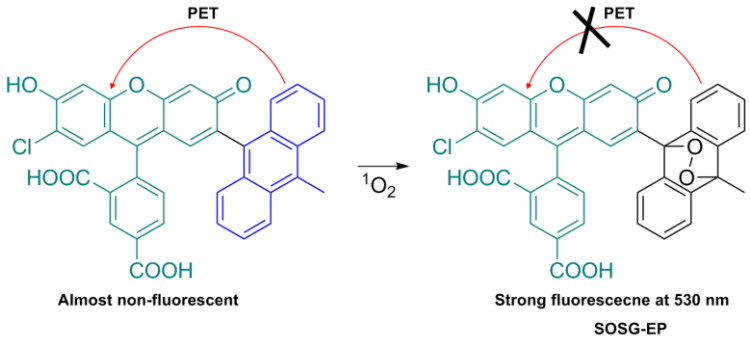


**Fig. 2.9** Formation of SOSG endoperoxide in the presence of singlet oxygen.

The SOSG molecule contains both a fluorescein and an anthracene moieties. Under irradiation, a photoinduced electron transfer (PET) occurs between anthracene and fluorescein and a weak fluorescence band at ~540 nm is observed (**Fig. 2.10,** red dashed line).

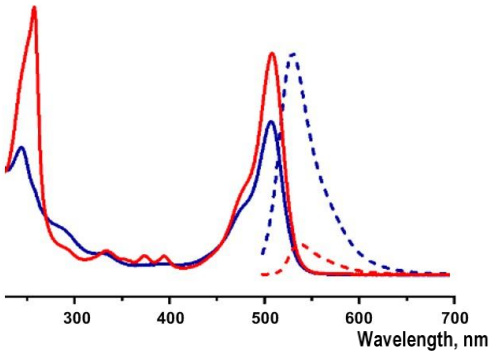


**Fig. 2.10** Normalized absorption (solid lines) and emission spectra (dashed lines, $\lambda_{ex}$ = 465 nm) of SOSG (red) and SOSG-EP (blue).[13]

In the presence of singlet oxygen, the anthracene core forms an endoperoxide leading to the quenching of PET in the molecule and fluorescein moiety shows an intensive fluorescence at 530 nm (**Fig. 2.10,** blue dashed line). The SOSG behaviour was described precisely by Majima group.[13] SOSG was applied to biological studies to determine the presence of singlet oxygen in cells[12] or to quantitatively control its quantum yield.[16] We also used SOSG for the determination of singlet oxygen quantum yield determination in this work.

Photosensitizers can be divided into two groups based on their stability in the presence of singlet oxygen. Instable compounds undergo self oxidation.

Concerning the photosensitive properties of P(V) porphyrins,[23–27] mainly their interaction with biological systems was investigated. DNA damage under visible irradiation in the presence of P(V) porphyrins was reported.[23,25] Protein damages in the presence of P(V) porphyrins under irradiation was also decribed.[24] Two probable mechanisms were proposed: electron transfer and oxidation by generation of active oxygen species. The latter mechanism was shown to be the predominant one. It is worth noting that, the reported studies were based on the use of tetraphenylporphyrin or similar symmetric P(V) derivatives. The quantum yields of singlet oxygen generation were also determined. The value of 0.28 was reported for $[P(TPP)(OH)_2]^+$ in ethanol.[25] The singlet oxygen was detected through its phosphorescence at 1270 nm. Two other contributions reported a quantum yield of 0.62-0.73 for the generation of singlet oxygen by phosphorus porphyrin derivatives (axially substituted alkoxy-complexes) in water.[24,26]

Within the framework of this thesis, we have undertaken an investigation of the two series of phosphorus porphyrins: TPP and MPyP differing by the nature of the axial ligands, the role played by the solvent. It should be mentioned that whereas the turnstile#1 is stable and can be isolated, the P(V) porphyrin bearing an aryloxy axial ligands behaves differently.

## 2. Photophysical properties of P(V) porphyrins

### 2.1 P(V) porphyrins as photosensitizers

In the first chapter we described the synthetic efforts to prepare P(V) porphyrin based turnstiles. Attempts to synthesize and isolate turnstile#2 and the model turnstile#2 were unsuccessful. These compounds undergo decomposition either during the purification procedure or directly in the solid state. Here we proposed that their instability is due to the photoreactivity of P(V) porphyrin core in the presence of oxygen. To prove this hypothesis, comparative photochemical experiments were carried out in the presence and in the absence of oxygen. Two solutions of $[P(MPyP)(OEt)_2]^+$ in chloroform were prepared. One of them was left for 4.5 h under laboratory UV lamp (BioBlock Scientific VL-4C, 254 nm) irradiation in an open vessel. The second one was bubbled with argon for 15 min and then irradiated for 4.5 h in a closed vessel. Both samples were monitored by UV-

Vis spectroscopy during the irradiation. The solution of the first sample was almost bleached (**Fig. 2.11**) under irradiation for 4.5 h, whereas for the second sample no change of the UV-vis spectrum was observed.

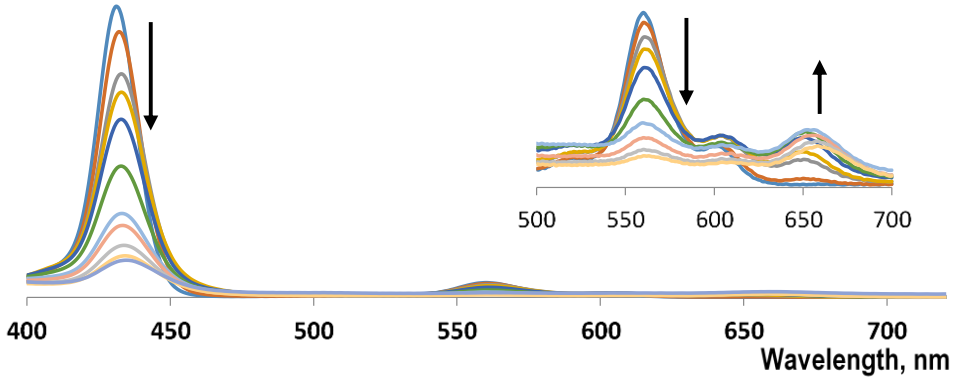


**Fig. 2.11** Photobleaching of $[P(MPyP)(OEt)_2]^+$ chloroform solution under UV-irradiation in air.

It can be deduced that $O_2$ is involved in the decomposition process under the irradiation. Moreover, keeping the solution of the first sample (open vessel) in the dark does not lead to rapid bleaching of the porphyrin. Thus, we can propose that the decomposition of our series of P(V) porphyrins is due to the formation of singlet oxygen under irradiation and its reaction with the porphyrin macrocycle. Based on these experiments, the P(V) porphyrins ((TPP or MPyP) prepared were systematically studied. The role played by the axial ligands (hydroxide, chloride, ethoxide or phenolate) and the solvent ($CHCl_3$, DMSO and water) was investigated.

## 2.2 Photophysical properties of P(V) porphyrins in chloroform

### 2.2.1 Experimental setup#1

As described above, two main methods based on observation of phosphorescence at 1268.7 nm or the use of a chemical traps may be employed to detect singlet oxygen generation. We used the standard method using DPBF as a trap. The experimental setup#1 depicted in **Fig. 2.12** was designed and constructed.

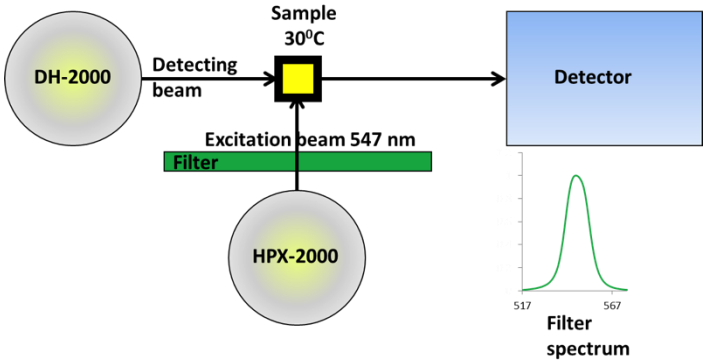


**Fig. 2.12** Experimental setup#1 for singlet oxygen detection.

All parts of the device are connected by optic fibers thus allowing to configure the setup for every particular purpose. In this case, a Xenon lamp (HPX-2000, Ocean Optics) was used as an irradiation source. The setup#1 was equipped with a narrow green filter (transmission maximum at 547 nm). This wavelength corresponds to the absorption band of the porphyrin in the first Q band region. Orthogonally, a halogen lamp (DH-2000, Ocean Optics) was connected to the cell containing the sample and the detector was installed in the opposite site. For decreasing the beam intensity an attenuator was used. The sample was placed into the 4-side quartz transparent cell, thermostated at 30 $^{o}$C and equipped with a magnetic stirrer. All samples were measured in an open vessel. Freshly distilled chloroform (over $CaH_2$) was used for all measurements. The solution was not degassed nor extra bubbled with air (or oxygen). The oxygen concentration in the solution is close to literature reported data 0.742 mole fraction at 30 $^{o}$C and 100 kPa.[28]

The sample was irradiated by the Xenon beam passed through the green filter. Simultaneously, a low intensity halogen lamp beam (modulated by the attenuator) covering the visible region was passed through the sample and analysed by the detector. The UV-Vis spectrum was recorded every 50 ms using this device, however, in the majority of cases spectra were recorded every 1-10 sec. Each sample was prepared in 2.4 ml of chloroform. The concentration of the porphyrin was ~$10^{-6}$ corresponding to intensity of Soret band ~ 1. 7 µl of a 0.017 M DPBF solution in chloroform was added. The DPBF concentration in the sample was thus $5 \cdot 10^{-5}$ M corresponding to *ca* 1 order excess of the trap.

### 2.2.2 Singlet oxygen generation measurements

Two series of P(V) porphyrins (TPP and MPyP) were chosen and for each, four different complexes were studied: $[P(TPP)Cl_2]^+$, $[P(TPP)(OH)_2]^+$, $[P(TPP)(OEt)_2]^+$, $[P(TPP)(OPhOMe)_2]^+$; $[P(MPyP)Cl_2]^+$, $[P(MPyP)(OH)_2]^+$, $[P(MPyP)(OEt)_2]^+$, $[P(MPyP)(OPhOMe)_2]^+$. All compounds were passed through Bio-Beads S-X3 column to remove all impurities formed during the storage. For each compound, experiments were carried out at least twice.

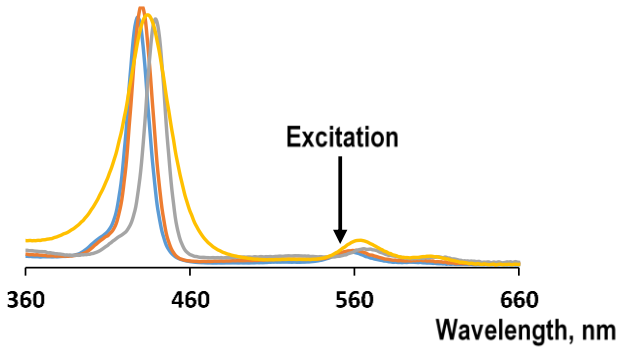


**Fig. 2.13** UV-Vis absorption spectra of $[P(MPyP)(OH)_2]^+$ (blue), $[P(MPyP)(OEt)_2]^+$ (orange), $[P(MPyP)Cl_2]^+$ (grey) and $[P(MPyP)(OPhOMe)_2]^+$ (yellow) in chloroform at room temperature.

The absorption spectra of P(V) MPyP complex in chloroform is similar to spectra of P(V)TPP complex (**Fig. 2.13**). $H_2TPP$ was applied as a standard. The quantum yield of the singlet oxygen generation in chloroform for $H_2TPP$ is $\Phi = 0.50$.[29]

The equation **1** was used for calculation of the singlet oxygen generation quantum yield. $\Phi$,$\Phi_{st}$ are quantum yields; R, $R_{st}$ are DPBF bleaching rates; I, $I_{st}$ are integral light absorptions for the samples and for the standards respectively:

$$\Phi = \Phi_{st} \frac{RI_{st}}{R_{st}I} \qquad (1)$$

The absorption spectrum of the DPBF solution is presented in the **Fig. 2.14a**. In most cases, the overlap of the porphyrin and the trap spectra is observed after addition of a DPBF solution into the sample (**Fig. 2.14b)**, except for $[P(TPP)Cl_2]^+$ for which two different peaks (417 nm and 440 nm) were observed (**Fig. 2.14c)**.

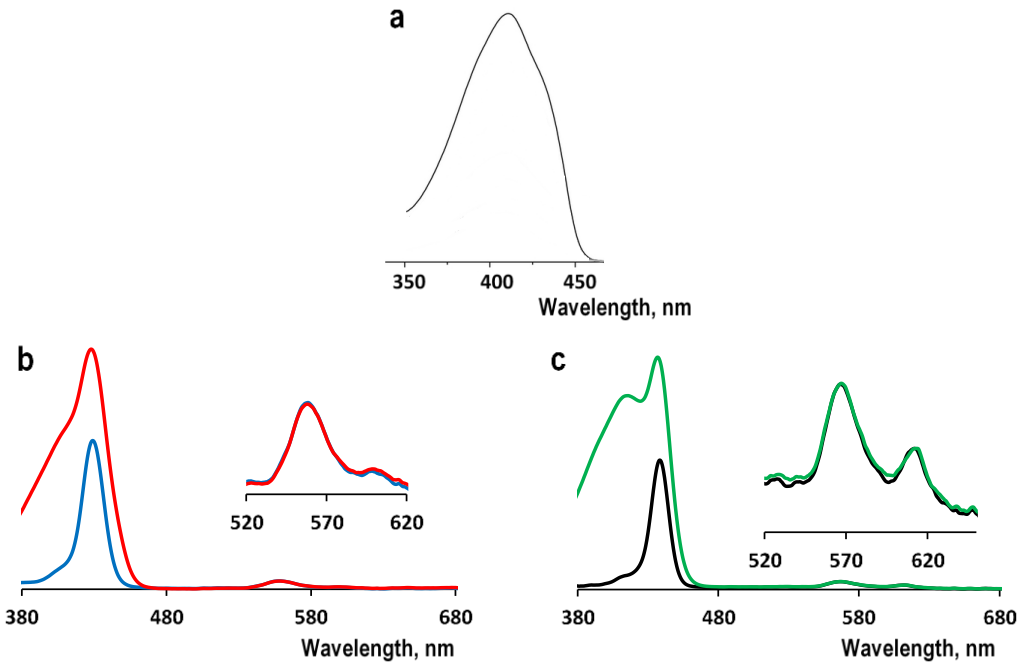


**Fig. 2.14** UV-Vis absorption spectra of a) DPBF solution in chloroform; b) $P(MPyP)(OEt)_2]^+$ (blue), mixed with DPBF (red) and c) $[P(TPP)Cl_2]^+$ (black), mixed with DPBF (green) solutions at 30 °C in chloroform.

The irradiation of the sample at 547 nm induces the decrease of the intensity of the "overlapped peak" (**Fig. 2.15**). After complete bleaching of DPBF, the spectrum corresponds to the spectrum of porphyrin. Thus, for further calculation we focused on the "overlapped peak" located at 425-430 nm corresponding to the porphyrin Soret band and the DPBF bands. The plot of the intensity of the peak against time displays a linear dependence of the DPBF bleaching (**Fig. 2.15**). The appearance of an invariable behaviour after 2000 s indicates the completion of DPBF bleaching and the presence of the porphyrin in solution.

In the case of $[P(TPP)Cl_2]^+$, two different peaks are observed (**Fig.12b**) and the process was monitored directly by the decrease of the intensity of the peak (417 nm) of DPBF.

Data are given in **table 2.1**. Although this method leads to large experimental errors, since all data were collected under similar conditions, their comparison reliable.

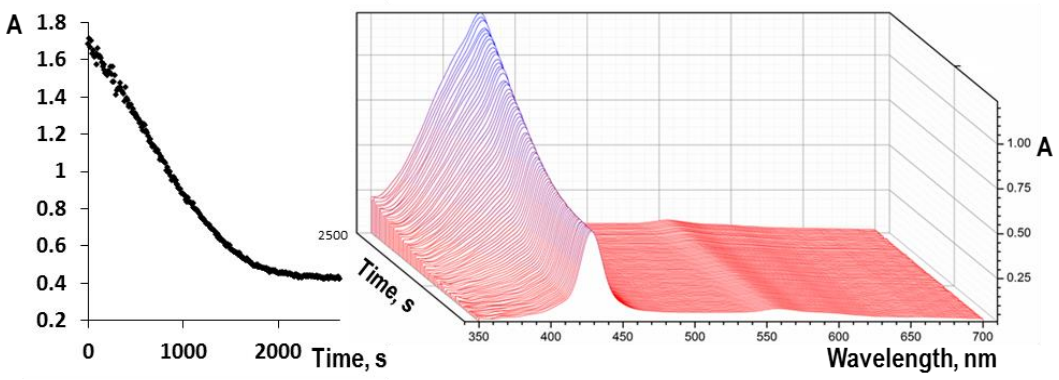


**Fig. 2.15** Plot of DPBF + $[P(MPyP(OEt)_2]^+$ peak (428 nm) bleaching *vs* time in chloroform at 30 $^oC$ (left) and changes of the UV-Vis spectra with time (right).

The P(V)TPP derivatives leads to an increase in the quantum yield of the singlet oxygen generation. The following trend was determined: $[P(TPP)(OPhOMe)_2]^+ < [P(TPP)(OH)_2]^+ < [P(TPP)(OEt)_2]^+ < [P(TPP)Cl_2]^+$. The same sequence holds for P(V)MPyP however values are *ca* 10-20% higher. Such high values indicate very weak fluorescence for almost all the investigated complexes. On the other hand, the complexes with aryloxy axial ligands ($[P(TPP)(OPhOMe)_2]^+$ and $[P(MPyP)(OPhOMe)_2]^+$) leads to extremely low quantum yields when compared to the other complexes (the explanation is given below).

**Table 2.1** Singlet oxygen generation quantum yields of P(V) porphyrins in chloroform.

| Name | $\Phi_\Delta$ |
|---|---|
| $[P(TPP)(OH)_2]^+$ | 0.73 |
| $[P(TPP)(OEt)_2]^+$ | 0.77 |
| $[P(TPP)Cl_2]^+$ | 0.93 |
| $[P(TPP)(OPhOMe)_2]^+$ | 0.19 |
| $[P(MPyP)(OH)_2]^+$ | 0.99 |
| $[P(MPyP)(OEt)_2]^+$ | 0.99 |
| $[P(MPyP)Cl_2]^+$ | 1.00 |
| $[P(MPyP)(OPhOMe)_2]^+$ | 0.16 |

### 2.2.3 Fluorescence measurements

The fluorescence of the complexes was measured at room temperature in freshly distilled chloroform. $H_2TPP$ was chosen as a standard ($\Phi = 0.11$ in toluene).[30] All samples, excited at 550 nm, showed fluorescence in the 620 and 700 nm range corresponding to $S_1$-$S_0$ transition with

characteristic Stokes shifts (**Fig. 2.16)**. P(V)TPP spectra are similar and not presented. During the fluorescence measurements, excitation spectra were also recorded; the similarity of excitation spectra with absorption ones indicated the purity of complexes studied.

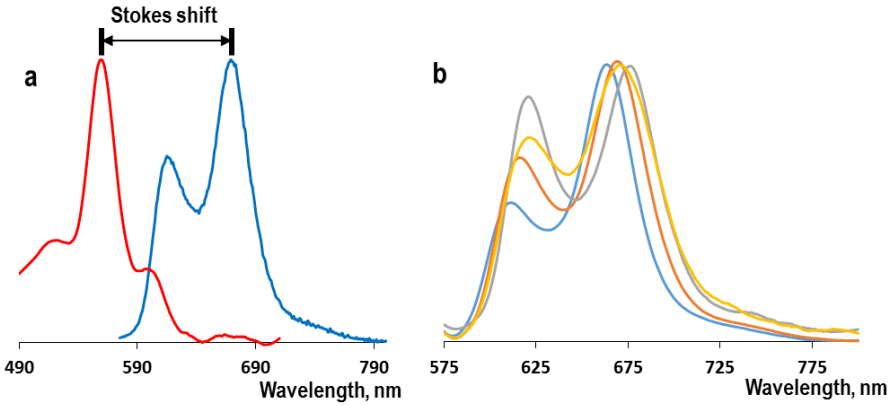


**Fig. 2.16** (a) Comparison of normalized absorption (red) and emission (blue) spectra of $[P(MPyP(OEt)_2]^+$ complex in chloroform ($\lambda_{ex}$ = 550 nm),
(b) fluorescence spectra ($\lambda_{ex}$ = 550 nm) of $[P(MPyP)(OH)_2]^+$ (blue), $[P(MPyP)(OEt)_2]^+$ (orange), $[P(MPyP)Cl_2]^+$ (grey), $[P(MPyP)(OPhOMe)_2]^+$ (yellow) complexes in chloroform at room temperature.

Quantum yields of fluorescence were calculated using **equation 2:**

$$\Phi = \Phi_{st} \frac{FA_{st}n^2}{F_{st}An_{st}^2} \qquad (2)$$

where $\Phi$, $\Phi_{st}$ are fluorescence quantum yields; F, $F_{st}$ are the areas under the fluorescence emission curves; A, $A_{st}$ are absorption values at excitation wavelength (550 nm); n, $n_{st}$ are refractive indices for the samples and for standard solvent respectively.

As presented in **table 2.2**, P(V) the fluorescence quantum yields of porphyrins studied are small. The lowest value (less than 1%) is observed for the aryloxy complexes. The data collected is in good correlation with literature reported for similar P(V)TPP complexes.[31]

**Table 2.2** Photophysical data of P(V) porphyrins in chloroform.

| Name | $\lambda_F$, nm | $\Phi_F$ | Stokes shift, nm |
|---|---|---|---|
| $[P(TPP)(OH)_2]^+$ | 609, 664 | 0.027 | 106 |
| $[P(TPP)(OEt)_2]^+$ | 610, 663 | 0.036 | 106 |
| $[P(TPP)Cl_2]^+$ | 622, 677 | 0.014 | 109 |
| $[P(TPP)(OPhOMe)_2]^+$ | 619, 672 | 0.009 | 107 |
| $[P(MPyP)(OH)_2]^+$ | 611, 663 | 0.029 | 107 |
| $[P(MPyP)(OEt)_2]^+$ | 616, 669 | 0.060 | 110 |
| $[P(MPyP)Cl_2]^+$ | 621, 676 | 0.012 | 110 |
| $[P(MPyP)(OPhOMe)_2]^+$ | 621, 671 | 0.005 | 107 |

A low fluorescence quantum yield implies an efficient intersystem crossing (ISC) for P(V) porphyrins. The photochemical behaviour of $[P(TPP)(OH)_2]^+$ complex in ethanol was described by A. Harriman in 1983.[31] It was stated that 80% of absorbed energy is engaged in ISC for the generation of triplet state.

Based on the above mentioned investigations, several conclusions may be drawn:

- the P(V) porphyrins are efficient photosensitizers in chloroform
- their behaviour as photosensitizers depends on the *meso*-substituents of the porphyrin backbone as well as on the axial ligands
- complexes with aryloxy axial ligands display low fluorescence quantum yields as well as singlet oxygen generation propensity
- potentially, these series of compounds may be used as photosensitizers in photodynamic therapy (PDT) due to their solubility in water
- additional flash-photolysis experiments should be performed for better understanding of the energy transfer processes in these complexes.

## 2.3 Photophysical properties of P(V) porphyrins in DMSO

### 2.3.1 Singlet oxygen generation measurements

Using DPBF as the chemical trap, the same experimental setup described above for measurements in $CHCl_3$ was used in the case of DMSO as the solvent. All techniques and concentrations were also identical. DMSO ($t_{melt}$=18.5 $^oC$) was frozen in the fridge (+6 $^oC$) and the excess of water was removed, the procedure was repeated until no liquid was detected. Residual solid DMSO was melted and used for the measurements. DMSO was chosen since it is nontoxic and widely applied in medicine. Furthermore, potential compounds for PDT were tested in this solvent.[32] All porphyrin derivatives prepared, $[P(TPP)Cl_2]^+$, $[P(TPP)(OH)_2]^+$, $[P(TPP)(OEt)_2]^+$, $[P(TPP)(OPhOMe)_2]^+$; $[P(MPyP)Cl_2]^+$, $[P(MPyP)(OH)_2]^+$, $[P(MPyP)(OEt)_2]^+$, and $[P(MPyP)(OPhOMe)_2]^+$, were studied. Absorption spectra of MPyP complexes in DMSO are represented at **Fig. 2.17**.

Again, $H_2TPP$ was used as the standard. The literature data for singlet oxygen generation quantum yield for $H_2TPP$ in DMSO varies between 5% and 50%[33,34] depending on the oxygen concentration. Thus, we remeasured the quantum yield of $H_2TPP$ in DMSO using the same technique as for P(V) porphyrins in chloroform and calculated a $\Phi_\Delta$ value of 17%. Taking this into account, we calculated the $\Phi_\Delta$ for all prepared complexes in DMSO. Calculations were made using the **Equation 1** and the data are presented in **table 2.3**.

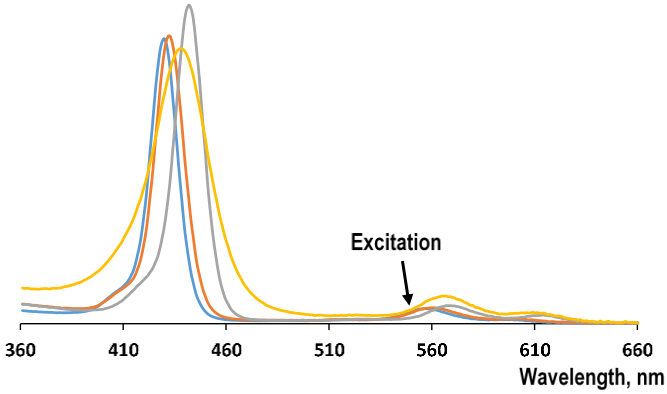


**Fig. 2.17** UV-Vis absorption spectra of $[P(MPyP)(OH)_2]^+$ (blue), $[P(MPyP)(OEt)_2]^+$ (orange), $[P(MPyP)Cl_2]^+$ (grey) and $[P(MPyP)(OPhOMe)_2]^+$ (yellow) complexes in DMSO at room temperature.

**Table 2.3** Singlet oxygen generation quantum yields of P(V) porphyrins in DMSO.

| Name | $\Phi_\Delta$ |
|---|---|
| $[P(TPP)(OH)_2]^+$ | 0.24 |
| $[P(TPP)(OEt)_2]^+$ | 0.34 |
| $[P(TPP)Cl_2]^+$ | 0.36 |
| $[P(TPP)(OPhOMe)_2]^+$ | 0.00 |
| $[P(MPyP)(OH)_2]^+$ | 0.31 |
| $[P(MPyP)(OEt)_2]^+$ | 0.37 |
| $[P(MPyP)Cl_2]^+$ | 0.40 |
| $[P(MPyP)(OPhOMe)_2]^+$ | 0.00 |

In the presence of DPBF, $[P(TPP)(OPhOMe)_2]^+$ and $[P(MPyP)(OPhOMe)_2]^+$ complexes did not lead to any bleaching in DMSO solution.

The dramatic decrease in the quantum yield upon switching from chloroform to DMSO may be due to the presence of higher number of hydrogen atoms in DMSO responsible for the quenching of singlet oxygen.[35–37] Interestingly, MPyP complexes are more effective than TPP with the following sequence (OPhOMe) < (OH) < (OEt) < Cl. The lower quantum yields in DMSO when compared to chloroform may be also explained by the lower stability of chloroform under irradiation. Indeed, the decomposition leads to the formation of radicals which could promote the destruction of the trap.

### 2.3.2 Fluorescence measurements

As in chloroform, the fluorescence experiments were performed at room temperature and under irradiation at $\lambda_{ex}$ = 550 nm. Complexes studied again displayed fluorescence in the 620-700 nm range with characteristic Stokes shifts (**Fig. 2.18).**

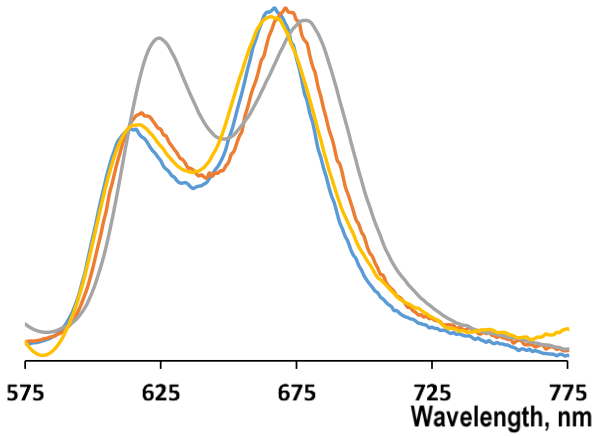


**Fig. 2.18** Fluorescence spectra ($\lambda_{ex}$ = 550 nm) of $[P(MPyP)(OH)_2]^+$ (blue), $[P(MPyP)(OEt)_2]^+$ (orange), $[P(MPyP)Cl_2]^+$ (grey), $[P(MPyP)(OPhOMe)_2]^+$ (yellow) complexes in DMSO at room temperature.

The fluorescence quantum yields were calculated using the Equation 2 and values are given **table 2.4**.

**Table 2.4.** Photophysical data for P(V) porphyrins in DMSO.

| Name | $\lambda_{Fmax}$, nm | $\Phi_F$ | Stokes shift, nm |
|---|---|---|---|
| $[P(TPP)(OH)_2]^+$ | 614, 667 | 0.126 | 109 |
| $[P(TPP)(OEt)_2]^+$ | 614, 666 | 0.125 | 109 |
| $[P(TPP)Cl_2]^+$ | 625, 679 | 0.016 | 111 |
| $[P(TPP)(OPhOMe)_2]^+$ | 618, 668 | 0.005 | 103 |
| $[P(MPyP)(OH)_2]^+$ | 612, 667 | 0.119 | 110 |
| $[P(MPyP)(OEt)_2]^+$ | 618, 671 | 0.104 | 111 |
| $[P(MPyP)Cl_2]^+$ | 624, 678 | 0.029 | 111 |
| $[P(MPyP)(OPhOMe)_2]^+$ | 617, 666 | 0.006 | 100 |

The fluorescence quantum yield increases dramatically for complexes with ethoxy and hydroxy axial ligands when compared to values obtained in chloroform. Very weak fluorescence was observed for the chloro and aryloxy porphyrin derivatives. Excitation spectra were found to be similar to absorption spectra.

The following conclusions may be drawn:

- the solvent has a substantial influence on the photochemical properties of P(V) porphyrins
- quantum yield values for singlet oxygen generation are higher in chloroform in contrast to fluorescence quantum yields

- complexes with aryloxy as axial ligands do not generate singlet oxygen in DMSO
- since P(V) porphyrins may be of interest for PDT studied, experiments in aqueous solution must be carried out

## 2.4 Photophysical properties of phosphorus porphyrins in aqueous solutions

### 2.4.1 Experimental setup#2

The setup of the spectrometer had to be changed due to the use of SOSG. In setup#1, the sample was irradiated at 547 nm but this is no longer possible due to the possible overlap with the emission peak of SOSG at 530 nm. Thus, the Xenon lamp was replaced by a violet diode laser with wavelength of 405 nm (STAR405F10, Roithner Laser Technik). This laser excites both the porphyrin core and SOSG. Since we detect the emission of SOSG, the setup does not require the second light source. The scheme of the fiber-optic spectrometer is presented in **Fig. 2.19.**

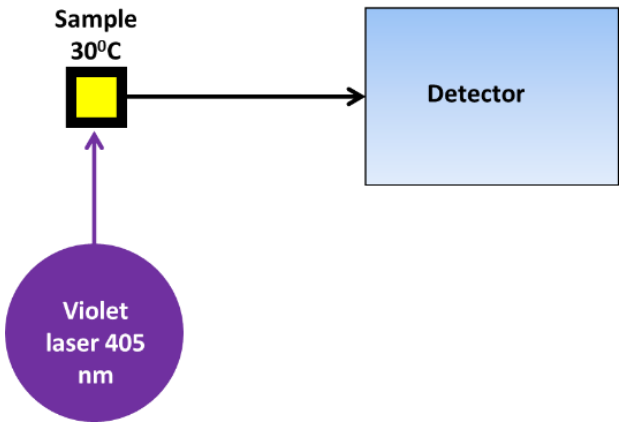


**Fig. 2.19** Experimental setup#2 for singlet oxygen determination in aqueous solutions using SOSG.

The sample was stirred at 30 ˚C. Only stirrers covered with Teflon can be used because of strong oxidation power of the solution. The detector connected was orthogonally placed to measure the emission.

### 2.4.2 Singlet oxygen generation measurements

An increase in the number of *meso*-pyridyl substituents on P(V) porphyrins enhances their solubility in water. The Free-base $H_2$TPP porphyrin is totally insoluble in water and cannot be used as a standard. The water-soluble 5,10,15,20-tetra(4-sulfophenyl)porphyrin ($H_2$TSP) was thus used. Its singlet oxygen generation quantum yield is reported to be 0.64.[38] All absorption spectra were recorded **(Fig. 2.20)**.

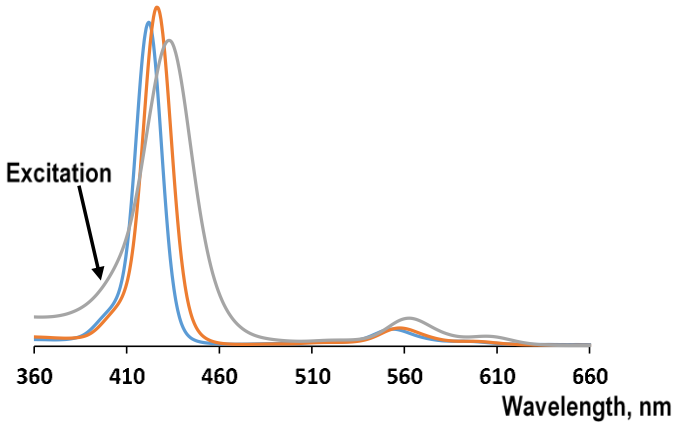


**Fig. 2.20** UV-Vis absorption spectra of $[P(MPyP)(OH)_2]^+$ (blue), $[P(MPyP)(OEt)_2]^+$ (orange) and $[P(MPyP)(OPhOMe)_2]^+$ (grey) complexes in distilled water at room temperature.

Since $[P(TPP)Cl_2]^+$ and $[P(MPyP)Cl_2]^+$ complexes are easily hydrolyzed in water, they were not studied. Thus only six P(V) porphyrin derivatives were investigated.

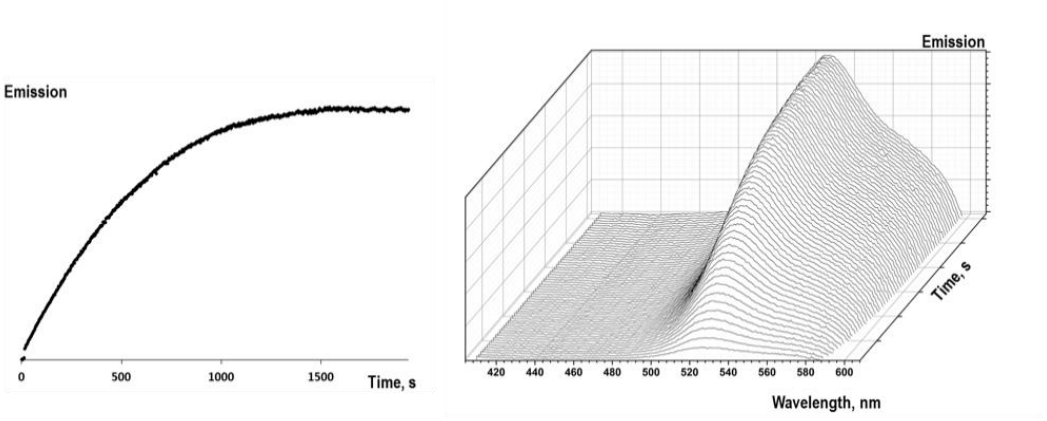


**Fig. 2.21** Plot of SOSG-EP emission increase at 530 nm *vs* time.

For calculations, the emission peak rate increase of SOSG was used. Only the linear part was considered. Plot of the emission at 530 nm against time is presented in **Fig. 2.21** and the data are given in **table 2.5**.

**Table 2.5** Singlet oxygen generation quantum yields of P(V) porphyrins in water.

| Name | $\Phi_\Delta$ |
|---|---|
| $[P(TPP)(OH)_2]^+$ | 0.11 |
| $[P(TPP)(OEt)_2]^+$ | 0.12 |
| $[P(TPP)(OPhOMe)_2]^+$ | 0.00 |
| $[P(MPyP)(OH)_2]^+$ | 0.25 |
| $[P(MPyP)(OEt)_2]^+$ | 0.46 |
| $[P(MPyP)(OPhOMe)_2]^+$ | 0.00 |

Trends observed in $CHCl_3$ and DMSO are again observed in water. Indeed, the photosensitizing efficiency of MPyP is higher than the one observed for TPP complexes, and the difference is even more pronounced in water than in organic solvents. $\Phi_\Delta$ for $[P(TPP)(OH)_2]^+$ and $[P(TPP)(OEt)_2]^+$ is only 0.11 and 0.12 respectively, whereas the values obtained for the corresponding MPyP are 0.25 and 0.46 respectively. The $[P(TPP)(OPhOMe)_2]^+$ and $[P(MPyP)(OPhOMe)_2]^+$ complexes did not generate any singlet oxygen in water.

The investigated P(V) porphyrins are stable in the aqueous environment even in the absence of SOSG. After 12 h of irradiation of $[P(TPP)(OH)_2]^+$, $[P(TPP)(OEt)_2]^+$, $[P(MPyP)(OH)_2]^+$, $[P(MPyP)(OEt)_2]^+$ at 405 nm, no solution bleaching was observed.

### 2.4.3 Fluorescence measurements

For fluorescence experiments, we used the same conditions and protocol as for experiments carried out in chloroform ($\lambda_{ex}$ = 550 nm, room temperature). The fluorescence spectra of TPP or MPyP complexes were found to rather similar, the fluorescence spectra of the MPyP series is given in **Fig. 2.22.**

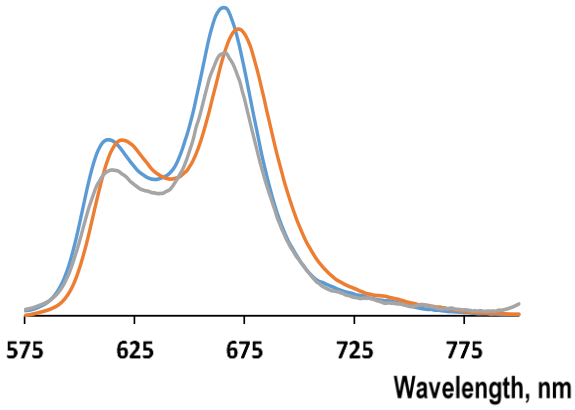


**Fig. 2.22** Fluorescence spectra ($\lambda_{ex}$ = 550 nm) of $[P(MPyP)(OH)_2]^+$ (blue), $[P(MPyP)(OEt)_2]^+$ (orange), $[P(MPyP)(OPhOMe)_2]^+$ (grey) complexes in water at room temperature.

**Table 2.6** Photophysical data of P(V) porphyrins in water.

| Name | $\lambda_{Fmax}$, nm | $\Phi_F$ | Stokes shift, nm |
|---|---|---|---|
| $[P(TPP)(OH)_2]^+$ | 614, 667 | 0.119 | 112 |
| $[P(TPP)(OEt)_2]^+$ | 621, 673 | 0.073 | 115 |
| $[P(TPP)(OPhOMe)_2]^+$ | 619, 671 | 0.008 | 107 |
| $[P(MPyP)(OH)_2]^+$ | 614, 667 | 0.113 | 113 |
| $[P(MPyP)(OEt)_2]^+$ | 618, 674 | 0.083 | 117 |
| $[P(MPyP)(OPhOMe)_2]^+$ | 616, 667 | 0.007 | 104 |

Data determined for all studied complexes are presented in **table 2.6.** In general, complexes with ethoxy and hydroxy axial ligands display fluorescence quantum yields of *ca* 10%, the hydroxy complex is slightly more efficient.

The following conclusions and trends may be drawn:

- P(V) porphyrins are efficient photosensitizers in water
- the efficiency of singlet oxygen generation and the fluorescence dramatically depends on:
  - the axial ligands with the following sequence Cl> OEt>OH>>OAr
  - the nature of the porphyrin substituents: MPyP better than TPP
  - the solvent: $CHCl_3$ better than DMSO or $H_2O$
- since P(V) porphyrins are water-soluble, they may be used for PDT
- P(V) porphyrins may be also used for photocatalysis (see part 3 of this chapter)
- Complexes with aryloxy axial ligands display different behaviour, an attempt to explain this difference is presented in the following part .

## 2.5 Electronic structure of aryloxy-complexes

$[P(TPP)(OPhOMe)_2]^+$ and $[P(MPyP)(OPhOMe)_2]^+$ complexes show specific photophysical features when compared to other P(V) porphyrins. Indeed, they display extremely low fluorescence and singlet oxygen generation quantum yields. Since, these complexes were used for the design of turnstiles (see chapter I), we tried to find an explanation for their peculiar properties.

Similar compounds with pyrene moieties in axial positions were described previously.[39] Owing to presence of the phosphorus atom in the cavity, the porphyrin ring is an electron acceptor. On the other hand, aromatic axial ligands are electron donors. For the pyrene complex described, since the energy of the HOMOs of the pyrene ligands is higher than the one of the porphyrin, a photoinduced electron transfer is expected. Upon excitation of the complex, 3 possible pathways for electron and energy transfer were described (**Fig. 2.23)**.

After excitation of the pyrene absorption band (337 nm), two possible processes (2 and 3) were found to occur. It was shown that in case of connection of the aromatic axial ligand directly to O-P group, only the process 2 (oxidative electron transfer) takes place. Upon excitation of the porphyrin moiety, the process 1 occurs. Both processes 1 and 2 lead to the formation of "charge-transferred" state of porphyrin for which the electron from the pyrene moiety is transferred to the porphyrin. This electron transfer leads to the quenching of the fluorescence as depicted in **Fig. 2.23**. Similar complexes based on phosphorus – N-containing axial aromatic ligands were also described[40] and PET from axial aromatic ligands to porphyrin ring was also observed.

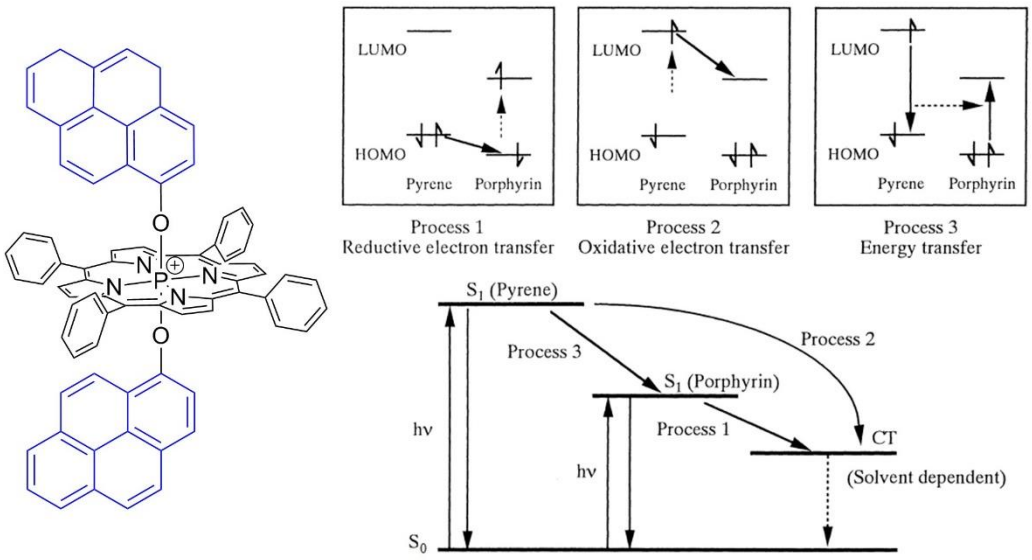


**Fig. 2.23** Pyrene substituted P(V) porphyrin and possible relaxation processes in the molecule.

We suggest that similar phenomenon could occur in P(V) complexes with aryloxy axial ligands described in this manuscript. According to the literature data, we may propose an electron transfer from the phenyl ring to porphyrin core. To prove this hypothesis, we performed quantum chemical calculations using the Spartan'14 software (Wavefunction Inc., CA, USA) with B3LYP(6-31G*) basic set for $[P(MPyP)(OPhOMe)_2]^+$ complex (**Fig. 2.24**).

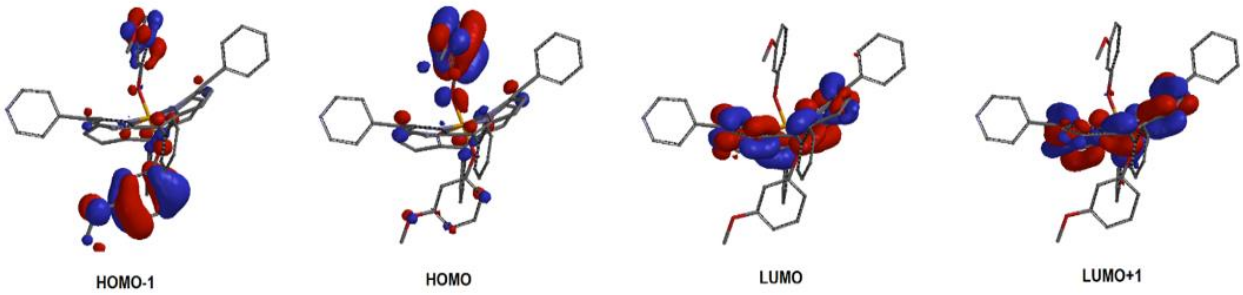


**Fig. 2.24** Calculated molecular orbitals for $[P(MPyP)(OPhOMe)_2]^+$ complex.

As we can see, both HOMO and HOMO-1 are located at phenoxy axial ligands and both LUMOs – at the porphyrin ring. This confirms the possibility of electron transfer in agreement with literature results and offers a possible explanation for the specific behaviour of our compounds under the irradiation. Most part of the absorbed energy goes to PET. Therefore, this type of P(V) porphyrins are bad photosensitizers. As described in the chapter I, the handle#1 contains aromatic part connected directly to the porphyrin. Consequently, the PET stabilizes the P(V) porphyrins towards irradiation. Indeed, the turnstile#1 bearing phenolates axial ligands was found to be more stable than the turnstile#2 bearing alkoxides in the axial positions. This feature allowed to isolate the turnstile#1 and to study its dynamic behaviour in solution.

# 3. Application of P(V) porphyrins in photocatalysis

## 3.1 Experiment description

Since P(V) porphyrins are effective photosensitizers, it appeared interesting to investigate their reactivity in photooxidation processes. Porphyrins (free-base or Zn(II) complex) were already used for this purpose.[41,42] They showed high efficiency in the oxidation of unsaturated cyclic organic compounds. To study the behaviour of P(V) complexes, the hydroquinone (HQ) oxidation was chosen as a model reaction since its photooxidation mechanism is well documented.[43–45] The oxidative process can be easily monitored by UV-Vis spectroscopy, since the main product of the photodegradation is hydroxybenzoquinone (BQ) (**Fig. 2.25**).

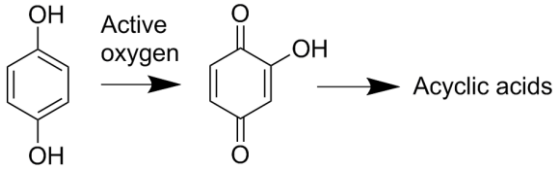


**Fig. 2.25** HQ oxidation by active forms of oxygen.

To prevent the influence of the pH in the experiment, we carried out the reaction using 0.1M potassium phosphate buffer (pH = 7). Four complexes were used in this study: $[P(TPP)(OH)_2]^+$, $[P(TPP)(OEt)_2]^+$, $[P(MPyP)(OH)_2]^+$, $[P(MPyP)(OEt)_2]^+$. It was difficult to predict the results, since HQ is sensitive to all forms of active oxygen (not only singlet oxygen) and probably to other photodestrucive mechanisms. The experiment was performed under visible light irradiation in a designed irradiation chamber BS-02 (Opsytec Dr. Gröbel). The spectrum of the lamp D-65 is presented in **Fig. 2.26**.

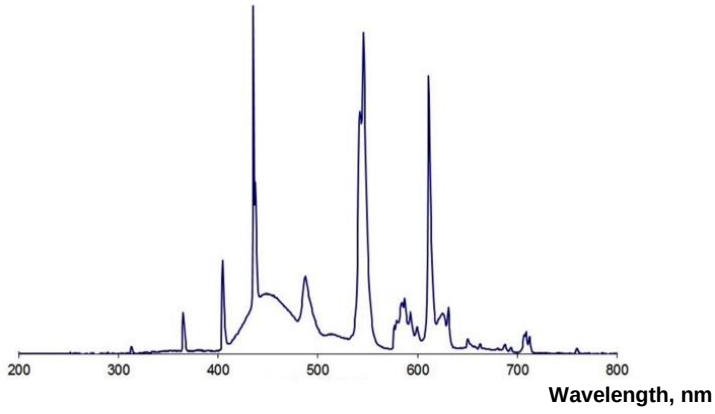


**Fig. 2.26** The spectrum of the lamp D-65 used for the photodestruction experiments.

The oxidation of HQ was monitored by UV-Vis spectrophotometry. Owing to higher ionic strength, the solubility of P(V) porphyrins decreases considerably in the buffered solution when compared to pure water. The experiments were performed in porphyrins buffered solutions ($1.4 \cdot 10^{-6}$ M). 10 μl of the HQ solution in phosphate buffer (0.09 M) was added to 2.4 ml of the porphyrin

solution in an open quartz cells. The final HQ:Porphyrin ratio was 270:1. The solution was irradiated at room temperature and then analysed by UV-Vis spectroscopy. The percentage of HQ and porphyrin was determined from the intensity of the corresponding bands.

### 3.2 Photooxidation of hydroquinone

All four samples were irradiated simultaneously in the chamber. Significant changes in the UV domain of the spectra were detected. All porphyrins displayed similar behaviours. Spectral changes for $[P(MPyP(OEt)_2]^+$ complex are presented in **Fig. 2.27** as an example.

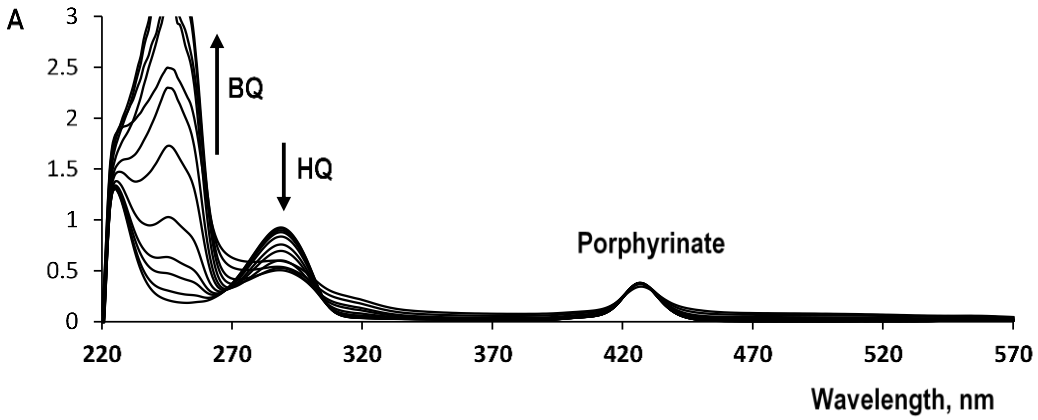


**Fig. 2.27** Photooxidation of HQ in the presence of $[P(MPyP)(OEt)_2]^+$ complex in phosphate buffer.

The band at 290 nm corresponds to the initial HQ and the peak at 246 nm to BQ formed during the irradiation. Due to the substantial difference in the molar absorption coefficients ($\varepsilon_{HQ}$(290nm) = 2500 L.mol$^{-1}$.cm$^{-1}$; $\varepsilon_{BQ}$(246nm) = 25000 L.mol$^{-1}$.cm$^{-1}$), the intensity of the BQ band increases rapidly above 3.

To visualise the efficiency of $[P(TPP)(OH)_2]^+$, $[P(TPP)(OEt)_2]^+$, $[P(MPyP)(OH)_2]^+$, $[P(MPyP)(OEt)_2]^+$, degradation curves of P(V) porphyrins and HQ were plotted **(Fig. 2.28)**.

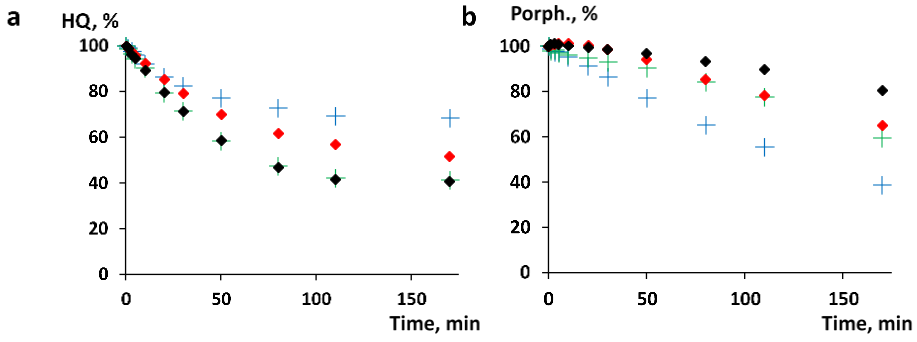


**Fig. 2.28** Photodegradation of HQ in the presence of P(V) porphyrins in phosphate buffer: $[P(TPP)(OH)_2]^+$ (blue crosses ), $[P(TPP)(OEt)_2]^+$ (green crosses), $[P(MPyP)(OH)_2]^+$ (red diamonds), $[P(MPyP)(OEt)_2]^+$ (black diamonds) (a) and simultaneous photodegradation of corresponding porphyrins (b).

Complexes with ethoxy axial ligands showed better efficiency in comparison with hydroxy analogues. After 170 min of irradiation, only ~40% of HQ remained (**Fig. 2.28a**). Further irradiation leads to further oxidation of BQ to carbonic acids as evidenced by the decrease of the BQ peak and the appearance of other bands in the spectrum. Consequently, it appeared difficult to quantify the processes after 170 min of exposure. $[P(TPP)(OH)_2]^+$ appeared to be a least efficient photocatalyst. After oxidation of ~30% of HQ, the oxidation process was stopped. Simultaneously, the intensity of $[P(TPP)(OH)_2]^+$ peak decreased by 60% when compared to the initial intensity **(Fig. 2.28b)**. The best result was obtained with $[P(MPyP)(OEt)_2]^+$: more than 80% of the initial porphyrin was still in the solution after 170 min of irradiation.

- MPyP complexes are more stable than TPP analogues
- $[P(MPyP)(OEt)_2]^+$ is the best photocatalyst among the studied compounds and shows with higher stability under irradiation
- as expected, the hydroxy P(V) porphyrins are less photo stable

## 4. Conclusions of the chapter

In this chapter, we have investigated in detail photophysical properties of a series of P(V) porphyrins (TPP and MPyP) and found this type of compounds to be efficient photosensitizers. This observation explains the low stability of P(V) porphyrins described in Chapter I. Indeed, it was shown that self-oxidizing processes take place under visible light irradiation in the presence of oxygen.

P(V) porphyrin derivatives (except complexes with aryloxy-axial ligands) display high quantum yields for singlet oxygen generation in chloroform. In DMSO and in water, the efficiency is noticeably lower. As it might be expected, an increase of the fluorescence quantum yields in DMSO and water with respect chloroform was observed. For a better understanding of these processes, flash-photolysis experiments are needed.

It was also found that fluorescence and singlet oxygen generation of P(V) porphyrin complexes bearing aryloxy axial ligands are quenched by electron transfer from the electron donor phenyl ring to the porphyrin macrocycle. This leads to a higher photo stability when compared to other P(V) porphyrins. Consequently, P(V) porphyrin complexes bearing aryloxy axial ligands are suitable to be used for the design of molecular turnstiles as described in chapter I.

Attempts to investigate photocatalytic properties of P(V) porphyrins were carried out. The dependence of photocatalytic activity on the substituents in the macrocycle and the nature of axial ligands were investigated. $[P(MPyP)(OEt)_2]^+$ complex was shown to be the best catalyst for hydroquinone oxidation in water. P(V) porphyrin derivatives prepared may thus be used as catalysts for photooxidation of other classes of compounds. Furthermore, P(V) porphyrins may

also be of interest for Photo Dynamic Treatment (PDT). These features need to be further investigated.

## 5. References


1 M. Gouterman, *J. Chem. Phys.*, 1959, **30**, 1139–1161.

2 M. Gouterman, G. H. Wagnière and L. C. Snyder, *J. Mol. Spectrosc.*, 1963, **11**, 108–127.

3 L. Bajema, M. Gouterman and B. Meyer, *J. Mol. Spectrosc.*, 1961, **27**, 225–235.

4 E. D. Sternberg, D. Dolphin and C. Brückner, *Tetrahedron*, 1998, **54**, 4151–4202.

5 J. Karolczak, D. Kowalska, A. Lukaszewicz and A. Maciejewski, *J.Phys.Chem A*, 2004, **108**, 4570–4575.

6 P. B. Merkel, D. R. Kearns and S. Effects, *J. Am. Chem. Soc.*, 1972, **94**, 1029–1030.

7 P. Ogilby and C. Foote, *J. Am. Chem. Soc.*, 1981, **103**, 3423–3430.

8 K. I. Salokhiddinov, I. M. Byteva and G. P. Gurinovich, *J. Appl. Spectrosc.*, 1981, **34**, 561–564.

9 J. R. Hurst, J. D. McDonald and G. B. Schuster, *J. Am. Soc.*, 1982, **104**, 2065–2067.

10 M. C. DeRosa and R. J. Crutchley, *Coord. Chem. Rev.*, 2002, **233-234**, 351–371.

11 F. Amat-Guerri, E. Lempe, E. a Lissi, F. J. Rodriguez and F. R. Trull, *J. Photochem. Photobiol. A Chem.*, 1996, **93**, 49–56.

12 A. Gollmer, J. Arnbjerg, F. H. Blaikie, B. W. Pedersen, T. Breitenbach, K. Daasbjerg, M. Glasius and P. R. Ogilby, *Photochem. Photobiol.*, 2011, **87**, 671–9.

13 S. Kim, M. Fujitsuka and T. Majima, *J. Phys. Chem. B*, 2013, **117**, 13985–13992.

14 N. A. Kuznetsova, N. S. Gretsova, O. A. Yuzhakova, V. M. Negrimovskii, O. L. Kaliya and E. A. Luk'yanets, *Russ. J. Gen. Chem.*, 2001, **71**, 36–41.

15 D. Lala, J. F. Rabek and B. Ranby, *Eur. Polym. J.*, 1980, **16**, 735–744.

16 H. Lin, Y. Shen, D. Chen, L. Lin, B. C. Wilson, B. Li and S. Xie, *J. Fluoresc.*, 2013, **23**, 41–47.

17 B. A. Lindig, M. A. J. Rodgers and P. A. Schaap, *J. Am. Chem. Soc.*, 1980, **102**, 5590–5593.

18 V. Nardello and J. Aubry, *Tetrahedron Lett.*, 1997, **38**, 7361–7364.

19 V. Nardello, D. Brault, P. Chavalle and J.-M. Aubry, *J. Photochem. Photobiol. B Biol.*, 1997, **39**, 146–155.

20 P. T. Nyffeler, N. A. Boyle, L. Eltepu, C. H. Wong, A. Eschenmoser, R. A. Lerner and P. Wentworth, *Angew. Chemie Int. Ed.*, 2004, **43**, 4656–4659.

21 A. Greer, *Acc. Chem. Res.*, 2006, **39**, 797–804.

22 T. Nyokong and V. Ahsen, *Photosensitizers in Medicine, Environment and Security*, Springer, 2012.

23 M. P. Gajewski and L. Czuchajowski, *J. Porphyr. Phthalocyanines*, 2005, **09**, 453–462.

24 K. Hirakawa, N. Fukunaga, Y. Nishimura, T. Arai and S. Okazaki, *Bioorganic Med.*

*Chem. Lett.*, 2013, **23**, 2704–2707.

25 K. Hirakawa, S. Kawanishi, T. Hirano and H. Segawa, *J. Photochem. Photobiol. B.*, 2007, **87**, 209–217.

26 J. Matsumoto, T. Shinbara, S. I. Tanimura, T. Matsumoto, T. Shiragami, H. Yokoi, Y. Nosaka, S. Okazaki, K. Hirakawa and M. Yasuda, *J. Photochem. Photobiol. A Chem.*, 2011, **218**, 178–184.

27 A. A. Ryan, M. M. Ebrahim, R. Petitdemange, G. M. Vaz, E. Paszko, N. N. Sergeeva and M. O. Senge, *Photodiagnosis Photodyn. Ther.*, 2014, **11**, 510–515.

28 K. Shirono, T. Morimatsu and F. Takemura, *J. Chem. Eng. Data*, 2008, **53**, 1867–1871.

29 R. Schmidt, K. Seikel and H.-D. Brauer, *J. Phys. Chem.*, 1989, **93**, 4507–4511.

30 J. P. Strachan, S. Gentemann, J. Seth, W. A. Kalsbeck, J. S. Lindsey, D. Holten and D. F. Bocian, *J. Am. Chem. Soc.*, 1997, **119**, 11191–11201.

31 A. Harriman, *J. Photochem.*, 1983, **23**, 37–43.

32 L. A. Lapkina, Y. G. Gorbunova, D. O. Gil, V. K. Ivanov, N. Y. Konstantinov and A. Y. Tsivadze, *J. Porphyr. Phthalocyanines*, 2013, **17**, 564–572.

33 M. Korínek, R. Dědic, a. Molnár, a. Svoboda and J. Hála, *J. Mol. Struct.*, 2005, **744-747**, 727–731.

34 A. R. Silva, A. C. Pelegrino, A. C. Tedesco and R. A. Jorge, *J. Braz. Chem. Soc.*, 2008, **19**, 491–501.

35 P. B. Merkel and D. R. Kearns, *Chem. Phys. Lett.*, 1971, **12**, 120–122.

36 T. Kajiwara and D. R. Kearns, *J. Am Chem Soc*, 1973, **95**, 5886–5890.

37 P. B. Merkel and D. R. Kearns, *J. Am. Chem. Soc.*, 1972, **94**, 7244–7253.

38 J. Davila and A. Harriman, *Photochem. Photobiol.*, 1990, **51**, 9–19.

39 K. Hirakawa and H. Segawa, *J. Photochem. Photobiol. A Chem.*, 1999, **123**, 67–76.

40 M. Fujitsuka, D. W. Cho, S. Tojo, A. Inoue, T. Shiragami, M. Yasuda and T. Majima, *J. Phys. Chem. A*, 2007, **111**, 10574–10579.

41 J. H. Cai, J. W. Huang, P. Zhao, Y. H. Zhou, H. C. Yu and L. N. Ji, *J. Mol. Catal. A Chem.*, 2008, **292**, 49–53.

42 T. Nagasawa, S. I. Allakhverdiev, Y. Kimura and T. Nagata, *Photochem. Photobiol. Sci.*, 2009, **8**, 174–180.

43 X. Li, J. W. Cubbage, T. a. Tetzlaff and W. S. Jenks, *J. Org. Chem.*, 1999, **64**, 8509–8524.

44 J. Von Sonntag, E. Mvula, K. Hildenbrand and C. Von Sonntag, *Chem. Eur. J.*, 2004, **10**, 440–451.

45 J. Bohuslavek, S. Chanama, R. L. Crawford and L. Y. Xun, *Biodegradation*, 2005, **16**, 353–362.

# Chapter III. A Molecular Break Based on a Zn(II) Porphyrin Dimer

# Contents


**1. Introduction** **109**

**2. Synthesis of the targeted Zn(II) dimer** **113**

**3. Behaviour of the Zn(II) dimer** **114**

**3.1 Investigation of the axial ligand coordination** **114**

**3.2 Handle#3 based system** **119**

**3.3 Acid/base trigger** **123**

**4. Conclusion of the chapter** **124**

**5. References** **126**

# 1. Introduction

As it was mentioned in the introduction part of this manuscript, the porphyrin backbone has been widely used for the design of dynamic systems.[1–7] Free-base porphyrin derivatives as well as their zinc complexes have been studied both in fundamental research and in materials science. After investigating P(V) porphyrin based molecular turnstiles (see chapter 1), we explored another design principle based on Zn(II) porphyrin dimer systems. The general idea on what may be called a molecular gear is represented in **Fig. 3.1.**

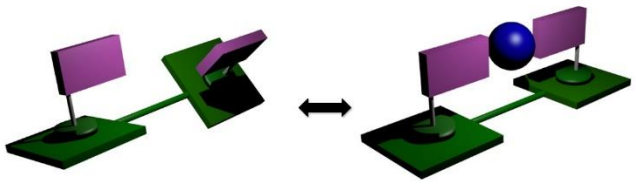

**Fig. 3.1** Schematic representation of Zn(II) porphyrin dimer as a molecular gear.

Two porphyrin moieties are linked *via* a non-flexible bridge (green parts). The bridge allows the free motion of the two parts with respect to each other. Usually in solution, zinc cation located within the porphyrin cavity is pentacoordinated and adopts a square based pyramidal coordination geometry. Thus, in addition to the four nitrogen centres of the tetraaza core of the porphyrin, it can bind one additional peripheral ligand in its axial position (violet moiety). The motion of the system can be blocked by a locker (blue sphere) between two axial ligands or by a bismonodentate ligand binding simultaneously to both Zn centres.

Among many possibilities, the porphyrin dimer may formed either by flexible or rigid connectors. For the latter design, one may use aromatic linkers or ethynyl type fragments. However, an aromatic bridge, for steric reasons, will impose a barrier to the motion. Hence, an ethynyl type connector was chosen. An a single ethynyl spacer, owing to π-conjugation with the porphyrin core, would also hinder the rotation.[8] For that reason, butadiyne was used as the bridge between the two porphyrin units.

Concerning the design of porphyrin macrocycle, three *meso*-positions of both macrocycles were occupied by phenyl rings and only one meso position on each porphyrin was used to interconnect them by the butadiyne moiety. The structure of the targeted porphyrin dimer is represented in **Fig. 3.2**.

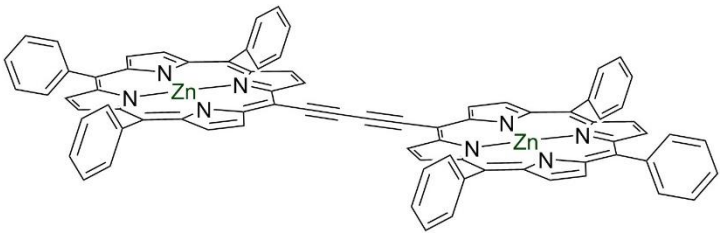


**Fig. 3.2** The porphyrin dimer designed to behave as molecular gear.

One of the first studies dealing with this subject was reported by the Harry Anderson in 1994.[9] In this publication, butadiyne-linked β-substituted porphyrin dimers were reported. Since this type of linker allows the rotation of two porphyrin cores, several conformers in solution may be expected. However, porphyrin dimers were found to aggregate *via* π-π stacking interactions[9,10] **(Fig. 3.3)** leading to a planar conformation of dimers with two parallel adjacent porphyrin molecules.

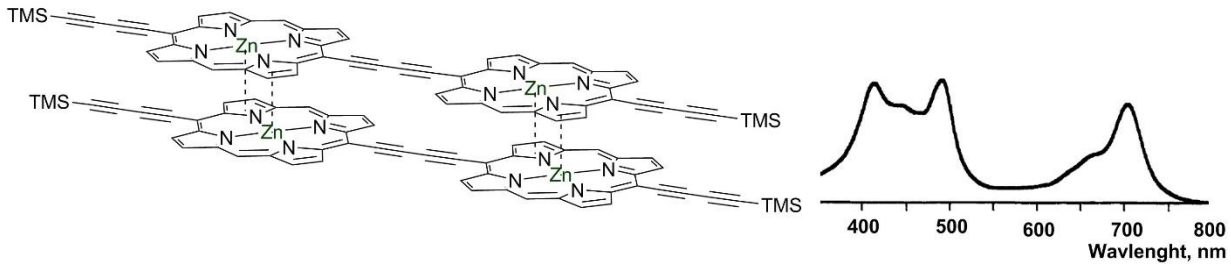


**Fig. 3.3** π-π stacking in porphyrin dimers (β-substituents in dimers are omitted for clarity) and UV-Vis spectrum of the system in DCM at room temperature.[9]

Dimers are shifted relative to each other, *i.e.* the centre of one molecule is located under the pyrrole part of the molecule. Owing to these interactions, the rotational motion is hindered and only the planar conformer is observed.

In the case of metallated porphyrins, an additional way to form planar complexes may occur. The use of a bis monodentate rigid ligand capable of binding two metal centres simultaneously, the two dimers may be bridged imposing thus the planar conformation. Indeed, it was demonstrated that Zn(II) dimer in DCM solution predominantly exists in aggregated form. Binding of DABCO as bridging ligand leads to a stable 2:2 complex with "ladder" type structures **(Fig. 3.4)**. The NMR spectrum of porphyrin dimer in the presence of DABCO in $CD_2Cl_2$ ($c = 10^{-3}$M) displays sharp signals for all porphyrin protons while DABCO signals are significantly upfield shifted due to the screening effect of neighbouring porphyrins (-4,6 ppm). The increase of the porphyrin-DABCO ratio to 1:2 (or more) leads to the formation of 1:2 porphyrin-DABCO complex with fast exchange between coordinated and uncoordinated DABCO molecules. These processes were also monitored by UV-Vis spectroscopy.

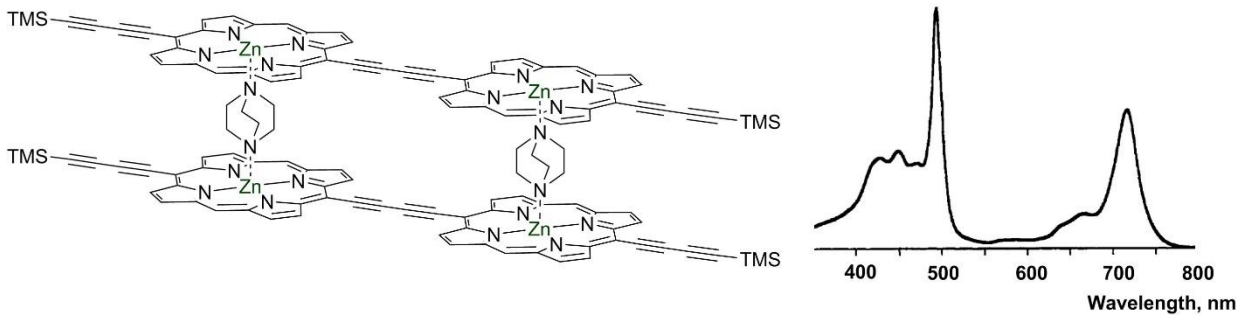


**Fig. 3.4** Porphyrin dimer-DABCO complex (2:2) and its UV-Vis absorption spectrum in DCM at room temperature.

In the presence of pyridine, the dimer forms a 1:2 porphyrin-pyridine complex (**Fig. 3.5)**. In that case, non planar oligomers can be formed for steric reasons. Thus, in solution, the pyridine complex occurs as a mixture of torsionally distinguished isomers. The UV-Vis spectrum of the mixture is different from the one of "planar DABCO complex". An explanation can be given by the point-dipole coupling theory developed by Kasha.[11]

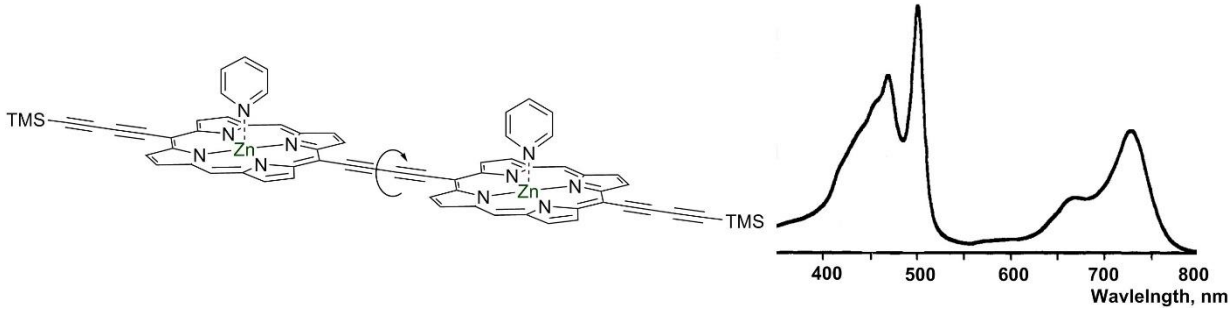


**Fig. 3.5** Porphyrin dimer-pyridine 1:2 complex and its UV-Vis absorption spectrum in DCM at room temperature.

The Soret band of the porphyrin includes $B_x$ and $B_y$ components **(Fig. 3.6)**. In the spectrum of a metallated porphyrin monomer, they are degenerated. In the spectrum of the dimer, they are split into two bands: $B_x$ transition corresponding to head-to-tail and $B_y$ corresponding to face-to-face arrangements respectively. Since they are not identical, two Soret-bands are observed. From data collected,[9,12] it was proposed that the blue-shifted $B_y$ component mainly corresponds to the non-planar conformation (mixture of torsionally free dimers) and the red-shifted $B_x$ band to the planar conformation.

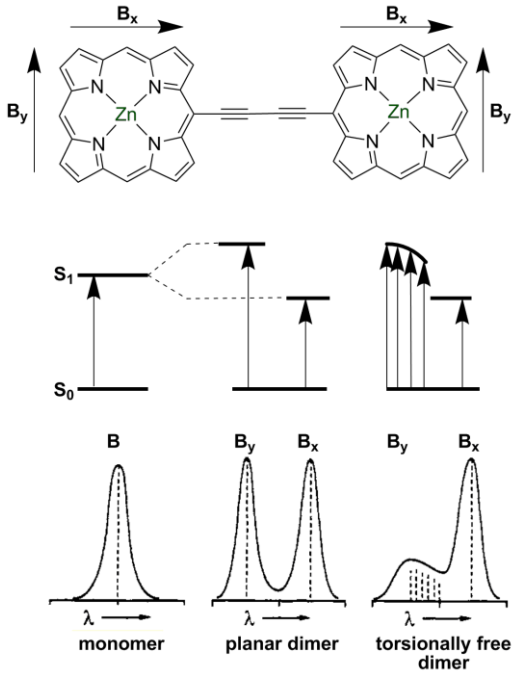


**Fig. 3.6** Kasha's model for exciton coupling.

Imposition of the orthogonal conformation was also described by Aida *et al*.[12] A monopyridyl *meso*-substituted dimer depicted in **Fig. 3.7** was synthesized. In the absence of any external

coordinating agent, it the compound forms orthogonal cages (tetramers of dimers) in solution due to self-assembling processes as confirmed by the UV-Vis absorption spectrum **(Fig. 3.7)**.

Later, Bo Albinsson *et al.* investigated similar dimers however without the presence of coordinating sites at the *meso*-positions **(Fig. 3.8)**.[13] It was found that the butadiyne bridge allows the motion of two moieties of the dimer. Interestingly, DFT calculations revealed considerable energetic barrier to free rotation about the butadiyne axis.[14] At room temperature, the free 360º rotation is not expected.

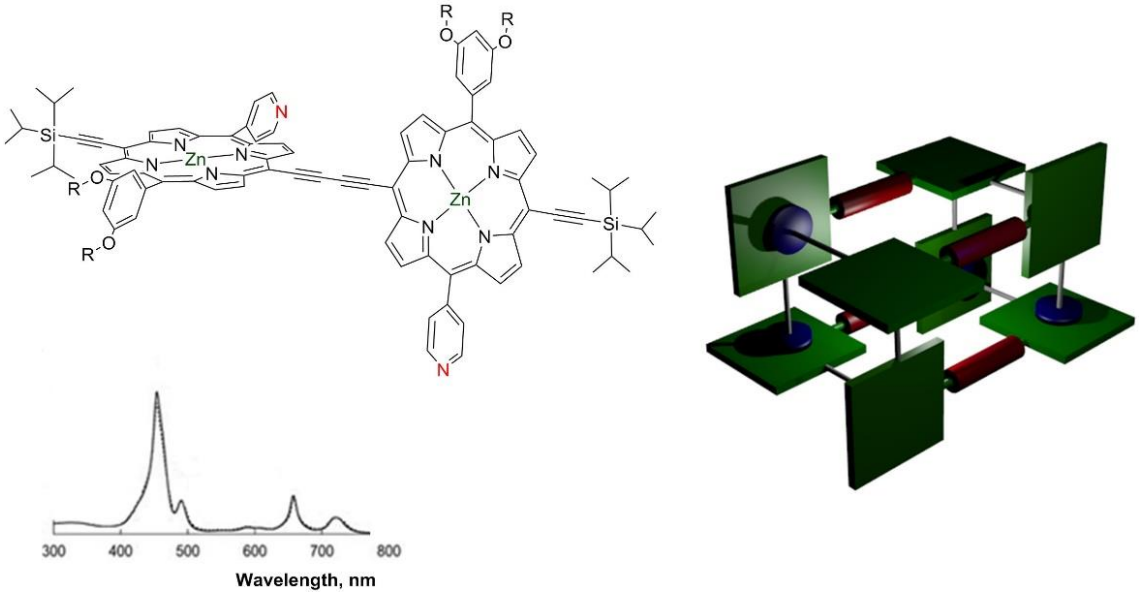


**Fig. 3.7** Formation of an orthogonal dimer conformer and its UV-Vis spectrum in DCM at room temperature.[12]

In order to impose a planar conformation of the dimer in solution, a non-flexible bidentate handle was prepared and used. Results obtained correlate well with the above mentioned data. In solution, a mixture of several conformers is observed and upon gradual addition of the handle to the solution significant changes in the absorption spectrum are observed **(fig. 3.8)**. The intensity of the blue-shifted $B_x$ component of the Soret band decreases dramatically, while simultaneously the intensity of the red-shifted $B_y$ component increases. Q-bands demonstrate the same behaviour.

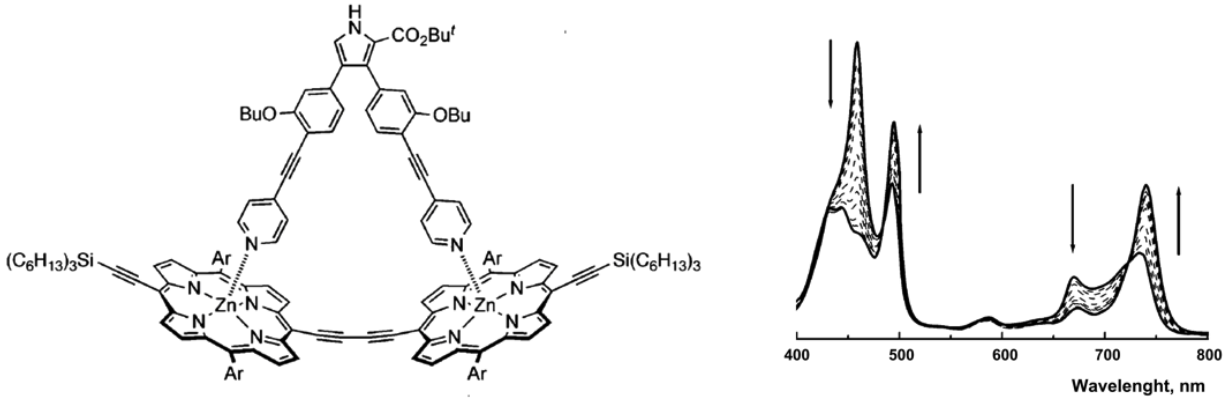


**Fig. 3.8** Structure of dimer bonded to a handle and UV-Vis spectrum in DCM during titration.

Several structures of butadyine-linked porphyrin Zn(II) dimers were investigated by other groups.[15–18] In the solid state, the dimer displays the planar (or close to planar) conformation. The zinc cation is penta-coordinated in almost all compounds. The two axial ligands are located either on the same side of the dimer[15] or on opposite sides.[16–18] The butadiyne linker is strictly linear. No examples of dimers bearing a bidentate handle in the axial position have been reported. The dimer bearing two pyridyl axial ligands[15] will be described more precisely and compared to compounds obtained during this work.

## 2. Synthesis of the targeted Zn(II) dimer

According to a described procedure[19,20], the first step involves a direct cross-condensation of a mixture of aldehydes affording a mixture of 6 porphyrins including the targeted porphyrin in rather low yield **(Fig. 3.9)**. The TMS protective group was removed by TBAF in quantitative yield. Then the porphyrin was metallated using Zn acetate under standard conditions affording the desired metalled porphyrin. The dimer was obtained in 65% yield by a Pd catalysed coupling reaction between the two monomer molecules. The overall yield was 3.25%.[21] The product was isolated by column chromatography (alumina, cyclohexane-toluene 1:1 as an eluent) and analysed by NMR and HR-ESI MS techniques.

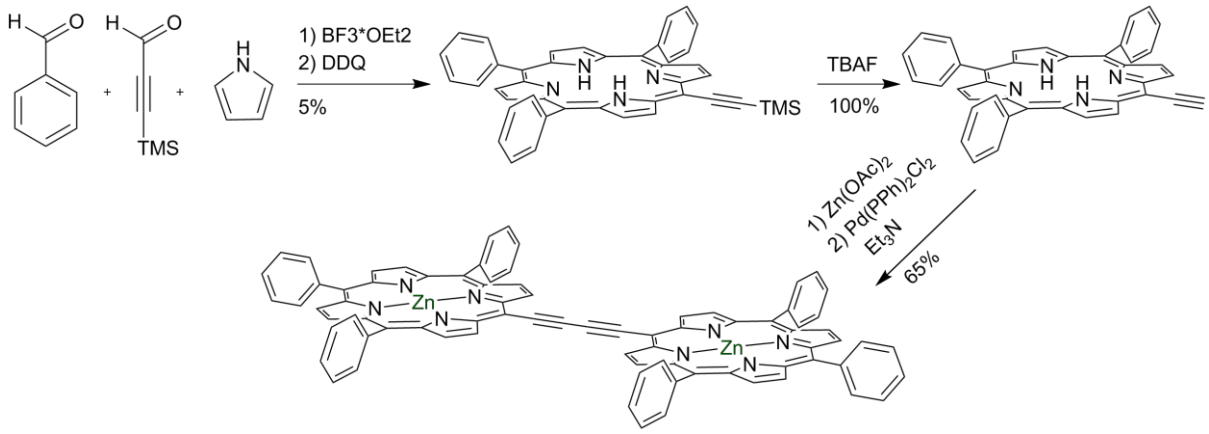


**Fig. 3.9** Synthetic strategy toward the target Zn(II) dimer.

The dimer appeared to be only slightly soluble in non-coordinative solvents due to π-π stacking interactions between porphyrins. However, it was found to be well soluble in coordinating solvent such as THF, DMSO and pyridine. Indeed, owing to their coordination in the axial positions of the Zn(II) and breaking π–π interactions between dimers, addition of the coordinating solvents to chloroform or toluene solutions of the dimer increased its solubility.

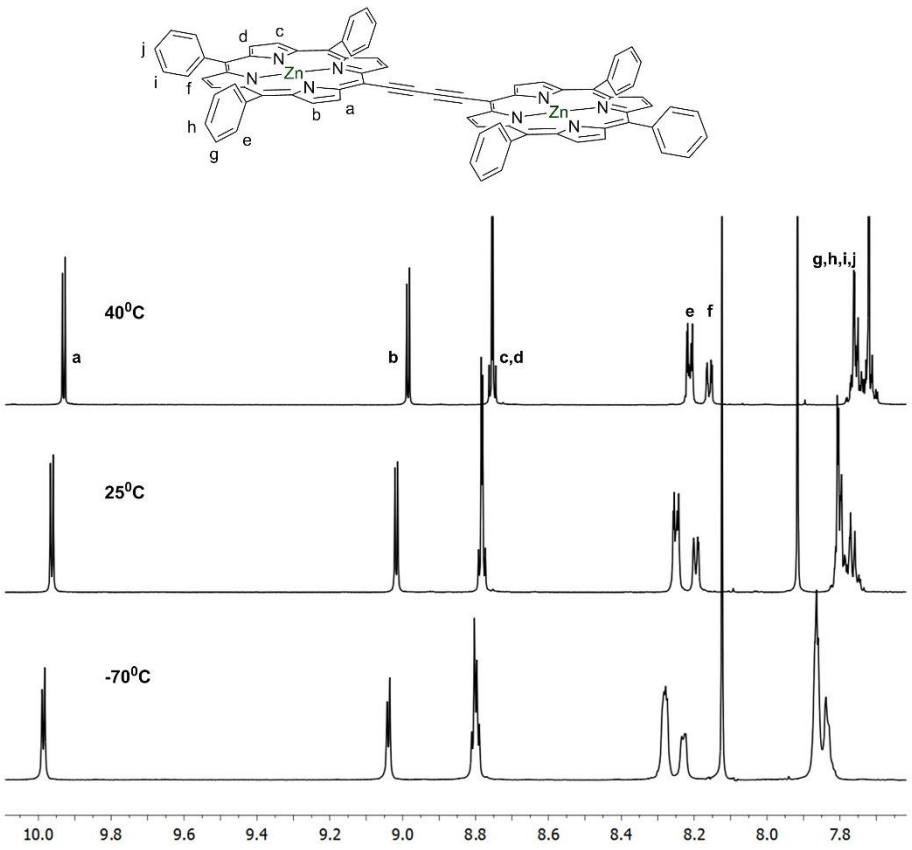


**Fig. 3.10** $^{1}$H-NMR spectrum of the dimer in THF-$d_8$ at different temperatures.

Due to the high symmetry of the molecule, all conformers should display the same $^{1}$H-NMR spectrum and consequently cannot be distinguished by this method at room temperature. In order to overcome this, $^{1}$H-NMR spectra were recorded at different temperatures in order to distinguish between different conformers. Unfortunately, cooling the THF-$d_8$ solution of dimer to -70 $^{\circ}$C did not afford any significant changes in the spectrum (**Fig. 3.10**).

# 3. Behaviour of the Zn(II) dimer

## 3.1 Investigation of the axial ligand coordination

The system described above **(Fig. 3.1)** requires the presence of one ligand in the axial position per Zn(II) centre. The most common axial ligand for such a complex is pyridine-based derivatives.[22] The binding constant for the coordination of pyridine by the monomer Zn(II) tetraphenylporphyrin (Zn(TPP)) was reported to be logK = 3.84 and 2.79 in DCM[23] and chloroform[24] respectively.

The binding of pyridine to the dimer was investigated by NMR titration experiments performed in $CDCl_3$ with traces of DMSO-$d_6$ (to solubilize the dimer) (**Fig. 3.11)**. The addition of one or two equivalents of pyridine leads to the appearance of signals corresponding to the pyridine protons significantly up-field shifted due to ring current of porphyrin indicating the binding of pyridines in the axial position of Zn(II). Owing to fast exchange between coordinated and non-coordinated

pyridine molecules, further addition of pyridine leads to a downfield shift of these signals up to the usual chemical shifts for a non-coordinated pyridine (for 30 eq.).

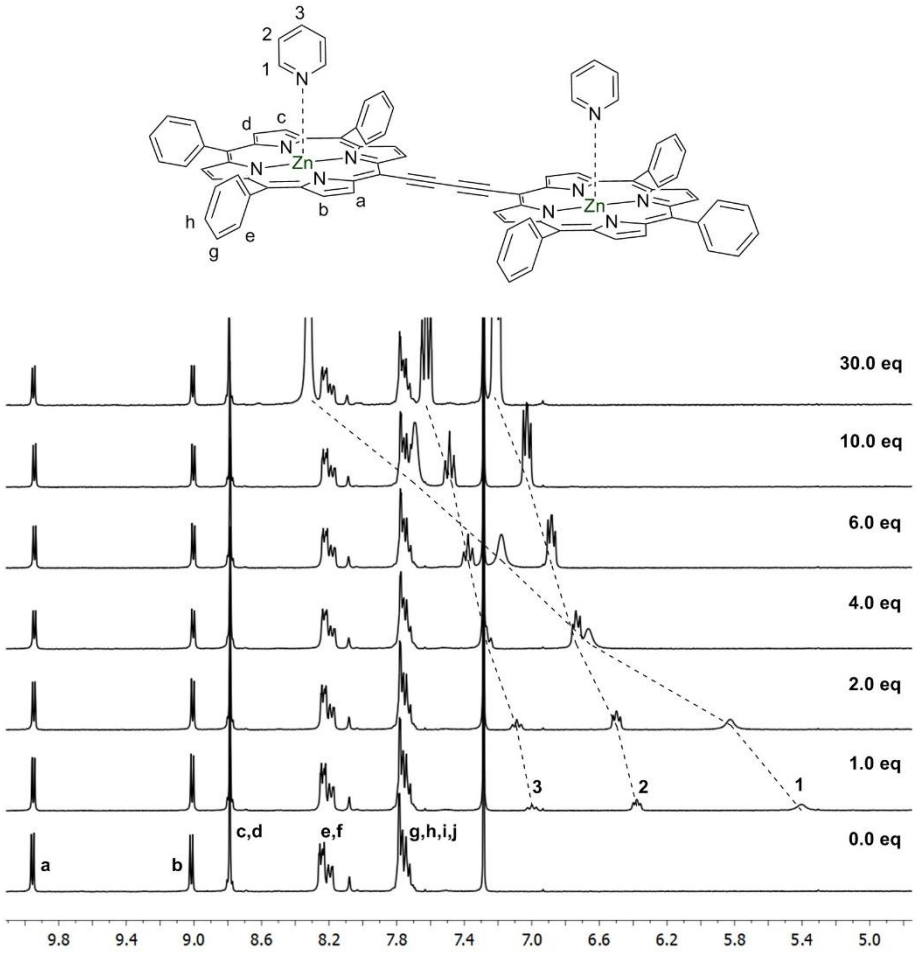


**Fig. 3.11** $^{1}$H-NMR of titration of the dimer (c = $2.1 \cdot 10^{-3}$ M) in $CDCl_3$ solution with a drop of DMSO-$d_6$ by pyridine.

The dimer is soluble enough in chloroform and DCM in concentrations less than $10^{-5}$M to perform the UV-Vis experiments. Thus, titration of the dimer solution by pyridine in both solvents was carried out **(Fig. 3.12)**. During the titration, we noticed a significant increase (4 times) in the intensity of all bands due to disaggregation of the stacked dimers in DCM. Furthermore, the binding of axial pyridines leads to a red shift of *ca* 10 nm of the Soret and Q-bands.

These changes correspond to two processes **(Fig. 3.12)**: disaggregation of aggregated dimer ($K_{Dis}$) and concomitant binding of pyridine ($K_L$). All titration curves were treated by HypSpec software.[25,26] logK = 6.941±0.0033 in DCM and logK = 7.507±0.0131 in chloroform were calculated. These constants can be represented as a result of two processes:

$$K = K_{Dis}K_L \qquad \textbf{(eq. 3.1)}$$

$$\log K = \log K_{Dis} + \log K_L \qquad \textbf{(eq. 3.2)}$$

In a first approximation we assume that the binding constant $K_L$ of the system with pyridine is the same as for Zn(II) tetraphenylporphyrin (as described previously[9,23,24], $\log K_L$ 3.84 in DCM and

2.79 in $CHCl_3$), since both binding processes occur independently. The disaggregation $K_{Dis}$ constant can be deduced from eq.3.1. Thus $\log K_{Dis}$ is 4.15 in DCM and 3.66 in chloroform.

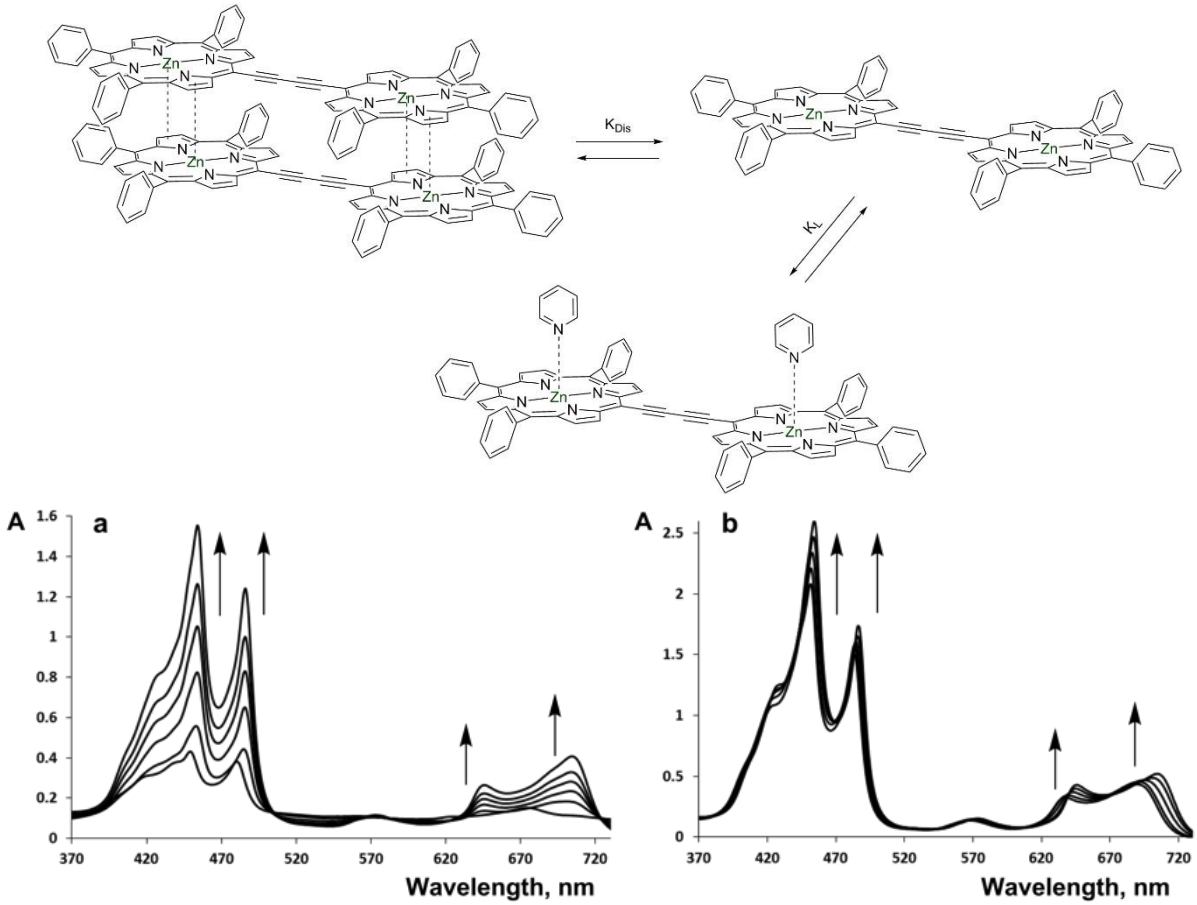


**Fig. 3.12** Titration of the dimer with pyridine **a**: in DCM, c = $4.7 \cdot 10^{-6}$ M, 0-220 eq. of pyridine and **b**: in chloroform, c = $8.0 \cdot 10^{-6}$ M, 0-400 eq. of pyridine

The titration of dimer by DMAP (*para*-dimethyl pyridine) in DCM solution was performed. Calculated logK appeared to be 9.1489±0.0119. This value is three orders of magnitude higher than the value obtained for pyridine and is consistent with the stronger basicity DMAP when compared to pyridine (pKa = 9.60 *vs* pKa = 5.17 for pyridine[27]). A value $\log K_L = 5.45$[28] for DMAP binding to Zn(TPP) was reported. Thus, the $\log K_{Dis}$ for the dimer in DCM is equal to 3.68.

These systems with monodentate axial ligands, pyridine or DMAP, are free to rotate. Spectra recorded are averaged and correspond to mixtures of all conformers in the solution.

As already described,[9] the addition of DABCO to a similar compound (**fig. 3.4**.) leading to the formation of a 2/2 complex, blocks the rotation and imposes a planar conformation. We also performed the titration of the dimer with DABCO. The resulting UV-Vis spectrum **(Fig. 3.13)** is similar to the one described earlier and corresponds to the planar conformation of the dimer after the addition of 15 eq. of DABCO. This spectrum will be used as a reference for further experiments.

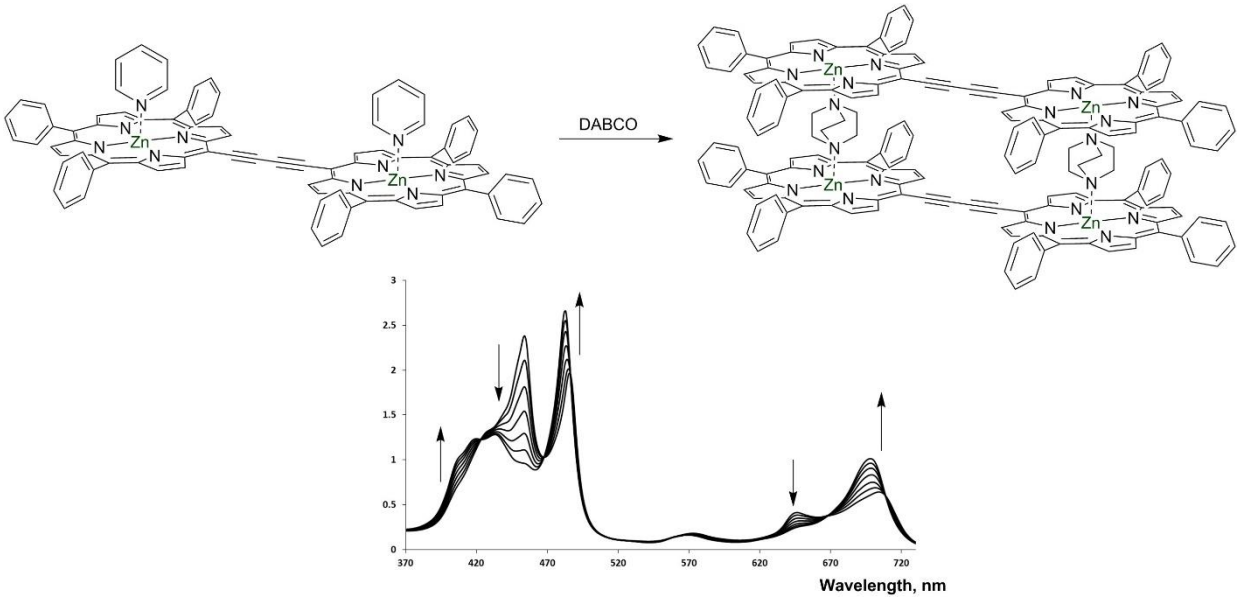


**Fig. 3.13** The formation of a planar 2:2 complex with DABCO in DCM (c = $8.0 \cdot 10^{-6}$ M, 40 eq. of pyridine, 0-15 eq. of DABCO).

Single crystals of the dimer have been obtained and studied by X-ray diffraction techniques. The single crystals were obtained at 25 $^{o}$C by vapour diffusion of pentane into the solution of dimer in chloroform with a drop of toluene and methanol in the presence of 2.5 equivalents of DMAP. The crystal (triclinic, P-1 space group) is composed of the dimer and 3 chloroform molecules which form short contacts with the dimer molecules. The X-ray structure is depicted in **Fig. 3.14**. Selected structural parameters are given in **table 3.1**.

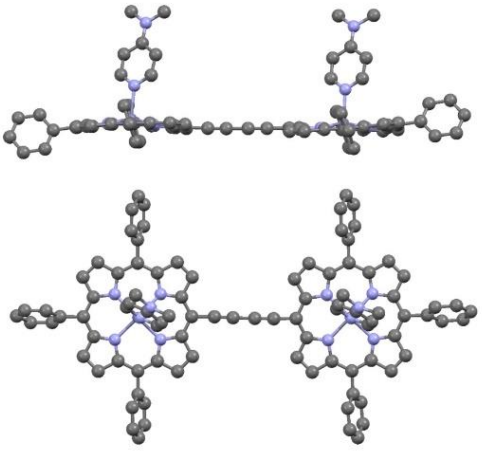

**Fig. 3.14** X-ray structure of the dimer complex with two DMAP molecules (solvent molecules and hydrogen atoms are omitted for clarity).

Both porphyrin rings are almost planar. The butadiyne linker is linear. Both Zn atoms are penta-coordinated and surrounded by four nitrogen atoms of the porphyrin cores (Zn-$N_{por}$ distances are 2.067(5) - 2.115(5) Å) and one nitrogen of the DMAP axial ligand ((Zn-$N_{DMAP}$ distances are 2.115(5) - 2.135(5) Å). Zinc cations are slightly displaced out of the porphyrin plane (distances between Zn and porphyrin plane (20 C and 4 N atoms of the porphyrin ring) are 0.314Å, 0.453Å).

Distance between two Zn atoms within the dimer is 13.515 Å. In the crystal, molecules are packed as cofacial dimers of dimers due to π-π stacking and both DMAP molecules are located on the same side of the dimer. Angles between DMAP planes and the porphyrin mean planes are 73.37° and 73.42°. The distance between two neighbouring dimer molecule planes (46 C and 8 N atoms: both porphyrin rings and butadyine bridge) is 3.423 Å (**Fig. 3.15**).

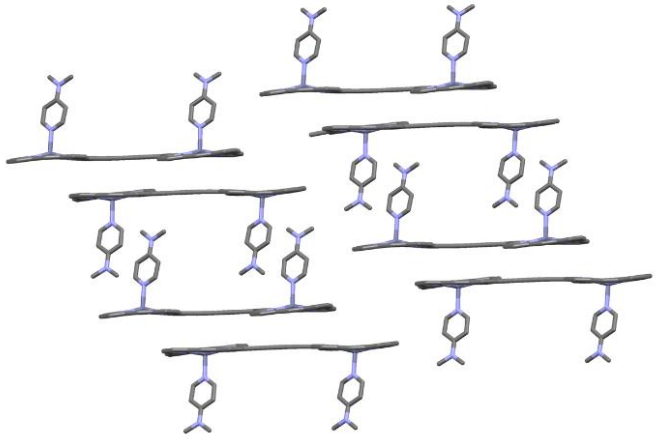

**Fig. 3.15** Crystal packing in the single crystal of the dimer(DMAP)$_2$ (solvent molecules and phenyl *meso*-substituents are omitted for clarity).

**Table 3.1** Selected X-ray data for dimers with DMAP and pyridine molecules.

| **Bond** | **Length (Å)** | | **Bond** | **Angle (degree)** | |
|---|---|---|---|---|---|
| | **Dimer (DMAP)** | **Dimer (pyridine)[15]** | | **Dimer (DMAP)** | **Dimer (pyridine)[15]** |
| Zn-$N_{Pyr.}$ | 2.115(5), 2.135(5) | 2.144(4), 2.163(4) | $N_{Pyr}$-Zn-$N_{Porph}$ | 95.0(2), 94.2(2) | 96.68, 96.41 |
| Zn-$N_{Porph.}$ | 2.067(5) – 2.115(5) | 2.052 – 2.080 | N-Zn-$N_{trans}$<br>N-Zn-$N_{cis}$ | 158.28(19) – 163.3(2);<br>87.7(2) – 89.0(2) | 159.82 – 161.22;<br>88.11 – 88.74 |

This structure should be compared to the structure of the Dimer(pyridine)$_2$ reported previously.[15] The structural parameters of both crystals are similar with only slight differences. The angle between two porphyrin planes is 1.64° in DMAP structure vs 5.51° in the case of Dimer(pyridine)$_2$ complex. The Zn atom displacements out of the porphyrin planes are almost the same: 0.327 Å and 0.424 Å for DMAP complex and 0.394 Å and 0.401 Å for pyridine complex. Since pyridine is less basic than DMAP, the distance between Zn and N atom of the axial ligand is larger for the pyridine complex (see **table 3.1**). In both structures, phenyl substituents are oriented almost orthogonally to porphyrin ring. Strong π-π stacking is observed in crystal of both

systems. Distances between two dimer molecules are 3.423 Å for the DMAP complex while it is larger for the pyridine complex (4.9 Å).

### 3.2 Handle#3 based system

To stop the rotation of two porphyrin moieties within the dimer, a bidentate locker, handle#3 (**fig 3.16**) was designed. This flexible linker is equipped with two pyridyl groups at its both extremities **(Fig. 3.16)**.

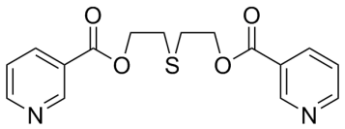

**Fig. 3.16** The handle#3 used to lock the dimer.

Addition of the handle to the dimer in DCM leads to the coordination of the bis monodentate ligand to the apical position of the two Zn(II) centres of the dimer, thus switching off the flipping of the porphyrin macrocycles. The coordination of the two pyridyls of the handle#3 could be monitored by UV-Vis spectroscopy. Indeed, the addition of the handle#3 to a DCM solution of the dimer leads to the formation of a planar 1:1 complex (**Fig. 3.17)** with logK = 4.665±0.022.

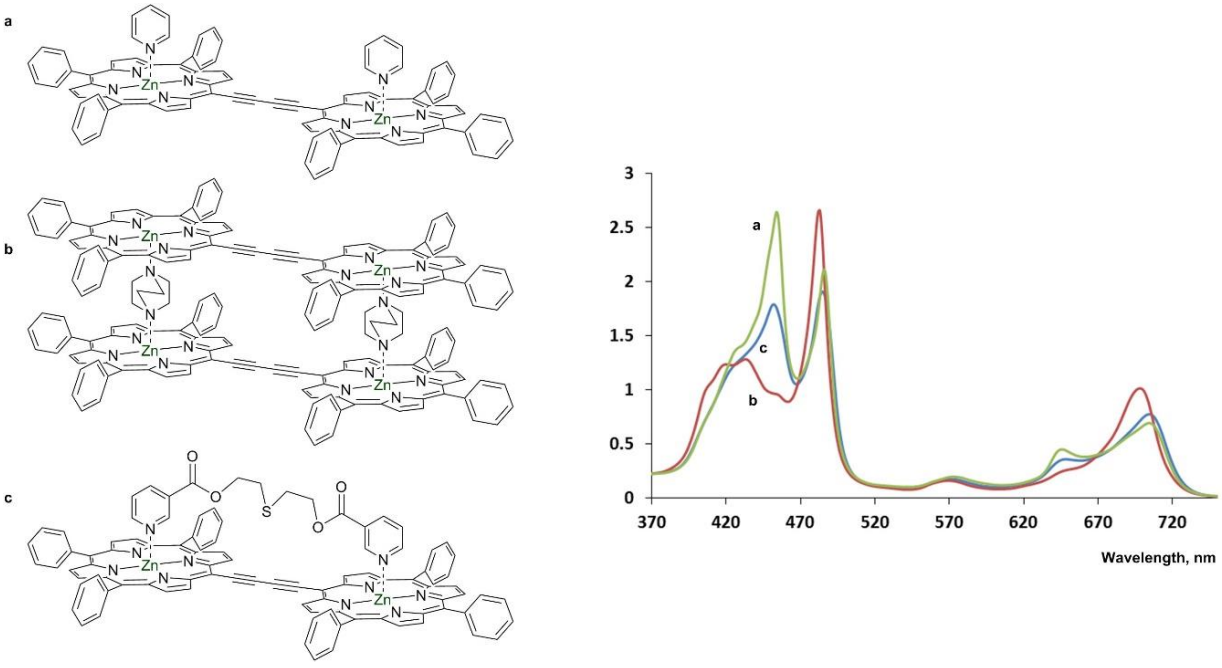


**Fig. 3.17** Comparison of the structures and UV-Vis spectra (in DCM) of the three different complexes of the dimer: Dimer(pyr)$_2$ (a, green), [Dimer(DABCO)]$_2$ (b, red), Dimer(handle#3) (c, blue).

By comparison with the DABCO 2:2 complex, the blue-shifted $B_x$ component of the Soret-band of the Dimer(handle#3) is more intense and sharper, thus indicating that there is still some "flipping" in the presence of the handle. There are three possible explanations for that: i) the handle#3 is flexible enough to allow the flipping of the dimer and to a decrease in the conjugation of π-electrons between the two porphyrin cores; ii) opposite of the reason mentioned above, the

handle is too rigid or short and only one of the two pyridyl units is involved in the binding process. However this is less likely since the distance between two Zn(II) is close to 13.5 Å and the expected distance between two nitrogen atoms in handle#3 (obtained by ChemDraw 3D software) is *ca* 13-14 Å. Moreover, the compatibility between the handle#3 and the Zn(dimer) is supported by examination of CPK models. iii) The third reason is the formation of a mixture containing partially bonded dimers. Among the three possibilities, the first one seems the most probable.

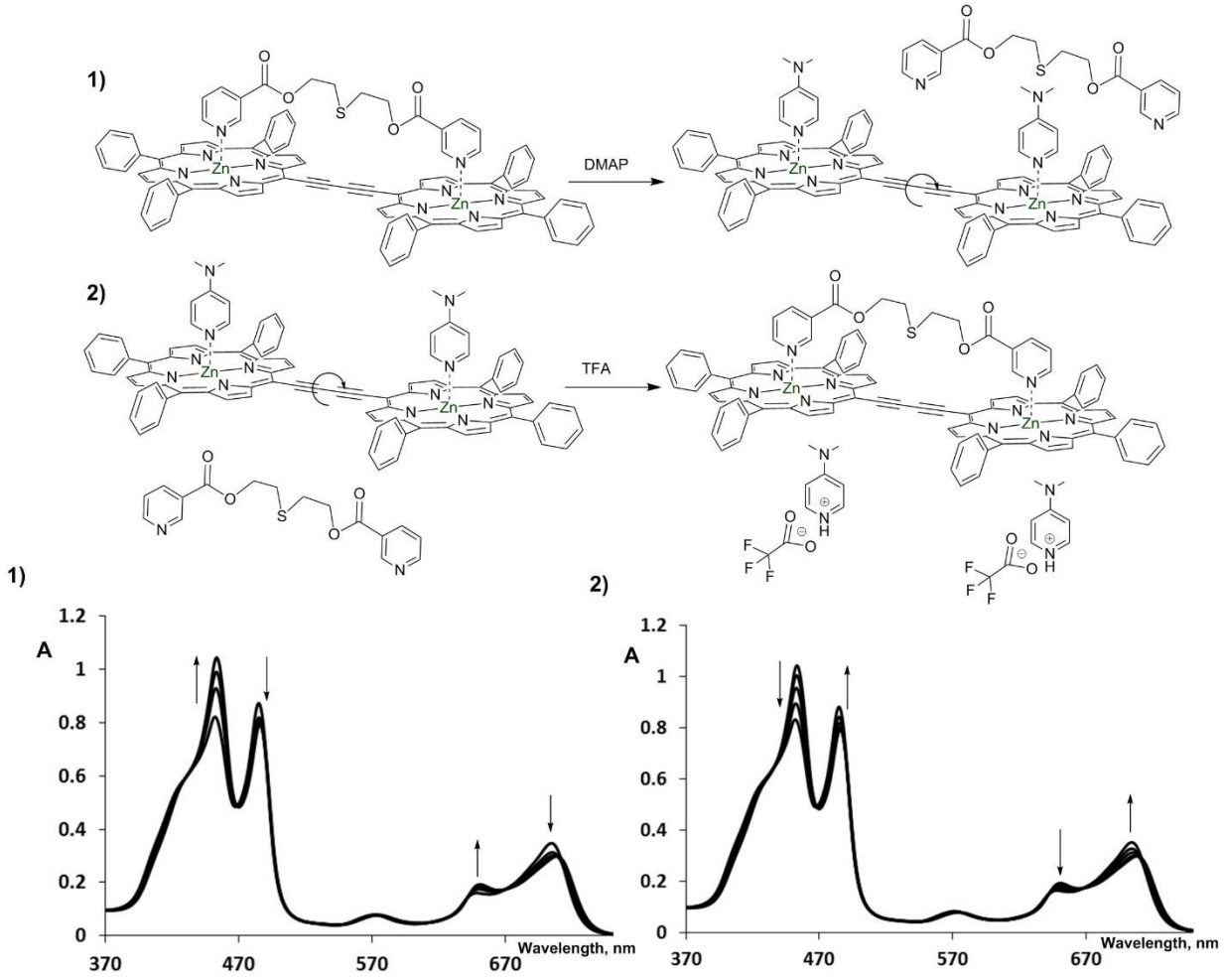


**Fig. 3.18** Opening and closing of the dimer (c = $4.7 \cdot 10^{-6}$ M) with handle#3 (5 eq.), DMAP (0-20 eq.) (upper spectrum) and TFA (5-15 eq.) (lower spectrum) in DCM at room temperature.

The re-opening of the system requires the disconnection of the handle#3. For this purpose, the competition between DMAP and the handle was investigated. Gradual addition of DMAP to the dimer in the presence of the handle#3 (preformed complex) leads to the formation of the mixture of "torsional free" Dimer$(DMAP)_2$. This process was monitored by UV-Vis spectroscopy **(Fig. 3.18)**. Disconnection of the handle leads to an increase of the intensity of the blue-shifted Soret and Q-bands while the intensity of the red shifted Soret and Q-bands decreased simultaneously indicating that the system is reopened.

Interestingly, this process is reversible and the closed state could be regenerated (**Fig. 3.18**). Indeed, stepwise addition of TFA leads to the protonation of the stronger base, DMAP, leading to

its decoordination from Zn(II) and the binding of the handle#3. This process was also followed by UV-Vis spectroscopy **(Fig. 3.18)**.

In addition to the study of the Dimer(handle#3) complex in solution, its characterization in the solid-state by X-Ray diffraction was also carried out. Single crystals were obtained at 25 ºC by vapour diffusion of pentane into a solution of the dimer in chloroform (containing drops of toluene and methanol) in the presence of 1.5 equivalents of the handle#3. Dimer(handle#3) complex crystallizes (monoclinic, c2/c space group) with one water molecule (**Fig. 3.19)**. Due to the low quality of the crystal, the structure was not finished. Unfortunately, it was not possible to determine the position of the flexible chain connected to the two pyridyl units and thus they are not represented in **Fig. 3.19**. Also one of the two pyridyl moieties was found to be disordered between two positions. The calculation of the structure could not be completed. It is difficult to say if the handle#3 is connected to one dimer molecule or to two neighbouring ones.

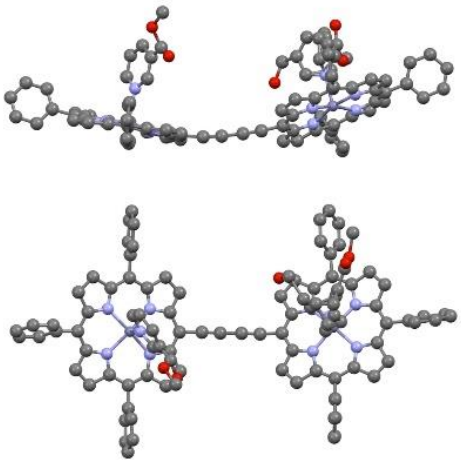

**Fig. 3.19** Partial X-ray structure of the dimer complex with handle#3 (solvent molecules are removed for clarity, one of the pyridine moiety is disordered).

Both Zn atoms are penta-coordinated and surrounded by four nitrogen atoms of the porphyrin cores and one nitrogen of the pyridyl axial ligand. They are both displaced out of porphyrin plane (the distances between Zn and porphyrin planes (20 C and 4 N atoms) are 0.232Å, 0.296 Å, which is twice less than in structure of dimer with DMAP). Unlike the structure of Dimer(DMAP)$_2$ , the torsional angle between two halves of the dimer is not 0º. In comparison with the previously described DMAP complex, the dimer is not planar. The butadiyne linker is not linear and the angle between two porphyrin planes (20 C and 4 N atoms) is about 36.66º and the Zn-Zn distance is 13.11 Å. Since we did not determine the position of all the atoms in the structure, we cannot explain why the butadiyne linker is not linear. But most likely, the convergent orientation of the two porphyrin mean planes and the bending of the dimer is due to the coordination of the handle to the Zn(II) that is probably not long enough to provide a planar conformation of the dimer in the solid state.

To test this proposal, we modelled the geometry of the handle#3 complex. The calculations were achieved using the Spartan'14 software (B3LYP 6-31G* basic set) **(Fig. 3.20)**. The optimized geometry is in good agreement with the obtained crystal data and the butadiyne linker was also found to be non linear. The torsional angle between two porphyrin rings is even larger that the angle observed experimentally. However this difference could arise from the fact that the calculations were performed for the molecule in vacuum, while in the single crystal X-ray structure, one has to consider the influence of the crystal packing on the final structure **(Fig. 3.21).**

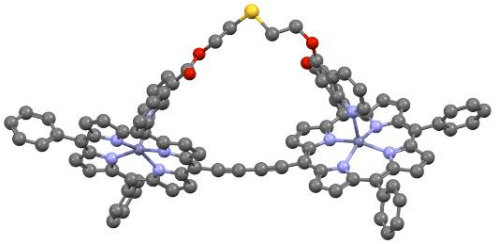

**Fig. 3.20** Calculated geometry of Dimer(handle#3) complex (B3LYP 6-31G* basic set).

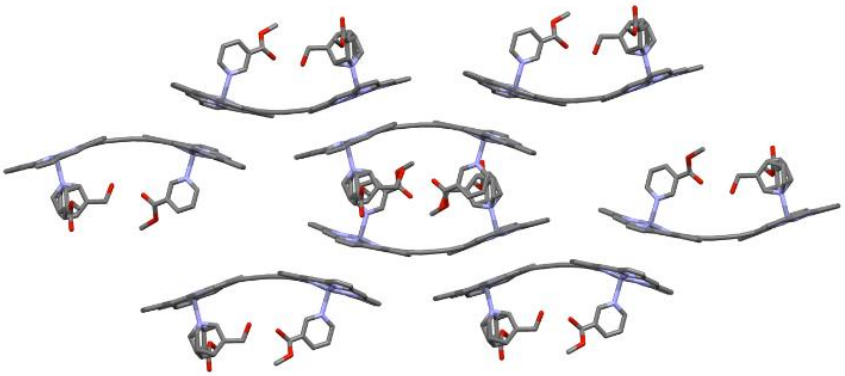

**Fig. 3.21** Crystal packing of the single crystal of the dimer(handle#3) complex (*meso*-phenyl substituents are omitted for clarity)

Crystal packing is significantly different from Dimer(DMAP)$_2$. Two molecules form pairs. Dimer molecules are oriented in the pair in a convergent manner. Pyridyl moieties of one dimer form π-π bonds with pyridyl units of another dimer. Simultaneously, each porphyrin forms π-π contacts with adjacent porphyrin ring of another dimer pair.

Several conclusions can be drawn:

- the motion of two moieties of the dimer can be switched off or at least partially by the addition of the handle#3
- the process may be monitored by UV-Vis absorption spectroscopy
- single crystals of the dimer with handle#3 and DMAP illustrate their structural peculiarities: DMAP complex is planar, handle#3 complex is not
- the handle#3 could not be determined in the crystal structure but its bending by the dimer in the solid state is in good accordance with the calculated structure

### 3.3 Acid/base trigger

Another possibility to stop the motion of the two porphyrin moieties within the dimer, may be based on a system bearing two small axial ligands bearing acid/base active entities and the use of an auxiliary molecules to lock the movement as shown **Fig. 3.1**. We first tried to introduce two nicotinic acids at the axial positions of the two Zn(II) in the dimer. Unfortunately, nicotinic acid is poorly soluble in most organic solvents, consequently it cannot be used as the dimer that is not soluble in water.

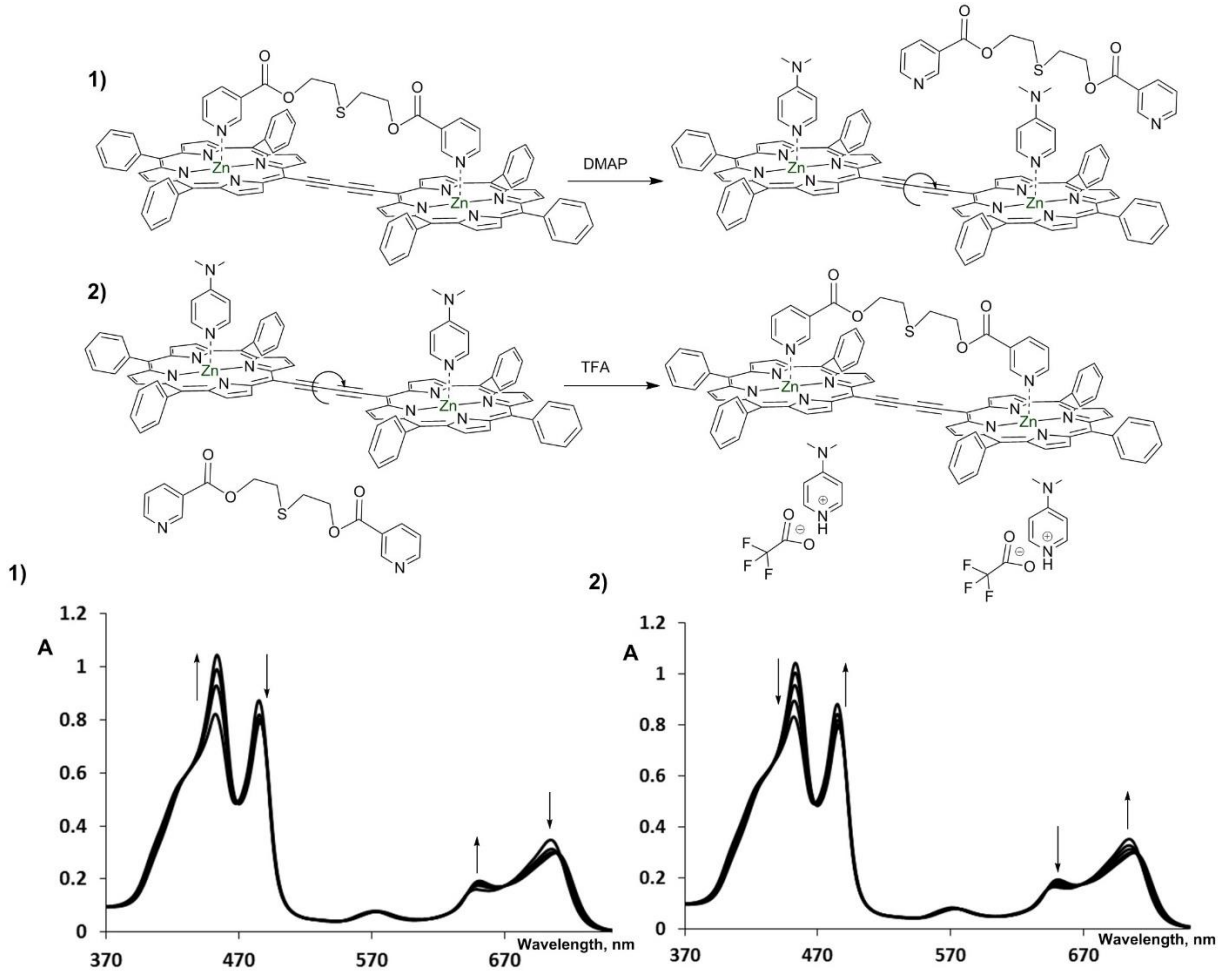


**Fig. 3.22** Closing/opening processes in the AP-SA dimer ($c = 8.0 \cdot 10^{-6}$ M) system in DCM at room temperature (AP – 40 eq., SA – 0-40 eq., upper) and $Et_3N$ – 0-90 eq. (lower).

Another way to proceed is to use an aminopyridine as an axial ligand and a dicarboxylic acid as a locker. Thus, the 4-aminomethyl pyridine (AP) was used as axial ligands: the pyridyl unit being coordinated to the Zn(II) while the amino groups could further interact with an appropriate diacid through H-bonds as a locker and thus switch off the flipping of the system.

Due to its rigidity and its pKa (2.554 for benzenesulfonic acid[29]), 4,4'-biphenyldisulfonic (SA) acid seems perfectly suited to lock the system. However this acid is insoluble in DCM, so for the titration, SA was added to a solution of methanol (**fig. 3.22**).

Addition of AP to the solution of the dimer in DCM was monitored by UV-Vis spectroscopy. Further addition of SA closes the system and switch off the motion. Formation of the planar conformation is shown by UV-Vis **(Fig. 3.22)**.

Moreover, the system can be reopened by addition of $Et_3N$. Indeed addition of $Et_3N$ leads to the deprotonation of the ammonium and thus to the reopening of the system (**Fig. 3.22)** and return to the open initial state. Further addition of SA to the solution leads to formation of a precipitate.

As conclusions for this part we have shown that:

- the dimer can be closed by AP/SA system
- only one open/close cycle can be achieved due to the precipitation

We tried to characterize the open and/or close state of the molecular gear in the solid state by X-Ray diffraction. Unfortunately, for the moment, we did not succeed in growing single crystals.

## 4. Conclusion of the chapter

In this chapter we reported the formation of molecular gears based on Zn(II) dimer composed of two porphyrin moieties connected by butadiyne bridge. In order to control the motion within the dimer, two approaches have been undertaken.

The first one consisted in the coordination of a bis monodentate handle (handle#3), bearing two pyridyl moieties, to the axial positions of the two Zn(II) centres of the dimer. The second strategy involved electrostatic interactions and hydrogen bonding between ammonium groups located at the axial pyridyls and 4,4'-biphenyldisulfonate anion. Due to the low solubility of the dimer in non-coordinating solvents, it appeared difficult to follow the processes by NMR techniques. Thus, we monitored the conformational changes by UV-Vis spectroscopy, since the spectrum of the dimer is sensitive to the torsional angle between the two moieties. Both systems studied are reversible, however for the second system based on ammonium and sulfonate units, due to precipitation only one cycle could be achieved.

In order to increase the solubility, one may replace the *meso*-phenyl groups by 3,5-tBuPhenyl or alkyl chains.

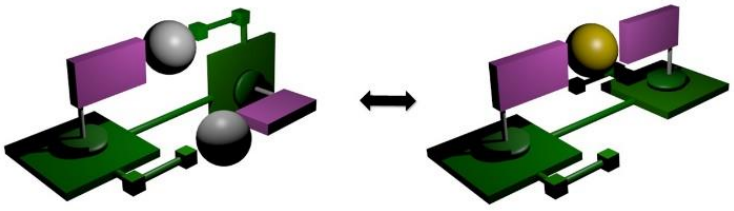

**Fig. 3.23** Schematic representation of a potential bistable gear.

Within this chapter, only a first step toward a functional molecular gear based on the Zn(II) dimer was investigated. One could introduce additional coordinating sites at the periphery of the porphyrin ring. The additional functionalization of one of the *meso*-positions would afford a system that could in principle be switched between two conformations: orthogonal and planar, as represented in **Fig. 3.23.** Further functionalization of the *meso*-positions of porphyrins could also leads to gears capable to interact with specific the surfaces. More complex gears composed of porphyrin trimer or tetramer.

## 5. References


1 S. Liu, D. V. Kondratuk, S. A. L. Rousseaux, G. Gil-Ramírez, M. C. O'Sullivan, J. Cremers, T. D. W. Claridge and H. L. Anderson, *Angew. Chemie Int. Ed.*, 2015, **54**, 5355–5359.

2 A. Sugasaki, K. Sugiyasu, M. Ikeda, M. Takeuchi and S. Shinkai, *J. Am. Chem. Soc.*, 2001, **123**, 10239–10244.

3 A. Robertson, M. Ikeda, M. Takeuchi and S. Shinkai, *Bull. Chem. Soc. Jpn.*, 2001, **74**, 883–888.

4 M. Ikeda, T. Tanida, M. Takeuchi and S. Shinkai, *Org. Lett.*, 2000, **2**, 1803–1805.

5 A. Sugasaki, M. Ikeda, M. Takeuchi and S. Shinkai, *Angew. Chemie Int. Ed.*, 2000, **39**, 3839–3842.

6 A. Sugasaki, M. Ikeda, M. Takeuchi, A. Robertson and S. Shinkai, *J. Chem. Soc. Perkin Trans. 1*, 1999, **1**, 3259–3264.

7 M. Takeuchi, T. Imada and S. Shinkai, *Angew. Chemie Int. Ed.*, 1998, **37**, 2096–2099.

8 V. S.-Y. Lin, S. G. DiMagno and M. J. Therien, *Science.*, 1994, **264**, 1105–1111.

9 H. L. Anderson, *Inorg. Chem.*, 1994, **33**, 972–981.

10 C. A. Hunter and J. K. M. Sanders, *J. Am. Chem. Soc.*, 1990, **112**, 5525–5534.

11 M. Kasha, H. R. Rawls and M. Ashraf El-Bayoumi, *Pure Appl. Chem.*, 1965, **11**, 371–392.

12 A. Tsuda, H. Hu, R. Tanaka and T. Aida, *Angew. Chemie Int. Ed.*, 2005, **44**, 4884–4888.

13 M. U. Winters, J. Kärnbratt, M. Eng, C. J. Wilson, H. L. Anderson and B. Albinsson, *J. Phys. Chem. C*, 2007, **111**, 7192–7199.

14 R. Stranger, J. E. McGrady, D. P. Arnold, I. Lane and G. A. Heath, *Inorg. Chem.*, 1996, **35**, 7791–7797.

15 S. R. Harper, M. C. Pfrunder, L. J. Esdaile, P. Jensen, J. C. McMurtrie and D. P. Arnold, *European J. Org. Chem.*, 2015, 2807–2825.

16 M. J. Langton, J. D. Matichak, A. L. Thompson and H. L. Anderson, *Chem. Sci.*, 2011, **2**, 1897–1901.

17 Y.-J. Chen, S.-S. Chen, S.-S. Lo, T.-H. Huang, C.-C. Wu, G.-H. Lee, S.-M. Peng and C.-Y. Yeh, *Chem. Commun.*, 2006, 1015–1017.

18 A. Berlicka, L. Latos-Grazynski and T. Lis, *Inorg. Chem.*, 2005, **44**, 4522–4533.

19 J.-W. Seo, S. Y. Jang, D. Kim and H.-J. Kim, *Tetrahedron*, 2008, **64**, 2733–2739.

20 M. Fathalla and J. Jayawickramarajah, *European J. Org. Chem.*, 2009, 6095–6099.

21 R. W. Wagner, T. E. Johnson, F. Li and J. S. Lindsey, *J. Org. Chem.*, 1995, **60**, 5266–5273.

22 A. Satake and Y. Kobuke, *Tetrahedron*, 2005, **61**, 13–41.

23 M. Nappa and J. S. Valentine, *J. Am. Chem. Soc.*, 1978, **100**, 5075–5080.

24 S. J. Cole, G. C. Curthoys, E. A. Magnusson and J. N. Phillips, *Inorg. Chem.*, 1972, **11**, 1024–1028.

25 P. Gans, A. Sabatini and A. Vacca, *Talanta*, 1996, **43**, 1739–1753.

26 *http://www.hyperquad.co.uk/*.

27 I. Kaljurand, A. Kutt, L. Soovali, T. Rodima, V. Maemets, I. Leito and I. A. Koppel, *J. Org. Chem.*, 2005, **70**, 1019–1028.

28 J. Otsuki, A. Yasuda and T. Takido, *Chem. Commun.*, 2003, 608–609.

29 J. A. Dean, in *Handbook of Organic Chemistry*, McGraw-Hill Book Co, New York, 1987, pp. 8–9.

# General Conclusions

The research carried out with the framework of this PhD training period was centred on the design and synthesis of new types of molecular turnstiles, photosensitizers and molecular gears.

The first chapter describes new molecular turnstiles based on P(V) porphyrin derivatives. Two families of molecular dynamic systems was prepared and their behaviour in solution was investigated. They were both based on P(V) porphyrin derivatives. They differ by the nature of the handle. The Turnstiles#1 is based a bidentate handle (handle#1) bearing two coordinating phenolate moieties while for the turnstiles#2, the bidentate handle (handle#2) is based on the coordination of non-aromatic alkoxide units at the axial position of P(V). Turnstiles#2 were found to be photo unstable and were not further studied. Concerning the two turnstiles#1, the one, based on phosphorus (V) tetraphenylporphyrin, was investigated as a model compound in order to test the synthetic pathway and to check the stability of compounds under acidic conditions. The dynamics of the movement in the one-station turnstile#1, based on P(V) [5-monopyridyl-(10,15,20)-triphenylporphyrin] and handle#1 was studied. The presence of a pyridyl group in the handle#1 allows the stopping of the movement either by addition of $Ag^+$ or $H^+$. Both processes are reversible and the addition of $NEt_4Br$ or $NEt_3$ respectively allows to switch between the close and open states.

Moreover, a new approach to the synthesis of P(V) porphyrins was elaborated. The use of $POBr_3$ to metallate the porphyrin cavity was found to be more efficient than the standard $POCl_3$&$PCl_5$ method. The molecular structures of phosphorus (V) complexes with 5-monopyridyl-(10,15,20)-triphenylporphyrin and hydroxyl axial ligands as well as oxyphenol axial groups were studied by single crystals X-ray diffraction. The $[P(MPyP)(OH)_2]^+$ complex forms a 1D zig-zag coordination polymer in the crystal due to hydrogen bonds between adjacent porphyrins. The geometry of P(V) MPyP complexes is similar to P(V) TPP complexes, the porphyrin core in all cases is not planar but strongly distorted (ruffled).

In the future, the formation of similar turnstiles bearing more than two coordinating sites at the *meso* positions of the porphyrin could in principle allow to master the directionality of the movement which is the final goal of this project. However, we noticed that the synthesis of such turnstiles might be rather difficult and would require new experimental strategies and conditions.

During the investigation of the P(V) based turnstiles, we noticed rather low photostability of the porphyrin based compounds in the presence of oxygen under irradiation. The second chapter of the manuscript describes photochemical properties of P(V) porphyrins. It was demonstrated that P(V) porphyrins are efficient photosensitizers. The studied compounds (except complexes with aryloxy- axial ligands) display high quantum yields for singlet oxygen generation in chloroform.

Lower values have been observed in DMSO and in water. In parallel, higher fluorescence quantum yields were observed in DMSO and water with respect to chloroform. The photophysical parameters depend on three main factors: nature of *meso*-substituents, axial ligands and the solvent. However, P(V) porphyrins bearing two aryloxy axial ligands behave differently probably due to PET. This explains the difference in photostability of the turnstile#1 and the turnstile#2. Flash-photolysis experiments are required to better understand the relaxation processes in the P(V) porphyrin derivatives upon excitation (especially ISC processes).

Some preliminary attempts to study photocatalytic properties of P(V) porphyrins were carried out. $[P(MPyP)(OEt)_2]^+$ complex showed the best results for hydroquinone oxidation in water. This type of P(V) porphyrin derivatives could be used for photo oxidation of other classes of compounds. They might also be of interest as PDT reagents.

The last part of the manuscript deals with a new type of molecular gears based on a Zn(II) porphyrin dimer. Two porphyrin moieties are linked with a non-flexible butadiyne bridge. In solution, the compound exists as a mixture of rotational conformers resulting from the flipping of the two porphyrins. We succeed in locking the system by blocking the flipping process. The first approach required the addition of a bis monodentate ligand (handle #3) that coordinates simultaneously to the axial position of both zinc (II) cation within the dimer. The reversibility of the process was shown from the addition of DMAP and TFA alternatively. The second design involves acid/base processes for the locking and unlocking of the molecular gear. The dynamic molecule is composed of the Zn(II) dimer and two axial monodentate ligands bearing either an acid (carboxylic) or a basic (amine) sites. The locking process is achieved through electrostatic interactions and H-bonding. Although the opening/closing processes are in principle reversible, only a single cycle could be achieved because of precipitation. Further functionalization of the porphyrin *meso*-positions of the dimer could open new perspectives in mastering the movement in such dimeric species.

# Experimental Part

## Materials and instruments

Unless otherwise noted, all chemicals and starting materials were obtained commercially from Acros® or Aldrich® and used without further purification.

Pyrrole was purified using chromatography on aluminum oxide. Dry pyridine was obtained by distillation over $CaH_2$. THF was dried and distilled over metallic sodium or using chromatography on aluminum oxide in the drying station. $Et_3N$ was dried over molecular sieves.

Aluminum Oxide 90 (Merck) and silica (Geduran, Silica Gel Si 60 from Merck) were used for column chromatography. BioRad Bio Beads S-X1 and S-X3 were used for the gel-permeation chromatography (GPC). Analytical thin-layer chromatography (TLC) was carried out using Merck silica gel 60 plates (precoated sheets, 0.2 mm thick, with fluorescence indicator F254). All reactions were performed under argon unless stated otherwise. Several reactions were carried out under microwave irradiation using Discover BenchMate microwave apparatus (CEM Corporation). The reactions were carried out in glass tubes equipped with a magnetic stirrer.

**$^{1}$H-NMR, $^{13}$C-NMR, $^{31}$P-NMR** and **$^{19}$F-NMR** spectra were acquired at 25 °C on Bruker Avance NMR spectrometers: AV 300 (300 MHz), AV400 (400 MHz), AV500 (500 MHz) or AV600 (600 MHz). NMR spectra were referenced to the residual solvent signal.

**UV-Vis absorption spectra** were obtained at room temperature on a Lambda 650S spectrometer (PerkinElmer) and Thermo Evolution 210 spectrometer in quartz cells with a 1 cm optical path. Spectrophotometric titrations were performed in 1 cm quartz cells with a Teflon stopper. Wavelengths (λ) are given in nm. Molar absorption coefficients (ε) are given in $L.mol^{-1}.cm^{-1}$.

**The photoluminescence spectra** ($\lambda_{ex}$ = 450 nm) at 25 °C were recorded on a Horiba Scientific Flourolog spectrofluorimeter with Fluorohub photon-counter for life-time measurements. Fluorescence quantum yields ($\Phi_F$) were determined by a comparative method using Eq. (1).

$$\Phi_F = \Phi_F^{St} \frac{F \cdot A^{St} \cdot n^2}{F^{St} \cdot A \cdot n_{St}^2} \qquad (1)$$

with F and $F^{St}$ areas under the fluorescence emission peaks of the samples and the standard, respectively; A and $A^{St}$ are absorbances of the samples and standard at the excitation wavelengths, respectively; $n^2$ and $n^2_{st}$ are the refractive indices of solvents used for the sample and standard, respectively. $H_2TPP$ (in toluene) ($\Phi_F$ = 0.11)[1] was used as the standard.

**Singlet oxygen quantum yield** ($\Phi_\Delta$) determination was carried out using the fiber-optic setup (Ocean Optics) described more in details in Chapter II. Singlet oxygen quantum yields were determined using $H_2TPP$ and $H_2TSP$ as references (see Chapter II). DPBF was used as a chemical

quencher for singlet oxygen in chloroform and DMSO. SOSG was used as a chemical quencher in distilled water. Eq. (2) was used for the calculations:

$$\Phi_{\Delta} = \Phi_{\Delta}^{St} \frac{R \cdot I^{St}}{R^{St} \cdot I} \qquad (2)$$

with $\Phi^{St}_{\Delta}$ the singlet oxygen quantum yield for the standard $H_2TPP$. R and $R^{St}$ are the DPBF photobleaching rates in non-aqueous solutions (or SOSG fluorescence increasing rates in water) in the presence of the sample and the standard, respectively. I and $I^{St}$ are the integral light absorption values of the sample and the standard, respectively. To avoid chain reactions induced by DPBF in the presence of singlet oxygen, the concentration of trap was lowered to $5\times10^{-5}$ M.

**Photodestruction experiments** were carried out in an irradiation chamber BS-02 (Opsytec Dr. Gröbel) with D65 lamps in time-controlling mode.

**MALDI TOF mass-spectra** were measured on a Bruker Daltonics Ultraflex(III) spectrometer without matrix.

**High-resolution mass spectra (HRMS) ESI-TOF** were recorded on the microTOF LC mass spectrometer (Bruker Daltonics).

**Elemental analysis** was performed on a Thermo Scientific Flash 2000.

**Quantum chemical calculations** were provided with Spartan'14 software (Wavefunction Inc., CA, USA) with B3LYP(6-31G*) basic set.

**Single-crystal X-ray diffraction experiments** were carried out on a Bruker APEX8 CCD diffractometer equipped with an Oxford Cryosystem liquid $N_2$ device at 173(2) K, using a molybdenum microfocus sealed tube generator with mirror-monochromated Mo-Kα radiation (λ = 0.71073 Å), operated at 50 kV/600 μA. The structures were solved using SHELX-97 and refined by full matrix least squares on $F^2$ using SHELX-97 with anisotropic thermal parameters for all non-hydrogen atoms. Hydrogen atoms were introduced at calculated positions and not refined (riding model).

## Synthetic procedures and characterizations.

| | |
|---|---|
| **5,10,15,20-tetraphenylporphyrin, $H_2$TPP (1a)**<br><br>**5-monopyridyl-(10,15,20)-triphenylporphyrin $H_2$MPyP (1b)**<br><br>**(5,15)-dipyridyl-(10,20)-diphenylporphyrin $H_2$DPyP (1c)** | 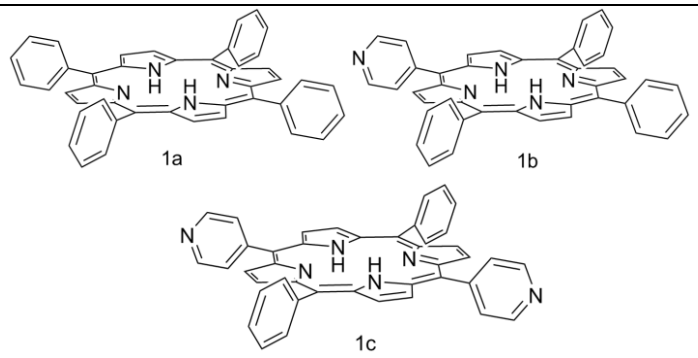 |

$H_2$MPyP was prepared according to a modified literature protocol[2] that leads to the formation of a mixture of porphyrins, including $H_2$TPP and $H_2$DPyP.

Pyrrole (4 ml, 57.65 mmol, 4 eq.), 4-pyridinecarboxaldehyde (1.35 ml, 14.33 mmol, 1 eq. and benzaldehyde (4.40 ml, 43.29 mmol 3 eq.) were added to a round-bottom flask (0,5 L) preliminary filled with 250 ml of propionic acid and the mixture bubbled with argon during 15 minutes. The reaction mixture was refluxed for 2 h, then cooled to the room temperature, diluted with ethanol (400 ml) and left in the fridge for 1 night. The purple solid was filtrated and washed several times with ethanol until the colorless filtrate. The resulting crude solid was dried under vacuum and purified by column chromatography on silica gel. $H_2$TPP **(1a)** was isolated (500 mg, 2.5%) as the first fraction using a cyclohexane-DCM mixture (1:1). $H_2$MPyP **(1b)** was isolated (440 mg, 5%) as the second fraction using DCM. Increasing the polarity of the eluent (DCM + 1vol % of MeOH) afforded $H_2$DPyP **(1c)** (130 mg, 3%).

**$H_2$TPP** - $^1$H-NMR ($CDCl_3$, 600 MHz) δ, ppm: -2.77 (s, 2H, NH), 7.77 (m, 12H, *m*- and *p*-phenyl), 8.22 (d, $^3J$ = 6.8 Hz, 8H, *o*-phenyl), 8.84 (s, 8H, β-pyrr).

**$H_2$MPyP** - $^1$H-NMR ($CDCl_3$, 600 MHz) δ, ppm: -2.80 (s, 2H, NH), 7.77 (m, 9H, *m*- and *p*-phenyl), 8.18 (m, 2H, *o*-pyridyl), 8.21 (m, 6H, *o*-phenyl), 8.80 (d, $^3J$ = 4.4 Hz, 2H, β-pyrr), 8.86 (s, 4H, β-pyrr), 8.89 (d, $^3J$ = 4.4 Hz, 2H, β-pyrr), 9.04 (m, 2H, *m*-pyridyl).

**$H_2$DPyP** - $^1$H-NMR ($CDCl_3$, 600 MHz) δ, ppm: -2.84 (s, 2H, NH), 7.78 (m, 6H, *m*- and *p*-phenyl), 8.18 (m, 4H, *o*-pyridyl), 8.21 (d, $^3J$ = 6.9 Hz, 4H, *o*-phenyl), 8.81 (d, $^3J$ = 4.3 Hz, 4H, β-pyrr), 8.91 (d, $^3J$ = 4.3 Hz, 4H, β-pyrr), 9.04 (m, 4H, *m*-pyridyl).

| | |
|---|---|
| **5-(pentafluorophenyl)-(10,15,20)-triphenylporphyrin, $H_2$MpFP (2).** | 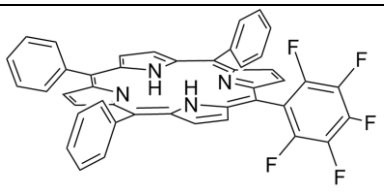 |

The porphyrin **2** was synthesized according to a described procedure.[3]

Pyrrole (5 ml, 72.07 mmol, 4 eq.), pentafluorobenzaldehyde (3.53 g, 18.02 mmol, 1 eq.) and benzaldehyde (5.5 ml, 54.05 mmol, 3 eq.) were added to a round-bottom flask (0.5 L) preliminary filled with 300 ml of propionic acid and the mixture bubbled with argon during 15 minutes. The reaction mixture was refluxed under argon during 2 h. After cooling to room temperature, ethanol was added (300 ml) and the mixture was left in the fridge overnight. The purple precipitate was filtrated and washed several times with ethanol until the colorless filtrate. Then it was dried under vacuum and purified by column chromatography on silica gel using toluene-petroleum ether mixture (3:7). The 5$^{th}$ fraction was collected, the solvent was evaporated to afford target product **2** (270 mg, 2.5%) as a purple solid.

$^{1}$H-NMR ($CDCl_3$, 500 MHz) δ, ppm: -2.73 (s, 2H, NH), 7.79 (m, 9H, *m*- and *p*-phenyl), 8.23 (m, 6H, *o*-phenyl), 8.79 (d, $^{3}J$ = 4.9 Hz, 2H, β-pyrr), 8.87 (s, 4H, β-pyrr), 8.96 (d, $^{3}J$ = 4.9 Hz, 2H, β-pyrr).

| **2,6-bis(chloromethyl)pyridine (3).** | 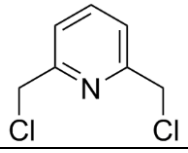 |
|---|---|



This compound was synthesized following a described procedure.[4]

The 2,6-bis(oxymethyl)pyridine (4 g, 28.75 mmol, 1 eq.) was dissolved in dry THF (100 ml). The mixture was bubbled with argon during 15 min and then $SOCl_2$ (5.5 ml, 71.87 mmol, 2.5 eq.) dissolved in THF (30 ml) was added dropwise during 1 h. The mixture was stirred during 24 h-at room temperature. Then the solvent was evaporated and the solid was dissolved in dichloromethane. The mixture was washed with 0.1 M $NaHCO_3$ (4 x 300 ml) and water (5 x 600 ml). The organic layer was evaporated and the residue was dried under vacuum to afford target product **3** with 93% yield (4.91 g).

$^{1}$H-NMR ($CDCl_3$, 300 MHz) δ, ppm 4.67 (s, 4H, $CH_2$), 7.44 (d, $^{3}J$ = 7.7 Hz, 2H, *m*-pyridyl), 7.77 (t, $^{3}J$ = 7.7 Hz, 1H, *p*-pyridyl).

| **2-(2-(2-((tetrahydro-2H-pyran-2-yl)oxy)ethoxy)ethoxy)ethanol (4).** | 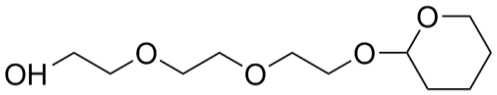 |
|---|---|



This compound was synthesized using a described procedure.[4]

The triethylene glycol (20 ml, 146.50 mmol, 3 eq.) and 3,4-dihydro-2H-pyran (DHP) (4.46 ml, 48.83 mmol, 1 eq.) were mixed in a 25 ml round-bottom flask and 7 drops of concentrated HCl were added as a catalyst. The mixture was stirred at room temperature during 24 h. Then it was diluted with 300 ml of chloroform and washed with 4 x 700 ml of 0.1 M $NaHCO_3$. The organic

layer was dried under vacuum and purified by $SiO_2$ column chromatography using methanol-ethyl acetate (1:9) affording compound **4** with 56% yield (6.40 g) as a colorless oil.

$^1$H-NMR ($CDCl_3$, 600 MHz) δ, ppm: 1.43 (m, 4H, $CH_{2\ THP}$), 1.62 (m, 1H, $CH_{2\ THP}$), 1.74 (m, 1H, $CH_{2\ THP}$), 3.41 (m, 2H, $CH_2O$), 3.54 (m, 10H, $CH_2O$), 3.77 (m, 2H, $CH_2O$), 4.54 (s, 1H, CH).
$^{13}$C-NMR ($CDCl_3$, 75 MHz) δ, ppm: 19.5 ($CH_{2\ THP}$), 25.3 ($CH_{2\ THP}$), 30.5 ($CH_{2\ THP}$), 61.7 ($CH_2O$), 62.1 ($CH_2O$), 62.4 ($CH_2O$), 66.6 ($CH_2O$), 66.8 ($CH_2O$), 70.4 ($CH_2O$), 72.4 ($CH_2O$), 99.1 ($CH_{THP}$).

| **2,6-bis((2-(2-(2-((tetrahydro-2H-pyran-2-yl)oxy)ethoxy)ethoxy)ethoxy)methyl)pyridine (5).** | 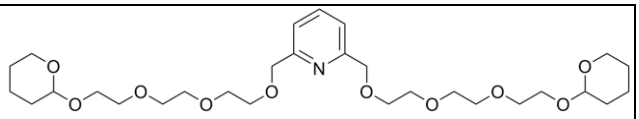 |
|---|---|

This compound was synthesized according to a described procedure.[4]

A suspension of NaH (1.09 g (60% dispersion in mineral oil), 27.32 mmol, 2.2 eq.) in dry THF (200 ml) was cooled to 0$^o$C and (6.4 g, 27.32 mmol, 2.2 eq.) of **4** (dissolved in dry THF (50 ml)) was added to the suspension. Then compound **3 (**2.2 g, 12.42 mmol, 1 eq.) dissolved in dry THF (50 ml) was added dropwise and the reaction mixture was refluxed during 5 days. The solvent was removed under vacuum. The brown solid was dissolved in 300 ml of chloroform. It was washed with water (4 x 300 ml). The organic layer was isolated. The solvents were removed under vacuum and the brown oil was purified by $Al_2O_3$ column chromatography using ethyl acetate-n-hexane (1:1) affording the compound **5** with 58% yield (4.10 g) as a colorless oil.

$^1$H-NMR ($CDCl_3$, 300 MHz) δ, ppm 1.44-1.81 (m, 12H, $CH_{2\ THP}$), 3.42-3.86 (m, 28H, $CH_2O$ and $CH_2O_{THP}$), 4.59 (m, 2H, CH), 4.63 (s, 4H, $PyCH_2$), 7.34 (d, $^3J$ = 7.7 Hz, 2H, m-pyridyl), 7.66 (t, $^3J$ = 7.8 Hz, p-pyridyl).
$^{13}$C-NMR ($CDCl_3$, 75 MHz) δ, ppm: 19.4 ($CH_{2\ THP}$), 25.3 ($CH_{2\ THP}$), 30.4 ($CH_{2\ THP}$), 62.1 ($CH_2O$), 66.5 ($CH_2O$), 70.2 ($CH_2O$), 70.4 ($CH_2O$), 70.5 ($CH_2O$), 70.6 ($CH_2O$), 73.9 ($PyCH_2$), 98.8 ($CH_{\ THP}$), 119.8 ($CH_{Py}$), 137.1 ($CH_{Py}$), 157.8 (C).

| **2,2'-((((((pyridine-2,6-diylbis(methylene))bis(oxy))bis(ethane-2,1-diyl))bis(oxy))bis(ethane-2,1-diyl))bis(oxy))diethanol (6).** | 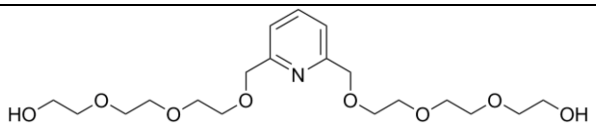 |
|---|---|

This compound was synthesized using a described procedure.[4]

A solution of **5** (4.10 g, 7.18 mmol, 1 eq.) in methanol (500 ml) with 10 drops of HCl was stirred at room temperature for 7 h. Solid $NaHCO_3$ was added to the mixture until pH 7 was reached. The solvent was evaporated and the solid residue was dissolved in diethyl ether and filtrated. The solvent was evaporated afforded compound **6** in quantitative yield (2.90 g) as a pale yellow oil.

$^{1}$H-NMR ($CDCl_3$, 600 MHz) δ, ppm: 3.53-3.78 (m, 24H, $CH_2O$), 4.67 (s, 4H, $PyCH_2$), 7.36 (d, $^{3}J$ = 7.6 Hz, 2H, *m*-pyridyl), 7.72 (t, *J*=7.8 Hz, *p*-pyridyl).

$^{13}$C-NMR ($CDCl_3$, 150 MHz) δ, ppm: 61.5 ($CH_2O$), 70.0 ($CH_2O$), 70.2 ($CH_2O$), 70.4 ($CH_2O$), 70.5 ($CH_2O$), 72.6 ($CH_2O$), 73.7 ($PyCH_2$), 120.4 ($CH_{Py}$), 137.4 ($CH_{Py}$), 157.5 (C).

| **((((((Pyridine-2,6-diylbis(methylene))bis(oxy))bis(ethane-2,1-diyl))bis(oxy))bis(ethane-2,1-diyl))bis(oxy))bis(ethane-2,1-diyl) dimethanesulfonate (7).** | 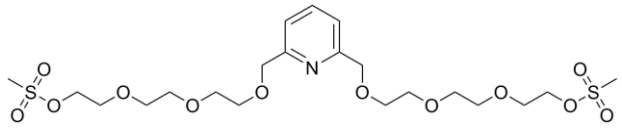 |
|---|---|

This compound was synthesized using a described procedure.[4]

A solution of **6** (2.90 g, 7.18 mmol, 1 eq.) in dry THF (200 ml) was bubbled with argon during 30 min. Then triethylamine (3.50 ml, 25.17 mmol, 3.5 eq.) and methanesulfonyl chloride (1.95 ml, 25.17 mmol, 3.5 eq.) were added under argon and the mixture was stirred during 5 h at room temperature. 200 ml of chloroform was added and the mixture was washed with 0.1M $NaHCO_3$ (4 x 400 ml) and water (4 x 400 ml). Chloroform was evaporated and the yellow oil thus obtained was dried under vacuum. The compound **7** was obtained in quantitative yield (4.03 g).

$^{1}$H-NMR ($CDCl_3$, 600 MHz) δ, ppm: 2.99 (s, 6H, $SCH_3$), 3.57-3.72 (m, 20H, $CH_2O$), 4.30 (m, 4H, $CH_2O$), 4.61 (s, 4H, $PyCH_2$), 7.33 (d, $^{3}J$ = 7.8 Hz, 2H, *m*-pyridyl), 7.70 (t, $^{3}J$ = 7.8 Hz, *p*-pyridyl).

$^{13}$C-NMR ($CDCl_3$, 150 MHz) δ, ppm: 37.3 ($SCH_3$), 69.0 ($CH_2O$), 69.2 ($CH_2O$), 70.2 ($CH_2O$), 70.5 ($CH_2O$), 70.6 ($CH_2O$), 70.7 ($CH_2O$), 74.0 ($PyCH_2$), 120.0 ($CH_{Py}$), 137.3 ($CH_{Py}$), 157.8 (C).

| **3-((tetrahydro-2H-pyran-2-yl)oxy)phenol (8).** | 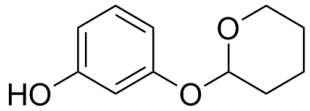 |
|---|---|

This compound was obtained using a described procedure.[5]

Resorcinol (5 g, 45.41 mmol, 1 eq.) was dissolved in 3,4-dihydro-2H-pyran (DHP) (4.55 ml, 49.95 mmol, 1.1 eq.). Then $AlCl_3{\cdot}6H_2O$ (121 mg, 45.40 mmol, 0.01 eq.) was added and the mixture was stirred during 20 h. The reaction mixture was purified by column chromatography on $SiO_2$ using ethyl acetate - *n*-hexane (1:9) to give 2.11 g of compound **8** (yield 24%).

$^{1}$H-NMR ($CDCl_3$, 600 MHz) δ, ppm: 1.67 (m, 4H, $CH_{2\ THP}$), 1.84 (m, 1H, $CH_{2\ THP}$), 1.99 (m, 1H, $CH_{2\ THP}$), 3.62 (m, 1H, $OCH_{2\ THP}$), 3.93 (m, 1H, $OCH_{2\ THP}$), 5.38 (t, $^{3}J$ = 3.2 Hz, 1H, $CH_{THP}$), 6.46 (dd $^{3}J$ = 8.0 Hz, $^{4}J$ = 2.2 Hz, 1H, $CH_{res}$), 6.58 (dd, $^{4}J$ = 2.6 Hz, $^{4}J$ = 2.6 Hz, 1H, $CH_{res}$), 6.60 (dd, $^{3}J$ = 7.8 Hz, $^{4}J$ = 2.2 Hz, 1H, $CH_{res}$), 6.67 (s, 1H, OH), 7.09 (dd, $^{3}J$ = 8.1 Hz, $^{3}J$ = 8.1 Hz, 1H, $CH_{res}$).

$^{13}$C-NMR ($CDCl_3$, 150 MHz) δ, ppm: 18.8 ($CH_{2\ THP}$), 25.2 ($CH_{2\ THP}$), 30.4 ($CH_{2\ THP}$), 62.2 ($OCH_{2\ THP}$), 96.5 ($CH_{THP}$), 104.1 ($CH_{res}$), 108.7 ($CH_{res}$), 109.0 ($CH_{res}$), 130.1 ($CH_{res}$), 157.1 (C), 158.2 (C).

| | |
|---|---|
| **2,6-bis((2-(2-(2-(3-((tetrahydro-2H-pyran-2yl)oxy)phenoxy)ethoxy)ethoxy) methyl)pyridine (9).** | 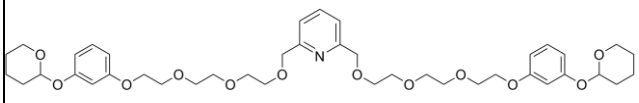 |

This compound was synthesized according to a described procedure.[4]

A suspension of NaH (0.87 g, 21.73 mmol, 4.4 eq., (60% dispersion in mineral oil)) in 150 ml of dry THF was bubbled with argon for 30 min and cooled down to 0 °C. A degassed solution of **8** (2.11 g, 10.87 mmol, 2.2 eq.) in 75 ml of dry THF was added dropwise and the mixture was stirred at 0 °C for 1.5 h. Then a degassed solution of **7** (2.76 g, 4.94 mmol, 1 eq.) in 80 ml of THF was added dropwise. The reaction mixture was refluxed under argon during 3 days. After evaporation of the solvent the brown residue was purified by column chromatography ($Al_2O_3$, *n*-hexane - ethyl acetate, 1:1) to give 2.63 g (70%) of the compound **9** as the pale yellow oil.

$^1$H-NMR ($CDCl_3$, 600 MHz) δ, ppm: 1.66 (m, 8H, $CH_{2\ THP}$), 1.83 (m, 2H, $CH_{2\ THP}$), 1.99 (m, 2H, $CH_{2\ THP}$), 3.55-3.92 (m, 24H, $CH_2O$), 4.10 (m, 4H, $OCH_{2\ THP}$), 4.65 (s, 4H, $PyCH_2$), 5.37 (t, $^3J$ = 3.4 Hz, 2H, $CH_{THP}$), 6.53 (m, 2H, $CH_{res}$), 6.64 (m, 4H, $CH_{res}$), 7.14 (dd, $^3J$ = 8.6 Hz, $^3J$ = 8.6 Hz, 2H, $CH_{res}$), 7.36 (d, $^3J$ = 7.7 Hz, 2H, *m*-pyridyl), 7.66 (t, $^3J$ = 7.8 Hz, 1H, *p*-pyridyl).

$^{13}$C-NMR ($CDCl_3$, 150 MHz) δ, ppm: 18.8 ($CH_{2\ THP}$), 25.2 ($CH_{2\ THP}$), 30.9 ($CH_{2\ THP}$), 62.1 ($CH_2O$), 67.4 ($CH_2O$), 69.8 ($CH_2O$), 70.3 ($CH_2O$), 70.6 ($CH_2O$), 70.7 ($CH_2O$), 70.8 ($CH_2O$), 74.1, 96.4 ($PyCH_2$), 103.6 ($CH_{res}$), 107.9 ($CH_{res}$), 109.0 ($CH_{res}$), 119.9 ($CH_{Py}$), 129.7 ($CH_{res}$), 137.3 ($CH_{Py}$), 157.9 (C), 158.3 (C), 159.9 (C).

| | |
|---|---|
| **3,3'-(((((((pyridine-2,6-diylbis(methylene))bis-(oxy))-bis-(ethane-2,1-diyl))bis(oxy))bis(ethane-2,1-diyl))bis(oxy))bis(ethane-2,1-diyl))bis(oxy))diphenol (10); Handle#1** | 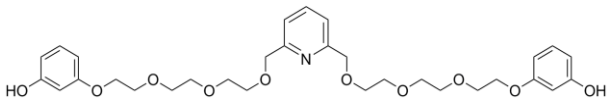 |

This compound was synthesized using a described procedure.[4]

A solution of **9** (2.63 g, 3.48 mmol, 1 eq.) in methanol (250 ml) in the presence of 25 drops of HCl was stirred at room temperature for 6 h. Solid $NaHCO_3$ was added to the solution until pH 7 was reached. After evaporation of methanol the crude product was purified by column chromatography ($SiO_2$, methanol - ethyl acetate, 1:9) to give pure **10** as a pale yellow oil (1.94 g, 95%).

$^1$H-NMR ($CDCl_3$, 600 MHz) δ, ppm: 3.64-3.70 (m, 16H, $CH_2O$), 3.80 (m, 4H, $CH_2O$), 4.06 (m, 4H, $CH_2O$), 4.70 (s, 4H, $PyCH_2$), 6.41 (dd, $^3J$ = 8.1 Hz, $^4J$ = 2.2 Hz, 2H, $CH_{res}$), 6.44 (dd, $^3J$ = 8.1 Hz, $^4J$ = 2.2 Hz, 2H, $CH_{res}$), 6.42 (dd, $^4J$ = 2.3 Hz, $^4J$ = 2.3 Hz, 2H, $CH_{res}$), 7.07 (dd, $^3J$ = 8.1 Hz, $^3J$ = 8.1 Hz, 2H, $CH_{res}$), 7.40 (d, $^3J$ = 7.7 Hz, 2H, *m*-pyridyl), 7.67 (t, $^3J$ = 7.8 Hz, 1H, *p*-pyridyl).

$^{13}$C-NMR ($CDCl_3$, 150 MHz) δ, 67.4 ($CH_2O$), 69.7 ($CH_2O$), 70.4 ($CH_2O$), 70.7 ($CH_2O$), 70.8 ($CH_2O$), 70.9 ($CH_2O$), 73.0 ($PyCH_2$), 102.8 ($CH_{res}$), 106.4 ($CH_{res}$), 108.5 ($CH_{res}$), 121.1 ($CH_{Py}$), 130.0 ($CH_{res}$), 157.2 ($CH_{Py}$), 157.6 (C), 159.9 (C), 159.9 (C).

| **2-(2-(2-(2-((tetrahydro-2H-pyran-2-yl)oxy)ethoxy)ethoxy)ethoxy)ethanol (11).** | 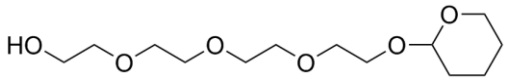 |
|---|---|

This compound was synthesized using a described procedure.[6]

The tetraethylene glycol (41.4 ml, 239.80 mmol, 3 eq.) and 3,4-dihydro-2H-pyran (DHP) (7.30 ml, 79.93 mmol, 1 eq.) were mixed in 25 ml round-bottom flask and 10 drops of concentrated HCl were added as a catalyst. The mixture was stirred at room temperature for 20 h, diluted with 120 ml of chloroform and washed with 0.1 M $NaHCO_3$ (4 x 700 ml). The organic layer was dried under vacuum at 60 ºC overnight to afford 17 g (yield 73%) of compound **11** as pale yellow oil.

$^1$H-NMR ($CDCl_3$, 300 MHz) δ, ppm 1.20-1.72 (m, 6H, $CH_{2\ THP}$), 3.10-3.75 (m, 16H, $CH_2O$), 4.40 (s, 1H, $OCH_{THP}$).

| **2,6-bis(13-((tetrahydro-2H-pyran-2-yl)oxy)-2,5,8,11-tetraoxatridecyl)pyridine (12).** | 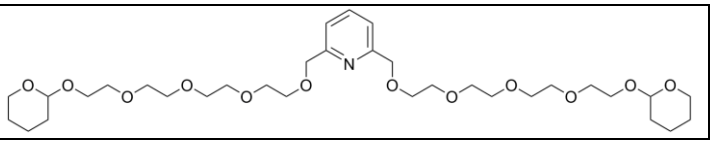 |
|---|---|

This compound was synthesized using a described procedure.[6]

A suspension of NaH (2.44 g, 61.08 mmol, 2.2 eq., 60% dispersion in mineral oil) in dry THF (300 ml) was cooled to 0ºC under argon and the compound **11** (17 g, 61.08 mmol, 2.2 eq.) dissolved in dry THF (100 ml)) was added dropwise to the suspension. After 45 min of stirring, compound **3** (4.89 g, 27.76 mmol, 1 eq.) dissolved in dry THF (100 ml) was added dropwise. The reaction mixture was refluxed for 120 h. After evaporation of solvent under vacuum, the brown solid was dissolved in DCM (400 ml) and washed with water (4 x 500 ml). The organic layer was isolated and DCM was evaporated under vacuum. The brown oil thus obtained was purified by column chromatography ($Al_2O_3$, ethyl acetate - petroleum ether, 6:4) to afford 11.82 g (yield 64%) of colorless oil **12**.

$^1$H-NMR ($CDCl_3$, 400 MHz) δ, ppm 1.43-1.88 (m, 12H, $CH_{2THP}$), 3.43-3.90 (m, 32H, $CH_2O$), 4.62 (m, 2H, $CH_{THP}$), 4.66 (s, 4H, $PyCH_2$), 7.37 (d, $^3J$ = 7.7 Hz, 2H, *m*-pyridyl), 7.70 (t, $^3J$ = 7.7 Hz, 1H, *p*-pyridyl).

$^{13}$C-NMR ($CDCl_3$, 150 MHz) δ, 19.5 ($CH_{2\ THP}$), 25.4 ($CH_{2\ THP}$), 30.6 ($CH_{2\ THP}$), 62.2 ($CH_2O$), 66.6 ($CH_2O$), 70.3 ($CH_2O$), 70.5 ($CH_2O$), 70.6 ($CH_2O$), 70.7 ($CH_2O$), 74.0 ($PyCH_2$), 98.9 ($CH_{THP}$), 119.9 ($CH_{Py}$), 137.2 ($CH_{Py}$), 157.9 (C).

| | |
|---|---|
| **1,1'-(pyridine-2,6-diyl)bis(2,5,8,11-tetraoxatridecan-13-ol) (13).** | 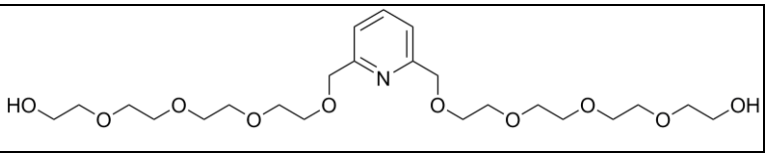 |

This compound was synthesized using a described procedure.[6]

A solution of **12** (11.32 g, 17.91 mmol) in methanol (1 L) with 10 ml of HCl was stirred at room temperature for 36 h. Solid $NaHCO_3$ was added to the mixture until pH 7 was reached. After evaporation of methanol, the solid residue was dissolved in diethyl ether. The mixture was filtrated and ether was evaporated. The compound **13** was isolated as colorless oil in 88% yield (7.37 g).

$^1$H-NMR ($CDCl_3$, 300 MHz) δ, ppm 3.51-3.73 (m, 32H, $CH_2O$), 4.63 (s, 4H, $PyCH_2$), 7.36 (d, $^3J$ = 7.7, 2H, *m*-pyridyl), 7.69 (t, $^3J$ = 7.7 Hz, 1H, *p*-pyridyl).

| | |
|---|---|
| **1,1'-(pyridine-2,6-diyl)bis(2,5,8,11-tetraoxatridecane-13,1-diyl)bis(4-methylbenzenesulfonate) (14). Handle#2** | 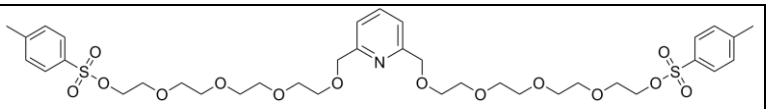 |

A solution of **13** (7.07 g, 14.38 mmol, 1 eq.) in dry THF **(**300 ml) was bubbled with argon during 30 min. Triethylamine (6.80 ml, 48.90 mmol, 3.4 eq.) and tosyl chloride (8.22 g, 43.15 mmol, 3.0 eq.) were added under argon and the reaction mixture was stirred at room temperature for 5 h. After addition of chloroform (600 ml) the reaction mixture was washed several times with 0.1M $NaHCO_3$ (4 x 500 ml) and water (4 x 500 ml). The organic layer was isolated and after evaporation of chloroform, the yellow oil was dried under vacuum affording the compound **14** (2.77 g, 25% yield).

$^1$H-NMR ($CDCl_3$, 300 MHz) δ, ppm: 2.40 (s, 6H, $CH_3$), 3.64 (m, 28H, $CH_2O$), 4.12 (m, 4H, $CH_2O$), 4.62 (s, 4H, $ArCH_2$), 7.30 (d, $^3J$ = 8.0 Hz, 4H, $CH_{tosyl}$), 7.33 (d, $^3J$ = 7.8 Hz, 2H, *m*-pyridyl), 7.66 (t, $^3J$ = 7.9, 1H, *p*-pyridyl), 7.75 (d, $^3J$ = 8.4, 4H, $CH_{tosyl}$).

$^{13}$C-NMR ($CDCl_3$, 125 MHz) δ, 21.6 ($CH_3$), 68.1 ($CH_2O$), 68.6 ($CH_2O$), 69.3 ($CH_2O$), 69.4 ($CH_2O$), 70.1 ($CH_2O$), 70.5 ($CH_2O$), 70.6 ($CH_2O$), 70.7 ($CH_2O$), 72.4 ($PyCH_2$), 125.9 ($CH_{Py}$), 127.9 ($CH_{Ts}$), 128.8 ($CH_{Py}$), 129.9 ($CH_{Ts}$), 133.7 (C), 144.9 (C), 154.2 (C).

Elemental analysis, %: calculated for $C_{37}H_{55}NO_{15}S_2 \cdot 0.71(CH_2Cl_2) \cdot 0.71(H_2O) \cdot 0.29(N_3Et)$: C, 52.48; H, 6.72; N, 2.00. Found C, 52.43; H, 6.76; N, 2.00

| | |
|---|---|
| **Dichloro(5,10,15,20-tetraphenylporphyrinato)phosphorus(V) chloride, $[P(TPP)Cl_2]^+Cl^-$ (15).** | 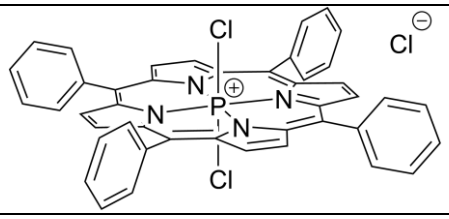 |

Porphyrin **15** was obtained according to a modified literature procedure.[7]

The free-base 5,10,15,20-tetraphenylporphyrin, $H_2TPP$ **(1a)** (0.1 g, 0.16 mmol, 1 eq.) was dissolved in 18 ml of pyridine under argon and $POCl_3$ (2 ml, 21.96 mmol, 135 eq.) was added dropwise to the mixture under stirring. A solution of $PCl_5$ **(**0.1 g, 0.48 mmol, 3 eq.) in 2 ml of pyridine was then added dropwise and the mixture was refluxed under argon during 24 h. After cooling to the room temperature and evaporation of pyridine under vacuum, the dark green solid was dissolved in 50 ml of $CH_2Cl_2$ and washed with distilled water (3 x 400 ml) to remove residual pyridine. The organic layer was isolated and after evaporation of DCM, the green solid was purified by column chromatography on alumina using DCM-methanol (95:5) as eluent. The major main fraction was isolated and evaporated to dryness before it was further purified by chromatography on Bio-Beads S-X3 column (eluent – chloroform) affording 0.1 g (yield 82%) of pure compound **15** as a green solid.

$^1$H-NMR ($CDCl_3$, 300 MHz) δ, ppm: 7.80 (m, 12H, *m*- and *p*-phenyl), 7.99 (m, 8H, *o*-phenyl), 9.14 (d, $^4J_{P\text{-}H}$ = 4.5 Hz, 8H, β-pyrr).

$^{31}$P-NMR ($CDCl_3$, 121 MHz) δ, ppm: -229

$^{13}$C-NMR ($CDCl_3$, 125 MHz) δ, ppm: 117.7 (C, $^3J_{P\text{-}C}$ = 3.3 Hz), 128.8 (CH), 130.5 (CH), 132.8 (CH, $^3J_{P\text{-}C}$ = 6.5 Hz), 133.3 (CH), 134.2 (C), 140.0 (C).

HR-ESI MS: *m/z* calcd. for $[C_{44}H_{28}Cl_2N_4P]^+$ : 713.1423; found: 713.1407 [**15**-Cl]$^+$.

UV-vis ($CHCl_3$): λ, nm (log ε) 440 (5.44), 568 (4.13), 613 (4.00).

| | |
|---|---|
| **Dihydroxy(5,10,15,20-tetraphenylporphyrinato)phosphorus(V) chloride, $[P(TPP)(OH)_2]^+Cl^-$ (16a).** | 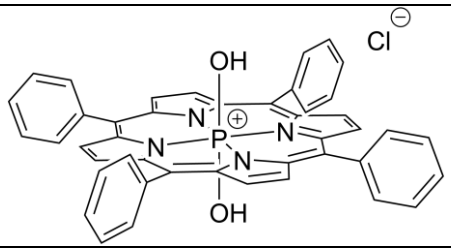 |

A previously described procedure was applied.[7]

The porphyrin $[P(TPP)Cl_2]^+Cl^-$ **(15) (**0.05 g, 0,07 mmol, 1 eq.) dissolved in a mixture of distilled water (15 ml) and pyridine (25 ml) and the mixture was refluxed overnight. Water and pyridine were removed under vacuum. The residue was dissolved in DCM (80 ml) and washed with distilled water (3 x 400ml) to remove residual pyridine. Solvent was evaporated under vacuum and the purple residue was purified by column chromatography on alumina with a mixture of DCM and methanol (from 0% to 5%) as an eluent affording 0.031 g (yield 65%) of a purple solid.

$^{1}$H-NMR ($CDCl_3$, 400 MHz) δ, ppm: 7.69 (m, 12H, *m*- and *p*-phenyl), 8.01 (m, 8H *o*-phenyl), 8.89 (d, $^{4}J_{P\text{-}H}$ = 2.7 Hz, 8H, β-pyrr).

$^{31}$P-NMR ($CDCl_3$, 162 MHz) δ, ppm: -193.

UV-vis ($CHCl_3$) λ, nm (logε): 428 (5.42), 556 (4.21), 596 (3.92).

| | |
|---|---|
| **Dihydroxy(5,10,15,20-tetraphenylporphyrinato)phosphorus(V) bromide,** **$[P(TPP)(OH)_2]^+Br^-$ (16b).** | 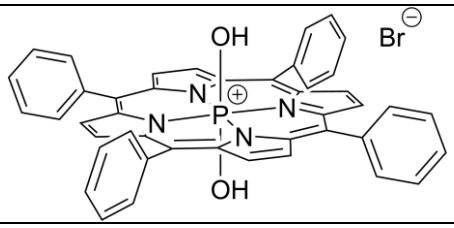 |

A procedure described for phthalocyanines[8] was modified and adapted for porphyrins.

The porphyrin $H_2TPP$ **(1a)** (0.1 g, 0.16 mmol, 1 eq.) was dissolved in pyridine (60 ml) under argon and $POBr_3$ (1.1 g, 4.06 mmol, 25 eq.) previously dissolved in pyridine (20 ml) was added dropwise to the mixture under stirring. The reaction mixture was refluxed during 80 min under argon and then cooled to room temperature. The green mixture was then poured into 150 ml of $CH_2Cl_2$ and 2L of distilled water was added and the mixture stirred during 2 days at room temperature until full hydrolysis of $[P(TPP)(Br)_2]^+Br^-$ to the dihydroxy complex $[P(TPP)(OH)_2]^+Br^-$ was completed. The organic layer was isolated and diluted with petroleum ether (150 ml). The mixture was poured directly on a $SiO_2$ chromatography column without evaporation of solvents. Increasing the polarity of the eluent using $CH_2Cl_2$-MeOH mixture (90:10) give the crude product. Further purification of product by Bio-Beads S-X1 GPC (eluent – chloroform-methanol 98:2) afforded 0,115 g of the pure purple compound **16b** in 95 % yield.

$^{1}$H-NMR ($CDCl_3$, 400 MHz) δ, ppm: 7.69 (m, 12H, *m*- and *p*-phenyl), 8.01 (m, 8H *o*-phenyl), 8.89 (d, $^{4}J_{P\text{-}H}$ = 2.7 Hz, 8H, β-pyrr).

$^{31}$P-NMR ($CDCl_3$, 162 MHz) δ, ppm: -193.

$^{13}$C-NMR ($CDCl_3$, 125 MHz) δ, ppm: 115.9 (C), 127.7 (CH), 128.7 (CH), 132.0 (CH), 133.7 (CH), 134.7 (C), 139.5 (C).

HR-ESI MS: *m/z* calcd. for $[C_{44}H_{30}N_4O_2P]^+$: 677.2101; found: 677.2084 [**16b**-Br]$^+$.

UV-vis ($CHCl_3$) λ, nm (logε): 428 (5.42), 556 (4.21), 596 (3.92).

| | |
|---|---|
| **Di-(3-methoxyphenoxy)-(5,10,15,20-tetraphenylporphyrinato)phosphorus(V) chloride,** **$[P(TPP)(OPhOMe)_2]^+Cl^-$ (17).** | 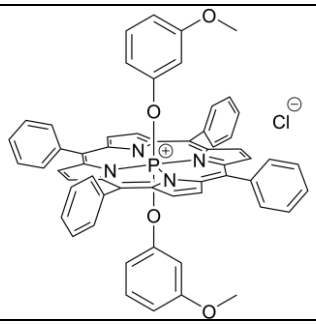 |

The porphyrin $[P(TPP)Cl_2]^+Cl^-$ **(15)** (0.04 g, 0.053 mmol, 1 eq.) was dissolved in pyridine (10 ml) then 3-methoxyphenol (17 µl, 0.155 mmol, 3 eq.) previously dissolved in 5 ml of pyridine was

added dropwise. The reaction mixture was refluxed overnight under argon. Pyridine was removed under vacuum and the solid residue was purified by column chromatography on alumina using a mixture of methanol-DCM as the eluent (from 0% to 10% of MeOH). Further purification by Bio-Beads S-X1 GPC (eluent - chloroform-methanol 98:2) afforded 24 mg of the pure green product **17** (50% yield).

$^{1}$H-NMR ($CDCl_3$, 500 MHz) δ, ppm: 1.25 (br., 2H, *o*-phenoxy), 1.80 (d, $^{3}J$ = 8.2 Hz, 2H, *o*-phenoxy), 3.11 (s, 6H, O-$CH_3$), 5.68 (d, $^{3}J$=8.3 Hz, 2H, *p*-phenoxy), 5.84 (dd, $^{3}J$ = 8.2 Hz, $^{3}J$ = 8.2 Hz, 2H , *m*-phenoxy), 7.76 (m, 20H, phenyl), 9.04 (d, $^{4}J_{P-H}$ = 2.7 Hz, 8H, β-pyrr).

$^{31}$P-NMR ($CDCl_3$, 162 MHz) δ, ppm: -196.

$^{13}$C-NMR ($CDCl_3$, 125 MHz) δ, ppm: 54.9 ($CH_3$), 101.5 (CH phenoxy., $^{3}J_{P-C}$ = 8.8 Hz), 106.8 (CH phenoxy., $^{3}J_{P-C}$ = 8.6 Hz), 107.6 (CH), 117.2 (C), 128.4 (CH), 128.6 (CH), 130.1 (CH), 133.4 (CH, $^{3}J_{P-C}$ = 6.1 Hz), 133.6 (CH), 134.9 (C), 139.6 (C), 150.1 (C phenoxy., $^{2}J_{P-C}$ = 17.4 Hz), 158.7 (C phenoxy.).

HR-ESI MS: *m/z* calcd. for $[C_{58}H_{42}N_4O_4P]^+$: 889.2938; found: 889.2944 [**17**-Cl]$^+$.

UV-vis ($CHCl_3$) λ, nm (logε): 435 (5.00), 565 (4.10), 606 (3.79).

| | |
|---|---|
| **Diethoxy(5,10,15,20-tetraphenylporphyrinato)phosphorus(V) bromide,** **[P(TPP)(OEt)$_2$]$^+$Br$^-$ (18).** | 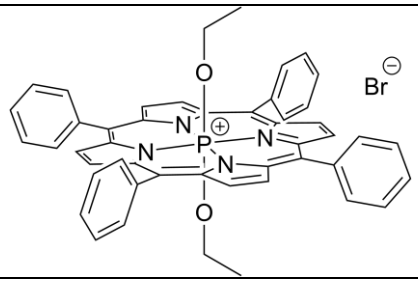  |

The porphyrin $H_2$TPP **(1a)** (0.1 g, 0.16 mmol, 1 eq.) was dissolved pyridine (60 ml) under argon before $POBr_3$ (1.1 g, 4.06 mmol, 25 eq.) previously dissolved in pyridine (20 ml) was added dropwise under stirring. The reaction mixture was refluxed during 80 min under argon and then cooled to room temperature. After addition of 100 ml of ethanol, the green mixture was stirred at room temperature for 48 h until full axial ligand substitution was completed and reaction mixture became purple. The mixture was diluted with DCM (200 ml) and washed with distilled water (3 x 500 ml) to remove pyridine and ethanol. The organic layer was isolated, diluted with 200 ml of petroleum ether and poured directly on a silica gel chromatography column without evaporation of solvents. Increasing the polarity of the eluent using DCM-MeOH mixture (90:10) give the crude product. Further purification by Bio-Beads S-X1 GPC (eluent - chloroform-methanol 98:2) afforded 84 mg of the pure purple compound **18** in 64% yield.

$^{1}$H-NMR ($CDCl_3$, 300 MHz) δ, ppm: -2.34 (dq, $^{3}J_{P-H}$ = 14.0 Hz, $^{3}J$ = 7.0 Hz, 4H, $CH_2$), -1.79 (td, $^{3}J$ = 7.3 Hz, $^{4}J_{P-H}$ = 2.1 Hz, 6H, $CH_3$), 7.79 (m, 12H, *m*- and *p*-phenyl), 7.95 (m, 8H, *o*-phenyl), 9.07 (d, $^{4}J_{P-H}$ = 2.7 Hz, 8H, β-pyrr).

$^{31}$P-NMR ($CDCl_3$, 162 MHz) δ, ppm: -179.

$^{13}$C-NMR ($CDCl_3$, 125 MHz) δ, ppm: 13.1 ($CH_3$, $^{3}J_{P\text{-}C}$ = 16.4 Hz), 56.9 ($CH_2$, $^{2}J_{P\text{-}C}$ = 15.0 Hz), 115.4 (C, $^{3}J_{P\text{-}C}$ = 2.0 Hz), 128.6 (CH), 129.9 (CH), 132.2 (CH, $^{3}J_{P\text{-}C}$ = 5.0 Hz), 133.3 (CH), 135.4 (C), 139.2 (C).

HR-ESI MS: *m/z* calcd. for $[C_{48}H_{38}N_4O_2P]^+$: 733.2727; found: 733.2737 [**18**-Br]$^+$.

UV-vis ($CHCl_3$) λ, nm (logε): 431 (5.44), 560 (4.23), 599 (4.02).

| **Model turnstile#1,**<br>**[P(TPP)handle#1]$^+$Cl$^-$ (19).** | 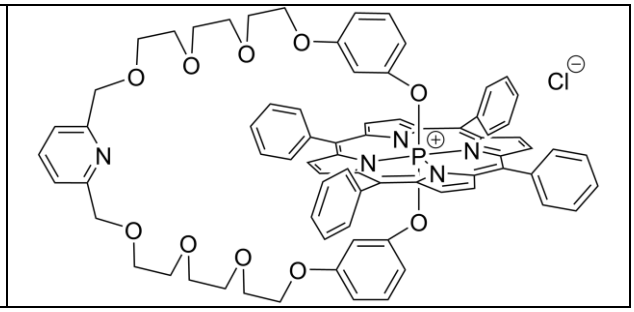 |
|---|---|

The porphyrin $[P(TPP)Cl_2]^+Cl^-$ **(15)** (0.02 g, 0.027 mmol, 1 eq.) and handle#1 **(10)** (0.018 g, 0.029 mmol, 1.1 eq.) were placed into a microwave tube and distilled pyridine (3 ml) was added under argon. The mixture was heated to 150$^o$C at 120 W during 2 h in the microwave oven using dry air cooler. The reaction mixture was cooled to room temperature and chloroform (20 ml) was added and the solution (without evaporation of solvents) was purified by silica gel column chromatography. The 3$^{rd}$ fraction (10% methanol and 90% of chloroform) was isolated and evaporated to give a green-brown solid. This fraction was further purified using Bio-Beads S-X1 GPC (eluent - chloroform-methanol 98:2). 10 mg (30% yield) of pure product **19** was obtained as a brown-green solid.

$^{1}$H-NMR ($CD_3OD$, 400 MHz) δ, ppm: 1.40 (td, $^{4}J_{P\text{-}H}$ =2.2 Hz, $^{4}J$ = 2.2 Hz, 2H, *o*-phenoxy), 2.27 (br. d, $^{3}J$ = 8.2 Hz, 2H, *o*-phenoxy), 3.34 (t, $^{3}J$ = 5.0 Hz, 4H, $CH_2O$), 3.51 (t, $^{3}J$ = 5.0 Hz, 4H, $CH_2O$), 3.56-3.69 (m, 16H, $CH_2O$), 4.51 (s, 4H, $CH_2O$), 5.74 (br. d, $^{3}J$ = 8.2 Hz, 2H, p-phenoxy), 5.90 (ddd, $^{3}J$ = 8.3 Hz, $^{3}J$ = 8.3 Hz, $^{4}J$ = 1.7 Hz, 2H, m-phenoxy), 7.22 (d, $^{3}J$ = 7.6 Hz, 2H, *m*-pyridyl$_{handle}$), 7.31 (t $^{3}J$ = 7.8 Hz, 1H, *p*-pyridyl$_{handle}$), 7.75 (m, 12H, *m*- and *p*-phenyl), 7.81 (m, 8H, *o*-phenyl), 9.08 (d, $^{4}J_{P\text{-}H}$ = 3.6 Hz, 8H, β-pyrr).

$^{31}$P-NMR ($CD_3OD$, 162 MHz): δ, ppm, -195.

$^{13}$C-NMR ($CD_3OD$, 100 MHz): δ, ppm 68.3 ($CH_2O$), 70.3 ($CH_2O$), 71.7 ($CH_2O$), 71.8 ($CH_2O$), 72.0 ($CH_2O$), 74.5 ($CH_2O$), 79.5 ($CH_2O$), 101.7 ($CH_{phenoxy}$, $^{3}J_{P\text{-}C}$ = 8.1 Hz), 108.9 (CH), 109.7 (CH), 118.4 (CH), 121.7 (C), 129.5 (CH), 130.9 (CH) 134.7 (CH), 134.8 (CH, $^{3}J_{P\text{-}C}$ = 6.0 Hz), 136.3 (CH), 138.9 (C), 140.8 (CH), 151.6 (C) 151.7 (C), 159.0 (C), 159.2 (C).

HR-ESI MS: *m/z* calcd. for $[C_{75}H_{68}N_5O_{10}P]^{2+}$: 614.7346; found: 614.7394 [**19**H-Cl]$^{2+}$, *m/z* calcd. for $[C_{75}H_{67}N_5O_{10}P]^+$: 1228.4620; found: 1228.4481 [**19**-Cl]$^+$.

UV-vis ($CHCl_3$) λ, nm (logε): 436 (4.96), 565 (3.95), 607 (3.57)

| | |
|---|---|
| **Model turnstile#2, [P(TPP)handle#2]$^{+}$OTs$^{-}$ (20).** | 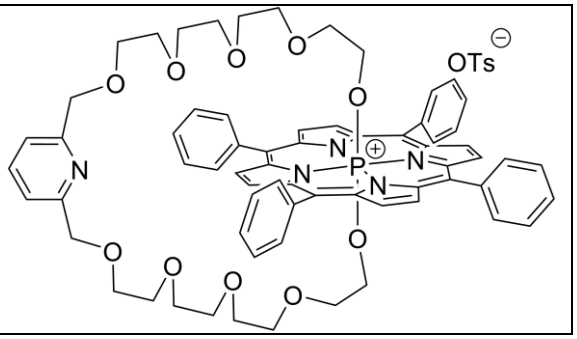 |

The synthesis was adapted from a described procedure for similar compounds.[9,10]

The porphyrin [P(TPP)(OH)$_2$]$^{+}$Br$^{-}$ **(16b)** (0.04 g, 0,053 mmol, 1 eq.) and handle#2 **(14)** (0.046 g, 0.058 mmol 1.1 eq.) were dissolved in acetonitrile (150 ml). The mixture was bubbled with argon during 30 min and then $Cs_2CO_3$ (0.023 g, 0.07 mmol, 1.32 eq.) and DMF (2 drops) were added. The reaction mixture was stirred overnight at 60 ºC. Approximately 100 ml of MeCN was evaporated under vacuum and the mixture was diluted with 100 ml of DCM. The suspension was directly poured (without evaporation of the solvents) onto a $SiO_2$ column with a mixture of DCM-methanol as eluent. Brown-red fraction (15% of methanol) was isolated and purified by Bio-Beads S-X1 GPC with chloroform as the eluent to afford 9 mg of red-brown solid that still containing a small amount of impurities.

$^{1}$H-NMR ($CD_3OD$, 400 MHz) δ, ppm: -2.20 (dt, $^{3}J_{P\text{-}H}$ = 10.1 Hz, $^{3}J$ = 5.5 Hz, 4H, P-O-$CH_2$), 0.65 (br., 4H, $CH_2O$), 2.38 (m, 4H, $CH_2O$), 2.63 (m, 4H, $CH_2O$), 2.93 (m, 4H, $CH_2O$), 3.18 (m, 4H, $CH_2O$), 3.38 (m, 4H, $CH_2O$), 3.49 (m, 4H, $CH_2O$), 4.45 (s, 4H, $CH_2O$), 7.22 (d, $^{3}J$ = 7.8 Hz, 2H, *m*-pyridyl$_{handle}$), 7.56 (t, $^{3}J$ = 7.6 Hz, 1H, *p*-pyridyl$_{handle}$), 7.81 (m, 12H, m and *p*-phenyl), 8.04 (m, 8H, *o*-phenyl), 9.12 (m, 8H, β-pyrr). *Spectra are described more precisely in Chapter I.*

$^{31}$P-NMR ($CD_3OD$, 162 MHz) δ, ppm: -181 (s).

MALDI-TOF MS: *m/z* calcd. for $[C_{67}H_{67}N_5O_{10}P]^{+}$: 1132.47; found: 1132.46 [**20**-OTs]$^{+}$.

UV-vis ($CHCl_3$) λ, nm: 433, 562, 603.

| | |
|---|---|
| **Dichloro(5-pyridyl-(10,15,20)-triphenylporphyrinato)phosphorus(V) chloride, [P(MPyP)Cl$_2$]$^{+}$Cl$^{-}$ (21).** | 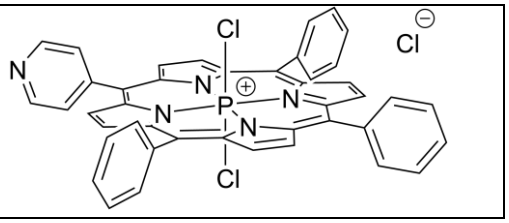 |

**Method A.**

The porphyrin $H_2$MPyP (5-monopyridyl-(10,15,20)-triphenylporphyrin) **(1b)** (0.1 g, 0.16 mmol, 1 eq.) was dissolved in pyridine (20 ml) and solutions of $POCl_3$ (2 ml, 21.93 mmol, 135 eq.) and $PCl_5$ (0.1 g, 0.49 mmol, 3 eq.) in 2 ml of pyridine were added dropwise under argon. The mixture was refluxed during 72 h under argon. The pyridine was evaporated under vacuum and the green residue was purified by column chromatography on alumina. Gradual addition of methanol up to 5% afforded the crude compound. After evaporation, the solid was further purified

by Bio-Beads S-X1 GPC with chloroform as the eluent affording 48 mg (yield 40%) of compound **21** as a green solid.

**Method B.**

The porphyrin $[P(MPyP)(OH)_2]^+Br^-$ **(22) (**19 mg, 0.038 mmol, 1 eq.), (see below) was dissolved in chloroform (5 ml) under argon and $SOCl_2$ (2 ml, 27 mmol, 720 eq.) was added. The mixture was stirred during 12 h at room temperature and the solvent as well as excess of thionyl chloride were removed under vacuum. Chloroform (5 ml) was added and the mixture was passed through Bio-Beads S-X1 GPC column with chloroform as eluent affording 19 mg (100% yield) of the compound **21** as a green solid.

$^1$H-NMR ($CDCl_3$ + DMSO-$d_6$, 300 MHz) δ, ppm: 7.48 (m, 9H, *m*- and *p*-phenyl), 7.63 (d, $^3J$ = 6.7 Hz, 6H *o*-phenyl), 7.79 (m, 2H *o*-pyridyl), 8.78-8.88 (m, 10H, β-pyrr, *m*-pyridyl).

$^{31}$P-NMR ($CDCl_3$+DMSO-$d_6$, 121 MHz) δ, ppm: -229.

$^{13}$C-NMR ($CDCl_3$ + DMSO-$d_6$, 125 MHz) δ, ppm: 111.5 (C), 118.4 (C, $^3J_{P-C}$ = 3.0 Hz) 118.7 (C, $^3J_{P-C}$ = 3.0 Hz), 127.7 (C), 128.1 (C), 128.9 (CH), 130.6 (CH, $^3J_{P-C}$ = 3.4 Hz), 133.1 (CH, $^3J_{P-C}$ = 6.6 Hz), 133.3 (CH, $^3J_{P-C}$ = 6.6 Hz), 133.4 (CH), 133.5 (CH), 134.0 (CH), 134.1 (CH), 134.6 (CH, $^3J_{P-C}$ = 6.5 Hz), 138.7 (C), 139.8 (C), 140.3 (C), 140.4 (C).

HR-ESI MS: *m/z* calcd. for $[C_{43}H_{27}Cl_2N_5P]^+$: 714.1376; found: 714.1341 [**21**-Cl]$^+$.

UV-vis ($CHCl_3$) λ, nm (logε): 439 (5.32), 570 (4.02), 608 (3.81).

| | |
|---|---|
| **Dihydroxy(5-pyridyl-(10,15,20)-triphenylporphyrinato)phosphorus(V) bromide, $[P(MPyP)(OH)_2]^+Br^-$ (22).** | 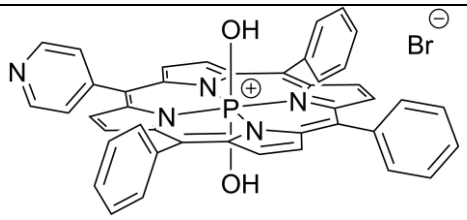 |

The porphyrin $H_2$MPyP (5-monopyridyl-(10,15,20)-triphenylporphyrin) **(1b)** (63 mg, 0.1 mmol, 1 eq.) was dissolved pyridine (30 ml) under argon and a solution of $POBr_3$ (1.17 g, 4.09 mmol, 40 eq.) in pyridine (20 ml) was added dropwise under stirring. The reaction mixture was refluxed during 1.5 h under argon and then cooled to room temperature. After adding $CH_2Cl_2$ (150 ml), to the green suspension 2 L of distilled water was added and the mixture stirred at room temperature during 1 day until full hydrolysis of $P(MPyP)(Br)_2]^+Br^-$ to the dihydroxy complex **[**$P(MPyP)(OH)_2]^+Br^-$ was completed. The organic layer was isolated and placed on a silica gel chromatography column without evaporation of $CH_2Cl_2$. Increasing the methanol ratio in the eluent up to 15% give the crude product. Further purification by Bio-Beads S-X1 GPC (eluent - chloroform-methanol 98:2) afforded 65 mg (85% yield) of the pure purple compound **22**.

$^1$H-NMR ($CDCl_3$, 400 MHz) δ, ppm: -3.85 (br., 2H, OH), 7.71 (m, 9H, *m*- and *p*-phenyl), 7.95 (m, 2H, *o*-pyridyl), 8.00 (m, 6H *o*-phenyl), 8.68 (dd, $^3J$ = 5.1 Hz , $^4J_{P-H}$ = 1.3 Hz, 2H, β-pyrr), 8.76

(d, $^{4}J_{P\text{-}H}$ = 1.3 Hz, 4H, β-pyrr), 8.78 (dd, $^{3}J$ = 5.1 Hz , $^{4}J_{P\text{-}H}$ =1.3 Hz, 2H, β-pyrr), 8.92 (m, 2H, *m*-pyridyl).

$^{31}$P-NMR ($CDCl_3$, 162 MHz) δ, ppm: -193.

$^{13}$C-NMR ($CDCl_3$, 125 MHz) δ, ppm: 111.8 (C), 116.2 (C), 116.4 (C), 126.9 (CH,), 127.8 (CH,), 128.3 (CH), 129.0 (CH), 129.5 (CH), 131.4 (CH), 132.4 (C), 132.5 (CH), 132.9 (CH), 133.6 (CH), 134.7 (CH), 138.3 (C), 139.4 (C), 139.5 (C), 147.6 (CH), 148.6 (CH).

HR-ESI MS: *m/z* calcd. for $[C_{43}H_{30}N_5O_2P]^{2+}$: 339.6063; found: 339.6031 [**22**+H-Br]$^{2+}$;

*m/z* calcd. for $[C_{43}H_{29}N_5O_2P]^{+}$: 678.2053; found: 678.2036 [**22**-Br]$^{+}$.

UV-vis ($CHCl_3$) λ, nm (logε): 428 (5.24), 556 (4.02), 598 (3.32).

| **Di-(3-methoxyphenoxy)(5-pyridyl-(10,15,20)-triphenylporphyrinato)phosphorus(V) chloride, $[P(MPyP)(OPhOMe)_2]^{+}Cl^{-}$ (23).** | 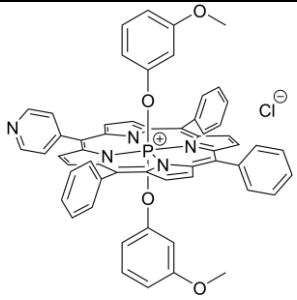 |
|---|---|

The porphyrin $[P(MPyP)Cl_2]^{+}Cl^{-}$ **(21)** (50 mg, 0.067 mmol, 1 eq.) was dissolved in pyridine (10 ml) and then a solution of 3-methoxyphenol (22 µl, 0.20 mmol, 3 eq.) in pyridine (5 ml) was added dropwise. The reaction mixture was refluxed overnight under argon. Pyridine was removed under vacuum and the solid residue was purified by column chromatography on silica gel using methanol-$CH_2Cl_2$ mixture as the eluent (from 0% to 15% of MeOH). Further purification by Bio-Beads S-X1 GPC (eluent - chloroform-methanol 98:2) afforded 30 mg (yield 50%) of the compound **23** as a green solid.

$^{1}$H-NMR ($CDCl_3$, 400 MHz) δ, ppm: 1.24 (br., 2H, *o*-phenoxy), 1.75 (br., 2H *o*-phenoxy), 3.11 (s, 6H, O-$CH_3$), 5.68 (d, $^{3}J$ = 8.0 Hz, 2H, *p*-phenoxy), 5.84 (dd, $^{3}J$ = 8.0 Hz, $^{3}J$ = 8.0 Hz, 2H, m-phenoxy), 7.69-7.81 (m, 17H, phenyl + *o*-pyridyl), 9.06 (m, 8H, β-pyrr), 9.12 (m, 2H, *m*-pyridyl).

$^{31}$P-NMR ($CDCl_3$, 162 MHz) δ ppm: -195.

$^{13}$C-NMR ($CDCl_3$, 125 MHz) δ, ppm: 55.0 ($CH_3$), 101.7 (CH, $^{3}J_{P\text{-}C}$ = 9.0 Hz), 106.8 (CH, $^{3}J_{P\text{-}C}$ = 9.1 Hz), 107.6, (CH), 117.8 (C) 128.5 (CH), 128.6 (CH), 130.2 (CH), 132.7 (CH), 133.6 (CH), 133.8 (CH), 134.4 (CH), 134.7 (CH), 139.5 (C), 139.7 (C), 139.8 (C), 150.0 (C), 158.7 (C).

HR-ESI MS: *m/z* calcd. for $[C_{57}H_{42}N_5O_4P]^{2+}$: 445.6482; found: 445.6458 [**23**H-Cl]$^{2+}$:

*m/z* calcd. for $[C_{57}H_{41}N_5O_4P]^{+}$: 890.2891; found: 890.2873 [**23**-Cl]$^{+}$.

UV-vis ($CHCl_3$) λ, nm (logε): 434 (5.00), 564 (4.00), 606 (3.61).

| | |
|---|---|
| **Diethoxy(5-pyridyl-(10,15,20)-triphenylporphyrinato)phosphorus(V) bromide, $[P(MPyP)(OEt)_2]^+Br^-$ (24).** | 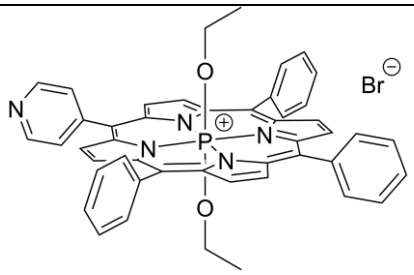 |

**Method A.**

This synthesis was achieved by modifying a reported procedure.[10]

The porphyrin $[P(MPyP)(OH)_2]^+Br^-$ **(22)** (10 mg, 0.013 mmol, 1 eq.) was dissolved in acetonitrile (30 ml) and then ethyl tosylate (6 mg, 0.03 mmol, 2.3 eq.) and $Cs_2CO_3$ (5.4 mg, 0.016 mmol, 1.3 eq.) were added. The reaction mixture was stirred at 50 °C for 12 h under the argon. After cooling to room temperature, the solvent was evaporated under vacuum and the residue was purified by column chromatography (silica gel, DCM-methanol). Gradually increasing eluent polarity up to 20% of methanol affording a crude product that was passed through Bio-Beads S-X1 GPC (eluent - chloroform-methanol 98:2) afforded 4 mg (yield 30%) of the complex **24** as a purple solid.

**Method B.**

The porphyrin $H_2MPyP$ **(1b)** (95 mg, 0.15 mmol, 1 eq.) was dissolved pyridine (30 ml) under argon and then a solution of $POBr_3$ (1.77 g, 6.17 mmol, 40 eq.) in pyridine (20 ml) was added dropwise under stirring. The mixture was refluxed for 1,5 h under argon and then cooled to room temperature. After addition of ethanol (200 ml), the green mixture was stirred at room temperature for 24 h until full axial ligand substitution occurred and the mixture became purple. The DCM (500 ml) was added and the mixture was washed with distilled water several times (5 x 500 ml). Organic layer was poured on a silica gel chromatography column without evaporation of DCM. Increasing the methanol ratio in the eluent up to 15% give the crude product. Further purification of product by Bio-Beads S-X1 GPC (eluent - chloroform-methanol 98:2) afforded 84 mg (yield 66%) of the pure compound **24** as a purple solid.

$^1$H-NMR ($CDCl_3$, 300 MHz) δ, ppm: -2.35 (dq, $^3J_{P-H}$ = 13.7 Hz, $^3J$ = 7.3 Hz, 4H, $CH_2$), -1.74 (td, $^3J$ = 7.0 Hz, $^4J_{P-H}$ = 2.1 Hz, 6H, $CH_3$), 7.55-7.75 (m, 9H, *m*- and *p*-phenyl), 7.82 (m, 8H, *o*-phenyl + *o*-pyridyl), 8.81-9.02 (m, 10H, β-pyrr + *m*-pyridyl).

$^{31}$P-NMR ($CDCl_3$, 162 MHz) δ, ppm: -179.

$^{13}$C-NMR ($CDCl_3$, 125 MHz) δ, ppm: 13.1 ($CH_3$, $^2J_{P-C}$ = 16.2 Hz), 56.9 ($CH_2$), 112.2 (C), 116.7 (C), 117.0 (C), 128.0 (CH), 128.7 (CH), 129.9 (CH), 130.0 (CH), 132.5 (CH, $^3J_{P-C}$ = 5.0 Hz), 133.4 (CH), 133.5 (CH, $^3J_{P-C}$ = 5.2 Hz), 133.6 (CH, $^3J_{P-C}$ = 5.4 Hz), 134.1 (CH, $^3J_{P-C}$ = 5.1 Hz), 135.1 (CH), 135.2 (C), 138.1 (C), 139.2 (C), 139.3 (C), 139.5 (C), 149.6 (CH).

HR-ESI MS: *m/z* calcd. for $[C_{47}H_{38}N_5O_2P]^{2+}$: 367.6376; found: 367.6361 [**24**H-Br]$^{2+}$;
*m/z* calcd. for $[C_{47}H_{37}N_5O_2P]^+$: 734.2679; found: 734.4825 [**24**-Br]$^+$.

UV-vis ($CHCl_3$) λ, nm (logε): 431 (5.16), 559 (3.92), 602 (3.50).

| | |
|---|---|
| **Di(ethane-l,2-diolato)-(5-pyridyl-(10,15,20)-triphenylporphyrinato)phosphorus(V) bromide, $[P(MPyP)(O(CH_2)_2OH)_2]^+Br^-$ (25).** | 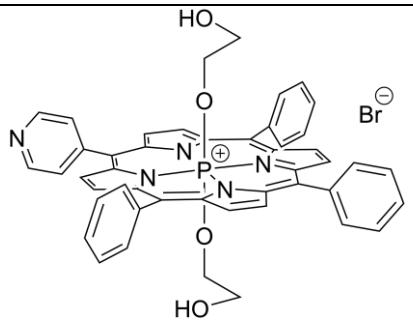 |

The porphyrin $H_2$MPyP **(1b)** (180 mg, 0.292 mmol, 1 eq.) was dissolved in pyridine (120 ml) under argon and then a solution of $POBr_3$ (3.35 g, 11.7 mmol, 40 eq.) in pyridine (30 ml) was added dropwise under stirring. The reaction mixture was refluxed for 80 min under argon. Then it was diluted with ethylene glycol (250 ml) and was further stirred at room temperature for 6 h. Approximately 80% of the solvents was evaporated under vacuum and then the mixture was diluted with $CH_2Cl_2$ (200 ml). The reaction mixture was washed 4 times with 400 ml of distilled water. The organic layer was isolated and poured directly on a $Al_2O_3$ chromatography column without evaporation of $CH_2Cl_2$. Increasing the methanol ratio in the eluent (DCM-methanol) up to 8% give a dark red fraction which was isolated and passed through a Bio-Beads S-X3 GPC column (eluent - chloroform-methanol 98:2) affording 180 mg (yield 73%) of the compound **25** as a purple solid.

$^1$H-NMR ($CDCl_3$, 400 MHz) δ, ppm: -2.34 (dt, $^3J_{P\text{-}H}$ = 12.1 Hz, $^3J$ = 6.0 Hz, 4H, P-O-$CH_2$), 0.60 (td, $^3J$ = 5.7 Hz, $^4J_{P\text{-}H}$ = 2.0 Hz, 4H, -$CH_2$-OH), 7.61-7.75 (m, 9H, *m*- and *p*-phenyl), 7.93 (m, 6H, *o*-phenyl), 7.99 (m, 2H, *o*-pyridyl), 8.77 (m, 2H, *m*-pyridyl), 8.84 (m, 2H, β-pyrr), 8.94 (m, 6H, β-pyrr).

$^{31}$P-NMR ($CDCl_3$, 162 MHz) δ, ppm: -180.

$^{13}$C-NMR ($CDCl_3$, 100 MHz) δ, ppm: 57.9 ($CH_2$, $^2J_{P\text{-}C}$ = 17.0 Hz), 63.1 ($CH_2$, $^2J_{P\text{-}C}$ = 14.5 Hz), 112.9 (C), 116.7 (C), 128.2 (C), 128.3 (CH), 128.3 (CH), 132.3 (CH), 133.2 (CH), 133.4 (CH), 133.5 (CH), 133.6 (CH), 135.4 (C), 138.5 (C), 139.5 (C), 143.8 (CH), 149.4 (CH).

UV-vis ($CHCl_3$) λ, nm (logε) 432 (5.20), 559 (3.98), 600 (3.46).

| | |
|---|---|
| **Di((3-oxypropyl)oxy)-(5-pyridyl-(10,15,20)-triphenylporphyrinato)phosphorus(V) bromide, $[P(MPyP)(O(CH_2)_3OH)_2]^+Br^-$ (26).** | 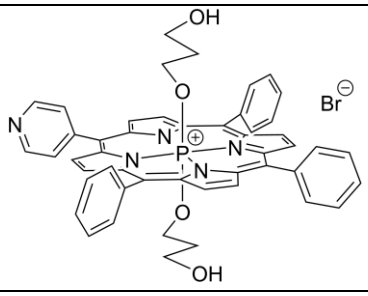 |

The porphyrin $H_2$MPyP **(1b)** (180 mg, 0.292 mmol, 1 eq.) was dissolved in pyridine (120 ml) under argon and then a solution of $POBr_3$ (3.35 g, 11.7 mmol, 40 eq.) in pyridine (30 ml) was

added dropwise under stirring. The reaction mixture was refluxed for 80 min under argon. Then it was diluted with propane-1,3-diol (250 ml) and was stirred at room temperature for 6 h. Approximately 80% of the solvents were evaporated under vacuum and the mixture was diluted with DCM (200 ml). The reaction mixture was washed 4 times with 400 ml of distilled water. The organic layer was isolated and poured directly on an alumina chromatography column without evaporation of DCM. Increasing the methanol ratio in the eluent (DCM-methanol) up to 8% give a dark red fraction which was passed through Bio-Beads S-X3 GPC column (eluent - chloroform-methanol 98:2) affording 172 mg (yield 67%)of the pure compound **26** as a purple solid.

$^{1}$H-NMR ($CDCl_3$, 400 MHz) δ, ppm: -2.26 (dt, $^{3}J_{P\text{-}H}$ = 12.0 Hz, $^{3}J$ = 5.9 Hz, 4H, P-O-$CH_2$), -1.27 (m, 4H, $CH_2$), 1.54 (t, $^{3}J$ = 5.8 Hz, 4H, -C$\underline{H}_2$-OH), 7.75 (m, 9H, *m*- and *p*-phenyl), 8.00 (m, 6H, *o*-phenyl), 8.08 (m, 2H, *o*-pyridyl), 8.95 (m, 2H, *m*-pyridyl), 8.98 (m, 2H, β-pyrr), 9.03 (m, 6H, β-pyrr).

$^{31}$P-NMR ($CDCl_3$, 162 MHz) δ, ppm: -180.

$^{13}$C-NMR ($CDCl_3$, 125 MHz) δ, ppm: 33.3 ($CH_2$, $^{2}J_{P\text{-}C}$ = 16.6 Hz), 57.0 ($CH_2$), 59.4 ($CH_2$, $^{2}J_{P\text{-}C}$ = 15.3 Hz), 113.6 (C), 117.9 (C), 118.3 (C), 129.4 (CH), 129.9 (CH), 130.9 (CH), 133.8 (CH), 134.6 (CH), 134.7 (CH), 135.0 (CH), 136.8 (C), 139.6 (C), 140.7 (C), 140.8 (C), 140.9 (C), 146.1 (C), 150.1 (CH)

HR ESI MS: *m/z* calcd. for $[C_{49}H_{41}N_5O_4P]^+$: 794.2891; found: 794.2821 [**26**-Br]$^+$.

UV-vis ($CHCl_3$) λ, nm (logε): 431 (5.26), 560 (4.00), 603 (3.39).

| | |
|---|---|
| **Di-(3-oxyphenoxy)(5-pyridyl-(10,15,20)-triphenylporphyrinato) phosphorus(V) bromide, $[P(MPyP)(OPhOH)_2]^+Br^-$ (27).** | 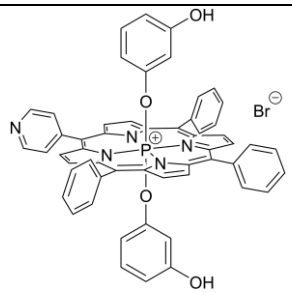 |

The porphyrin $H_2$MPyP **(1b)** (100 mg, 0.162 mmol, 1 eq.) was dissolved in pyridine (50 ml) under argon and then a solution of $POBr_3$ (1.86 g, 6.50 mmol, 40 eq.) in pyridine (20 ml) was added dropwise under stirring. The reaction mixture was refluxed for 1.5 h under argon and then cooled to room temperature. The suspension was diluted with chloroform (200 ml) and resorcinol (5 g, 45 mmol, 454 eq.) was added and the mixture was stirred at room temperature for 48 h until the axial ligand exchange was achieved. The organic layer was washed three times with distilled water (3 x 500 ml). The green-brown organic layer was poured on a silica gel chromatography column without evaporation of chloroform. Increasing the polarity of the eluent (DCM-methanol) up to 15% of MeOH give a crude product which was further purified on a Bio-Beads S-X3 GPC (eluent - chloroform-methanol 98:2) column affording 82 mg (yield 55%) of the pure compound **27** as a green-brown solid.

$^{1}$H-NMR ($CDCl_3$, 400 MHz) δ, ppm: 1.46 (br. d, $^{3}J$ = 8.2 Hz, 2H, *o*-phenoxy), 1.97 (m, 2H, *o*-phenoxy), 5.57 (ddd, $^{3}J$ = 8.3 Hz, $^{3}J$ = 8.3 Hz, $^{4}J$ = 1.4 Hz, 2H, *m*-phenoxy), 5.79 (br. d, $^{3}J$ = 8.2 Hz, 2H, *p*-phenoxy), 7.62 (m, 9H, *m*-phenyl + *p*-phenyl), 7.83 (m, 8H, *o*-phenyl + *o*-pyridyl), 8.13 (s, 2H, OH), 8.67 (m, 2H, *m*-pyridyl), 8.76 (dd, $^{3}J$ = 5.2 Hz, $^{4}J_{P\text{-}H}$ = 3.2 Hz, 2H, β-pyrr), 8.87 (dd, $^{3}J$ = 5.2 Hz, $^{4}J_{P\text{-}H}$ = 3.2 Hz, 2H, β-pyrr), 8.94 (d, $^{4}J_{P\text{-}H}$ = 3.2 Hz, 4H, β-pyrr).

$^{31}$P-NMR ($CDCl_3$, 162 MHz) δ ppm: -194.

$^{13}$C-NMR ($CDCl_3$, 125 MHz) δ, ppm: 103.1 (CH, $^{3}J_{P\text{-}C}$ = 8.6 Hz), 104.6 (CH, $^{3}J_{P\text{-}C}$ = 8.2 Hz), 110.8 (C), 113.4 (C), 117.5 (CH), 127.5 (CH), 128.3 (CH), 128.5 (CH), 129.7 (CH), 132.3 (CH), 133.3 (CH), 133.4 (CH), 133.6 (CH), 133.7 (CH), 135.1 (C), 138.6 (C), 139.5 (C), 139.7 (C), 139.8 (C), 143.7 (C), 149.2 (CH), 149.7 (C), 149.8 (C), 157.2 (C).

HR-ESI MS: *m/z* calcd. for $[C_{55}H_{38}N_5O_4P]^{2+}$: 431.6283; found: 431.6283 [**27**H-Br]$^{2+}$;
*m/z* calcd. for $[C_{55}H_{37}N_5O_4P]^{+}$: 862.2578; found: 862.2525 [**27**-Br]$^{+}$.

UV-vis ($CHCl_3$) λ, nm (logε): 436 (4.95), 565 (3.94), 607 (3.56)

| | |
|---|---|
| **Turnstile#1a,**<br>**[P(MPyP)handle#1]$^{+}$Cl$^{-}$ (28a).** | 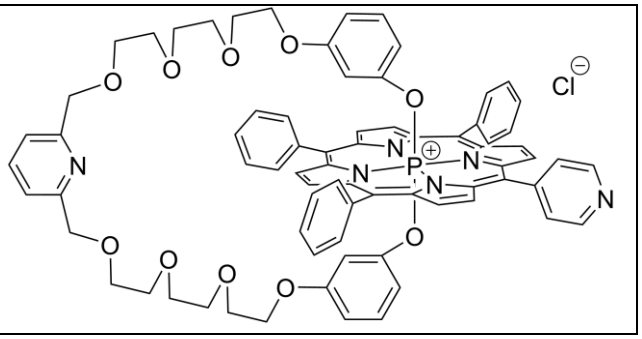 |

The porphyrin [P(MPyP)$Cl_2$]$^{+}$Cl$^{-}$ **(21)** (21 mg, 0.028 mmol, 1 eq.) and handle#1 **(10)** (18 mg, 0.03 mmol, 1.1 eq.) were placed into a microwave tube, distilled pyridine (3 ml) was added under argon and the mixture was heated to 140 ºC at 120 W during 45 min in the microwave oven using air cooling. The mixture was cooled to room temperature, chloroform (20 ml) was added and the reaction mixture was purified by silica gel column chromatography. The 3$^{rd}$ fraction (15% of methanol and 85% of DCM) was isolated as a green-brown solid. This fraction was further purified using Bio-Beads S-X1 GPC column (eluent - chloroform-methanol 98:2) affording 1.5 mg (yield 5%) of the pure product **28a** as a brown-green solid. This method is not reproducible and was successful only once.

$^{1}$H-NMR ($CD_3OD$, 400 MHz) δ, ppm: 1.41 (ddd, $^{4}J$ = 2.2 Hz, $^{4}J$ = 2.2 Hz, $^{4}J_{P\text{-}H}$ = 2.2 Hz, 2H, o-phenoxy), 2.24 (ddd, $^{3}J$ = 8.2 Hz, $^{4}J$ = 2.2 Hz, $^{4}J_{P\text{-}H}$ = 2.2 Hz, 2H *o*-phenoxy), 3.35 (m, $CH_2O$), 3.51 (m, $CH_2O$), 3.56-3.68 (m, 16H, $CH_2O$), 4.48 (s, 4H, $CH_2O$), 5.74 (dt, $^{3}J$ = 8.2 Hz, $^{4}J$ = 1.4 Hz, 2H, *p*-phenoxy), 5.92 (td, $^{3}J$ = 8.2 Hz, $^{4}J$ = 1.7, 2H, *m*-phenoxy), 7.17 (d, $^{3}J$ = 7.7 Hz, 2H, *m*-pyridyl$_{handle}$), 7.30 (t, $^{3}J$ = 7.8 Hz, 1H, *p*-pyridyl$_{handle}$), 7.75 (m, 9H, *m*- and *p*-phenyl), 7.82 (m, 6H, *o*-phenyl), 7.90 (m, 2H, *o*-pyridyl), 8.95 (m, 2H, *m*-pyridyl), 9.13 (m, 8H, β-pyrr).

| | |
|---|---|
| **Turnstile#1,**<br>**[P(MPyP)handle#1]$^{+}$Br$^{-}$ (28b).** | 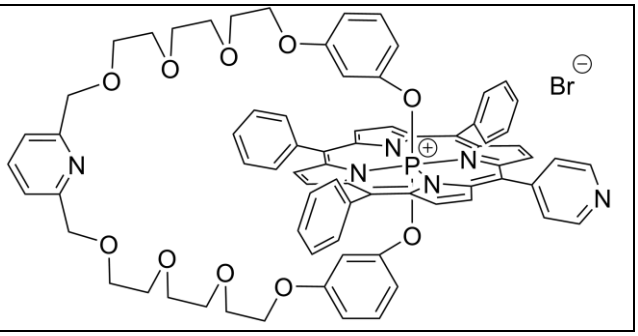 |

A 2-necked 250 ml round-bottom flask was filled with argon, the porphyrin [P(MPyP)$(OH)_2$]$^{+}$Br$^{-}$ **(22)** (100 mg, 0.13 mmol, 1 eq.) was dissolved in 5 ml of dry DCM and placed into the flask together with $SOBr_2$ (0.39 ml, 5.03 mmol, 38 eq.). The mixture was stirred at room temperature under argon during 3 h. DCM and the excess of $SOBr_2$ were removed under low pressure. The reaction mixture was left under vacuum overnight. Freshly distilled pyridine (25 ml) was added and the solution was transferred to a 0.5L 2-necked round-bottom flask, previously vacuumed and filled with argon and equipped with a reflux condenser. The handle#1 **(10)** (90 mg, 0.153 mmol, 1.16 eq.) previously dissolved in freshly distilled pyridine (25 ml) was added under argon under stirring. After addition of freshly distilled pyridine (100 ml), the mixture was stirred at 50 $^{o}$C during 24 h and further refluxed for 2 h. The reaction mixture was cooled to room temperature and dissolved in cyclohexane (200 ml). Without evaporation of solvents, it was purified by column chromatography on $SiO_2$. Using different eluents: DCM-cyclohexane (1:1), DCM and gradually increasing methanol ratio in DCM-methanol mixtures up to 12% give set of complexes. Further purification by Bio-Beads S-X3 (eluent - chloroform-methanol 98:2) removed small impurities from the mixture. Extra purification on Bio-Beads S-X1 column (eluent - 98/2 chloroform-methanol 98:2) afforded 18 mg (yield 10%) of the pure compound **28b** as a green solid.

$^{1}$H-NMR ($CD_3OD$, 400 MHz) δ, ppm: 1.41 (ddd, $^{4}J$ = 2.2 Hz, $^{4}J$ = 2.2 Hz, $^{4}J_{P-H}$ = 2.2 Hz, 2H, *o*-phenoxy), 2.24 (ddd, $^{3}J$ = 8.2 Hz, $^{4}J$ = 2.2 Hz, $^{4}J_{P-H}$ = 2.2 Hz, 2H *o*-phenoxy), 3.35 (m, $CH_2O$), 3.51 (m, $CH_2O$), 3.56-3.68 (m, 16H, $CH_2O$), 4.48 (s, 4H, $CH_2O$), 5.74 (dt, $^{3}J$ = 8.2 Hz, $^{4}J$ = 1.4 Hz, 2H, *p*-phenoxy), 5.92 (td, $^{3}J$ = 8.2 Hz, $^{4}J$ = 1.7, 2H, *m*-phenoxy), 7.17 (d, $^{3}J$ = 7.7 Hz, 2H, *m*-pyridyl$_{handle}$), 7.30 (t, $^{3}J$ = 7.8 Hz, 1H, *p*-pyridyl$_{handle}$), 7.75 (m, 9H, *m*- and *p*-phenyl), 7.82 (m, 6H, *o*-phenyl), 7.90 (m, 2H, *o*-pyridyl), 8.95 (m, 2H, *m*-pyridyl), 9.13 (m, 8H, β-pyrr).

$^{31}$P-NMR ($CD_3OD$, 162 MHz) δ, ppm: -195.

$^{13}$C-NMR ($CD_3OD$, 125 MHz) δ, ppm: 68.3 ($CH_2O$), 70.2 ($CH_2O$), 71.6 ($CH_2O$), 71.7 ($CH_2O$), 72.0 ($CH_2O$), 74.4 ($CH_2O$), 74.4 ($CH_2O$), 101.8 (CH, $^{3}J_{P-C}$ = 8.2 Hz), 106.7 (CH), 108.8 (CH, $^{3}J_{P-C}$ = 8.3 Hz), 109.0 (CH), 109.7 (CH), 118.8 (C), 119.1 (C), 121.6 (CH), 129.6 (CH), 129.7 (CH), 131.0 (CH), 134.2 (CH, $^{3}J_{P-C}$ = 5.2 Hz), 134.7 (CH), 135.0 (CH, $^{3}J_{P-C}$ = 5.4 Hz), 135.2, (CH, $^{3}J_{P-C}$ = 5.6 Hz), 135.4 (CH, $^{3}J_{P-C}$ = 5.3 Hz), 136.1 (C), 138.9 (CH), 139.7 (C), 140.7 (C), 140.8 (C), 141.0 (C), 145.2 (C), 150.3 (CH), 151.5 (C), 151.6 (C), 159.0 (C), 159.2(C).

HR-ESI MS: *m/z* calcd. for $[C_{74}H_{67}N_6O_{10}P]^{2+}$: 615.2323; found: 615.2312 [**28b**H-Br]$^{2+}$;

*m/z* calcd. for $[C_{74}H_{66}N_6O_{10}P]^+$: 1229.4573; found 1229.4590 [**28b**-Br]$^+$.

UV-vis ($CHCl_3$) λ, nm (logε): 434 (4.92), 565 (3.86), 607 (3.45).

| | |
|---|---|
| **Turnstile#2,**<br>**[P(MPyP)handle#2]$^+$OTs$^-$ (29).** | 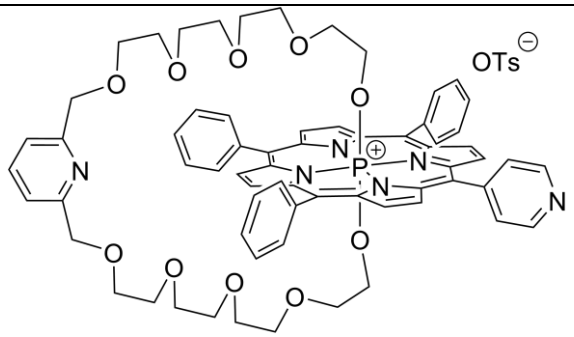 |

[P(MPyP)$(OH)_2]^+$Br$^-$ **(22) (**54 mg, 0.07 mmol, 1 eq.) and handle#2 **(14)** (68 mg, 0.085 mmol, 1.2 eq.) were dissolved in MeCN (80 ml). The mixture was bubbled 30 min with argon and $Cs_2CO_3$ (82 mg, 0.25 mmol, 3.5 eq.) was added and the reaction mixture was stirred at 50 $^oC$ for 36 h. Approximately half of MeCN was evaporated under vacuum and the mixture was diluted with DCM (100 ml). The reaction mixture was directly poured on a $SiO_2$ chromatography column and eluted with a mixture DCM-methanol. Brown-red fraction (15% of MeOH) was isolated and purified by Bio-Beads S-X1 GPC with chloroform as the eluent affording 10 mg of the compound **29** along with impurities.

$^1$H-NMR ($CD_3OD$, 400 MHz) δ, ppm: -2.23 (m, 4H, P-O-$CH_2$), 0.65 (br., 4H, $CH_2O$), 2.12 (m, 4H, $CH_2O$), 2.63 (m, 4H, $CH_2O$), 2.94 (m, 4H, $CH_2O$), 3.18 (m, 4H, $CH_2O$), 3.38 (m, 4H, $CH_2O$), 3.49 (m, 4H, $CH_2O$), 4.46 (s, 4H, $CH_2O$), 7.23 (d, $^3J$ = 7.9 Hz, 2H, *m*-pyridyl$_{handle}$), 7.55 (t $^3J$ = 7.6 Hz, 1H, *p*-pyridyl$_{handle}$), 7.82 (m, 9H, m and *p*-phenyl), 8.04 (m, 6H, *o*-phenyl), 8.15 (m, 2H, *o*-pyridyl), 8.98 (m, 2H, *m*-pyridyl), 9.14 (m, 8H, β-pyrr). *Spectra are described more precisely in Chapter I.*

$^{31}$P-NMR ($CD_3OD$, 162 MHz) δ, ppm: -181.

MALDI-TOF MS: *m/z* calcd. for $[C_{67}H_{67}N_5O_{10}P]^+$: 1132.47; found 1133.48 [**29**-OTs]$^+$.

UV-vis ($CHCl_3$) λ, nm: 433, 563, 602.

| | |
|---|---|
| **Dichloro-((5,15)-dipyridyl-(10,20)-diphenylporphyrinato)phosphorus(V) chloride,**<br>**[P(DPyP)$Cl_2]^+$Cl$^-$ (30).** | 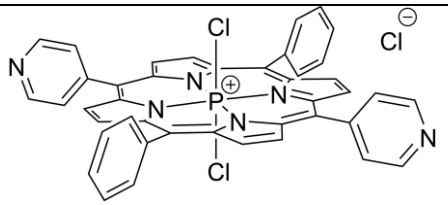 |

The (5,15)-dipyridyl-(10,20)-diphenylporphyrin, $H_2$DPyP **(1c)** (75 mg, 0.12 mmol, 1 eq.) was dissolved in pyridine (25 ml) under argon and solutions of $POCl_3$ (18 ml, 19.37 mmol, 160 eq.) and $PCl_5$ (9 mg, 0.43 mmol, 3,5 eq.) in pyridine (2 ml) were added dropwise under argon and then the mixture was refluxed during 7 days. The mixture was cooled to room temperature and the pyridine was evaporated under vacuum. The green solid was purified by column chromatography on silica gel. Mixture of MeOH and $CH_2Cl_2$ was used as the eluent and the green solid was isolated

at 8% of methanol. The residue was purified by Bio-Beads S-X1 GPC with chloroform as the eluent affording 5 mg (yield 5%) of compound **30**. This complex is hydrolyzing very rapidly in air and should be kept under argon in the absence of light and moisture.

$^{1}$H-NMR (DMSO-$d_6$ + $CDCl_3$, 300 MHz) δ, ppm: 7.78 (m, 6H, *m*- and *p*-phenyl), 7.93 (m, 4H, *o*-phenyl), 8.07 (m, 4H, *o*-pyridyl), 9.00 - 9.30 (m, 12H, *o*-pyridyl + β-pyrr).

$^{31}$P-NMR (DMSO-$d_6$ + $CDCl_3$, 162 MHz) δ, ppm: -229.

$^{13}$C-NMR (DMSO-$d_6$ + $CDCl_3$, 125 MHz) δ, ppm: 113.4 (C), 116.5 (C), 117.5 (C), 127.8 (CH), 128.2 (CH), 129.7 (CH), 129.9 (CH), 132.9 (CH), 133.3 (CH), 138.2 (C), 139.6 (C), 142.8, (C), 148.2 (CH).

HR-ESI MS: *m/z* calcd. for $[C_{42}H_{27}Cl_2N_6P]^{2+}$: 358.0700; found: 358.0716 [**30**H-Cl]$^{2+}$;
*m/z* calcd. for $[C_{42}H_{26}Cl_2N_6P]^{+}$: 715.1328; found: 715.1315 [**30**-Cl]$^{+}$.

UV-vis ($CHCl_3$) λ, nm: 438, 570, 608.

| | |
|---|---|
| **Dihydroxy-((5,15)-dipyridyl-(10,20)-diphenylporphyrinato)phosphorus(V) bromide, $[P(DPyP)(OH)_2]^{+}Br^{-}$ (31).** | 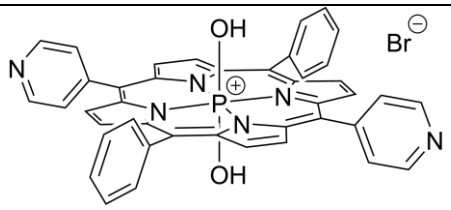 |

The (5,15)-dipyridyl-(10,20)-diphenylporphyrin, $H_2$DPyP **(1c)** (73 mg, 0.118 mmol, 1 eq.) was dissolved in pyridine (50 ml) under argon and then a solution of $POBr_3$ (1.8 g, 6.3 mmol, 53 eq.) in pyridine (10 ml) was added dropwise under stirring. The reaction mixture was refluxed for 1.5 h under argon and then cooled to room temperature. After dissolving in DCM (200 ml), to the green mixture 2 L of distilled water was added and stirred at room temperature during 1 day until full hydrolysis of $P(DPyP)(Br)_2]^{+}Br^{-}$ to the dihydroxy complex $[P(DPyP)(OH)_2]^{+}Br^{-}$ was achieved and the mixture became purple. The organic layer was then isolated and purified by column chromatography (silica gel, DCM-methanol mixture as the eluent). Increasing the methanol ratio in the eluent up to 25% afforded the crude product. Further purification by Bio-Beads S-X3 GPC (eluent - 98/2 chloroform-methanol 98:2) afforded 62 mg (yield 69%) of the pure compound **31** as a purple solid.

$^{1}$H-NMR ($CDCl_3$, 500 MHz) δ, ppm: 7.65-7.76 (m, 6H, m and p-phenyl), 7.89 (d, $^{3}J$ = 5.4 Hz, 2H, o-pyridyl), 7.97 (d, $^{3}J$ = 7.4 Hz, 2H, o-phenyl), 8.53 (d, $^{3}J$ = 4.8 Hz, 2H, m-pyridyl), 8.72 (dd, $^{3}J$ = 5.3 Hz, $^{4}J_{P\text{-}H}$ = 1.9 Hz, 4H, β-pyrr.), 8.89 (dd, $^{3}J$ = 5.3 Hz, $^{4}J_{P\text{-}H}$= 1.8 Hz, 4H, β-pyrr.).

$^{31}$P-NMR ($CDCl_3$, 121 MHz) δ: ppm -180.

$^{13}$C-NMR ($CDCl_3$, 125 MHz): 112.4 (C), 116.5 (C), 128.0 (CH,), 128.2 (CH,), 129.2 (CH), 131.6 (CH), 133.0 (CH), 133.5 (CH), 137.0 (C), 138.3 (C), 139.6 (C), 145.8 (C), 148.6 (CH).

HR-ESI MS: *m/z* calcd. for $[C_{42}H_{29}N_6O_2P]^{2+}$: 340.1039; found: 340.1026 [**31**H-Br]$^{2+}$;
*m/z* calcd. for $[C_{42}H_{28}N_6O_2P]^{+}$: 679.2006; found: 679.2008 [**31**-Br]$^{+}$.

UV-vis ($CHCl_3$) λ, nm (logε): 428 (5.07), 557 (3.93), 598 (3.48).

| | |
|---|---|
| **Dipropoxy-((5,15)-dipyridyl-(10,20)-diphenylporphyrinato)phosphorus(V) bromide, $[P(DPyP)(OPr)_2]^+Br^-$ (32).** | 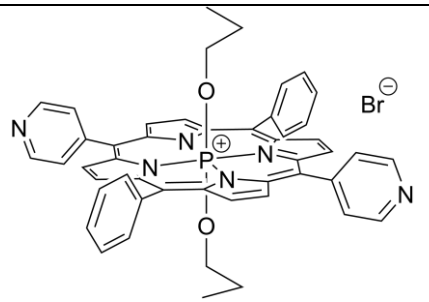 |

This synthesis was achieved by modification of a reported procedure.[10]

The porphyrin $[P(DPyP)(OH)_2]^+Br^-$ **(31) (**7 mg, 0.009 mmol, 1 eq.) was dissolved in acetonitrile (15 ml) and then 1-iodopropane (3 µl, 0.003 mmol, 3.3 eq.) and $Cs_2CO_3$ (7.5 mg, 0.0023 mmol, 2.5 eq.) were added. The reaction mixture was stirred at 50 $^oC$ during 24 h under argon. After cooling to room temperature, the solvent was evaporated under vacuum. The residue was purified by column chromatography (silica gel, DCM-methanol). The product was isolated at 20% of methanol in the eluent. Then it was passed through Bio-Beads S-X1 GPC (eluent - chloroform-methanol 98:2) afforded 1.5 mg (yield 20%) of compound **32**.

$^1$H-NMR ($CDCl_3$, 400 MHz) δ, ppm -2.48 (br., 4H, P-O-$CH_2$), -1.49 (br., 4H $CH_2$), -1.14 (br., 6H, $CH_3$) 7.81 (m, 6H, *m*- and *p*-phenyl), 8.00 (m, 8H, *o*-phenyl + *o*-pyridyl), 9.13 (m, 10H, *m*-pyridyl + β-pyrr).

$^{31}$P-NMR ($CDCl_3$, 162 MHz) δ, ppm, -179.

UV-vis ($CHCl_3$) λ, nm: 432, 560, 600.

| | |
|---|---|
| **Dihydroxy(5,10,15,20-tetrapyridylporphyrinato)phosphorus(V) bromide, $[P(TPyP)(OH)_2]^+Br^-$ (33)** | 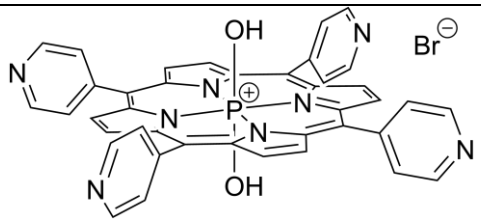 |

5,10,15,20-tetrapyridylporphyrin, $H_2TPyP$ **(**105 mg, 0.17 mmol, 1 eq.) was dissolved in pyridine (50 ml) under argon and then a solution of $POBr_3$ (4.80 g, 17 mmol, 100 eq.) in pyridine (10 ml) was added dropwise under stirring and the reaction mixture was refluxed for 2.5 h before it was cooled to room temperature. After dissolving in DCM (200 ml), to the green mixture 2 L of distilled water was added and the mixture stirred at room temperature during 1 day until full hydrolysis of $P(TPyP)(Br)_2]^+Br^-$ to the dihydroxy complex $[P(TPyP)(OH)_2]^+Br^-$ was achieved. The organic layer was isolated and poured directly on a silica gel chromatography column without evaporation of the solvents. Increasing the methanol ratio in the eluent up to 50% give the crude product. Further purification by Bio-Beads S-X1 GPC (eluent - chloroform-methanol 98:2) afforded 16 mg (yield 13%) of the pure compound **33** as a purple solid. This compound is unstable and decomposes even under argon and thus must be kept in the absence of light in the fridge.

$^{1}$H-NMR ($CD_3OD$, 500 MHz) δ, ppm: 8.17 (m, 8H, *o*-pyridyl), 8.97 (m, 8H *m*-pyridyl), 9.04 (d, $^{4}J_{P-H}$ =1.7 Hz, 8H β-pyrr).

$^{31}$P-NMR ($CD_3OD$, 121 MHz) δ, ppm: -175.

$^{13}$C-NMR ($CD_3OD$, 125 MHz) δ, ppm: 114.3 (C), 130.0 (CH), 133.5 (CH, $^{3}J_{P-C}$ = 3.3 Hz), 139.9 (C), 147.9 (C), 149.7 (CH).

HR-ESI MS: *m/z* calcd. for $[C_{40}H_{26}N_8O_2P]^+$: 681.1911; found: 681.1821 [**33**-Br]$^+$.

UV-vis ($CHCl_3$) λ, nm (logε): 427 (5.13), 557 (3.92), 594 (3.50).

| | |
|---|---|
| **Dishydroxy(5-(pentafluorophenyl)-(10,15,20)-triphenylporphyrinato)phosphorus(V) bromide, $[P(MpFP)(OH)_2]^+Br^-$ (34).** | 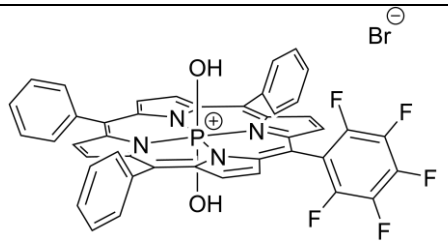 |

The 5-pentafluorophenyl-10,15,20-triphenylporphyrin, $H_2$MpFP **(2)** (270 mg, 0.38 mmol, 1 eq.) was dissolved in pyridine (150 ml) under argon and then a solution of $POBr_3$ (4.39 g, 15.3 mmol, 40 eq.) in pyridine (10 ml) was added dropwise under stirring. The mixture was refluxed for 1.5 h under argon and then cooled to room temperature. After dissolving in DCM (200 ml) to the green mixture, 2L of distilled water was added and the mixture stirred at room temperature during 1 day until it became purple. The organic layer was isolated and diluted with petroleum ether (200 ml). The mixture was poured directly on a silica gel chromatography column without evaporation of the solvents. Increasing the methanol ratio in the eluent up to 15% give the crude product. Further purification by Bio-Beads S-X3 GPC column (eluent - chloroform-methanol 98:2) afforded 170 mg (yield 55%) of the pure compound **34**.

$^{1}$H-NMR ($CD_3OD$, 500 MHz) δ, ppm: 7.80 (m, 9H, *m*- and *p*-phenyl), 8.04 (m, 6H *o*-phenyl), 9.06 (m, 4H, β-pyrr), 9.08 (m, 2H, β-pyrr), 9.14 (m, 2H, β-pyrr).

$^{31}$P-NMR ($CD_3OD$, 121 MHz) δ, ppm: -189.

$^{19}$F-NMR ($CD_3OD$, 282 MHz) δ, ppm: -164.3 (td, $^{3}J_{F-F}$ = 21.7 Hz, $^{4}J_{F-F}$ = 6.5 Hz, 2F, o-phenyl), -151.1 (t, $^{3}J_{F-F}$ = 21.0 Hz, 1F, p-phenyl), -140.6 (m, 2F, m-phenyl).

$^{13}$C-NMR ($CD_3OD$, 125, MHz) δ, ppm: 117.6 (C, $^{3}J_{P-C}$ = 1.8 Hz), 118.5 (C, $^{3}J_{P-C}$ = 1.8 Hz), 120.0 (CH), 120.1 (CH), 130.5 (CH), 132.8 (CH, $^{3}J_{P-C}$ = 4.1 Hz), 133.9 (CH, $^{3}J_{P-C}$ = 4.7 Hz), 134.3 (CH, $^{3}J_{P-C}$ = 4.7 Hz), 134.6 (CH), 134.7 (CH), 135.0 (CH, $^{3}J_{P-C}$ = 4.7 Hz), 137.7 (CH), 137.8 (C), 140.0 (C), 140.2 (C), 140.6 (C), 140.9 (C).

HR-ESI MS: *m/z* calcd. for $[C_{44}H_{25}F_5N_4O_2P]^+$: 767.1630; found: 767.1563 [**34**-Br]$^+$.

UV-vis ($CHCl_3$) λ, nm (logε): 425 (5.29), 555 (4.13), 593 (3.79).

| | |
|---|---|
| **5-(2-(trimethylsilyl)ethynyl)-10,15,20-triphenyl-porphyrin,**<br>**$H_2$TMSP (35).** | 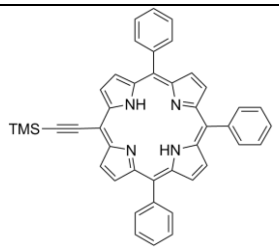 |

The compound was synthesized following a described procedure.[11,12]

To a mixture of pyrrole (1.18 ml, 17 mmol, 2.5 eq.), benzaldehyde (1.04 ml, 10.2 mmol, 1.5 eq.) and (trimethylsilyl)propiolaldehyde (1 ml, 6.8 mmol, 1 eq.) in chloroform (1.5 L) and trifluoroboron etherate (0.14 ml, 1.23 mmol, 0.18 eq.) were added. The reaction mixture was stirred at room temperature for 6 h in the dark. DDQ (1.93 g, 8.5 mmol, 1.25 eq.) was added and the resulting mixture was further stirred for 1 h. The solvent was evaporated to dryness under reduced pressure. The desired porphyrin was separated from the crude residue by column chromatography (silica gel, eluting with DCM-cyclohexane mixture 3:7). The 5$^{th}$ green fraction was collected. After recrystallization from DCM and cyclohexane, the product was isolated in 5% yield (0.1 g).

$^1$H-NMR ($CDCl_3$, 400 MHz) δ, ppm: -2.39 (s, 2H, NH), 0.63 (s, 9H, TMS), 7.78 (m, 9H m- and *p*-phenyl.), 8.21 (m, 6H, *o*-phenyl), 8.78 (s, 4H, β-pyrr), 8.90 (d, $^3J$ = 4.7 Hz, 2H, β-pyrr), 9.68 (d, $^3J$ = 4.8 Hz, 2H, β-pyrr).

$^{13}$C-NMR ($CDCl_3$, 75 MHz) δ, ppm: 0.8 ($CH_3$), 99.4 (C), 102.3 (C), 107.5 (C), 121.4 (C), 122.4 (C), 127.0 (CH), 127.1 (CH), 128.2 (CH), 134.7 (CH), 134.8 (CH), 142.1 (C), 142.3 (C).

| | |
|---|---|
| **5-ethynyl-10,15,20-triphenyl-porphyrin,**<br>**$H_2$EtP (36).** | 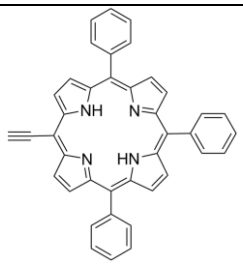 |

The compound was synthesized according to a described procedure.[12,11]

A solution of TBAF (0.2 ml, 0.2 mmol, 1.3 eq., 1M in THF) was slowly added to a solution of porphyrin **35** (100 mg, 0.16 mmol, 1 eq.) in a mixture of dry THF-DCM (4:1). A spatula of $CaCl_2$ was added to quench the reaction after 1 h. The reaction mixture was washed with water (3 x 200 ml), the organic layer was dried over anhydrous $Na_2SO_4$ and concentrated. The solvent was evaporated. The solid was recrystallized from chloroform-methanol afforded 90 mg (quantitative yield) of pure compound **36**.

$^{1}$H-NMR ($CDCl_3$, 400 MHz) δ, ppm: -2.44 (s, 2H, NH), 4.19 (s, 1H, ethynyl), 7.79 (m, 9H *m*- and *p*-phenyl.), 8.20 (m, 6H, *o*-phenyl), 8.79 (s, 4H, β-pyrr), 8.92 (d, $^{3}J$ = 4.3 Hz, 2H, β-pyrr), 9.70 (d, $^{3}J$ = 4.5 Hz, 2H, β-pyrr).

$^{13}$C-NMR ($CDCl_3$, 100 MHz) δ, ppm: 84.0 (CH), 121.0 (C), 126.7 (CH), 126.8 (CH), 127.9 (CH), 134.4 (CH), 134.5 (CH), 141.7 (C), 142.0 (C).

| **Zinc dimer (37).** | 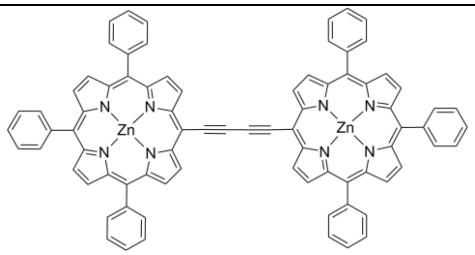 |
|---|---|

The compound was synthesized according to a described procedure.[13]

The porphyrin **36** (90 mg, 0.16 mmol, 1 eq.) was dissolved in a chloroform-methanol mixture (150/30 ml). Zinc acetate dihydrate (0.5 g, 2.28 mmol, 14 eq.) was added. The mixture was stirred during 4 h before solvents were evaporated under reduced pressure. The solid was dissolved in $CHCl_3$, washed with water, the organic fraction was concentrated and passed through a pad of silica and evaporated. The violet solid was dissolved in 50 ml of toluene. Trimethylamine (10 ml) and bis(triphenylphosphine)palladium(II) dichloride (56 mg, 0,08 mmol, 0.5 eq) were added and the mixture was stirred during 24 h at 50 ºC in air. The solvent was removed under reduced pressure and the crude solid was purified by column chromatography (alumina, cyclohexane-toluene 1:1) afforded 65 mg (yield 65%) of the pure product **37** as a green solid.

$^{1}$H-NMR (THF-d8, 400 MHz) δ, ppm: 7.85 (m, 18H *m*- and *p*-phenyl.), 8.27 (m, 12H, *o*-phenyl), 8.83 (s, 8H, β-pyrr), 9.06 (d, $^{3}J$ = 4.6 Hz, 4H, β-pyrr), 10.01 (d, $^{3}J$ = 4.7 Hz, 4H, β-pyrr).

$^{13}$C-NMR ($CDCl_3$+DMSO-$d_6$, 100 MHz) δ, ppm: 102.9 (C), 121.7 (C), 126.0 (CH), 126.1 (CH), 127.1 (CH), 131.2 (CH) 131.7 (CH), 132.7 (CH), 133.7 (CH), 133.8 (CH), 142.0 (C), 148.8 (C), 149.0 (C), 149.9 (C), 152.4 (C).

HR-ESI MS: *m/z* calcd. for $[C_{80}H_{46}N_8Zn_2]^+$: 1246.2423; found: 1246.2414 [**37**]$^+$.

UV-vis (THF) λ, nm (logε): 451 (5.58), 483 (5.36), 569 (4.43), 637 (4.80), 690 (4.83).

## References


1 J. P. Strachan, S. Gentemann, J. Seth, W. A. Kalsbeck, J. S. Lindsey, D. Holten and D. F. Bocian, *J. Am. Chem. Soc.*, 1997, **119**, 11191–11201.

2 M. T. Barton, N. M. Rowley, P. R. Ashton, C. J. Jones, N. Spencer, M. S. Tolleya and L. J. Yellowleesb, *New J. Chem.*, 2000, **24**, 555–560.

3 M. Jurow, C. Farley, C. Pabon, B. Hageman, A. Dolor and C. M. Drain, *Chem. Commun.*, 2012, **48**, 4731–4733.

4 A. Guenet, E. Graf, N. Kyritsakas and M. W. Hosseini, *Inorg. Chem.*, 2010, **49**, 1872–1883.

5 V. V. Namboodiri and R. S. Varma, *Tetrahedron Lett.*, 2002, **43**, 1143–1146.

6 N. Zigon, A. Guenet, E. Graf and M. W. Hosseini, *Chem. Commun.*, 2013, **49**, 3637–3639.

7 C. J. Carrano and M. Tsutsui, *J. Coord. Chem.*, 1977, **7**, 79–83.

8 M. O. Breusova, V. E. Pushkarev and L. G. Tomilova, *Russ. Chem. Bull. Int. Ed.*, 2007, **56**, 1456–1460.

9 K. Kunimoto, H. Segawa and T. Shimidzu, *Tetrahedron Lett.*, 1992, **33**, 6327–6330.

10 Y. Andou, K. Ishikawa, K. Shima, T. Shiragami and M. Yasuda, *Bull. Chem. Soc. Jpn.*, 2002, **75**, 1757–1760.

11 M. Fathalla and J. Jayawickramarajah, *European J. Org. Chem.*, 2009, 6095–6099.

12 J.-W. Seo, S. Y. Jang, D. Kim and H.-J. Kim, *Tetrahedron*, 2008, **64**, 2733–2739.

13 R. W. Wagner, T. E. Johnson, F. Li and J. S. Lindsey, *J. Org. Chem.*, 1995, **60**, 5266–5273.

# Crystallographic Data

## $[P(TPP)(OEt)_2]^+$ (not finalized)

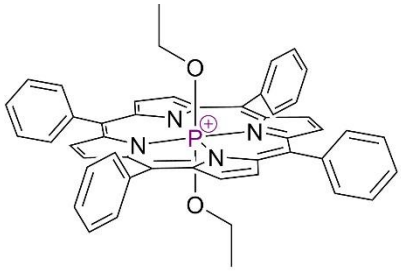


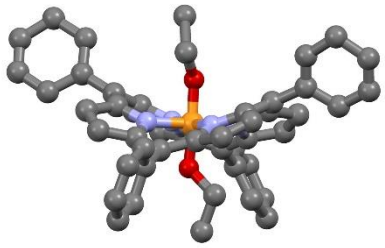

**Crystallization conditions:** Single crystals were obtained by vapor diffusion of n-pentane into a solution of porphyrin in chloroform with a few drops of methanol.

| | | |
|---|---|---|
| Identification code | e3463a | |
| Empirical formula | C70 H Cl3 N O P | |
| Formula weight | 1009.04 g/mol | |
| Temperature | 296(2) K | |
| Wavelength | 0.71073 Å | |
| Crystal system | triclinic | |
| Space group | P-1 | |
| Unit cell dimensions | a = 10.2750(4) | α = 83.6210(15) |
| | b = 16.5072(6) | β = 79.5842(15) |
| | c = 17.5546(6) | γ = 78.0722(15) |
| Volume | 2856.75(18) $Å^3$ | |
| Z | 2 | |
| Density (calculated) | 1.173 $g/cm^3$ | |
| Absorption coefficient | 0.231 $mm^{-1}$ | |
| F (000) | 1004 | |
| Crystal size | 0.08 x 0.06 x 0.06 mm | |
| Theta range for data collection | 1.664º to 30.123º | |
| Index ranges | -14<=h<=14, -23<=k<=22, -24<=l<=23 | |
| Reflections collected | 57989 | |
| Independent reflections | 15375 | |
| Completeness to theta = 30.123º | 91.2 % | |
| Absorption corrections | Semi-empirical from equivalents | |
| Max. and min. transmissions | 0.9908 and 0.9817 | |
| Refinement method | Full-matrix least-squares on $F^2$ | |
| Data / restraints / parameters | 15375 / 0 / 622 | |
| Goodness-of-fit $F^2$ | 3.926 | |
| Final R indices [I>2sigma (I)] | R1 = 0.2634, wR2 = 0.5489 | |
| R indices (all data) | R1 = 0.2114, wR2 = 0.5719 | |
| Largest diff. peak and hole | 2.952 and -1.386 $eÅ^{-3}$ | |

## $[P(MPyP)(OH)_2]^+$

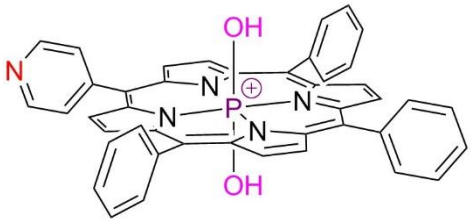


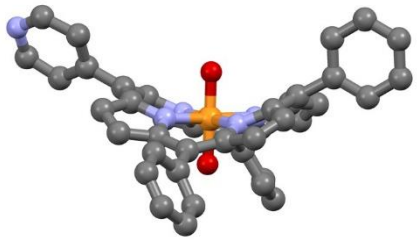

**Crystallization conditions:** Single crystals were obtained by vapor diffusion of n-pentane into a solution of porphyrin in chloroform.

| | |
|---|---|
| Identification code | e3714a_a |
| Empirical formula | C44.62 H28.62 Br0.62 Cl5.24 N5 O2 P |
| Formula weight | 932.72 g/mol |
| Temperature | 173(2) K |
| Wavelength | 0.71073 Å |
| Crystal system | monoclinic |
| Space group | P 1 21/c 1 |
| Unit cell dimensions | a = 17.106(2) Å α = 90° |
| | b = 14.2223(18) Å β = 102.067(4)° |
| | c = 17.709(2) Å γ = 90° |
| Volume | 4213.2(10) $Å^3$ |
| Z | 4 |
| Density (calculated) | 1.470 $g/cm^3$ |
| Absorption coefficient | 1.029 $mm^{-1}$ |
| F (000) | 1892.3 |
| Crystal size | 0.040 x 0.040 x 0.050 mm |
| Theta range for data collection | 1.85° to 27.55° |
| Index ranges | -22<=h<=19, -18<=k<=18, -22<=l<=19 |
| Reflections collected | 9485 |
| Independent reflections | 9485 [R(int) = 0.0534] |
| Completeness to theta = 27.55° | 97.4 % |
| Absorption corrections | Semi-empirical from equivalents |
| Max. and min. transmissions | 0.9510 and 0.9310 |
| Refinement method | Full-matrix least-squares on $F^2$ |
| Data / restraints / parameters | 9485 / 3 / 539 |
| Goodness-of-fit $F^2$ | 1.004 |
| Final R indices [I>2sigma (I)] | R1 = 0.0812, wR2 = 0.2242 |
| R indices (all data) | R1 = 0.1710, wR2 = 0.2522 |
| Largest diff. peak and hole | 1.121 and -0.634 $eÅ^{-3}$ |

## $[P(MPyP)(OPhOH)_2]^+$

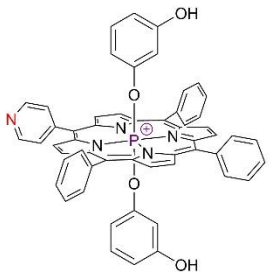


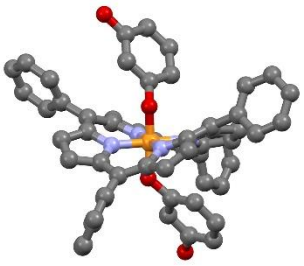

**Crystallization conditions:** Single crystals were obtained by slow diffusion of n-hexane into a chloroform solution of the complex in the presence of traces of methanol and toluene.

| | | |
|---|---|---|
| Identification code | RMI224 | |
| Empirical formula | C56 H38 Br0.50 Cl3.50 N5 O4 P | |
| Formula weight | 1039.73 g/mol | |
| Temperature | 100 K | |
| Wavelength | 0.71073 Å | |
| Crystal system | triclinic | |
| Space group | P-1 | |
| Unit cell dimensions | a = 11.2720(6) Å | α = 76.446(6)° |
| | b = 11.8839(8) Å | β = 80.822 (4)° |
| | c = 18.7479(11) Å | γ = 78.554(4)° |
| Volume | 2376.0(3) $Å^3$ | |
| Z | 2 | |
| Density (calculated) | 1.453 $g/cm^3$ | |
| Absorption coefficient | 0.731 $mm^{-1}$ | |
| F (000) | 1066.0 | |
| Crystal size | 0.200 x 0.020 x 0.400 mm | |
| Theta range for data collection | 4.11° to 25.00° | |
| Index ranges | -13<=h<=12, -14<=k<=14, -22<=l<=22 | |
| Reflections collected | 16695 | |
| Independent reflections | 8268 [R(int) = 0.0786] | |
| Completeness to theta = 25.00° | 98.8 % | |
| Absorption corrections | Semi-empirical from equivalents | |
| Max. and min. transmissions | 0.7590 and 0.9860 | |
| Refinement method | Full-matrix least-squares on $F^2$ | |
| Data / restraints / parameters | 8268 / 2 / 660 | |
| Goodness-of-fit $F^2$ | 1.021 | |
| Final R indices [I>2sigma (I)] | R1 = 0.0765, wR2 = 0.1791 | |
| R indices (all data) | R1 = 0.1557, wR2 = 0.2170 | |
| Largest diff. peak and hole | 1.642 and -1.063 $eÅ^{-3}$ | |

## Dimer(DMAP)$_2$

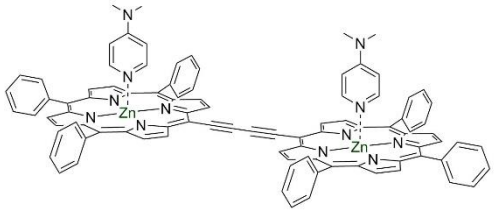
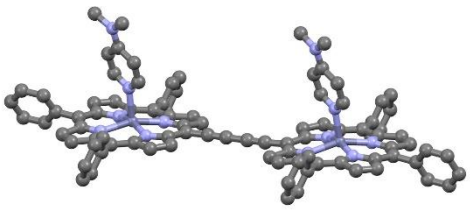

**Crystallization conditions:** Single crystals were obtained by vapor diffusion of n-pentane into a chloroform solution of the dimer (1 eq.) and DMAP (2.5 eq.) in the presence of traces of methanol and toluene.

| | | |
|---|---|---|
| Identification code | e3708a | |
| Empirical formula | C95.70 H67.70 Cl5.10 N12 Zn2 | |
| Formula weight | 1697.30 g/mol | |
| Temperature | 173(2) K | |
| Wavelength | 0.71073 Å | |
| Crystal system | triclinic | |
| Space group | P-1 | |
| Unit cell dimensions | a = 12.5752 Å | α = 106.0120(10)° |
| | b = 16.1287(8) Å | β = 92.051(2)° |
| | c = 23.4657 Å | γ = 111.422(2)° |
| Volume | 4208.8(5) Å$^3$ | |
| Z | 2 | |
| Density (calculated) | 1.339 g/cm$^3$ | |
| Absorption coefficient | 0.787 mm$^{-1}$ | |
| F (000) | 1745.2 | |
| Crystal size | 0.020 x 0.020 x 0.400 mm | |
| Theta range for data collection | 0.91° to 27.53° | |
| Index ranges | -16<=h<=16, -19<=k<=12, -30<=l<=30 | |
| Reflections collected | 31007 | |
| Independent reflections | 18140 [R(int) = 0.0684] | |
| Completeness to theta = 27.53° | 93.5 % | |
| Absorption corrections | Semi-empirical from equivalents | |
| Max. and min. transmissions | 0.9690 and 0.9850 | |
| Refinement method | Full-matrix least-squares on F$^2$ | |
| Data / restraints / parameters | 18140 / 12 / 1067 | |
| Goodness-of-fit F$^2$ | 1.029 | |
| Final R indices [I>2sigma (I)] | R1 = 0.0854, wR2 = 0.2322 | |
| R indices (all data) | R1 = 0.1770, wR2 = 0.2875 | |
| Largest diff. peak and hole | 1.896 and -0.847 eÅ$^{-3}$ | |

## Dimer(handle#3) (not finalized)

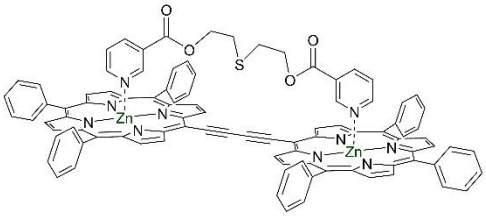


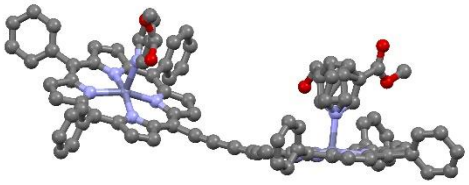

**Crystallization conditions:** Single crystals were obtained by vapor diffusion of n-pentane into the chloroform solution of the dimer (1 eq.) and handle#3 (1.5 eq.) in the presence of traces of methanol and toluene.

| | | |
|---|---|---|
| Identification code | e3731a | |
| Empirical formula | C94 HN10 O3.50 Zn2 | |
| Formula weight | 1420.63 g/mol | |
| Temperature | 173(2) K | |
| Wavelength | 0.71073 Å | |
| Crystal system | monoclinic | |
| Space group | C 1 2/c 1 | |
| Unit cell dimensions | a = 48.046(9) Å | α = 90° |
| | b = 13.475(2) Å | β = 132.023(16)° |
| | c = 32.273(7) Å | γ = 90° |
| Volume | 15522(6) $Å^3$ | |
| Z | 8 | |
| Density (calculated) | 1.247g/$cm^3$ | |
| Absorption coefficient | 0.676 $mm^{-1}$ | |
| F (000) | 5784 | |
| Crystal size | 0.050 x 0.050 x 0.060 mm | |
| Theta range for data collection | 1.62° to 27.69° | |
| Index ranges | -58<=h<=59, -15<=k<=17, -29<=l<=42 | |
| Reflections collected | 35994 | |
| Independent reflections | 16817 [R(int) = 0.0259] | |
| Completeness to theta = 27.693° | 92.5% | |
| Absorption corrections | Semi-empirical from equivalents | |
| Max. and min. transmissions | 0.9710 and 0.9600 | |
| Refinement method | Full-matrix least-squares on $F^2$ | |
| Data / restraints / parameters | 16817 / 9 / 910 | |
| Goodness-of-fit $F^2$ | 2.195 | |
| Final R indices [I>2sigma (I)] | R1 = 0.1033, wR2 = 0.3163 | |
| R indices (all data) | R1 = 0.1347, wR2 = 0.3293 | |
| Largest diff. peak and hole | 1.550 and -0.727 e$Å^{-3}$ | |

# Résumé

Le contrôle du mouvement moléculaire est un sujet étudié par les chimistes depuis deux décennies. L'utilisation de différents stimuli externes[1–9] a été mise à profit pour contrôler le mouvement. On peut citer notamment la formation ou la rupture d'une liaison de coordination[4], une variation de pH[9] ou encore des phénomènes de photoisomérisation[8].

Au cours des dernières années, notre groupe a étudié la synthèse de tourniquets moléculaires à base notamment de porphyrines de Sn(IV)[10–15], et de porphyrines à anse.[16,17] Des complexes non porphyriniques de Pt (II) et purement organique ont également été étudiés.[18–22] Le but poursuivi avec les porphyrines d'étain est décrit schématique sur la **Fig. 1**.

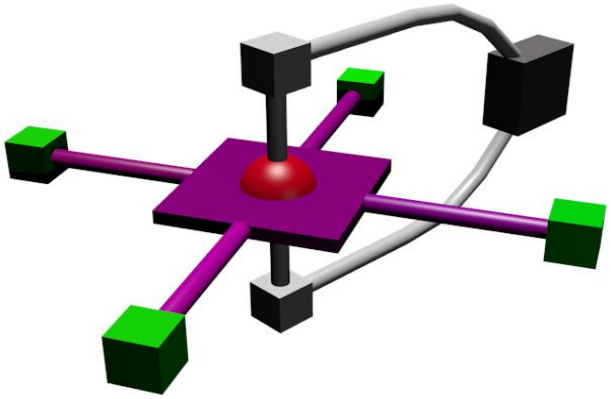

**Fig. 1** Représentation schématique du tourniquet.

Il s'agissait d'utiliser le Sn(IV) comme une charnière entre un rotor (l'anse) et un stator (la porphyrine). Le mouvement est fondé sur la rotation de la porphyrine autour de la liaison O-Sn-O. Dans une telle entité, le mouvement du tourniquet devait pourvoir être contrôlé par l'introduction de 4 stations différenciées en position *méso* du macrocycle porphyrinique. Il a effectivement été possible de générer un tourniquet moléculaire en utilisant une porphyrine symétrique de type $A_2B_2$[13–15]. Malheureusement, la diminution du pH conduisait à la destruction du tourniquet du fait de la labilité de la liaison Sn-O dans ces conditions[9].

La première partie de ce travail de thèse a été consacrée à la synthèse d'un tourniquet moléculaire à base de porphyrines de phosphore (V). La substitution du Sn(IV) par du P(V) dans la cavité porphyrinique devait permettre d'augmenter la stabilité de la liaison entre le rotor et le stator en milieu acide. Le but ultime poursuivi est la formation d'un tourniquet moléculaire dont on maitriserait le sens de rotation grâce à l'implication séquentielle d'au moins trois positions *méso* différenciées. Le mouvement serait maitrisé par la formation successive de liaisons de coordination et/ou d'interactions ioniques impliquant des substituants coordinants et/ou basiques présents sur des positions *méso* adjacentes.

Le deuxième chapitre du manuscrit aborde les propriétés photochimiques particulières des porphyrines de P(V) étudiées. En effet, l'irradiation, en présence d'oxygène, des complexes de

P(V) permet de générer de l'oxygène singulet avec des rendements quantiques quasi-quantitatifs dans certaines conditions ce qui pourrait permettre leur utilisation comme photo-sensibilisateurs très efficaces.[23–25] Nous avons étudié l'influence du solvant et des ligands présents en position axiale du P(V) sur les caractéristiques photophysiques des complexes ainsi que leur efficacité en tant que photo-sensibilisateurs.

La dernière partie du manuscrit concerne la maitrise du mouvement moléculaire dans un dimère de porphyrines de Zn(II) *méso*-substituées et liées *via* un pont acétylénique.[26–28] Le but poursuivi est de maitriser la mise en mouvement ou à l'inverse l'arrêt du mouvement des deux macrocycles porphyriniques en utilisant les propriétés basiques des ligands présents en positions apicales des ions Zn(II). Le stimulus utilisé serait ici d'ordre chimique avec l'ajout d'une molécule «sandwich» interagissant simultanément avec les deux ligands axiaux des Zn (II) conduisant ainsi à l'arrêt de la rotation, une variation du pH devant quant à elle permettre de réenclencher le mouvement des deux macrocycles. Nous aurions ainsi un système bis-porphyrinique pour lequel nous maitriserions la mise en mouvement ou son arrêt.

## Chapitre I. Des tourniquets moléculaires à base de porphyrines de P(V).

Le premier chapitre du manuscrit traite de la synthèse, la caractérisation et l'étude du mouvement de tourniquets moléculaires à base de porphyrine de P(V).

### 1) Synthèse

Les articles décrivant la synthèse et la caractérisation des porphyrines de P(V) *méso*-substituées sont peu nombreux.[29–33] Les porphyrines de P(V) ont une réactivité particulière pouvant en partie être expliquée par une déformation importante du macrocycle porphyrinique du fait du faible rayon ionique du P(V). La procédure habituelle de métallation des porphyrines *méso*-substituées par du P(V) utilise un mélange de $POCl_3$ et $PCl_5$.[29] Il semble également possible d'échanger les ligands présents en positions axiales du métal.[30,32,33]

Nous avons tout d'abord mis au point la synthèse d'un composé de référence à base de *méso*-tétraphénylporphyrine. L'accès à un tel complexe nécessite tout d'abord l'insertion du P(V) dans la cavité porphyrinique puis la coordination de l'anse en position axiale du P(V) (**Schéma 1**).

L'anse utilisée est obtenue *via* une synthèse multi-étape mise au point au laboratoire lors de l'étude sur les tourniquets à base de porphyrines d'étain.[10] Celle-ci porte un groupement pyridine dont la fonction serait de bloquer la rotation de l'anse en milieu acide ou en présence de cations métalliques. Les groupements phénols présents à chaque extrémité de l'anse devrait, chacun, former une liaison de coordination en positions axiales du P(V).

L'insertion du P(V) dans la cavité porphyrinique a été effectuée grâce à un mélange $POCl_3/PCl_5$

dans la pyridine à reflux.[29] Le complexe $[PCl_2(TPP)]Cl$ a ainsi pu être isolé avec un rendement de 82%. L'introduction de l'anse en position axiale du phosphore a pu être effectuée uniquement *via* l'utilisation de micro-ondes et à des températures élevées *(***Schéma 1***)*. Le rendement optimal obtenu n'est que de 30 % et on observe au cours de cette réaction la formation de nombreux sous-produits issus notamment de la déphosphoration de la porphyrine ou de la destruction du macrocycle.

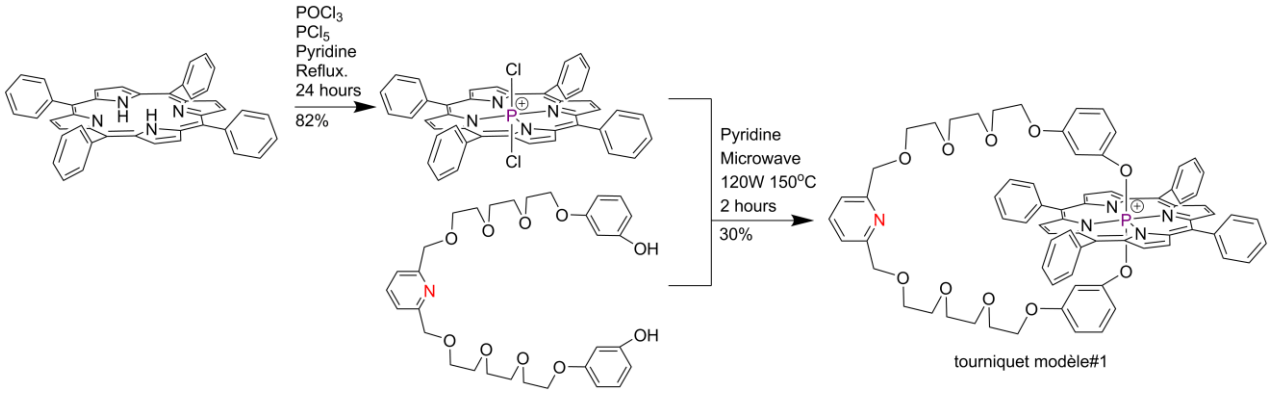


**Schéma 1.** Synthèse du système à base de tétraphenylporphyrine – tourniquet modèle#1.

Nous avons ensuite tenté d'adapter les conditions d'introduction de phosphore à des macrocycles porphyriniques portant un nombre croissant de groupements pyridines en position *méso* (**Schéma 2**). L'utilisation du mélange $POCl_3/PCl_5$ a permis d'accéder au complexe possédant une seule *méso*-pyridine mais avec rendement que de 40%. Par contre, les complexes des porphyrines possédant deux ou quatre pyridines en positions *méso* n'ont pu être obtenus selon ce protocole.

Par contre, l'utilisation de $POBr_3$ suivi de l'échange des ions $Br^-$ par des hydroxydes par hydrolyse a permis d'isoler l'ensemble des 4 complexes de P(V) ciblés (**Schéma 2**). On remarque néanmoins que, l'augmentation du nombre de groupements pyridyl en position *méso* conduit à une diminution drastique des rendements et ce malgré une augmentation de la quantité de réactif phosphoré utilisé et un prolongement des temps de réaction. Ainsi le rendement optimal obtenu avec la *méso*-tétrapyridylporphyrine reste très faible et ce malgré l'utilisation de 100 eq. de $POBr_3$ et près de 2 h 30 min de reflux à 130 °C.

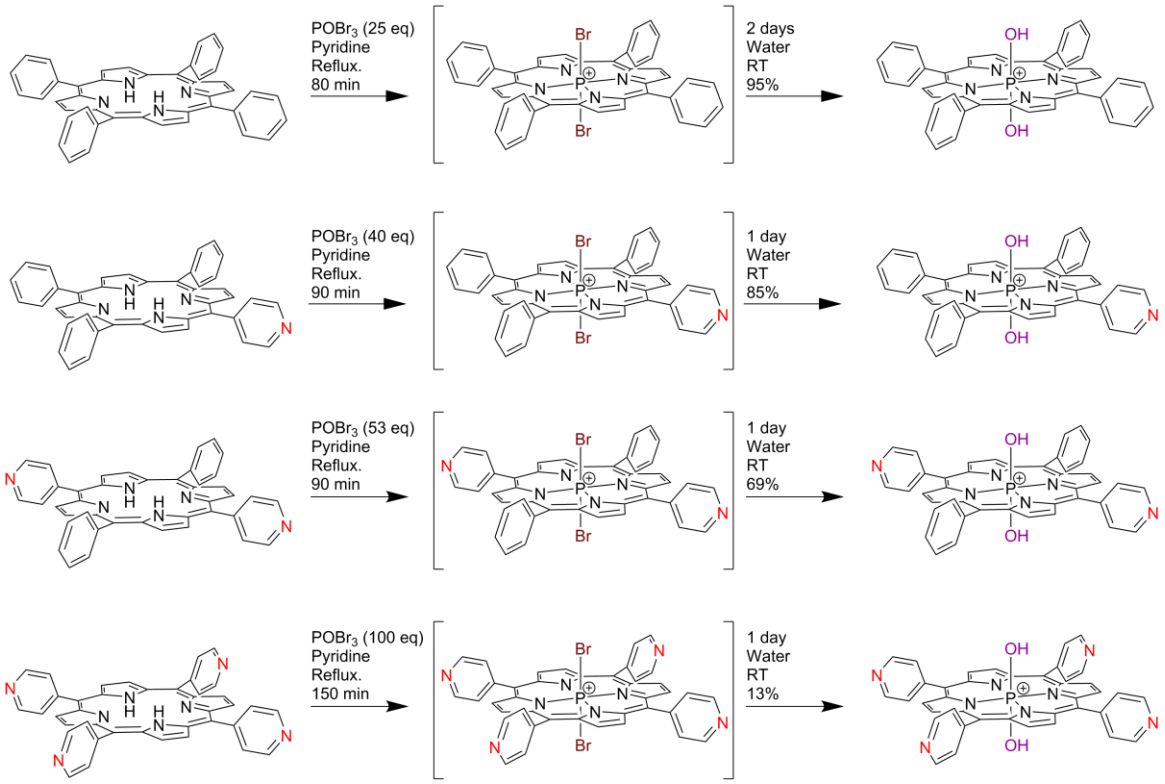


**Schéma 2.** Métallation de méso-pyridylporphyrines par du P(V).

L'insertion de l'anse sur ces complexes possédant deux hydroxo en position axiale du P(V) selon la méthode mise au point pour l'analogue dichloro de la tetraphénylporphyrine (**Schéma 1**) n'a pas conduit aux composés ciblés. Nous avons néanmoins réussi à isoler le complexe mono-pyridine incluant l'anse connectée en positions axiales, tourniquet#1, en introduisant directement cette dernière sur le complexe intermédiaire dibromé (**Schéma 3**).

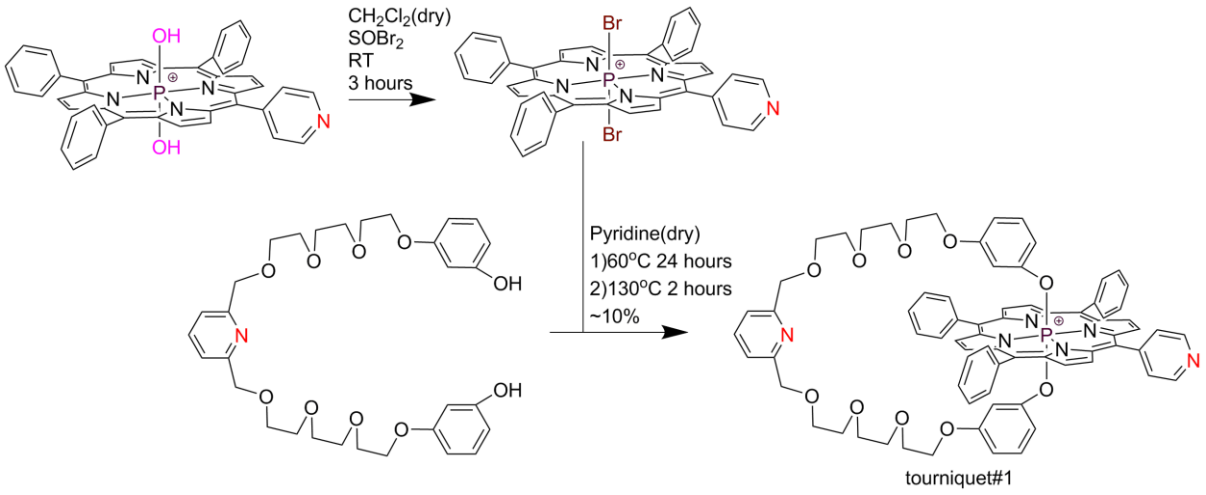


**Schéma 3.** Synthèse du tourniquet#1**.**

Nous avons également mis au point la synthèse du tourniquet#2, utilisant une anse légèrement modifiée (**Schéma 4**)[34]. Le complexe formé s'est révélé extrêmement instable en présence d'$O_2$ et

son étude n'a pas été poursuivie.

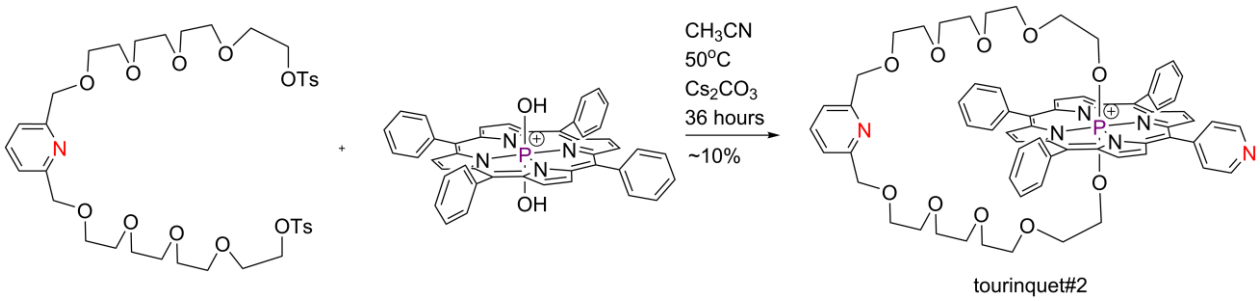


**Schéma 4.** Synthèse du tourniquet#2**.**

### 2) Mouvement moléculaire de tourniquet#1

Nous avons étudié le mouvement de l'anse dans **1** en présence de sels d'argent (**Schéma 5**) et avons pu mettre en évidence par RMN $^{1}$H (1-D et 2-D NOESY) un arrêt du mouvement dans la molécule par interaction des deux groupements pyridyl *via* une liaison de coordination avec un cation argent. L'ajout de bromure de tétraéthylammonium conduit à la formation de bromure d'argent et au déblocage du système.

Un stimulus acido-basique peut également être utilisé. En effet, l'ajout d'acide triflique permet l'arrêt du système grâce à une interaction pyridinium/pyridine. Dans ce cas, la mise en mouvement du système est possible par simple ajout de base, en l'occurrence la triéthylamine **(Schéma 5)**. Ainsi le système peut être verrouillé avec de l'acide triflique et déverrouillé avec $Et_3N$.

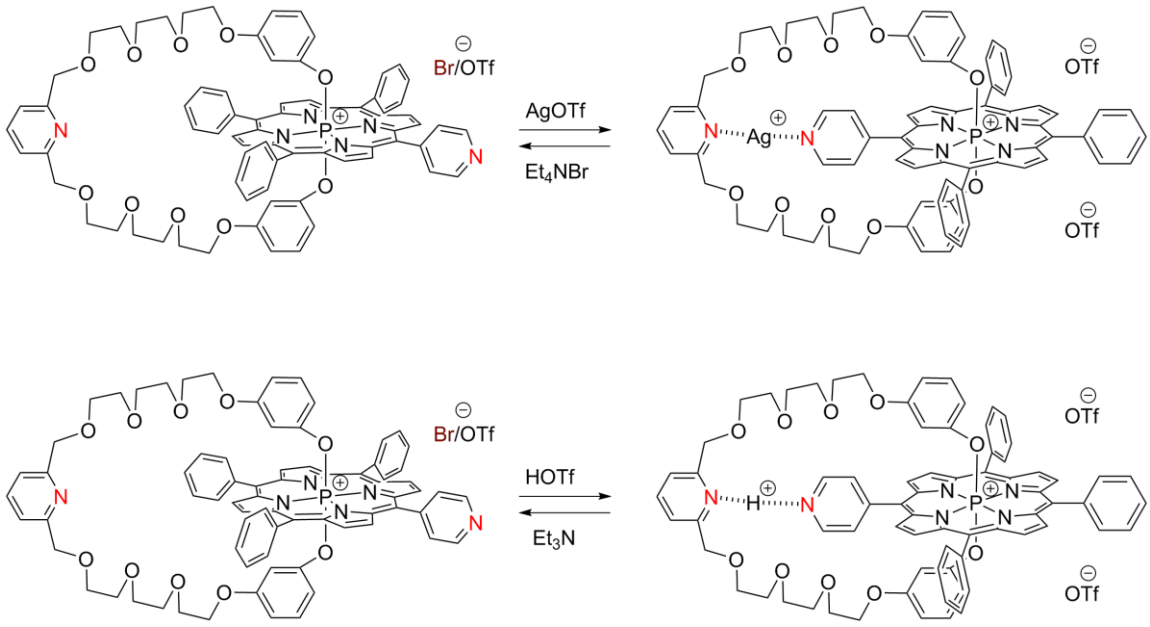


**Schéma 5.** Maitrise du mouvement de l'anse dans tourniquet#1.

**Chapitre II. Porphyrines de P(V): propriétés photochimiques.**

Au cours de notre étude sur les tourniquets moléculaires, nous avons noté une augmentation croissante de l'instabilité des complexes porphyriniques de P(V) en fonction du nombre de pyridines présentent en position *méso*. Les porphyrines de P(V) sont connues pour conduire à la formation d'oxygène singulet sous irradiation[35] ce qui pourrait notamment expliquer la décomposition observée des macrocycles porphyriniques. En effet, les complexes obtenus montrent des rendements quantiques de fluorescence extrêmement faibles. La désexcitation implique un état triplet, qui en présence d'$^3O_2$ conduirait efficacement à la génération d'$^1O_2$.

Nous avons voulu étudier l'irradiation des complexes de P(V) de la tétraphénylporphyrine et de la *méso*-monopyridinepophyrine, en fonction de la nature des ligands présents en position axiale du P(V) (chloro, hydroxy, 3-méthoxyphénoxo, et diéthoxy), ainsi que la nature du solvant ($CHCl_3$, DMSO et $H_2O$). Les conclusions de cette étude font apparaitre que les rendements quantiques de formation d'$^1O_2$ sont supérieurs avec la porphyrine possédant une pyridine. Concernant les ligands axiaux, une efficacité optimale est obtenue en présence de chlorures en position axiale de P(V) puis viennent les ligands éthoxy puis les hydroxo. Le rendement quantique très faible observé pour les ligands méthoxyphénoxo pourrait provenir d'une délocalisation de charges impliquant le ligand aromatique axial. Une telle observation est en parfaite adéquation avec la stabilité du tourniquet#1 par rapport au tourniquet#2 beaucoup plus instable. Enfin, le rendement quantique de génération d'oxygène singulet diminue avec la polarité du solvant.

**Chapitre III. Un frein moléculaire à base d'un dimère de porphyrine de Zn(II).**

Le dimère ciblé a été synthétisé selon le schéma synthétique détaillé sur le **Schéma 6.**[36,37]

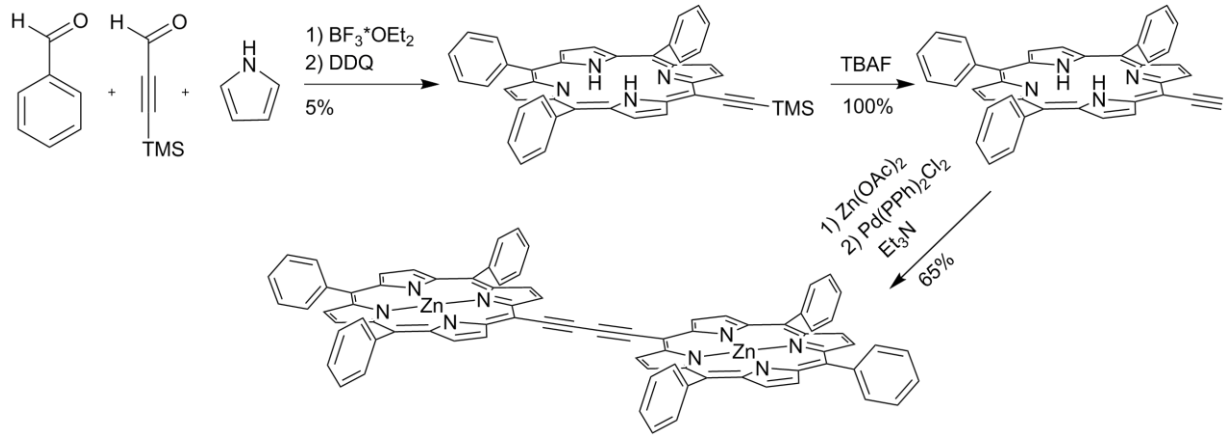


**Schéma 6.** Synthèse du dimère de Zn(II).

En solution, le dimère est en mouvement et existe comme un mélange de plusieurs conformères non plans. Le mouvement peut être bloqué par un stimulus chimique basé sur la formation d'un lien supplémentaire entre les deux ions métalliques *via* leurs positions axiales. Nous avons

notamment pu montrer que l'ajout d'acide [1,1'-biphenyl]-4,4'-disulfonique sur le système après coordination préalable de pyridin-4-yl-méthylamine en positions axiales des Zn(II) conduisait au blocage du système (**Schéma 7**). Le système peut être déverrouillé par simple ajout de triéthylamine.

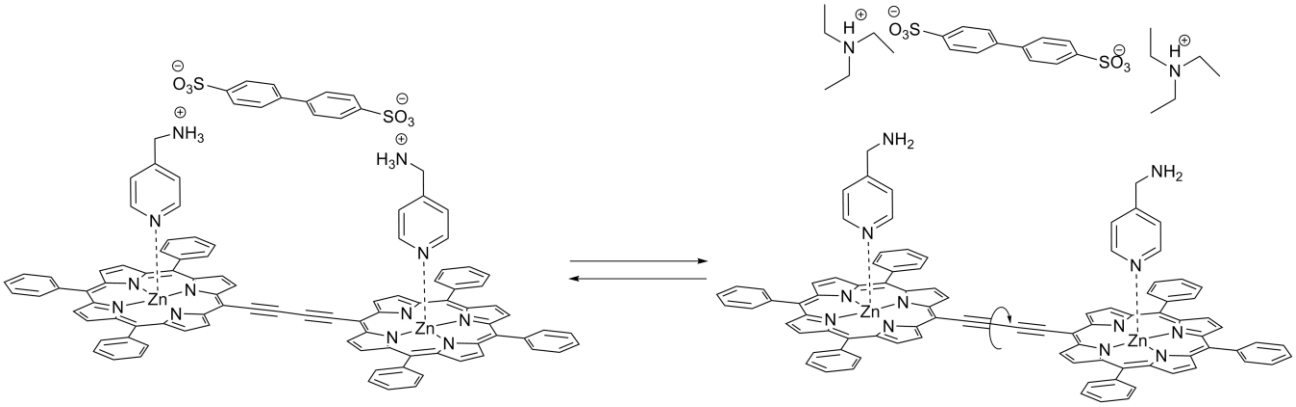

**Schéma 7.** Maitrise du mouvement dans le dimère **3.**

## Conclusion

Lors de ce travail de thèse, nous avons mis au point la synthèse d'un tourniquet moléculaire à base de porphyrine de P(V). La chimie des porphyrines de phosphore est loin d'être triviale, ceci est notamment lié à la faible taille du cation P(V) qui conduit à une très importante déformation du macrocycle ainsi qu'à la photo-décomposition des complexes générés.

Nous avons élaboré une méthode d'insertion du P(V) dans la cavité porphyrinique qui a permis d'accéder à des complexes porphyriniques substitués en position *méso* par des groupements pyridyl. Nous avons étudié l'échange de ligands en position axiale du P(V) et avons pu isoler 2 nouveaux tourniquets moléculaires. L'un d'entre eux s'est révélé être suffisamment stable et parfaitement adapté pour répondre à un stimulus chimique tel qu'une variation de pH ou l'ajout d'un cation métallique de type $Ag^+$. Dans les deux cas, la réversibilité des processus a pu être démontrée. Nous avons également effectué une étude photophysique des complexes porphyriniques de P(V) obtenus afin de mettre en évidence les paramètres conduisant à l'instabilité des systèmes obtenus.

Enfin, nous avons élaboré un deuxième système basé sur un dimère de porphyrines de Zn(II) dans lequel le mouvement peut être contrôlé à l'aide d'un stimulus chimique mettent en jeu les propriétés acido-basiques des ligands présents en position axiale des ions Zn(II)

## Bibliographie


1 K. Kinbara, T. Muraoka and T. Aida, *Org. Biomol. Chem.*, 2008, **6**, 1871–1876.

2 W. R. Browne and B. L. Feringa, *Nat. Nanotechnol.*, 2006, **1**, 25–35.

3 V. Serreli, C.-F. Lee, E. R. Kay and D. A. Leigh, *Nature*, 2007, **445**, 523–527.

4 M. C. Jiménez, C. Dietrich-Buchecker and J.-P. Sauvage, *Angew. Chemie (Int. Ed.)*, 2000, **39**, 3284–3287.

5 A. Mateo-Alonso, D. M. Guldi, F. Paolucci and M. Prato, *Angew. Chemie (Int. Ed.)*, 2007, **46**, 8120–8126.

6 P. R. Ashton, R. Ballardini, V. Balzani, I. Baxter, A. Credi, M. C. T. Fyfe, M. T. Gandolfi, M. Gómez-López, M. V. Martínez-Díaz, A. Piersanti, N. Spencer, J. Fraser Stoddart, M. Venturi, A. J. P. White and D. J. Williams, *J. Am. Chem. Soc.*, 1998, **120**, 11932–11942.

7 J. D. Badjic, M. Ronconi, J. F. Stoddart, V. Balzani, S. Silvi and A. Credi, *J. Am. Chem. Soc.*, 2006, **99**, 1489–1499.

8 T. Muraoka, K. Kinbara and T. Aida, *Nature*, 2006, **440**, 512–515.

9 J. D. Badjic, V. Balzani, A. Credi, S. Silvi and J. Fraser Stoddart, *Science*, 2004, **303**, 1845–1849.

10 A. Guenet, E. Graf, N. Kyritsakas, L. Allouche and M. W. Hosseini, *Chem. Commun.*, 2007, 2935–2937.

11 A. Guenet, E. Graf, N. Kyritsakas and M. W. Hosseini, *Inorg. Chem.*, 2010, **49**, 1872–1883.

12 A. Guenet, E. Graf, N. Kyritsakas and M. W. Hosseini, *Chem. Eur. J.*, 2011, **17**, 6443–6452.

13 T. Lang, E. Graf, N. Kyritsakas and M. W. Hosseini, *Dalt. Trans.*, 2011, **40**, 5244–5248.

14 T. Lang, E. Graf, N. Kyritsakas and M. W. Hosseini, *Dalt. Trans.*, 2011, **40**, 3517–3523.

15 T. Lang, A. Guenet, E. Graf, N. Kyritsakas and M. W. Hosseini, *Chem. Commun.*, 2010, **46**, 3508–3510.

16 T. Lang, E. Graf, N. Kyritsakas and M. W. Hosseini, *Chem. Eur. J.*, 2012, **18**, 10419–26.

17 T. Lang, E. Graf, N. Kyritsakas and M. W. Hosseini, *New J. Chem.*, 2013, **37**, 112.

18 N. Zigon, A. Guenet, E. Graf and M. W. Hosseini, *Chem. Commun.*, 2013, **49**, 3637–3639.

19 N. Zigon, P. Larpent, A. Jouaiti, N. Kyritsakas and M. W. Hosseini, *Chem. Commun.*, 2014, **50**, 5040–5042.

20 N. Zigon, P. Larpent, A. Jouaiti, N. Kyritsakas and M. W. Hosseini, *Dalt. Trans.*, 2014, **43**, 15779–15784.

21 N. Zigon, N. Kyritsakas and M. W. Hosseini, *Dalt. Trans.*, 2014, **43**, 152–157.

22 N. Zigon and M. W. Hosseini, *Chem. Commun.*, 2015, **51**, 12486–12489.

23 K. Hirakawa, S. Kawanishi, T. Hirano and H. Segawa, *J. Photochem. Photobiol. B.*, 2007, **87**, 209–17.

24 K. Hirakawa, N. Fukunaga, Y. Nishimura, T. Arai and S. Okazaki, *Bioorganic Med. Chem. Lett.*, 2013, **23**, 2704–2707.

25 J. Matsumoto, T. Shinbara, S. I. Tanimura, T. Matsumoto, T. Shiragami, H. Yokoi, Y. Nosaka, S. Okazaki, K. Hirakawa and M. Yasuda, *J. Photochem. Photobiol. A Chem.*, 2011, **218**, 178–184.

26 H. L. Anderson, *Inorg. Chem.*, 1994, **33**, 972–981.

27 A. Tsuda, H. Hu, R. Tanaka and T. Aida, *Angew. Chemie Int. Ed.*, 2005, **44**, 4884–4888.

28 M. U. Winters, J. Kärnbratt, M. Eng, C. J. Wilson, H. L. Anderson and B. Albinsson, *J. Phys. Chem. C*, 2007, **111**, 7192–7199.

29 C. J. Carrano and M. Tsutsui, *J. Coord. Chem.*, 1977, **7**, 79–83.

30 T. A. Rao and B. G. Maiya, *Inorg. Chem.*, 1996, **35**, 4829–4836.

31 K. Hirakawa and H. Segawa, *Photochem. Photobiol. Sci.*, 2010, **9**, 704.

32 K. Kunimoto, H. Segawa and T. Shimidzu, *Tetrahedron Lett.*, 1992, **33**, 6327–6330.

33 T. Xu, R. Lu, X. Liu, X. Zheng, X. Qiu and Y. Zhao, *Org. Lett.*, 2007, **9**, 797–800.

34 Y. Andou, K. Ishikawa, K. Shima, T. Shiragami and M. Yasuda, *Bull. Chem. Soc. Jpn.*, 2002, **75**, 1757–1760.

35 A. Harriman, *J. Photochem.*, 1983, **23**, 37–43.

36 J.-W. Seo, S. Y. Jang, D. Kim and H.-J. Kim, *Tetrahedron*, 2008, **64**, 2733–2739.

37 R. W. Wagner, T. E. Johnson, F. Li and J. S. Lindsey, *J. Org. Chem.*, 1995, **60**, 5266–5273.

## List of products

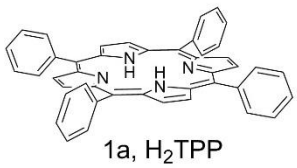

1a, $H_2TPP$

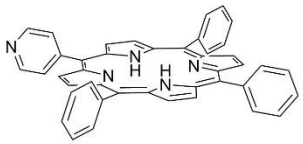

1b, $H_2MPyP$

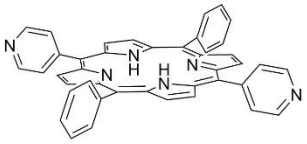

1c, $H_2DPyP$

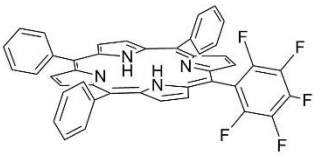

2, $H_2MpFP$

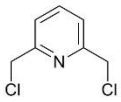

3

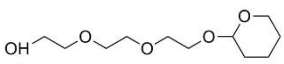

4

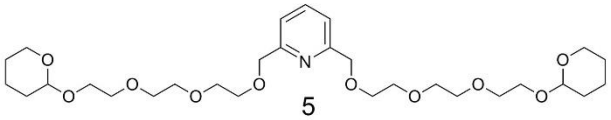

5

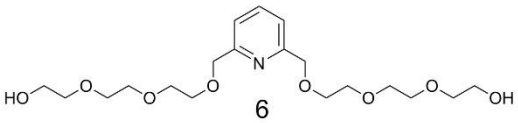

6

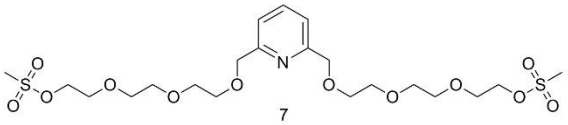

7

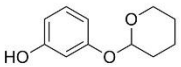

8

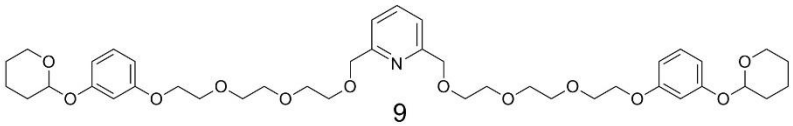

9

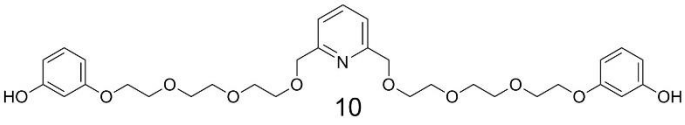

10

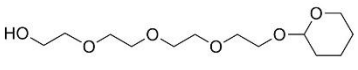

11

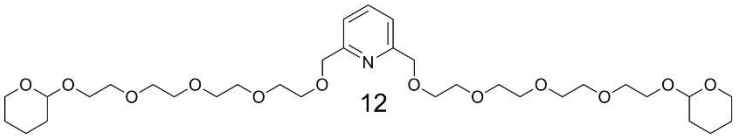

12

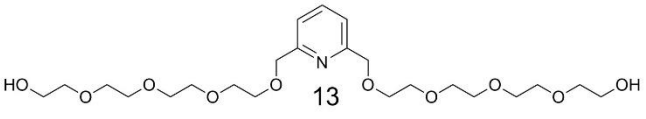

13

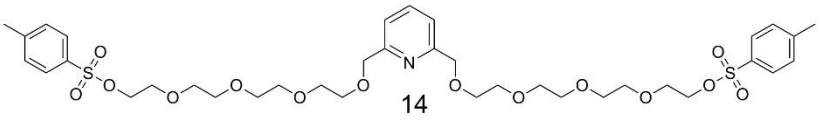

14

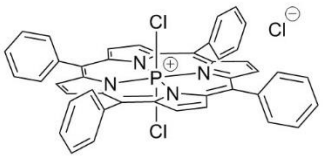

15, $[P(TPP)Cl_2]^+Cl^-$

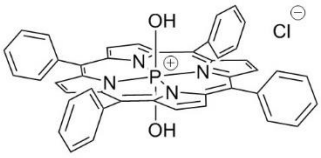

16a, $[P(TPP)(OH)_2]^+Cl^-$

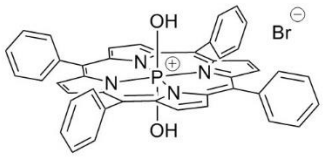

16b, $[P(TPP)(OH)_2]^+Br^-$

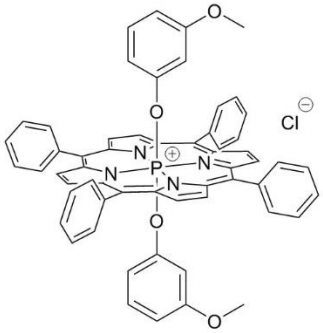

17, $[P(TPP)(OPhOMe)_2]^+Cl^-$

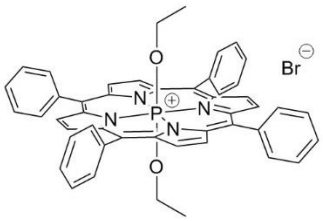

18, $[P(TPP)(OEt)_2]^+Br^-$

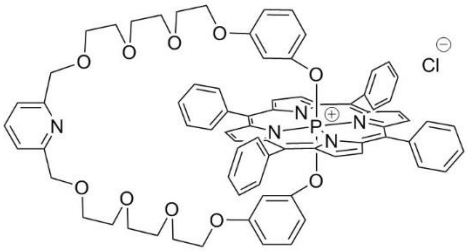

19, Model turnstile#1

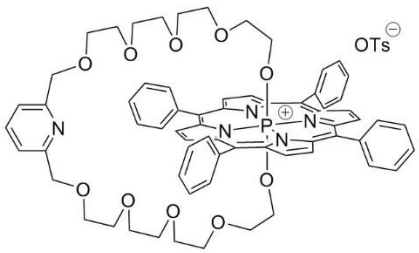

20, Model turnstile#2

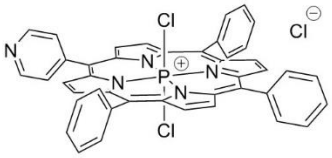

21, $[P(MPyP)Cl_2]^+Cl^-$

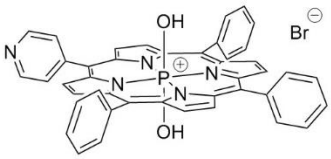

22, $[P(MPyP)(OH)_2]^+Br^-$

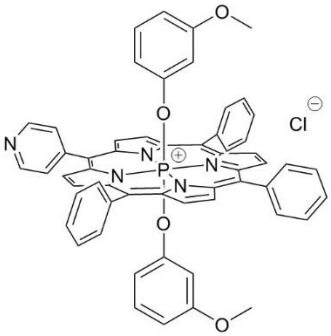

23, $[P(MPyP)(OPhOMe)_2]^+Cl^-$

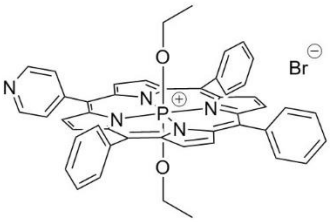

24, $[P(MPyP)(OEt)_2]^+Br^-$

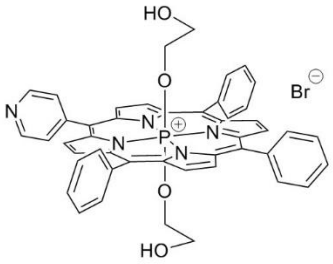

25, $[P(MPyP)(OEtOH)_2]^+Br^-$

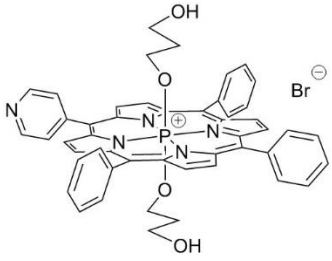

26, $[P(MPyP)(OPrOH)_2]^+Br^-$

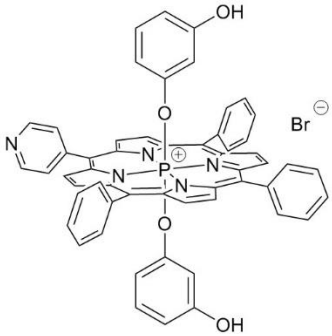

27, $[P(MPyP)(OPhOH)_2]^+Br^-$

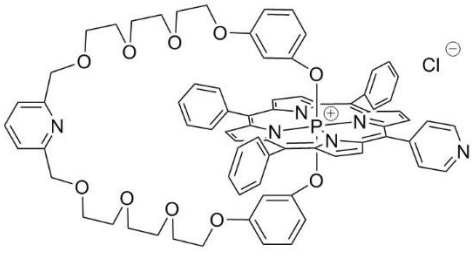

28a, Turnstile#1a

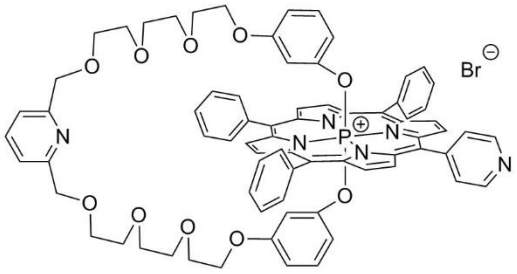

28b, Turnstile#1

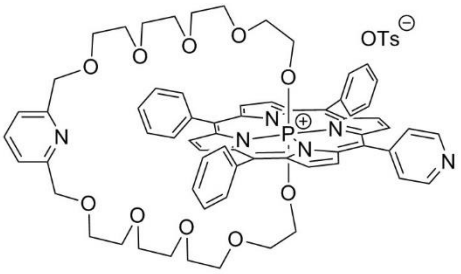

29, Turnstile#2

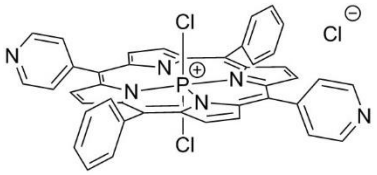

30, $[P(DPyP)Cl_2]^+Cl^-$

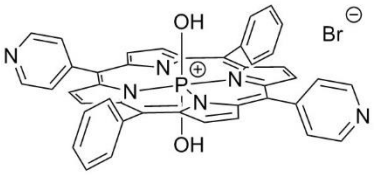

31, $[P(DPyP)(OH)_2]^+Br^-$

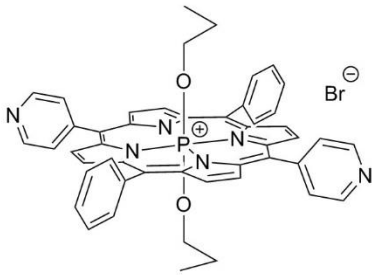

32, $[P(DPyP)(OPr)_2]^+Br^-$

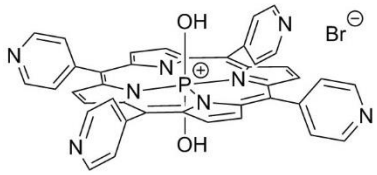

33, $[P(TPyP)(OH)_2]^+Br^-$

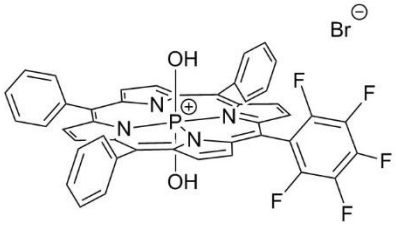

34, $[P(MpFP)(OH)_2]^+Br^-$

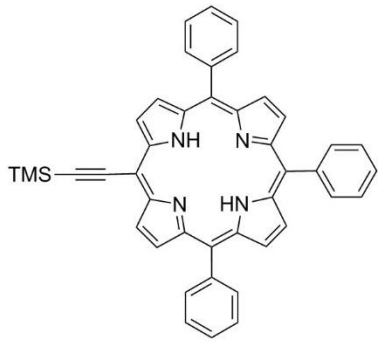

35, $H_2TMSP$

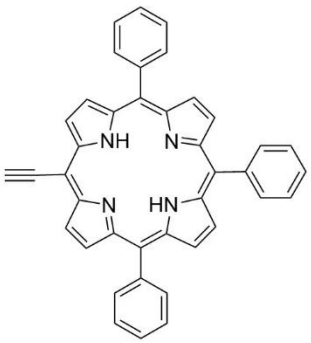

36, $H_2EtP$

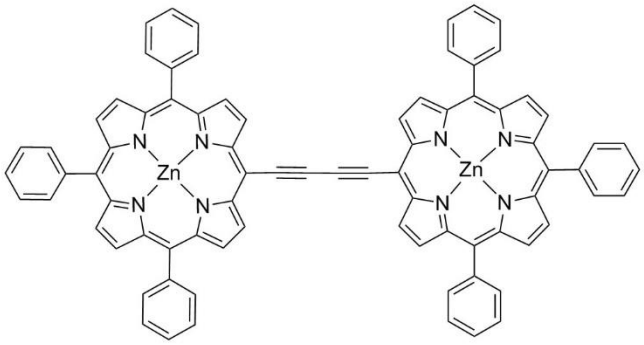

37, Zinc dimer

**Oral presentations:**

- "V International Conference of Physical Chemistry of Crown-compounds, Porphyrins and Phthalocyanines" Tuapse, Russia, September 2014
  *"Molecular switches based on P (V) porphyrinates"*
  I.N. Meshkov, Yu. G. Gorbunova, A. Yu. Tsivadze, V. Bulach, M.W. Hosseini

- "Journée des Doctorants", Strasbourg, France, November 2015
  *"Molecular turnstiles based on P (V) porphyrins"*
  I.N. Meshkov, Yu. G. Gorbunova, A. Yu. Tsivadze, V. Bulach, M.W. Hosseini

**Poster presentations:**

- "XXVI International Chugaev Conference on Coordination Chemistry", Kazan, Russia, October 2014
  *"Molecular turnstiles based on P (V) porphyrins"*
  I.N. Meshkov, Yu. G. Gorbunova, A. Yu. Tsivadze, V. Bulach, M.W. Hosseini

Ivan MESHKOV

# Contrôle du Mouvement Moléculaire à Base de Porphyrines


## Résumé

Les travaux décrits dans ce manuscrit s'intéressent au contrôle du mouvement moléculaire.

Après une introduction dédiée à l'état de l'art des machines moléculaires, le premier chapitre s'intéresse à la conception de tourniquets moléculaires à base de complexes porphyriniques de P(V). Le mouvement moléculaire a pu être contrôlé de manière réversible soit par l'utilisation des sites de coordination présents à la périphérie du système soit par des variations de pH. Le deuxième chapitre s'intéresse aux propriétés photophysiques des porphyrines de P(V) obtenues et plus particulièrement à leur capacité à générer de l'oxygène singulet avec une application potentielle en Thérapie Photodynamique (PDT).

Le troisième chapitre concerne l'élaboration d'un complexe contenant deux porphyrines de Zn(II) dont le mouvement relatif a pu être bloqué réversiblement par l'utilisation des positions axiales des cations métalliques.


Mots clés : machine moléculaire, tourniquet moléculaire, chimie supramoléculaire, porphyrine de P(V), chimie de coordination, oxygène singulet, porphyrin de Zn(II).


## Résumé en anglais

The manuscript focuses on molecular machines and the control of their movement. Two different devices have been designed, synthetized and characterized. Moreover, a series of new potential photosensitizer was obtained.

The introduction gives a general overview on molecular machines, reported during the past 20 years. The first chapter describes the synthesis of molecular turnstiles based on P(V) porphyrins. The molecular motion was controlled reversibly using either coordination chemistry or by changing the pH. The second part is dedicated to the study of the photophysical properties of P(V) porphyrins and especially their capacity to generate singlet oxygen under irradiation., making them potential photosensitizers that can be use in Photodynamic Therapy (PDT) or as catalyst.

The third chapter is devoted to the study of a molecular break based on a Zn (II) porphyrin dimer. The control of the movement was performed using the coordination of a bidentate ligand in the axial position of the metal cations.


Keywords: Molecular machines, Molecular turnstiles, supramolecular chemistry, P (V) porphyrins, Coordination chemistry, Singlet oxygen, Zn (II) porphyrins.